DOE/PC/90365--T20

Contract No. DE-AC22-91PC-90365

FUNDAMENTAL MECHANISMS IN FLUE GAS CONDITIONING

FINAL REPORT

Prepared for

U.S. DEPARTMENT OF ENERGY
Pittsburgh Energy Technology Center
P.O. Box 10940
Pittsburgh, PA 15236

Southern Research Institute

FUNDAMENTAL MECHANISMS IN FLUE GAS CONDITIONING

FINAL REPORT

SRI-ENV-96-146-7375-F

Contract No. DE-AC22-91PC90365

March 20, 1996

Todd R. Snyder
P. Vann Bush
Robert S. Dahlin

SOUTHERN RESEARCH INSTITUTE
2000 Ninth Avenue South
P.O. Box 55305
Birmingham, Alabama 35255-5305

Prepared for

Thomas D. Brown, Project Manager
UNITED STATES DEPARTMENT OF ENERGY
PITTSBURGH ENERGY TECHNOLOGY CENTER
Post Office Box 10940, MS 922
Pittsburgh, Pennsylvania 15236-0940

TABLE OF CONTENTS

1 EXECUTIVE SUMMARY

The U.S. Department of Energy's Pittsburgh Energy Technology Center (DOE/PETC) initiated this project as a part of a program to study the control of fine particles from coal combustion. Our project focus was flue gas conditioning. Various conditioning processes have lowered operating costs and increased collection efficiency at utility particulate control devices. By improving fine particle collection, flue gas conditioning also helps to control the emission of toxic metals, which are concentrated in the fine particle fraction. By combining a review of pertinent literature, laboratory characterizations of a variety of fine powders and ashes, pilot-scale studies of conditioning mechanisms, and field experiences, Southern Research Institute has been able to describe many of the key processes that account for the effects that conditioning can have on fine particle collection.

The overall goal of this research project was to explain the mechanisms by which various flue gas conditioning processes alter the performance of particulate control devices. Flue gas conditioning of fine particles can take place through many different methods. Conditioning involves the modification of one or more of the parameters which determine the magnitude of the forces acting on the fly ash particles. Resistivity, chemistry, cohesivity, size distribution, and particle morphology are among the basic properties of fly ash that significantly influence fine particle collection. Modifications of particulate properties can result in improved or degraded control device performance. These modifications can be caused by:

- Changes to the process design or operation that affect properties of the flue gas.
- Addition of particulate matter such as flue gas desulfurization (FGD) sorbents to the process effluent stream.
- Injection of reactive gases or liquids into the flue gas.

This project began with an extensive literature search to assemble existing theories and data covering two primary areas of interest. The first area focused on the characteristics of binary mixtures of FGD sorbents and coal fly ashes. The second area of interest was an examination of the effects of various conditioning agents on fine ash particles to determine the mechanisms by which these agents alter the physical properties of ash. We completed this phase of the project with publication of two special Topical Reports (Dahlin *et al*, 1992, Bush *et al*, 1992).

The primary forces or physical changes that affect the interaction of particles, and subsequently the performance of particulate control devices are van der Waals forces, electrostatic forces, ionic forces, adsorbed liquid layers, capillary forces (liquid bridges), and solid bridges. van der Waals forces, adsorption, and liquid and crystalline bridges all intimately depend upon the nature of the particle surface. The morphology of particles, their

surface chemistry, and the adsorption of vapors (in particular, water vapor) determine the forces of interaction among particles.

The literature search identified several areas where various types of conditioning can significantly alter the key characteristics of the particulate material to be collected. In high-temperature sorbent injection applications (where a sorbent such as limestone is inserted into the boiler, for example), the resistivity of the mixtures of sorbent and ash particles have significantly higher resistivities than the base line fly ashes. Electrostatic precipitators (ESPs) collecting these mixtures often have problems with back corona. Although SO_3 conditioning is generally not effective for reducing the resistivities of these mixtures, water vapor conditioning has been used successfully to accomplish this goal. For low-temperature sorbent injection applications (such as spray dryers or in-duct slurry injection), a primary concern is that the electrical resistivity of the ash/sorbent mixture may become too low. As the resistivity of the mixture drops much below 1×10^8 ohm-cm, the electrical force holding the particles on the ESP plates vanishes and then reverses direction to become a repulsive force. If this repulsive force becomes large enough, it can overcome the tensile strength of the particulate layer, resulting in reentrainment of the particles into the flue gas.

The deposition of layers of liquid on the surfaces of fly ash particles is the most common mechanism for altering the behavior of these particles during filtration or precipitation. Ammonium bisulfate, generated on fly ash particle surfaces during conditioning with ammonia in the presence of SO_3, has been shown to be effective in field applications for reducing resistivity and for increasing cohesivity. The effectiveness of this compound for increasing cohesivity is linked to the fact that it melts at 296 °F. Because it may exist as a liquid at the flue gas temperatures encountered in many particle control devices, it can collect at the contact points between particles through capillary action. When this occurs, liquid bridges are formed between adjacent particles. These liquid bridges form strong bonds between particles and significantly increase the bulk cohesivity of the ash. This is the most common mechanism for increasing ash cohesivity. Water adsorbed from the flue gas can also form these liquid bridges.

The primary variable determining the degree to which water adsorbs on suspended fly ash and sorbent particles is the relative humidity of the flue gas. As the relative humidity of the flue gas is increased, additional water is deposited on the surfaces of these particles. Even at the temperatures commonly encountered in fabric filters and electrostatic precipitators (~300 °F), layers of water are present on the surfaces of the entrained fly ash particles. Depending on the physical and chemical characteristics of the particles, enough water may become available to affect the strength of the bonds between particles through liquid bridge formation, or to reduce resistivity by providing conductive paths along the surfaces of the particles. The water initially deposited on fly ash particles usually forms strong chemical bonds with the compounds on the surfaces of the ash particles. Subsequent layers of water that are adsorbed as relative humidity increases become physically bonded to the particles. This physically bonded water is more

mobile than the chemically bonded water, and can form liquid bridges and/or dissolve soluble salts on the particle surfaces. In some cases the evaporation of previously adsorbed surface water has caused dissolved salts to be collected at interparticle contact points. Salt bridges formed in this way can greatly increase ash cohesivity.

Because water affects the key characteristics of particles through the same mechanisms that have been successfully applied to baghouses and precipitators, and because it is universally present in flue gas, we structured a parametric laboratory research program around the affects that water vapor conditioning has on various fly ashes and fine powders. The program was intended to assess the effects that relative humidity, particle morphology, and particle chemistry have on key particle characteristics. Water thus served as a generic conditioning additive.

We found that the amount of water adsorbed on the ashes and powders we tested was a function of the relative humidity used to condition them, and also strongly affected by the surface chemistry and morphology of the particles. Water adsorption was promoted by the presence of soluble salts and acids on the surfaces of fly ash particles. Water adsorbed on hydrophobic surfaces (often high in silica), was more likely to migrate to interparticle contact points than similar amounts of water adsorbed onto hydrophilic particle surfaces. The fate of adsorbed water was also strongly affected by the structure of the particles. Porous sorbent particles sequestered water in the interior of the particles, rendering it unavailable for building liquid bridges. Calcium in ashes often forms hydrates with adsorbed water, limiting the ability of the water to form liquid bridges.

After completing this laboratory program we performed pilot-scale evaluations at Southern Research Institute's 6 million Btu/hr Coal Combustion Facility (CCF) to verify the effects of water vapor conditioning on fabric filter and precipitator operation. Following these pilot-scale tests, we developed modifications to existing fabric filtration and electrostatic precipitation models developed by Southern Research Institute for the Electric Power Research Institute and the U.S. Environmental Protection Agency. The modifications to the filtration model account for reductions in the specific resistance of the filter cake due to adsorbed water on the fly ash particles resulting from flue gas humidification. Adjustments to the precipitation model were developed to account for the effects of electrostatic reentrainment observed during the collection of mixtures of sorbents and ashes from cool, moist flue gas.

We recommend that humidification should be seriously considered as a flue gas conditioning option. Humidification is a flue gas conditioning technique applicable to both electrostatic precipitators and fabric filters to improve particulate control. Unlike many flue gas conditioning systems, humidification does not add any toxic or hazardous compound to the plant site, flue gas, or collected ash. Our studies have shown that water adsorbed on ash particles during humidification of flue gas can increase bulk ash cohesivity and decrease bulk ash resistivity. An additional benefit of humidification is reduction in gas volume due to

evaporative cooling. Reductions in gas volume lead directly to increased specific collection area (SCA) in precipitators and reduced tubesheet pressure drop in fabric filters. Other potential benefits of increasing the cohesivity of the ash layer that builds on the ESP plates are reductions in rapping emissions and emissions from hopper boil up when ash dislodged from the plates during rapping falls into the collection hopper. Parallel benefits during cleaning cycles in fabric filters can also be expected from increased ash cohesivity.

2 INTRODUCTION

The U.S. Department of Energy's Pittsburgh Energy Technology Center initiated this project to develop a comprehensive understanding of the effects that various flue gas conditioning processes have on the on-site collection of fine fly ash particles generated by utility coal-fired boilers. In commissioning Southern Research Institute to perform this study to explain why conditioning processes alter fine particle collection, the U.S. Department of Energy's Pittsburgh Energy Technology Center (DOE/PETC) has attempted to consolidate utility experiences with various flue gas conditioning techniques with a fundamental understanding of particle-to-particle interactions. By combining a review of pertinent literature, laboratory characterizations of a variety of fine powders and ashes, pilot-scale verifications of conditioning mechanisms on the collection of fly ash particles from actual flue gas streams, and field experiences with a wide range of conditioning processes at utility installations, Southern Research Institute has been able to describe many of the key processes that account for the effects that conditioning can have on fine particle collection. DOE/PETC intends that this knowledge will provide a theoretical framework which can help guide the development and application of flue gas conditioning processes to enhance the collection of fine particles.

Southern Research Institute began this project with an extensive literature search to assemble existing theories and data covering two primary areas of interest. The first of these areas focused on the characteristics of binary mixtures of flue gas desulfurization sorbents and coal fly ashes. The second area of interest was an examination of the effects of various conditioning agents on fine ash particles to determine the mechanisms by which these agents alter the physical properties of ash. We completed this phase of the project with publication of two special Topical Reports (Dahlin *et al*, 1992, Bush *et al*, 1992). During the next phase of the project we analyzed a variety of fly ashes and fine powders in the laboratory. Based on the results of our literature search, the primary experimental parameter we set for these analyses was the relative humidity of the gas surrounding the particles. These laboratory studies were designed to assess the effects that relative humidity has on the key characteristics of bulk samples of fly ashes and powders. We then performed pilot-scale evaluations at Southern Research Institute's 6 million Btu/hr Coal Combustion Facility (CCF) to verify the results we obtained in these laboratory analyses. We issued this Final Report to summarize the results of our laboratory and pilot-scale work and to include discussions of modeling the effects of flue gas conditioning on fabric filtration and electrostatic precipitation.

2.1 BACKGROUND

Although many programs have successfully demonstrated the advantages of flue gas conditioning for improving particulate collection, most of the fundamental mechanisms involved in these processes remain poorly understood. Conditioning of fine particles can take place through many different methods. Flue gas conditioning involves the modification of one or more of the parameters which determine the magnitude of the forces acting on the fly ash

particles. The development of conditioning processes for the enhancement of fine particle collection is hampered by a lack of a comprehensive understanding of these forces.

A significant body of research exists describing the factors that influence the effectiveness of conventionally operated electrostatic precipitators (ESPs) and fabric filters. Much of this research has been directed toward the characterization of fly ash particles and bulk fly ash behavior. Resistivity, chemistry, cohesivity, size distribution, and particle morphology are among the basic properties of fly ash that significantly influence fine particle collection. In some cases the mechanisms by which these fly ash particles influence fine particle collection have been identified, while in other cases proposed mechanisms are based primarily on empirical evidence.

Modifications of particulate properties can result in improved or degraded control device performance. These modifications can be caused by changes to the flue gas, addition of particulate matter such as flue gas desulfurization (FGD) sorbents or the addition of reactive gases or liquids. When the mechanisms by which conditioning agents and FGD sorbents react with fly ash particles are better understood, selective application of appropriate conditioning agents can result in significantly improved fine particle collection at lower capital and operating costs.

2.2 OBJECTIVES

The overall goal of this research project was to describe the mechanisms by which various flue gas conditioning processes alter the performance of particulate control devices. One of our specific objectives was to determine how sorbent injection processes modify the characteristics of the particulate matter entrained in the flue gas, and to identify the mechanisms by which FGD processes affect the collection of fine particles in ESPs and fabric filters. The second specific objective of this project was to identify the mechanisms by which conditioning agents, including chemically active compounds, modify the key properties of fine fly ash particles.

The first specific objective has the potential to affect the broad implementation of technologies currently available or under development to control SO_2 emissions. The second specific objective provides for the effective development of advanced approaches to flue gas conditioning of fine fly ash particles. In both cases, the focus of the research was an evaluation of the fundamental mechanisms that are responsible for controlling or changing the key physical properties of the particulate matter. These objectives required us to apply theoretical descriptions of the relationships between interparticle forces and the characteristics of the particles, and to conduct empirical trials to assess the relative magnitudes of these forces. We then incorporated our findings into models describing the operation of ESPs and fabric filters.

3 LITERATURE SURVEY

Southern Research Institute assembled and examined the theories and data applicable to this project's objectives. We performed an abstract search through the DIALOG Information Services. This computer-based service was used to access the National Technical Information Service (NTIS), COMPENDEX PLUS, and Chemical Abstracts data bases. The results of the laboratory data and the articles obtained in the literature reviews performed for DOE/PETC under Contract No. DE-AC22-88PC88868 and Contract No. DE-AC22-88PC88851 were also included in this review. In addition to the information obtained through these literature reviews and abstract searches, operating experiences with ash conditioning were assembled for analysis. The specific details of the search and review procedures we used are presented in Appendix A. Over 35,000 abstracts were returned from this search and examined. 136 articles and reports that appeared to contain information describing the factors involved in either the interactions of ashes and sorbents or in the general conditioning of ash or other fine particles were selected for detailed review. We produced written reviews of the articles and reports and grouped them according to their applicability to sorbent or general conditioning applications.

3.1 ASH AND SORBENT INTERACTIONS

The following discussion is a condensed summary of our first Topical Report (Dahlin *et al*, 1992) derived from the literature review described above. In this discussion, we review what we learned about the effects of sorbent injection processes on particulate properties. The effects on the fundamental properties of size, shape, and chemistry are addressed, along with the effects on the flue gas environment and the bulk properties of electrical resistivity and cohesivity. Although resistivity and cohesivity are not fundamental properties, they are certainly key parameters in determining control device performance. Resistivity, in particular, is a parameter that has been measured in almost every study of sorbent injection that has been performed to date. One reason that resistivity effects have received so much attention is that the sorbent injection processes currently under development are primarily intended for the retrofit market. Over 90 % of the existing coal-fired generating capacity is equipped with ESPs. In a study by the Environmental Protection Agency (EPA), information on particulate control devices was compiled for 191 boilers at the 60 power plants with the highest SO_2 emissions (Emmel and Kaplan, 1988). This survey revealed that 174 out of the 191 boilers, or 91 % of this population of boilers, were equipped with ESPs. Therefore, there has been relatively little research on the effects of sorbent injection on fabric filter performance. Nevertheless, the fundamental information on particulate properties obtained in the ESP-related studies is equally applicable to fabric filters, since the effects of sorbent injection on particulate properties are independent of the type of control device.

For this discussion, it is most convenient to separate the sorbent injection processes into two categories: (1) high-temperature processes, involving injection of calcium-based sorbents into

the furnace or economizer; and (2) low-temperature processes, involving conventional lime spray drying, in-duct lime spray drying, or dry injection of hydrated lime with humidification. It is desirable to discuss these two categories of sorbent injection processes separately because the high-temperature sorbent injection processes produce fundamentally different effects on particulate properties than do the low-temperature processes. This results in different sets of concerns relative to control device performance. For example, with high-temperature sorbent injection a primary concern is high resistivity and the potential for back corona in an ESP. With low-temperature sorbent injection a primary concern is that the resistivity may become too low, resulting in electrical reentrainment in the ESP.

3.1.1 Effects of High-Temperature Sorbent Injection

Injection of calcium-based sorbents (limestone or hydrated lime) into the furnace or economizer produces substantial changes in particulate properties relative to those of the baseline fly ash. At furnace temperatures, the limestone or hydrated lime is rapidly calcined, and the resulting lime (CaO) undergoes a pozzolanic reaction with the aluminosilicates in the fly ash, forming a modified ash with cementitious qualities (Dahlin et *al*, 1986). At low temperatures (ca 300 °F), hydrated lime does not decompose, no pozzolanic reaction occurs, and the resulting ash is not significantly cementitious (Henzel and Ellison, 1990). This difference is partly responsible for the different effects of high-temperature and low-temperature sorbent injection on the properties of the ash.

3.1.1.1 Effect on Electrical Resistivity

Numerous studies have shown that the furnace injection of either limestone or hydrated lime produces a substantial increase in electrical resistivity, unless this effect is controlled by flue gas humidification or conditioning with SO_3. Studies have shown that when hydrated lime is injected at the furnace exit, the high resistivities of the ash/sorbent mixture are difficult to reduce with SO_3 conditioning in conventional concentrations. This effect was attributed to the higher specific surface area and reactivity of the hydrated lime (Gooch *et al*, 1987). These tests also confirmed that humidification of the flue gas with a water spray, which cooled the gas from about 300 °F to about 180 °F, was effective for reducing resistivity. At the same time, it was noted that the humidification eliminated the severe back corona in the pilot ESP used in the study.

3.1.1.2 Effect on Particle Size Distribution

In general, there is agreement that furnace sorbent injection produces a shift in the particle size distribution toward smaller particles. This is to be expected when hydrated lime is used as the sorbent, since the mass mean diameter of commercial hydrated lime is typically about 3 to 6 μm (Boynton, 1966). The mass mean diameter of fly ash from bituminous coals is typically about 16 μm (Dahlin and Altman, 1983). For limestone, the smallest mean size that can be

produced commercially in a dry grinding circuit is about 10 μm (Boynton, 1966). When subjected to rapid heating, as in furnace injection, virtually all limestones decrepitate (Boynton, 1966) producing a particle size distribution that is considerably finer than that of the parent material. Because of this decrepitation, limestone injection also tends to produce a shift in the size distribution toward smaller particle sizes.

3.1.1.3 Effect on Particle Morphology, Surface Area, and Pore Structure

Particle morphology and surface area have been shown to be key parameters in determining the performance of fabric filters (Bush *et al*, 1989). Relatively smooth particles tend to produce a low bulk ash cohesivity. In general, cohesivity increases as the particles become rougher and smaller. Ashes with low cohesivities tend to pack tighter into smooth dust cakes. Particle morphology is also important in ESPs in that rougher particles are subject to greater drag forces, resulting in lower electrical migration velocities (White, 1963). Surface roughness and surface area also affect the ability of the particles to adsorb water vapor and other conditioning agents that influence the electrical resistivity of the ash (Bickelhaupt, 1975). The effects on cohesivity that are important with regard to fabric filter performance are also important in determining the tendency of the ash to be reentrained from ESP plates.

Surface area is an important factor governing the ability of the sorbent to adsorb water vapor and other potential conditioning agents. Bush *et al* (1989) reported BET surface areas for 18 fly ashes and 6 ash/sorbent mixtures from fluidized-bed combustors and spray dryers. The ash/sorbent mixtures, particularly those from the fluidized-bed combustors, generally had higher surface areas than the fly ashes that did not contain any sorbent. Ash/sorbent mixtures from furnace sorbent injection processes have also been shown to possess slightly elevated surface areas, in comparison to the baseline fly ashes (Dahlin *et al*, 1987).

CaO particles produced from hydrated lime tend to be smaller than those produced from limestone, because of the finer size of the hydrated lime. However, the CaO particles produced from hydrated lime have a much greater tendency to agglomerate. CaO produced from hydrated lime also differs from limestone-derived CaO in terms of the distribution of pore volume with pore size. CaO derived from hydrated lime tends to possess more pore volume in larger pores than does limestone-derived CaO (Gullett and Bruce, 1987). This tends to make the hydrate-derived CaO less susceptible to pore closure and, therefore, more reactive towards SO_2 and other gases, which may explain why the ash/sorbent mixtures produced from hydrated lime tend to be more difficult to condition than those produced from limestone.

Certain additives that have been employed to promote the reactivity of sorbents have also been shown to alter morphology. A dramatic alteration of morphology has been observed when chromium oxide, Cr_2O_3, is used to promote the reactivity of limestone injected near the burner. Slaughter *et al* (1988) reported that the addition of 5 wt. % Cr_2O_3 to limestone injected at 2150 to 2600 °F converted the rough, angular sorbent particles to smooth spheres.

Slaughter *et al* suggest that the Cr_2O_3 reacts with the CaO to form a low-melting eutectic mixture, which would be a liquid at temperatures above about 1830 °F. Less pronounced morphological effects have been noted with other promoters, particularly the alkali metals, and with dispersants and surfactants.

Reductions in particle size and changes in pore structure have also been observed when surfactants and dispersants have been used to produce a modified hydrated lime. Kirchgessner and Lorrain (1987) prepared a modified hydrated lime by adding calcium lignosulfonate, a byproduct of the paper industry, to the water of hydration. They found that the modified hydrates containing calcium lignosulfonate had smaller mass mean particle sizes than the unmodified hydrates produced under the same hydration conditions. The presence of the large lignosulfonate molecule at the $Ca(OH)_2$ grain boundaries is believed to reduce grain boundary mobility, resulting in slower sintering. The smaller particle size obtained with the lignosulfonate has been attributed to the ability of the large lignosulfonate molecule to obstruct the formation of liquid bridges between the sorbent particles, resulting in less agglomeration (Kirchgessner and Lorrain, 1987).

3.1.1.4 Effect on Particle Cohesivity

To date, there have been no studies that have examined the effect of furnace sorbent injection on ash cohesivity. The only related studies that we are aware of pertain to the cohesivity of ash from fluidized bed combustors. These studies may not be relevant, however, because the ash/sorbent mixtures produced by atmospheric fluidized-bed combustors (AFBCs) differ from those produced by furnace sorbent injection. The AFBCs operate at lower temperatures than pulverized coal-fired (PC-fired) furnaces, producing ash particles that are much rougher and more angular than those produced by PC-fired utility boilers. The ash produced by a PC-fired boiler tends to be relatively smooth and spherical because it has passed through a semi-molten state in the high-temperature regions of the furnace. The operating temperatures of the AFBCs are well below the ash fusion point, so the ash never reaches a semi-molten state, but retains the rough, angular shapes of the coal mineral inclusions. These rough, angularly shaped particles result in a highly cohesive ash (Bush *et al*, 1987; Cushing *et al*, 1991). This result may also apply to ash/sorbent mixtures from furnace injection of limestone, which tends to produce rough, angular particles. However, it is doubtful that these observations could be extrapolated to furnace injection of hydrated lime, because of the substantial difference in particle size and morphology.

The inherent cohesivities of ashes are predominantly controlled by particle morphology. In general, cohesivity increases with decreasing size and with increasingly irregular particle shapes. Although surface chemistry can also affect cohesivity, ashes with similar chemistries can have widely different inherent cohesivities because of differences in morphology. Morphology may control cohesivity by altering the coordination number (average number of contact points per particle), and/or the proximity of the surfaces of adjacent particles.

3.1.2 Effects of Low-Temperature Sorbent Injection

Low-temperature sorbent injection processes include conventional spray drying, in-duct spray drying, dry sorbent injection with humidification, spray drying within an existing ESP casing (the E-SO_X process), and duct injection of advanced sorbents prepared by reacting lime with fly ash (Advanced silicate, or ADVACATE). The spray drying processes (conventional, in-duct, and E-SO_X) use an aqueous slurry of lime that is atomized into the flue gas by either rotary atomizers or pneumatic spray nozzles. In-duct and E-SO_X spray drying processes use pneumatic nozzles to spray the lime slurry into the duct or ESP casing. The ADVACATE process uses a similar injection system with a modified sorbent that is prepared by reacting lime and fly ash at a temperature of about 180 to 195 °F (Jozewicz *et al*, 1988).

3.1.2.1 Effect on Electrical Resistivity

With regard to ESP performance, a primary concern is that the electrical resistivity of the ash/sorbent mixture may become too low. When resistivity is in the desirable range, about 1 x 10^8 to 2 x 10^{10} ohm-cm according to White (1963), the electrical binding force acts with adhesive and cohesive forces to hold the particles on the ESP plates. As the resistivity drops much below 1 x 10^8 ohm-cm, the electrical force holding the particles on the ESP plates vanishes and then reverses direction to become a repulsive force (White, 1963). If the repulsive force becomes large enough, it can overcome the tensile strength of the particulate layer, resulting in reentrainment of the particles back into the flue gas. This electrical reentrainment can drastically reduce the collection efficiency of an ESP. A theoretical development of the criterion for the onset of electrical reentrainment was presented by Pontius and Marchant (1991).

Brown *et al* (1988) suggested that the unexpectedly poor performance of a pilot ESP operated downstream from a spray dryer was attributable to reentrainment. Although the authors did not report any data on resistivity, a low value would be expected under the specified operating conditions (20 °F approach temperature, calcium-to-sulfur molar ratio of 1.3:1, and coal sulfur content of 2.5 % to 4 %). In later work, supporting laboratory studies showed that electrical reentrainment occurred when the resistivity of the ash/sorbent mixture from the spray dryer fell below about 1 x 10^8 ohm-cm (Durham, Holstein *et al*, 1991). As the resistivity was further reduced by lowering the temperature in the laboratory test cell, the rate of particle ejection from the grounded electrode was observed to increase. Particle ejection ceased when the temperature reached about 135 °F, presumably because of the increase in particulate cohesivity with increasing relative humidity. The addition of calcium chloride to the ash/sorbent mixture was found to greatly reduce the reentrainment by increasing the relative humidity in the immediate vicinity of the particles, thereby increasing adsorption of water, and subsequently increasing cohesivity.

Calcium chloride addition to the lime slurry was subsequently investigated as a means of improving the performance of the pilot ESP collecting the spray dryer effluent (Durham, Holstein *et al*, 1991). At an approach temperature of 18 °F, the chloride addition dramatically improved ESP performance because of increased cohesivity.

Landham *et al* (1991) observed a gradual degradation in the performance of an ESP collecting spray dryer effluent that was found to be correlated with an increase in the lime slurry feed rate. Model predictions suggested that the ESP performance should have improved with increasing slurry feed rate as a result of the lower gas temperature, lower gas flow rate and velocity, higher specific collection area (SCA), lower gas viscosity, higher gas density, and higher field strength. The discrepancy between the observations and model predictions indicated the presence of a non-ideal effect such as electrical reentrainment. Resistivity measurements made in the laboratory under simulated spray dryer conditions yielded values of 4 to 6 x 10^7 ohm-cm, which are low enough to cause electrical reentrainment. The mechanism for this reduction in resistivity is the increased adsorption of surface water due to the increased partial pressure of water vapor in the flue gas. Water that resides on the surfaces of the ash particles mobilizes charge-carrying ions (principally sodium ions) contained in the aluminosilicate matrix of the fly ash particles.

There have also been indications that electrical reentrainment associated with low resistivity limits the performance of ESPs collecting effluent from dry sorbent injection. Durham, Ebner *et al* (1991) found that even the base line performance of the ESP, with no sorbent injection, was degraded by electrical reentrainment. This effect was attributed to inadequate insulation that allowed the gas temperature in the ESP to drop to 258 °F, producing resistivities of 10^7 to 10^8 ohm-cm. Field trials suggest that very small ESPs (SCA $\leq$ 150 ft^2/kacfm) must be enlarged to adequately control ashes with very low resistivities, such as the effluents from dry sorbent injection.

Other data from in-duct spray drying and dry sorbent injection tests suggest that it is possible to avoid the electrical reentrainment problem by operating the ESP at a higher gas temperature. Of course, this entails some sacrifice in SO_2 capture, but operation at higher temperatures may be necessary to avoid excessive electrical reentrainment.

Measurements of the collection efficiency of an ESP collecting the effluent from EPA's E-SO_X process have also suggested the presence of electrical reentrainment (Pontius and Marchant, 1991). Laboratory measurements revealed that the cohesive strength of the E-SO_X ash/sorbent mixture was at the low end of the range measured for a large number of fly ash samples. The resistivity of the E-SO_X solids was also shown to be extremely sensitive to temperature, dropping from 10^{10} ohm-cm at 170 °F to 10^8 ohm-cm at 140 °F. Apparently the process conditions caused the resistivity to be low enough to induce electrical reentrainment, especially considering the low cohesivity of the E-SO_X solids.

3.1.2.2 Effect on Particulate Loadings

Control devices installed downstream from conventional spray dryers, or other low-temperature sorbent injection processes, are generally subjected to much higher particulate loadings than are control devices collecting only fly ash. For higher sulfur coals, the increase in inlet loading is quite large, because of the larger amount of sorbent that must be injected. Spray dryers generally produce at least a doubling of the particulate mass, and order of magnitude increases in particulate loading are possible with higher sulfur coals.

3.1.2.3 Effect on Particle Size Distributions

Low-temperature sorbent injection processes also alter the size distribution of particles entering the downstream control device. Conventional spray dryers tend to make the size distribution coarser, because of the relatively large lime agglomerates produced in this process. Dry sorbent injection processes tend to make the size distribution finer, because the dry hydrate particles are generally smaller than the mass mean particle size of the fly ash. The effect of in-duct spray drying lies somewhere between the effects of conventional spray drying and dry sorbent injection. Dry injection would be expected to produce the lowest degree of sorbent agglomeration.

In case studies of spray dryers, the sorbent was found to be concentrated in relatively large particles. Comparison of the sorbent and ash size distributions reveals that the sorbent particles are larger than the fly ash particles, and the sorbent mass is substantially larger than the mass of fly ash. The relatively large size of the sorbent particles tends to lessen the effect of the large increase in particulate mass on ESP performance, because the larger particles are easier to collect.

Analysis of cascade impactor samples taken at the ESP inlet and outlet suggests that the E-SO_x sorbent actually breaks up in the ESP (Pontius and Marchant, 1991). Pontius and Marchant suggest that the break up occurred because the electrostatic forces acting on the sorbent agglomerates became large enough to overcome the agglomerates' tensile strength. To date, this type of breakup of sorbent particles has been reported only in connection with the E-SO_x process. However, it is possible that this breakup mechanism occurs in other low-temperature sorbent injection processes but has not yet been recognized.

Preparation of ADVACATE sorbent by reaction of $Ca(OH)_2$ and fly ash at elevated temperature reportedly produces a modified sorbent with a mass mean diameter of 66 to 112 μm (Sedman *et al*, 1991). This suggests that ADVACATE sorbent particles are much larger than sorbent particles used in other low-temperature processes. Since the mass mean particle size of $Ca(OH)_2$ is typically 2 to 6 μm, and that of fly ash is typically 15 to 20 μm, the much larger size of the ADVACATE sorbent particles suggests that this sorbent is highly agglomerated.

The effect of dry sorbent injection processes on the particle size distribution appears to be dependent upon the location of the humidification sprays relative to the sorbent injection nozzles. Injection of the water upstream of the sorbent results in the formation of a sulfuric acid aerosol. Durham, Ebner *et al* (1991) reported that the acid aerosol formed by this mechanism caused a doubling of the mass concentration of particles smaller than 0.4 μm. In this size range, the acid aerosol accounted for almost all of the observed increase in particulate mass, and the increase was virtually eliminated when the water was injected downstream from the sorbent nozzles. With the downstream humidification, the SO_3 vapor appears to be captured by the lime before it has a chance to condense in the water sprays. With either upstream or downstream humidification, the sorbent caused a significant increase in particle mass in the size range of 0.5 to 1 μm. Both this effect and the acid aerosol were observed to cause some quenching of the corona current in the inlet ESP field. The sorbent effect produced a 44 % reduction in current density, while the combined effect of the sorbent and acid aerosol produced a 93 % reduction, effectively shutting down the inlet field. Thus, upstream humidification is definitely not recommended for those cases where SO_3 concentration is significant.

Felix *et al* (July, 1991) observed the same corona quenching phenomenon discussed above with dry sorbent injection, but reported that slurry injection (i.e., in-duct spray drying) had no adverse effect on ESP electrical operation. This suggests that the acid aerosol is not formed during in-duct spray drying. It is postulated that the dense fog of slurry droplets created by in-duct spray drying captures the SO_3 as vapor before it condenses. In the case of dry injection with downstream humidification, the sorbent particles also appear to be capable of capturing SO_3 as vapor. However, in the case of dry injection with upstream humidification, the SO_3 is condensed as an ultrafine aerosol before coming into contact with the sorbent. Ultrafine acid aerosols are also produced in wet scrubbers, where the flue gas is rapidly quenched prior to entering the spray tower absorber (Dahlin and Brown, 1991). The rapid quenching prior to the absorber favors acid condensation, allowing little opportunity for capture of SO_3 as vapor. The quenching of the flue gas is much slower during in-duct spray drying, resulting in more opportunity for capture of SO_3 prior to condensation.

3.1.2.4 Effect on Particle Morphology, Surface Area, and Pore Structure

Like the high-temperature processes discussed earlier, low-temperature sorbent injection processes tend to significantly alter the morphology, surface area, and pore structure of the particles to be collected. Fly ash particles are predominantly smooth spheres, with no visible pore openings that might suggest any internal porosity. The absence of intraparticle porosity is confirmed by relatively low values of BET surface area, which are generally less than 4 m^2/g for fly ash (Bush *et al*, 1989). In contrast to the smooth, relatively non-porous fly ash particles, sorbent particles are more irregular in shape and are covered with many pore openings. These pore openings may actually be spaces between primary $Ca(OH)_2$ particles in

a sorbent agglomerate. In any case, sorbent particles have more surface area and porosity than ordinary fly ash. This conclusion is consistent with measurements showing that particles in spray dryer effluents have relatively high values of BET surface area (Livengood *et al*, 1988; Jǿns *et al*, 1986).

Sorbent particles produced by in-duct spray drying and dry sorbent injection are generally smaller than those produced by conventional spray dryers. This is attributable to the smaller droplet sizes used in the duct injection processes. Despite this difference in particle size, the surface areas of the ash/sorbent mixtures produced from conventional spray drying and duct injection appear to be comparable. This similarity in surface area attests to the fact that most of the surface area is contained within pores inside the individual particles; the particle surfaces make a relatively small contribution to total surface area.

Compared to ordinary fly ash, the solid effluents from low-temperature sorbent injection exhibit elevated surface areas and porosities. This increased surface area and porosity allow greater adsorption of water vapor and other potential conditioning agents, just as these factors allow greater SO_2 removal. Laboratory studies of the conversion of $Ca(OH)_2$ to $CaSO_3$ under differential reaction conditions have shown that the ultimate conversion is linearly correlated with surface area (Yoon *et al*, 1986; Borgwardt and Bruce, 1986; Blythe *et al*, 1986). Klingspor (1983) showed a direct proportionality between the BET surface area of hydrated lime and the amount of water adsorbed at a given relative humidity. It is reasonable to expect that the uptake of water vapor and other potential conditioning agents by ash/sorbent mixtures follows a similar trend with surface area. The adsorbed water and other species, such as sulfuric acid, play a key role in interparticle bonding, which is a key determinant of cohesivity or tensile strength. Therefore, electrical reentrainment in ESPs and the pressure drop across fabric filter dust cakes are ultimately affected by the elevated surface area and porosity associated with the effluents from low-temperature sorbent injection.

3.1.2.5 Effect on Particle Cohesivity

Several studies have shown that the ash/sorbent mixtures from low-temperature sorbent injection generally have lower tensile strengths (i.e., lower cohesivities) than do ordinary fly ashes (Bush *et al*, 1989; Pontius and Marchant, 1991). This result is contrary to what might be expected. At the lower temperatures and higher moisture levels associated with these processes, one would expect more adsorption of water vapor. With all other factors being equal, the presence of this adsorbed water should make the material more cohesive, as a result of increased liquid bridging and hydrogen bonding (Zimon, 1982). The low cohesivities suggest the presence of other mechanisms that prevent or offset the expected effects of the increased adsorption of water. One possible explanation is that the water is sequestered in the sorbent particles in such a manner that it is no longer available for bridging and hydrogen bonding. Some of the water could chemically react with the sorbent to produce a hydrate such as $CaSO_3 \cdot 2H_2O$. The water could also be drawn into pores by capillary action. This

hypothesis suggests that tensile strength should decrease with increasing porosity. Miller *et al* (1991) reported this type of relationship between cohesivity and the bulk (interparticle) porosity. Intraparticle porosity can be important in governing the capillary movement of water into the particle interior, and thereby affect cohesivity.

In general, low cohesivity is undesirable because of the potential for electrical reentrainment in ESPs and the potential for low dust cake porosity and high pressure drop in baghouses. If necessary, cohesivity can be increased by the use of deliquescent additives that help retain water at the particle surface. Durham, Holstein *et al* (1991) showed that the addition of calcium chloride to a spray dryer slurry resulted in a more cohesive ash/sorbent mixture and eliminated electrical reentrainment in a ESP collecting spray dryer effluent. Doyle *et al* (1986) suggested that a high alkali content in the fly ash tended to make spray dryer solid effluents more cohesive. They based this hypothesis on a study of two similar spray dryer installations. The installation with the higher alkali ash produced ash/sorbent mixtures that were more highly agglomerated, stickier, and more likely to cause deposition problems than were the ash/sorbent mixtures from the low-alkali ash. Thus, the ultimate cohesivity of an ash/sorbent mixture depends on ash chemistry as well as on the operating conditions of the sorbent injection process. Jǿns *et al* (1986) adjusted the residual moisture content of the dust cake at a baghouse collecting spray dryer effluent by manipulating the approach temperature. Thus, the control of process temperature and the use of deliquescent additives are two potential approaches to the control of cohesivity.

3.2 INTERACTIONS OF ASHES AND CONDITIONING AGENTS

The following section contains a discussion of mechanisms that govern the relationships between particles in a bulk agglomerate, including descriptions of the fundamental interparticle forces and how they are related. Emphasized in the discussion are those forces dominant in the regime of particles having the properties of fly ash. Several paragraphs are devoted to descriptions of the surface chemistry of fly ash. Then there is a discussion of what the mechanisms and fly ash properties suggest can be accomplished to modify particulate properties to improve their collection.

3.2.1 Mechanisms

Interactions of particles and interparticle forces are relevant at the collecting surfaces of particulate control devices: electrostatic precipitator plates, cyclone walls, or baghouse filtering fabric. At these surfaces, characteristics of the particles, the surfaces, and their environment yield a conglomerate of particles with resultant bulk properties that govern the performance of the particulate control device. Chemical reactions and physical forces will dictate the nature of the conglomerate.

Mechanisms by which particles interact define the applicable forces, and formalize the relationships between these forces, the effective range of the forces, the relative magnitudes of the forces, and the influences that can be applied to modify the strengths of the forces. Understanding these mechanisms allows prediction and modification of bulk particulate properties, and ultimately the improvement of the performance of particulate control devices.

3.2.1.1 Interparticle Forces

Forces that should be considered of influence in the regime of fly ash particles are listed in Table 3-1.

Table 3-1
Primary Interparticle Forces

Force	Effective range	Significant features
van der Waals	3 to 500 Å	very important because of the relatively long range of action; interparticle forces for particles of one micron diameter are four to six orders of magnitude greater than the gravitational force on the particles (Jayasinghe, 1972; Keller, 1973).
electrostatic (in the absence of an external electric field)	contact	quickly dissipated by grounded surfaces or humidity; greater than van der Waals forces only if particles exposed to corona charging (Visser, 1974); a small factor for particles 1 to 10 μm diameter unless $> 10^5$ charges are on particles (Keller, 1973)
ionic	≤ 2 lattice spacings	10 times stronger than van der Waals force, but charges quickly cancel at distance (Hobbel, 1988); initial layer(s) of adsorbed water may form hydrogen bonds that can contribute 99 % of the total adhesive force (van Oss, 1988)
adsorbed layers	<5 Å to contact	increases adhesion due to van der Waals forces by as much as 5 times up to several layers of adsorption (Visser, 1974); chemisorbed vapors are usually a monolayer thick, whereas physisorbed vapors, less tightly bound, can be many layers thick (Hench, 1971; Rietma, 1984)
capillary (liquid bridges)	contact	stronger than van der Waals forces, depending on tensile strength of the adsorbed film and the solid/liquid contact angle (Luckham, 1989); develop above a critical humidity (Coelho and Harnby, 1978)
solid bridges	contact	dissolving a water-soluble salt and then evaporating the water can leave a solid bond 10^4 times stronger than before the salt was dissolved (Williams and Nosker, 1983)

In the particle size regime of coal fly ash, van der Waals forces are generally considered the most fundamental of the interparticle forces. Other forces are usually subsidiary; that is, they become important after the van der Waals forces have attracted particles close enough together for the shorter-range forces to participate in the adhesion. At this point, the subsidiary forces may become dominant, as in the case of capillary forces, for example.

Particle size, shape, and surface roughness (traits that combine to describe particle morphology) govern the van der Waals forces. Since the distance over which these forces have significant influence is less than 0.05 μm, particle shape and the surface roughness have a large effect on the van der Waals forces. In fact, the intensity of the van der Waals force is proportional to the radii of curvature of surface asperities at the contact points (Donsi and Masimilla, 1974). Particle morphology combined with external forces applied to the particles (electrical or fluid dynamic forces) determine the number of contacts, or points of close proximity, each particle has with neighboring particles or surfaces. Adhesive forces increase with increasing proximate or contact area (Visser, 1974). Thus, decreasing particle size, particle sphericity, or particle surface smoothness will generally increase the strength of adhesive forces between particles.

Physical adsorption of gases is attributed to van der Waals forces and depends largely on particle morphology. Geometry of the particles near the contact point will promote adsorption and condensation of molecules from the gas phase (Hobbel, 1988). Adsorption will occur even when the concentration of gas molecules is far below the level for condensation. Physical adsorption can result in multiple layers of adsorbed molecules on the surface of particles. The adsorbed layers increase the area over which the interparticle forces are acting, effectively decrease the separation distance between particles, and, if extensive enough, can lead to the formation of liquid bridges between particles. Adsorbed layers may increase adhesion due to van der Waals forces by as much as a factor of five (Visser, 1974).

Only the first atomic layers on the surface of particles interact in van der Waals forces, so surface chemistry is important in determining adhesion (Lauga *et al*, 1991). However, compared to the morphology the chemical nature of the particle surface is of secondary importance for van der Waals forces (Luckham, 1989). The surface chemistry is a governing feature for some shorter-range forces. Work functions of materials, zeta potentials, and oxidation states are properties that can generate electrostatic and ionic bonds between particles.

Chemical properties of particle surfaces also affect the adsorption of gases (Fuller and Thompson, 1987). (This is, of course, the guiding principle in the development of specific sorbents to collect gaseous pollutants.) Chemical adsorption is usually limited to a monolayer, and creates stronger bonds than do physically adsorbed gases (Rietma, 1984). These strong chemical bonds normally involve ionic-covalent interactions (Hench, 1971), as is often the case with adsorbed water. The hydrogen-bonding component of interactions with adsorbed

water generally makes a far greater contribution to the adhesion than the change in van der Waals forces (van Oss and Good, 1988).

Adsorbed water is almost a universal factor in the interaction of particles, even in cases of very low relative humidities (Gillespie, 1987). Monolayer coverage of adsorbed water is reported to occur at 10 % relative humidity for most oxides (Fuller and Thompson, 1987). Adsorption of water is specifically pertinent in the case of fly ash under virtually all flue gas conditions (Rothenberg, 1980). The literature is extensive in its treatment of the effects of adsorbed water on interparticle adhesion. Water can be present in different forms: adsorbed monolayers or multilayers on particle surfaces, 'free' mobile water on the surface, physically adsorbed within pores in the particles, or strongly bound by chemisorption (Khan and Pilpel, 1986). The form of the water depends on the relative humidity of the gas, the morphology of the particles, the geometry of the contact points, and the surface chemistry of the particles. Hydrophilic particles provide binding sites all over the particle surface allowing the formation of a monolayer and then subsequent multilayers of water. Consequently, many particle-to-water bonds and water-to-water bonds can be formed on hydrophilic particles. For a hydrophobic particle surface there may be only a few sites suitable for water binding, which when saturated act as anchor points for adsorbed droplets (Buckton, 1990). Net adhesive force can vary by an order of magnitude depending on whether the particle surface is hydrophobic or hydrophilic (Leong *et al*, 1981). Agents can be applied to particles to alter the affinity of their surfaces to water, and thereby affect adhesion of water.

Adsorbed water will form liquid bridges between particles when the relative humidity (RH) exceeds some critical level for condensation to occur at contact points, reported to be between 65 and 80 % RH (Coelho and Harnby, 1978). A meniscus forms around the point of contact between particles, and surface tension of the liquid exerts a capillary force between the particles. The solid/liquid contact angle and the principle radii of curvature of the liquid bridge, together with the liquid surface tension, determine the magnitude of the capillary force, and depend on the surface chemistry. There is typically a peak in the adhesive force associated with adsorbed water near 90 % RH.

Drying surfaces after liquid bridges have been formed can leave residual solid bridges between particles. Any water-soluble salt can act as an adhesive in this way (Williams and Noker, 1983). Hydroxides of the alkali metals, abundant in fly ash and in FGD sorbents, are very soluble in water. Sulfur oxides are prevalent on the surface of fly ash particles and can yield salts upon reaction with water. Solid bridges are the strongest of interparticle bonds. Conventional particulate control devices typically operate in such a way as to systematically, or occasionally create liquid and consequential solid bridges between collected particles.

In summary, van der Waals forces, adsorption, and liquid and crystalline bridges all intimately depend upon the nature of the particle surface. The morphology of particles, their surface chemistry, and the adsorption of vapors (in particular, water vapor) determine the forces of

interaction among particles. The physical and chemical nature of the surfaces of fly ash particles is a primary determinant of the types of interactions that occur between fly ash particles, or between fly ash particles and conditioning agents. In the case of fly ash, the morphology and surface chemistry of the particles are generally a consequence of the chemical composition, preparation, and combustion of the coal. Adsorption of vapors onto the fly ash is dependent on the composition and temperature of the flue gas.

3.2.1.2 Chemical Characteristics of the Surfaces of Fly Ash Particles

The mineral core of ash particles is generally composed of an aluminosilicate glass along with the minerals quartz, mullite, hematite, and magnetite, although ashes from lignite and subbituminous coals tend to have more and different crystalline phases than these four mineral types (Buck *et al*, 1983). Because of the mechanisms involved in fly ash particle formation, the chemical environment on the surfaces of fly ash particles is relatively complex. Surface enrichment of many trace elements results in concentrations up to 75 times greater than those measured for bulk ash samples. Elements concentrated on the particle surface include As, Cd, Cu, Cr, Ga, Mo, Na, Ni, Pb, S, Sb, Se, Tl, and Zn (Klein *et al*, 1975; Davison *et al*, 1974). Natusch (1978) determined that an outer layer, 50 to 300 Å thick, is the region where the many different trace elements that are volatilized in the combustion process reside as sulfate salts on the fly ash particles. This layer is completely soluble in water, but accounts for only 2 to 3 % of the total weight of the ash.

In addition to the condensation of species on the surface of particles, vapors are adsorbed on the particle surfaces. Sulfur exists primarily as a surface layer a few nm thick on the mineral core (Mamane *et al*, 1986). The relative amounts of S and Ca indicate more S present than can be accounted for by $CaSO_4$. Some of the sulfur on the particle surface is the result of adsorption of SO_2, SO_3, or H_2SO_4 (Natusch, 1978; Kaufherr *et al*, 1985). Analyses show a correlation between the amounts of residual sulfur and calcium in dust cake ash (Bush *et al*, 1989). There is no such correlation for ash that does not have prolonged exposure to the flue gas. These results suggest that calcium and other alkalis on the fly ash surface can continue to combine with adsorbed sulfur oxides until the available alkali is completely reacted. Sulfur adsorbed in excess of this amount is then present on the surface in other forms. Time resolved surface leaching (TRSL) techniques demonstrated that surface sulfur is present exclusively in the +6 oxidation state. TRSL also suggests that, although Ca is distributed more or less uniformly throughout fly ash particles, it may be present in a different, more soluble form near the particle surface (Natusch *et al*, 1980). Ca and Mg are probably present as soluble oxides or hydroxides on the surfaces of fly ash particles (Tidy, 1986). Surface iron is primarily in the +3 oxidation state, although the iron distributed throughout the bulk of the fly ash particles has an oxidation number of +2.

Water is readily adsorbed on fly ash particles, and its presence may increase rates of adsorption and oxidation of SO_2 by several orders of magnitude over the rates associated with

a gas-solid reaction. Even at temperatures as high as 400 °F, appreciable amounts of water are still chemically adsorbed on the surface of ash particles. As the temperature of the gas surrounding the fly ash particles is reduced, multimolecular layers of water rapidly develop. As is the case with the micropores on many other adsorbates, the adsorption and desorption of water to or from the micropores on fly ash particles occurs very slowly, usually requiring more than a minute to equilibrate at typical flue gas temperatures (Rothenberg, 1980). The amount of water adsorbed on ash particles depends on the relative humidity, and also on the chemical makeup of the ash particles. Ashes high in silica and alumina are difficult to wet (Harker and Pimparker, 1988).

The mineral constituents and the condensation and adsorption of volatile species determine the surface chemistry of fly ash particles. We know, mainly from empirical correlations, that certain constituents of the ash surface chemistry are controlling factors in particulate control device performance. Key constituents on the surface include sulfur, alkali metals (calcium and sodium, in particular), and water.

3.2.2 Implications for Particulate Collection

The synergism between the inherent properties of fly ash particles and the flue gas environment determines the resistivity and cohesivity of the bulk ash collected in ESPs and fabric filters. These two bulk properties are determinants of the performance of the particulate control devices.

Modifications to the inherent properties of the particles generally requires the addition of material into the furnace with the coal, changes in the fineness of the coal injected into the burners, or alteration of the combustion temperature/residence time history of the particles. Some particulate additives have been injected into furnaces or upstream of particulate control devices to affect the bulk properties of the collected material. Sodium sulfate is added to coal having low sodium content to provide an enriched sodium concentration on the surface of fly ash particles. Sodium ions serve as the principal charge carriers in fly ash at elevated temperatures (Bickelhaupt *et al*, 1984). In ESPs operated at 700 to 800 °F these charge carriers can become depleted in the layer of ash contiguous with the collecting electrode because of the high mobility of the sodium ions at these temperatures. The addition of sodium to the ash provides sufficient charge carriers to keep the ash resistivity from becoming so high as to degrade ESP performance.

There has been little use of particulate additives to improve fabric filter performance. Several products are offered for use as "precoat" materials: they are to be applied to new bags to provide a protective filtering dust cake. Aluminum silicate, diatomaceous earth, limestone, and coal ash are the most common materials used for this purpose. Limited tests have shown that precoating bags can improve fabric filter performance (Snyder *et al*, 1990; Carr *et al*, 1991; Merritt *et al*, 1991). Particles can also be added continuously to the gas stream to

modify the filtration performance of the fly ash. Fine particles can be added in concentrations as low as 0.1 % by weight to ash to reduce the cohesivity of fly ash (Snyder *et al*, 1990). These particulate additives primarily decrease van der Waals forces by increasing the ash particle separation distances and contact area.

Though primarily a function of the coal chemistry, the flue gas environment offers the best opportunity to affect the particle properties and interparticle forces through adsorption on particle surfaces. Altering the flue gas environment through gaseous additives is a common technique to improve ESP performance. Resistivity of fly ash is controlled by the characteristics of the surfaces of the ash particles at temperatures below 400 to 450 °F. Since surface chemistry controls ash resistivity, the physical and chemical processes that control the nature of the particle surfaces and their surrounding environment ultimately determine ESP performance. Alkali metal ions, which serve as charge carriers, are mobilized on the glassy surfaces of fly ash particles by water and acid (Bickelhaupt, 1975). As SO_3, H_2SO_4, NH_2SO_2OH, or NH_3 are adsorbed onto ash particles in increasing amounts, the resistivity drops until the surfaces of the particles are effectively saturated with the adsorbed compound, at which point resistivity remains constant with additional adsorption of conditioning compound. Higher particle surface area and lower temperature, both factors that influence adsorption, result in lower resistivity. Bickelhaupt (1975) suggests that the relationship between resistivity and temperature may result from more water molecules being present on a given amount of surface area at lower temperatures. Adsorption of water can be limited by the surface chemistry of the ash (high silica and alumina content, for example), which can limit the effectiveness of water conditioning for resistivity reduction.

Modifying the flue gas environment has also been demonstrated to change the cohesivity of ash. NH_3 alone or in conjunction with SO_3 injected into the flue gases entering ESPs diminish rapping emissions (Dalmon and Tidy, 1972; Dismukes, 1975). This effect is attributed to an increase in the cohesiveness of the ash collected on the grounded plates in the ESP. Solid bridges, postulated to be ammonium sulfate, have been observed between particles that were exposed to NH_3 injection. Ash cohesivity has been altered in tests of NH_3 and SO_3 injection into flue gases entering fabric filters. Felix *et al* (1986) and Miller and Laudal (1987) reported significant improvement in particle collection as a result of the changes in ash cohesivity caused by NH_3 and SO_3. The mechanism by which these chemicals alter ash cohesivity has been postulated to be sequential adsorption of the gases on the particle surfaces, creating liquid bridges of ammonium bisulfate between particles that can become solid bridges of ammonium sulfate, given adequate concentrations of reactants and sufficient reaction time (Snyder *et al*, 1990).

The addition of water to the flue gas has been demonstrated to reduce pressure drop in fabric filters (Ariman and Helfritch, 1977; Snyder *et al*, 1990). The pressure drop is reduced because the dust cake formed by the ash has a higher porosity, resulting from a higher ash cohesivity. Increasing the humidity of the flue gas increases the amount of adsorbed water on

the particles. Increased van der Waals forces, hydrogen-bonding of adsorbed water on neighboring particles, capillary forces due to liquid bridges, and formation of solid bridges from the dissolution of surface salts may all result from the increased surface water. These changes in interparticle forces increase the adhesion of particles and the bulk ash cohesivity.

Other types of flue gas additives to alter interparticle adhesion were also identified in our literature review. Since adsorbed water is a critical component of the particle surface, injecting agents to moderate the particle's affinity to water should change the bulk particulate properties. Silanizing agents and other hydrophobic agents (for example, certain carboxylic acids such as stearic acid) can inhibit or even preclude the formation of liquid bridges (Karra and Fuerstenau, 1977), which would lower particulate cohesivity. Surfactants such as lignosulfonate have been used to decrease particle adhesion by decreasing the surface tension of water, and thus weakening the liquid bridges between particles. Trials of anionic and cationic surfactants have been suggested for this purpose (Snyder *et al*, 1990). Deliquescent materials, with their high affinity for water, can promote adsorption and the consequential formation of liquid bridges with their capillary forces. This action would increase particulate cohesivity.

4 LABORATORY ANALYSES

In our Topical Reports and in the summaries in the preceding section, we emphasized the roles adsorbed water can have in controlling bulk properties of powders. The experiments we performed in the laboratory were primarily designed to define the extent to which water affects key properties of ashes, powders, and mixtures of sorbents and ashes. In order to assess these effects, we assembled a broad variety of ashes and powders. Our objective in assembling these samples and analyses was to execute a matrix of tests that could independently examine, to the extent possible, the effects that particle morphology and ash chemistry have on the adsorption of water and its resultant effects. We also collected ash samples from field installations where various flue gas conditioning processes were being utilized, potentially affecting the characteristics of the ash and the performance of the baghouse or ESP collecting the conditioned ash.

4.1 DATA BASE OF ASHES AND POWDERS

Table 4-1 provides a brief description of the samples of ashes, powders, and mixtures of sorbents and ashes that we assembled for these laboratory analyses.

Table 4-1
Identification of Samples

	ID #	Description of Sample
base line	2870	Muskingum base line ESP hopper ash
	2871	Duct Injection Test Facility (DITF) dry $Ca(OH)_2$ injection
ashes and	2872	DITF $Ca(OH)_2$ slurry injection
	2873	DITF $Ca(OH)_2$ slurry injection with $CaCl_2$ addition
mixtures of	2884	Kintigh base line ESP hopper ash
	2885	spray dryer ash (High Sulfur Test Center)
sorbents and	2883	Edgewater furnace $Ca(OH)_2$ injection
	2890	ADVACATE injection
ashes	2907	Yorktown furnace injection of lignosulfonate-modified lime
	2029	Monticello dust cake ash
dust cake	2101	Scholz dust cake ash
	2515	Harrington dust cake ash
ashes	1994	AFBC dust cake ash

Table 4-1 (continued)

	ID #	Description of Sample
powders	3063	ultrafine silicon dioxide powder
	3064	ultrafine silicon dioxide powder
	3065	ultrafine silicon dioxide powder
	1856	glass beads
	2769	diatomaceous earth
	2874	alumina powder
	3238	aluminosilicate powder
leached dust cake ashes	2029-W	leached Monticello dust cake ash (first set)
	2101-W	leached Scholz dust cake ash (first set)
	2515-W	leached Harrington dust cake ash (first set)
	1994-W	leached AFBC dust cake ash (first set)
	2029-L	leached Monticello dust cake ash (second set)
	2101-L	leached Scholz dust cake ash (second set)
	2515-L	leached Harrington dust cake ash (second set)
	1994-L	leached AFBC dust cake ash (second set)
ashes and powders conditioned with organo-siloxane	2029-L-S	leached Monticello dust cake ash, conditioned with organosiloxane
	2101-L-S	leached Scholz dust cake ash, conditioned with organosiloxane
	2515-L-S	leached Harrington dust cake ash, conditioned with organosiloxane
	1994-L-S	leached AFBC dust cake ash, conditioned with organosiloxane
	1856-S	glass beads, conditioned with organosiloxane
	2769-S	aluminosilicate powder, conditioned with organosiloxane
	2874-S	diatomaceous earth, conditioned with organosiloxane
	3238-S	alumina powder, conditioned with organosiloxane
ashes and powders conditioned with SO_3	2029-A	Monticello dust cake ash, conditioned with SO_3
	2101-A	Scholz dust cake ash, conditioned with SO_3
	2515-A	Harrington dust cake ash, conditioned with SO_3
	1994-A	AFBC dust cake ash, conditioned with SO_3
	1856-A	glass beads, conditioned with SO_3
	2769-A	aluminosilicate powder, conditioned with SO_3
	2874-A	diatomaceous earth, conditioned with SO_3
	3238-A	alumina powder, conditioned with SO_3
	2029-L-A	leached Monticello dust cake ash, conditioned with SO_3
	2101-L-A	leached Scholz dust cake ash, conditioned with SO_3
	2515-L-A	leached Harrington dust cake ash, conditioned with SO_3
	1994-L-A	leached AFBC dust cake ash, conditioned with SO_3
pilot-scale tests	4058	ESP plate ash January 1994 (second pilot-scale test)
	4118	baghouse hopper ash November 1994 (third pilot-scale test)

We selected the first set of samples listed in Table 4-1 (base line ashes and mixtures of sorbents and ashes) because of their characteristics and operating histories. Analyses of these mixtures allowed us to quantify increases in surface area, changes in particle morphology, and increases in cohesivity that result when sorbents are mixed with ashes. These analyses demonstrated the importance of both particle morphology and chemistry in determining their behavior. We identified those sorbents that should represent the extremes of important physical characteristics (size and surface area) and sorbent injection applications that are widely used or have a high potential for wide application. Among the samples from low-temperature sorbent injection applications, the primary characteristics that were expected to determine the ease of final particle collection included particle size, degree of agglomeration, amount and distribution of surface area, and special chemical additives.

We obtained samples from three types of tests performed at the U.S. Department of Energy (DOE) Duct Injection Test Facility (DITF) at the Muskingum Plant of Ohio Edison in Beverly, OH. Sorbent and ash mixtures from $Ca(OH)_2$ slurry injection tests, injection tests of dry $Ca(OH)_2$ (coplanar with water spray), and $Ca(OH)_2$ slurry injection tests performed with $CaCl_2$ additive were obtained from the stockpile of samples generated under Contract DE-AC22-88PC88851. As would be expected with the addition of a deliquescent salt, addition of $CaCl_2$ to the slurry injected at the DITF apparently caused a high potential for water adsorption. Gas phase utilization of the sorbent increased as increasing amounts of $CaCl_2$ were added to the slurry. (Similar results have been observed in other tests of $CaCl_2$ addition.) We believe the $CaCl_2$ increases the partial pressure of water around the sorbent particle, thereby promoting SO_2 capture. In order to compare the characteristics and behavior of these three samples with unmodified ash from this plant, we also obtained base line (unconditioned) fly ash from the ESP hoppers at the Muskingum Plant.

Other samples in the first set included base line ESP hopper ash from Plant Kintigh in Somerset, NY, and ash from the spray dryer facility that is part of the EPRI High Sulfur Test Center (HSTC) located at this plant. We also obtained a sample of ash from the injection of recycled ADVACATE material from tests conducted at Southern Research Institute's CCF. The sample was collected from the hopper of the pulse-jet baghouse serving the CCF. The last ash sample in this first set was generated from the furnace injection of lignosulfonate-modified lime at the Yorktown plant (ID # 2907). This sample was collected from the Unit #2 inlet field ESP hopper.

We selected dust cake ashes from Gulf Power Company's Plant Scholz, Texas Utilities' Monticello Station, Southwestern Public Services Company's Harrington Station, and the 20 MW AFBC pilot facility located at TVA's Shawnee Generating Station. The first three pulverized-coal ash samples represent a variety of coal types, particle morphologies, and ash chemistries. Although the chemical composition of these samples is discussed in more detail

later in Section 4, the following table summarizes some of the primary differences between these samples.

Table 4-2
Chemical Differences Between the Dust Cake Ashes

Source	acid/alkali	Ca concentration	SO_3, soluble $SO_4^=$
Monticello	alkali	high	low
Scholz	acid	low	medium
Harrington	alkali	high	medium
AFBC	alkali	high	high

We included an array of powders in our laboratory analyses to refine our techniques for discriminating the effects of particulate chemistry and morphology. ID #'s 3063, 3064, and 3065 are commercially-produced, ultrafine, fumed silicon dioxide (98 % silica) powders. Glass beads used for pavement marking were also included in our studies because of their simple spherical shapes and relatively simple chemical composition. Sample ID # 2769 is a naturally occurring diatomaceous earth that is about 91 % silica. We also included an alumina powder because of its nearly pure chemical makeup (99.9 % Al_2O_3). The aluminosilicate powder we tested (ID # 3238) is a commercial product manufactured and marketed for precoating filter bags. It was added to our analyses because of its relatively simple chemistry and its shard-like particle shapes.

All but the last two of the remaining samples listed in Table 4-1 were derived from the dust cake ashes or powders described above. The procedures used to generate these samples are discussed later in this section. The last two samples listed in Table 4-1 were generated during our proof-of-concept tests performed at the Southern Research Institute CCF, and are discussed in Section 5.

4.2 ANALYTICAL METHODS

Throughout this project, we have used a variety of standard and customized analyses to characterize the ashes and powders described above. The tests we performed on these samples included measurements of size distribution, specific surface area, uncompacted bulk porosity, particle density, tensile strength, resistivity, specific gas flow resistance, and drag equivalent diameter. We also examined the morphology of many of the samples with a Scanning Electron Microscope (SEM) and performed mineral analyses and selected other chemical analyses on most of the samples in our data base. The procedures we used for many of the analyses we performed, and the significance of the type of results we obtained, are discussed in more detail in Appendix B.

4.3 RESULTS OF LABORATORY ANALYSES

The data we gathered in the laboratory are summarized and discussed below according to the type of analysis we performed. (In some of the tables summarizing these data, some data may be included for leached dust cake ash samples, dust cake ash and powder samples conditioned with organosiloxane or SO_3, and samples generated in our pilot-scale tests. The reader is instructed to refer back to these tables when these samples are discussed near the end of Section 4.) Overall conclusions from the laboratory research are presented in Section 7 in combination with conclusions drawn from our pilot-scale tests.

4.3.1 Morphology

The size and shape of the particles in a powder often control many of its bulk attributes. In order to assess the morphology of the ash and powder particles in our data base, we measured bulk characteristics such as particle density, specific surface area, and permeability. We also measured particle size distributions and examined the appearance of the ash and powder particles with an SEM. Table 4-3 summarizes the particle densities and specific surface areas we measured, as well as mass median diameters (MMD) data obtained from our measurements of the size distributions of the samples in our data base. Appendix C contains detailed size distributions measured for these samples. The permeabilities we measured for the samples in our data base are presented in Table 4-4. Figures 4-1 through 4-14 show SEM photographs of most of these samples.

Table 4-3
Physical Characteristics of Ash and Powder Samples

ID #	Stokes' MMD, μm	Particle density, g/m^3	Specific surface area, m^2/g
2870	14	2.56	0.62
2871	6.7	2.47	5.2
2872	6.9	2.52	7.5
2873	5.7	2.51	6.0
2884	22	2.47	1.1
2885	9.8	2.53	10.7
2883	11	2.59	4.2
2890	9.4	2.45	15.1
2907	--	--	5.2
2029	4.6	2.47	0.98
2101	8.9	2.44	3.00
2515	5.7	2.66	1.5
1994	2.7	2.65	20.9
1856	24	2.43	0.19
3063	--	--	100
3064	--	--	200
3065	--	--	380
2769	13	2.2	1.4
2874	36	3.9	0.85
3238	13	2.3	1.4
2029-W	--	2.47	1.6
2101-W	--	2.52	8.3
2515-W	--	2.59	7.1
1994-W	--	2.70	18.4
2029-L-S	--	--	0.8
2101-L-S	--	--	3.4
2515-L-S	--	--	10.1
1994-L-S	--	--	13.9
1856-S	--	--	0.1
2769-S	--	--	1.0
2874-S	--	--	0.9
3238-S	--	--	0.4
4058	7.7	2.29	--
4118	7.7	2.66	--

-- not measured

Table 4-4
Permeability Data Measured for Ash and Powder Samples

ID #	Estimated dust cake porosity*, %	Drag-equivalent diameter, μm	Specific gas flow resistance, in. H_2O·min·ft/lb
2029	67	3.46	3.3
2101	76	2.62	2.1
2515	76	2.32	2.5
1994	83	0.69	13
2029-L	64	3.31	4.9
2101-L	72	2.35	4.1
2515-L	79	1.66	3.5
2769	93	1.16	1.4
3238	95	0.90	1.7
4118	74	2.44	2.8

* based on uncompacted bulk porosity measurements, discussed in Section 4.3.4.1.

When compared to the corresponding data for the base line ashes from Muskingum and Kintigh, the surface areas and MMDs for the mixtures of ashes and sorbents show that the addition of sorbent material to fly ashes results in mixtures of particles with finer size distributions and higher overall specific surface areas. The SEM photographs of these base line ashes and the mixtures of sorbents and ashes illustrate the effects that sorbent addition has on particle appearance. Like almost all other pulverized-coal fly ash particles, the base line ash particles from Plant Kintigh and the Muskingum Plant are generally spherical, with relatively smooth surfaces. When sorbent is added, the particles in the resultant mixture clearly show how the addition of sorbent decreases mean size and sphericity.
These data agree with the information we obtained in our literature review (Dahlin *et al*, 1992).

The high specific surface area of ID # 2907 illustrates the effect of lignosulfonate-modified lime injection on the bulk morphology of the resultant mixture of sorbent and ash. This result also agrees with the information reported by Dahlin *et al* (1992). SEM pictures of the ADVACATE injection ash show that, as with the other mixtures of sorbents and ashes, this sample apparently contains a mixture of relatively smooth, spherical ash particles and irregularly-shaped sorbent particles.

The surface area and sizing measurements performed on the dust cake ashes demonstrate the effects of coal type on ash particle morphology. Monticello ash particles (ID # 2029), which are derived from the combustion of lignite, closely resemble smooth spheres. The Harrington ash particles, derived from the combustion of a subbituminous Powder River Basin coal, are also spherical, with somewhat rougher surfaces than the Monticello ash particles. The Scholz ash particles are derived from the combustion of high-sulfur bituminous coal. Their surfaces

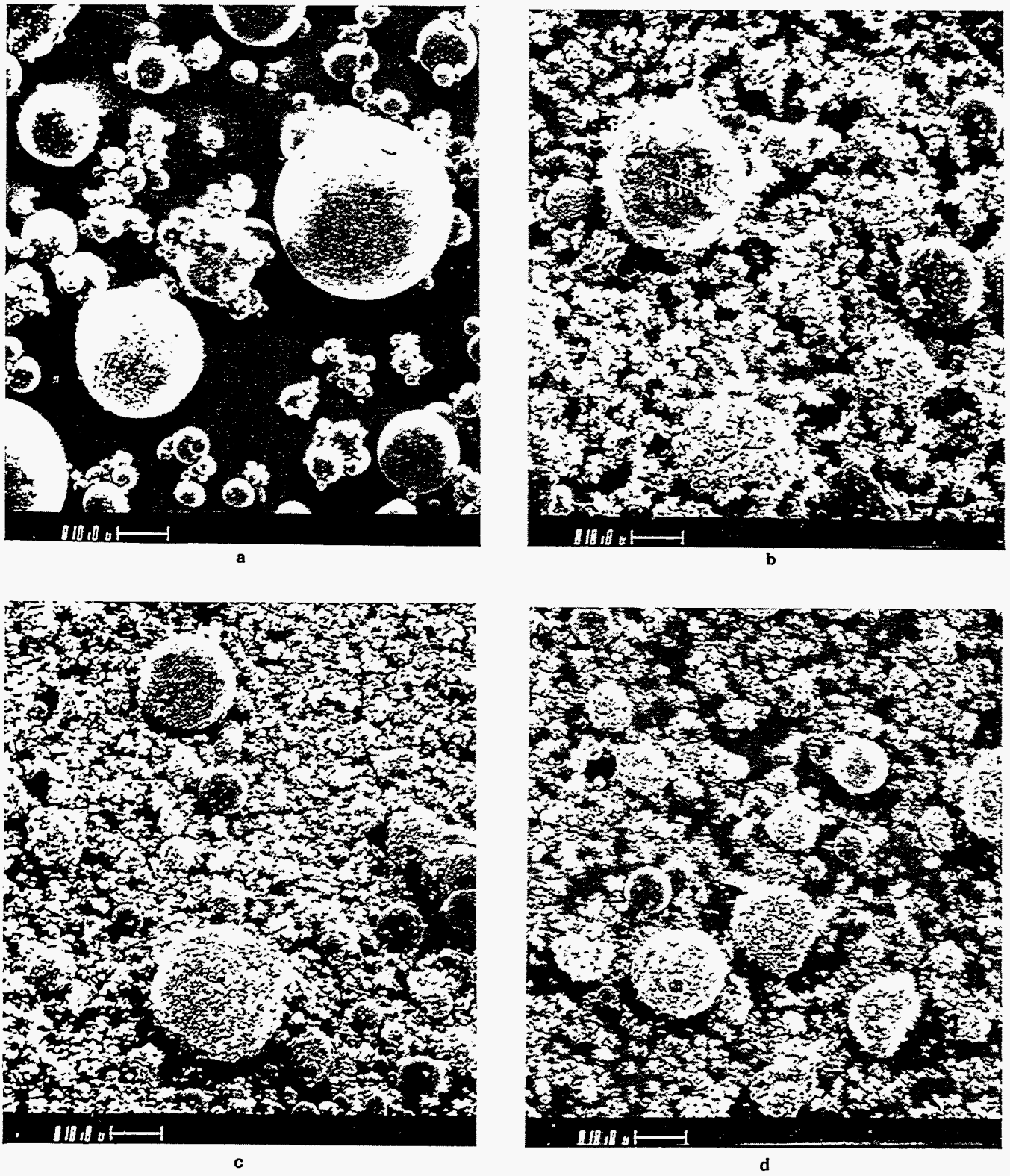

Figure 4-1. SEM photographs of a) Muskingum base line ESP hopper ash (ID # 2870), b) DITF dry $Ca(OH)_2$ injection ash (ID # 2871), c) DITF $Ca(OH)_2$ slurry injection ash (ID # 2872), and d) DITF $Ca(OH)_2$ slurry injection with $CaCl_2$ addition ash (ID # 2873) taken at a magnification of 1000X.

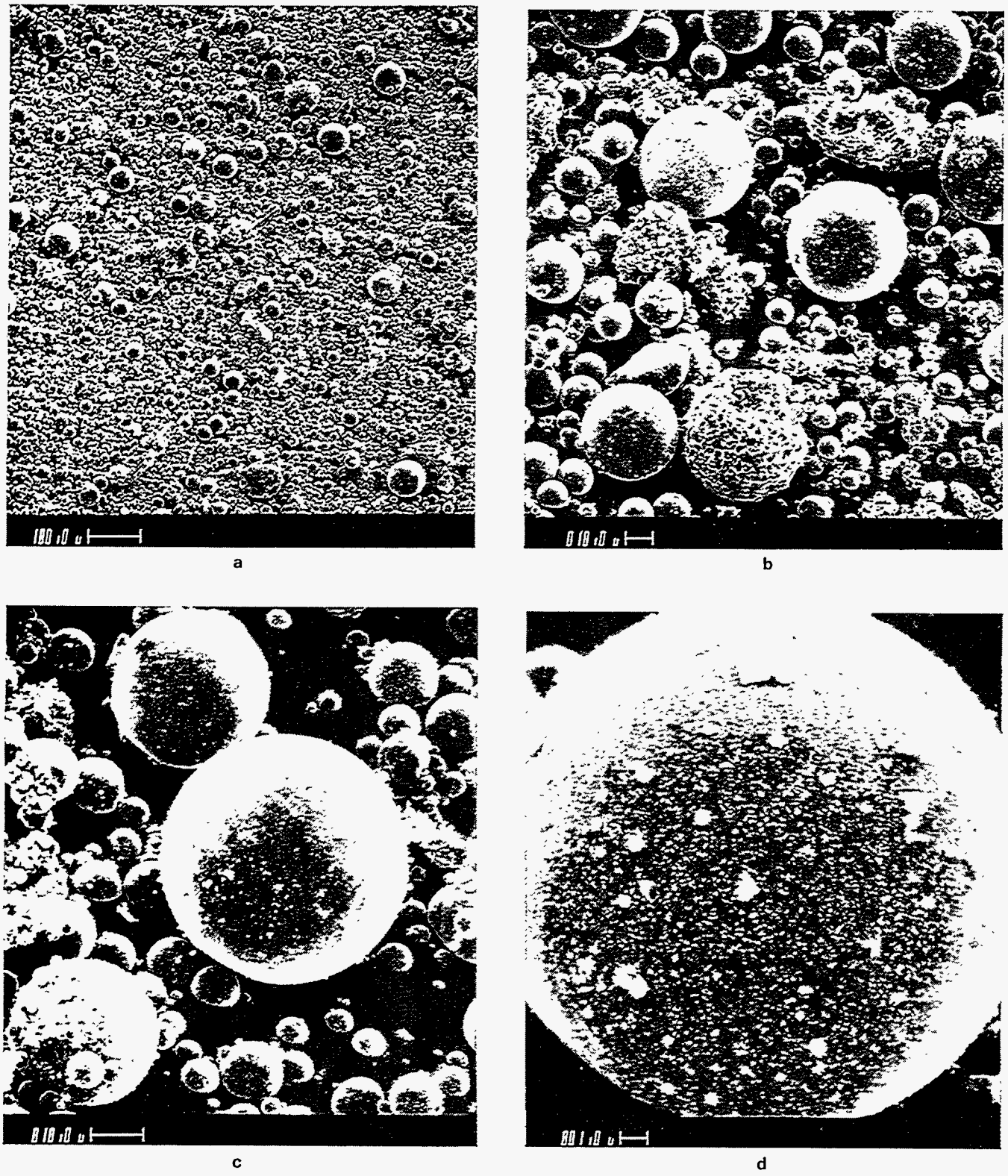

Figure 4-2. SEM photographs of Plant Kintigh base line ESP hopper ash (ID # 2884) taken at magnifications of a) 100X, b) 500X, c) 1000X, and d) 5000X.

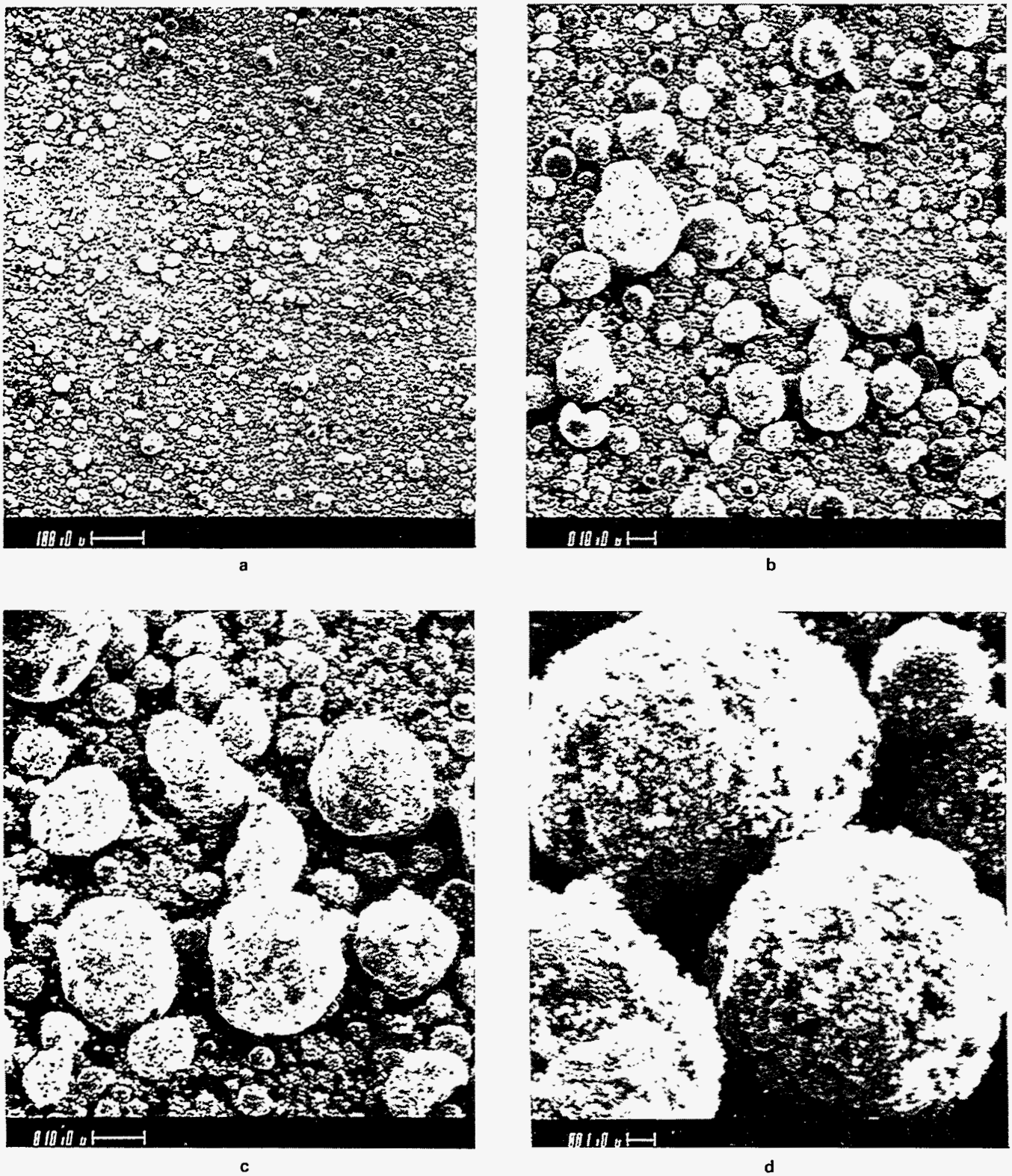

Figure 4-3. SEM photographs of the sorbent and ash mixture produced in the conventional spray dryer located at the High Sulfur Test Center (ID # 2885) taken at magnifications of a) 100X, b) 500X, c) 1000X, and d) 5000X.

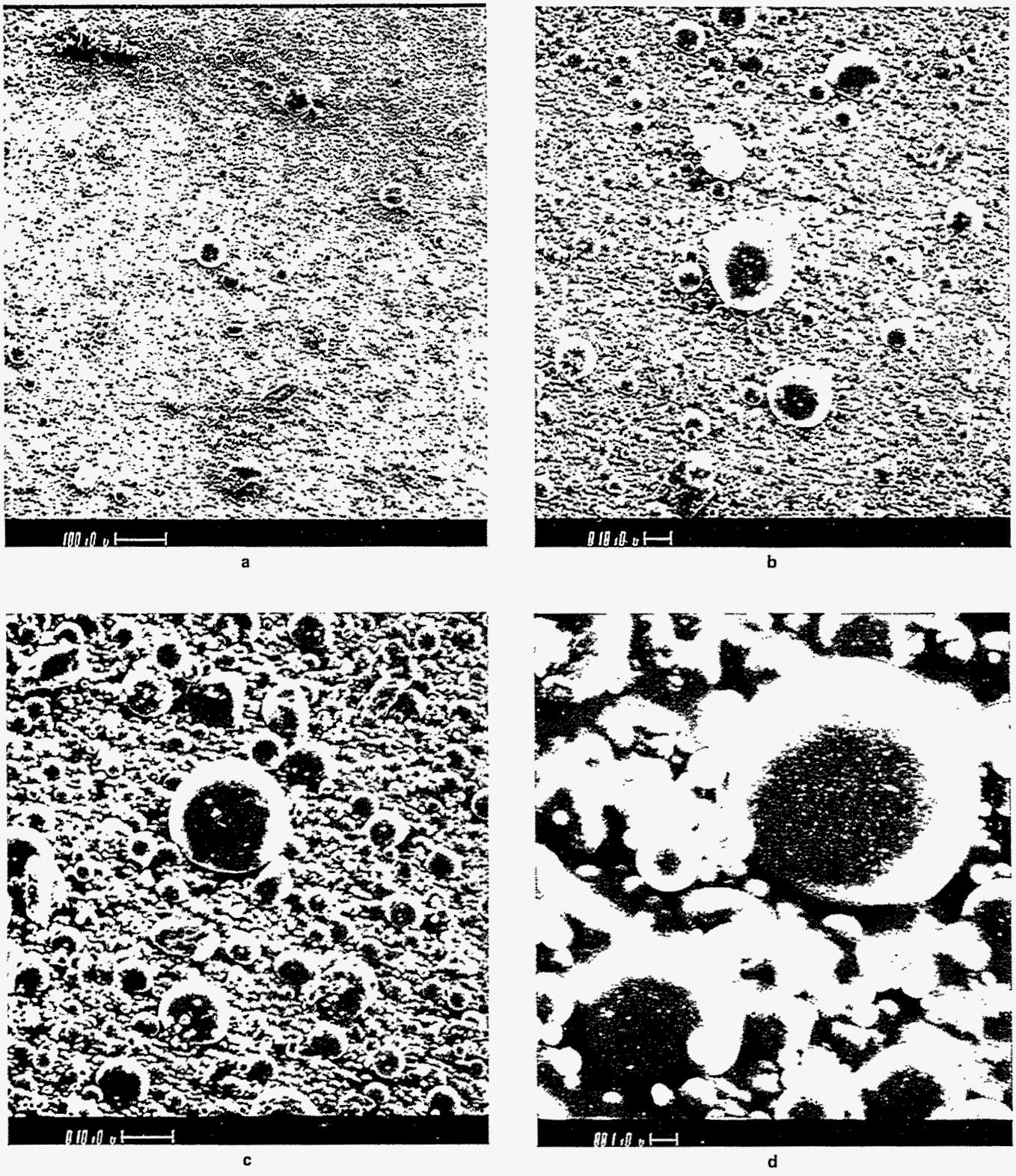

Figure 4-4. SEM photographs of Monticello dust cake ash (ID # 2029) taken at magnifications of a) 100X, b) 500X, c) 1000X, and d) 5000X.

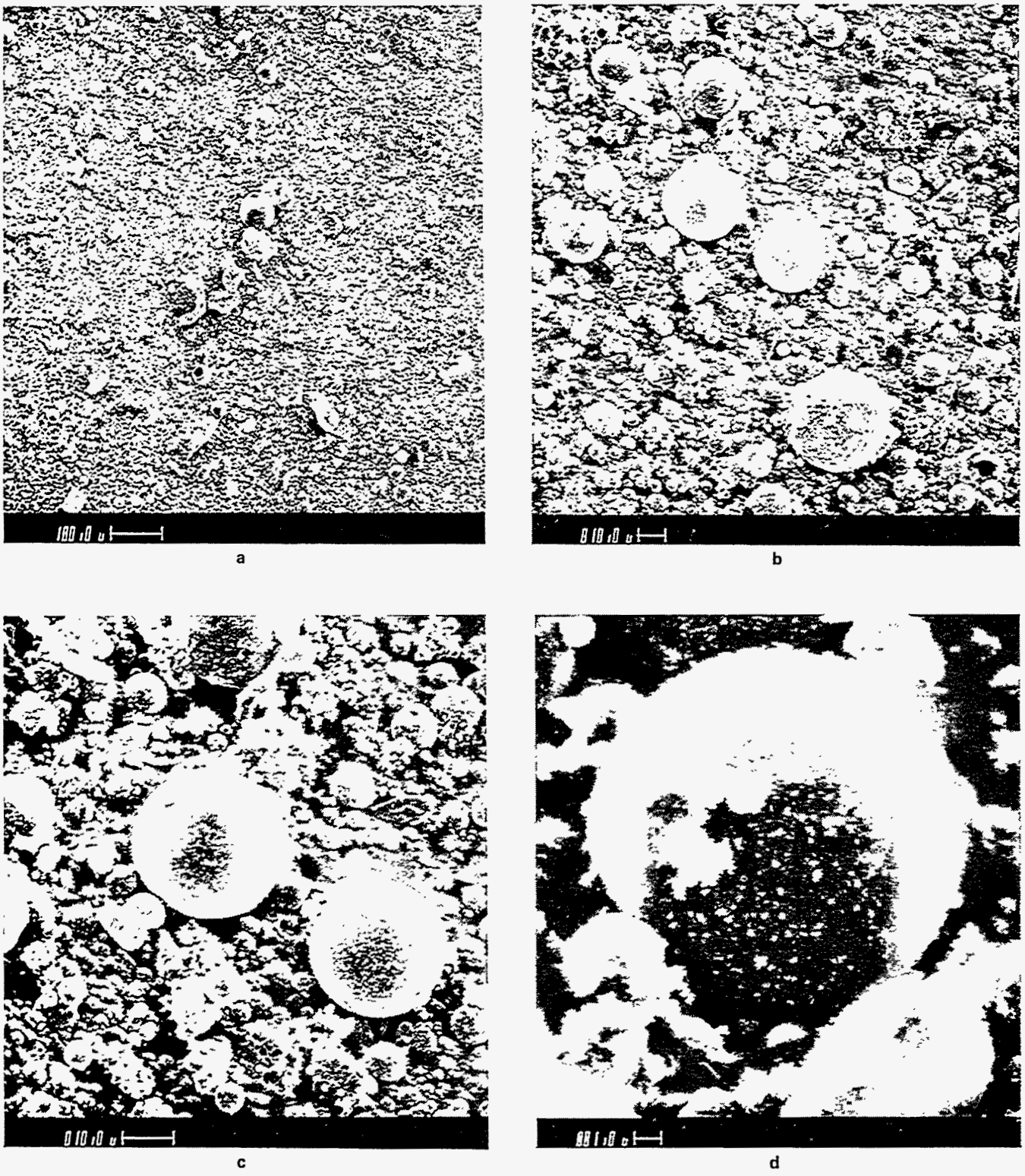

Figure 4-5. SEM photographs of Scholz dust cake ash (ID # 2101) taken at magnifications of a) 100X, b) 500X, c) 1000X, and d) 5000X.

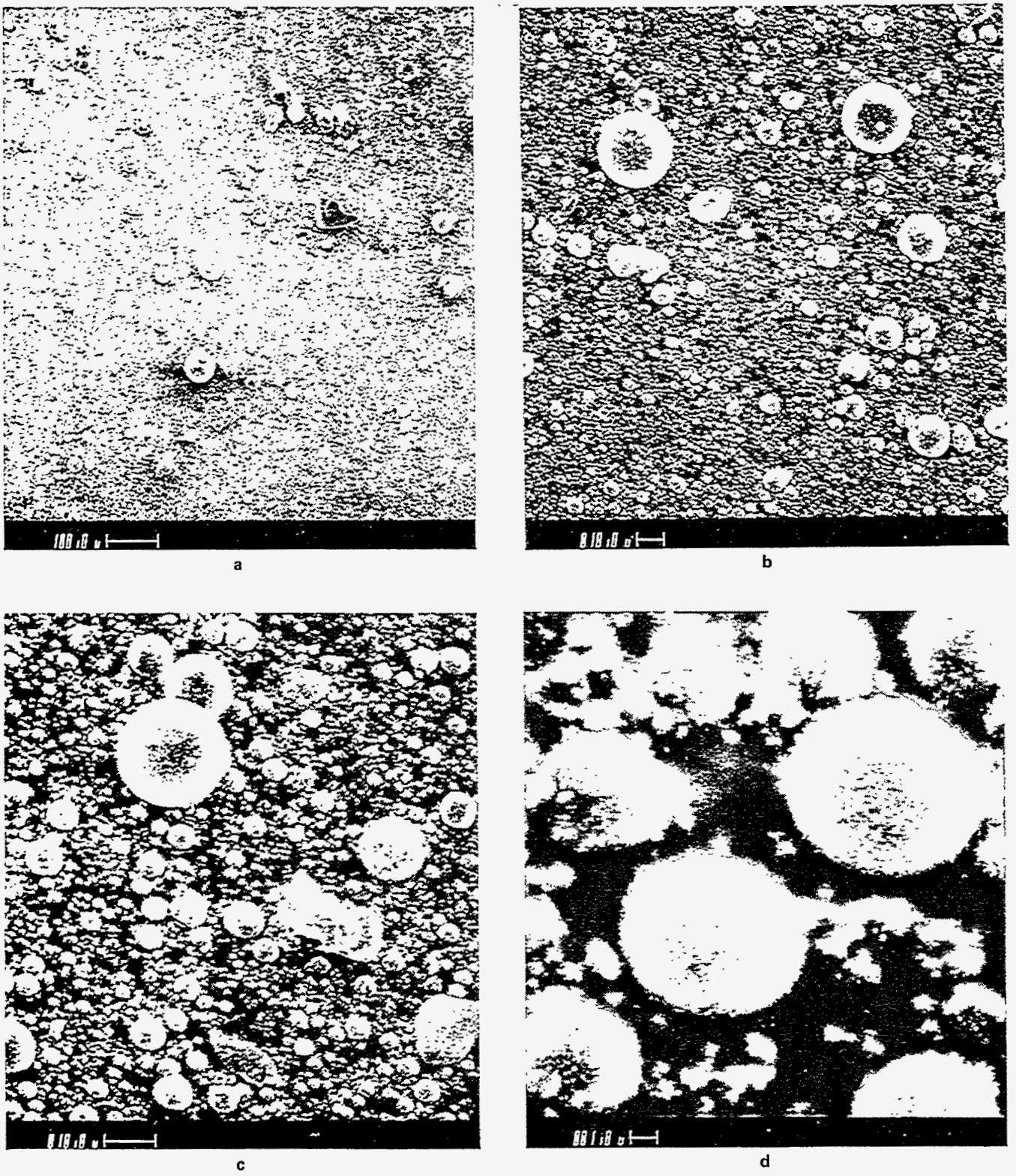

Figure 4-6. SEM photographs of Harrington dust cake ash (ID # 2515) taken at magnifications of a) 100X, b) 500X, c) 1000X, and d) 5000X.

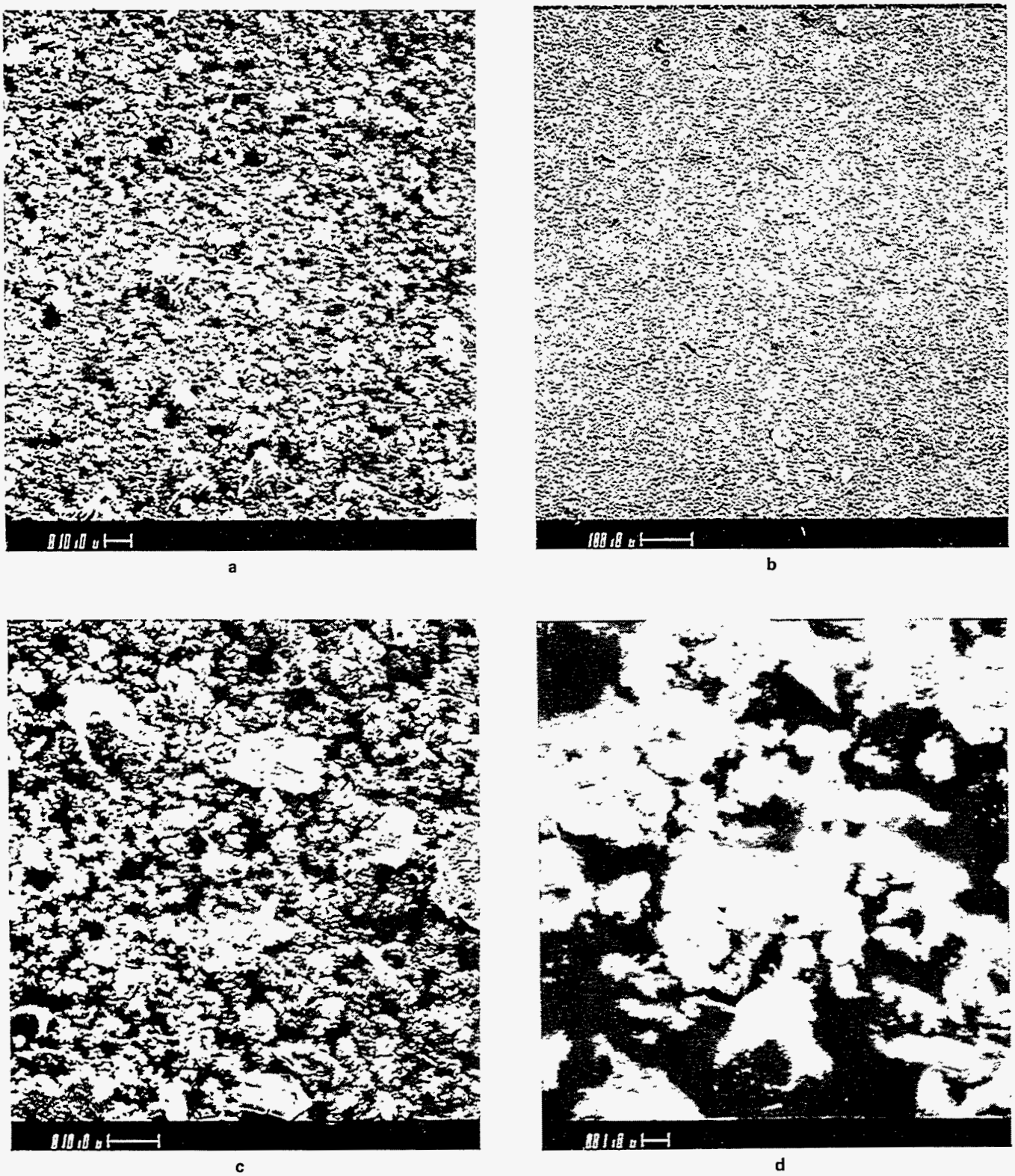

Figure 4-7. SEM photographs of AFBC dust cake ash (ID # 1994) taken at magnifications of a) 100X, b) 500X, c) 1000X, and d) 5000X.

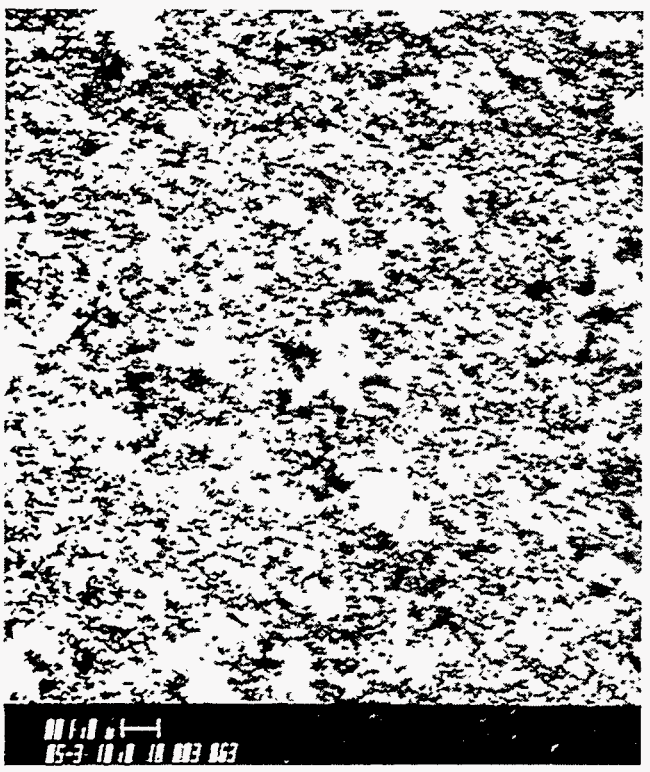

(a)

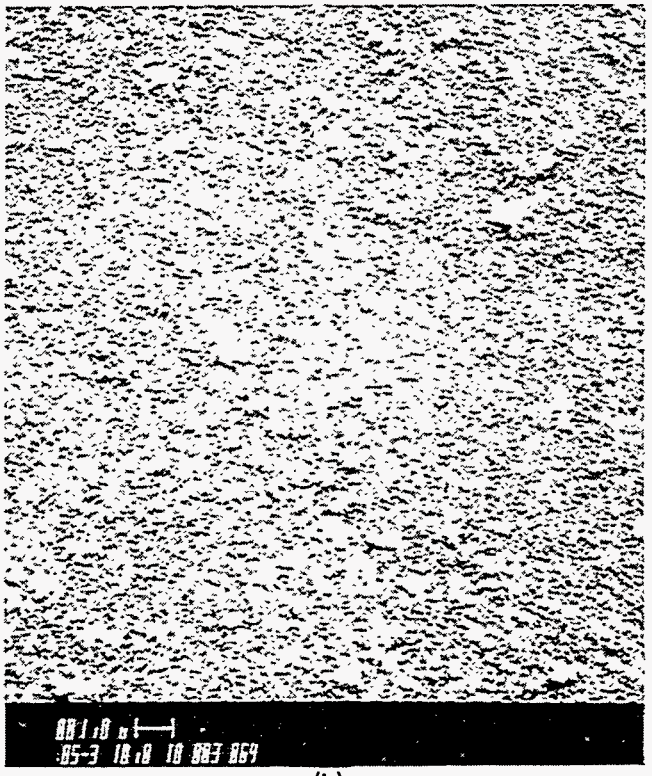

(b)

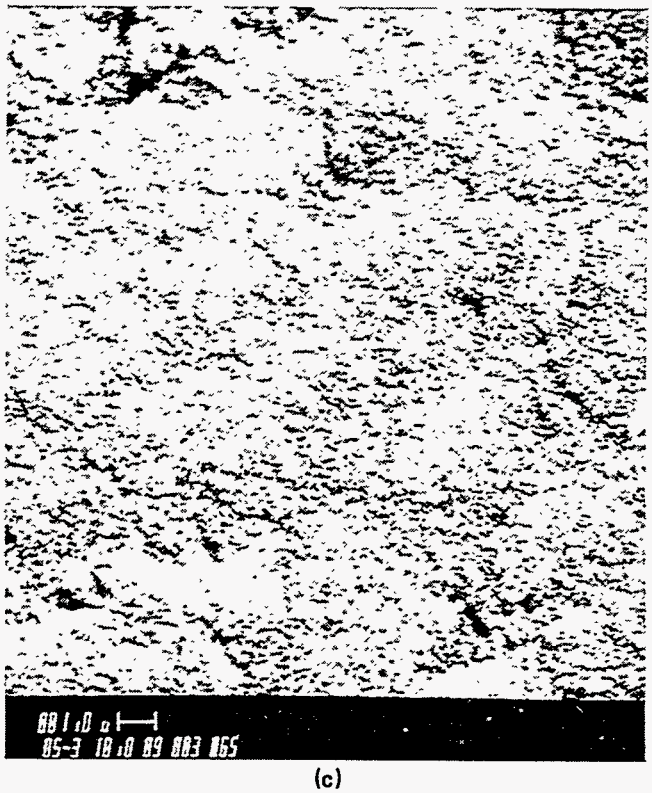

(c)

Figure 4-8. SEM photographs of the ultrafine silicon dioxide powders: a) ID # 3063, b) ID # 3064, and c) ID # 3065, taken at a magnification of 5000X.

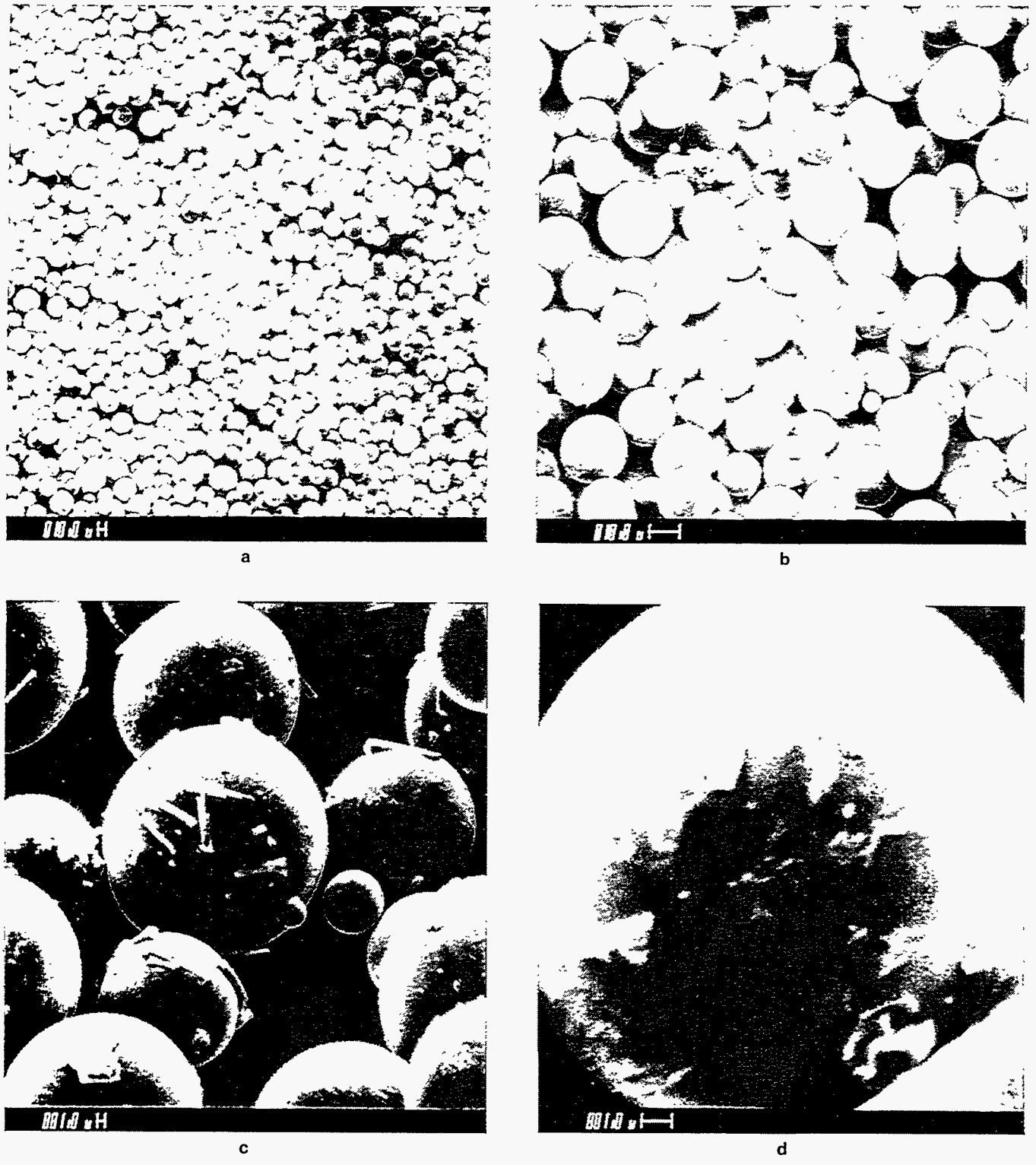

Figure 4-9. SEM photographs of glass beads (ID # 1856) taken at magnifications of a) 100X, b) 500X, c) 1000X, and d) 5000X.

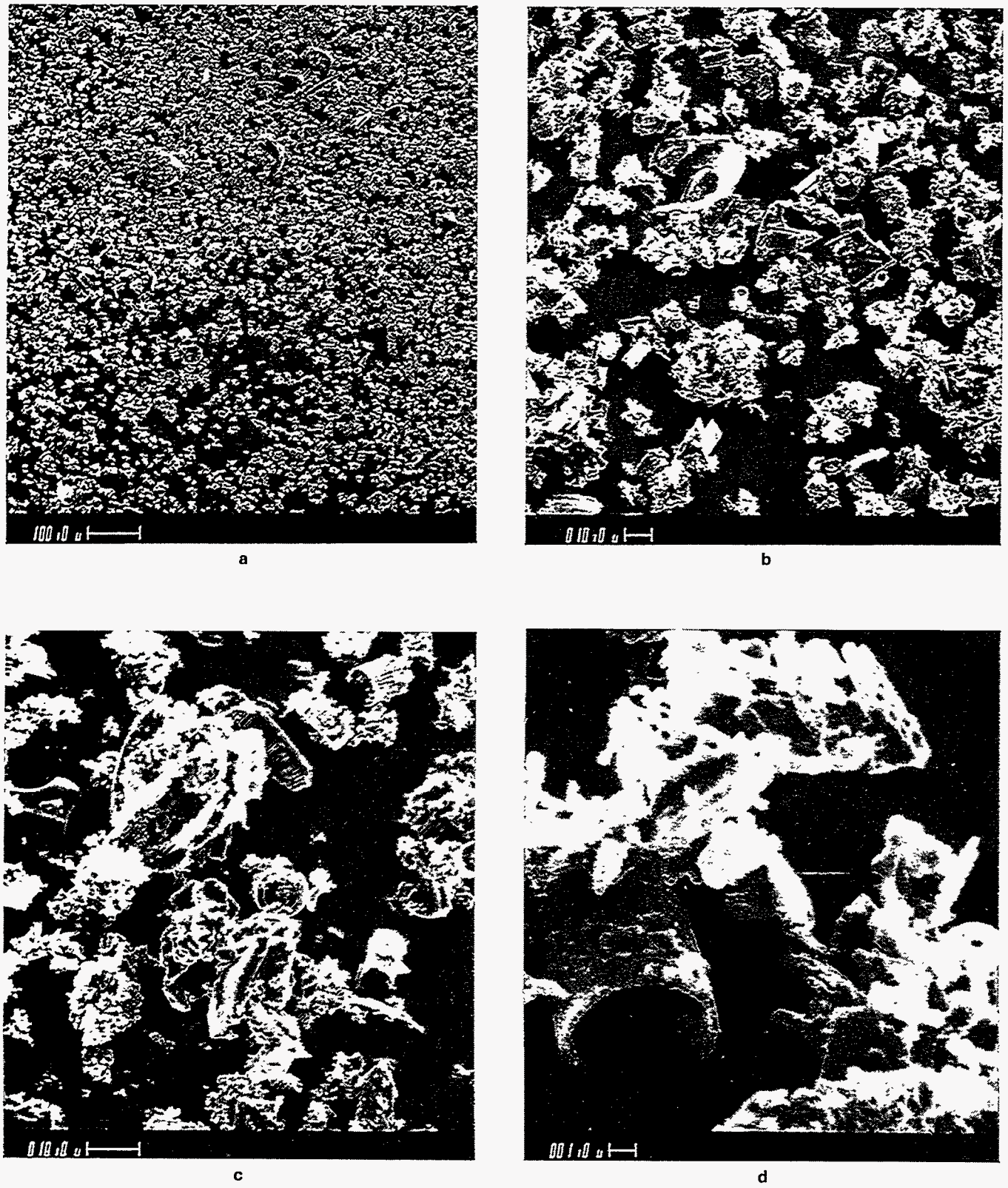

Figure 4-10. SEM photographs of diatomaceous earth (ID # 2769) taken at magnifications of a) 100X, b) 500X, c) 1000X, and d) 5000X.

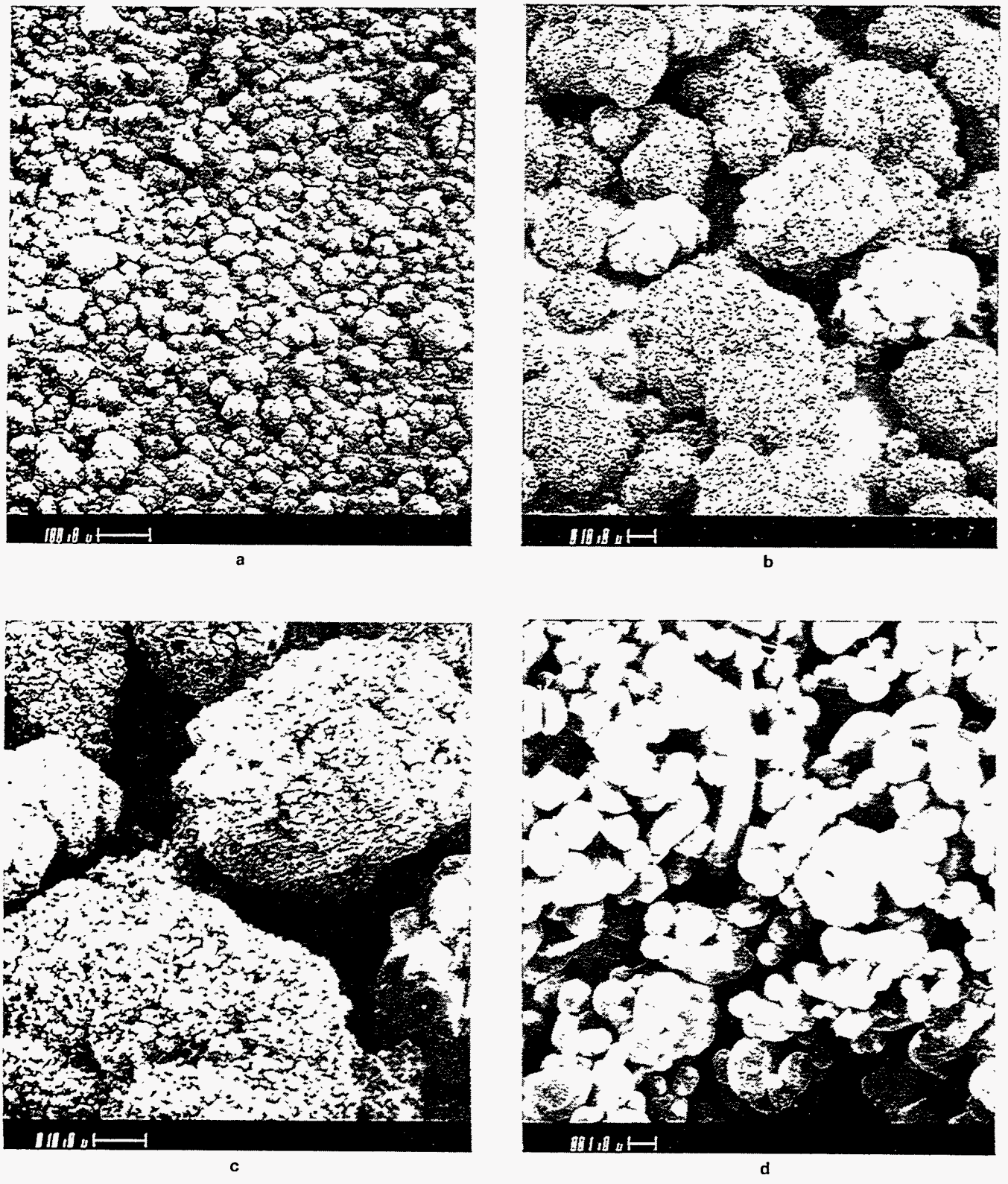

Figure 4-11. SEM photographs of alumina powder (ID # 2874) taken at magnifications of a) 100X, b) 500X, c) 1000X, and d) 5000X.

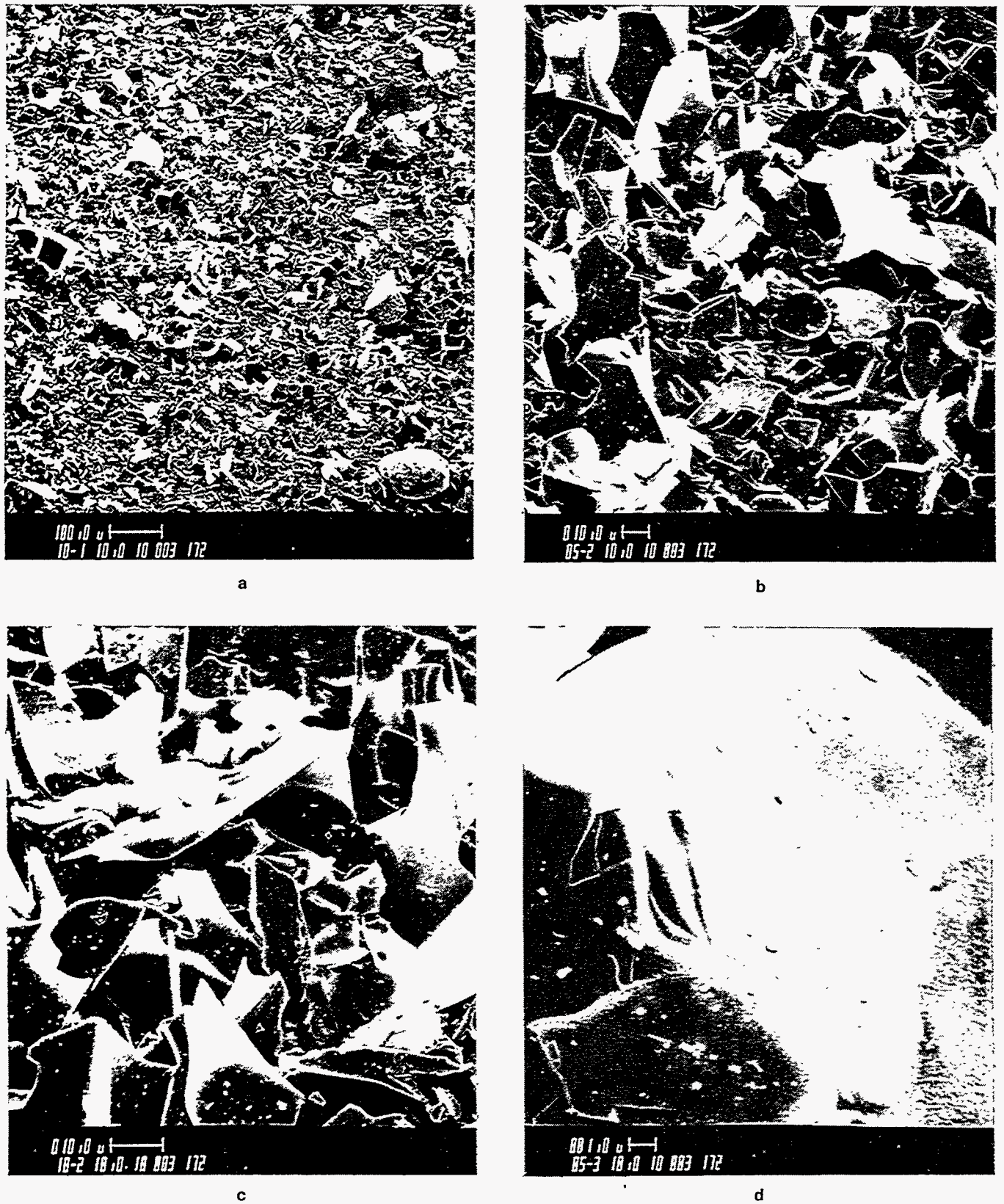

Figure 4-12. SEM photographs of aluminosilicate powder (ID # 3238) taken at magnifications of a) 100X, b) 500X, c) 1000X, and d) 5000X.

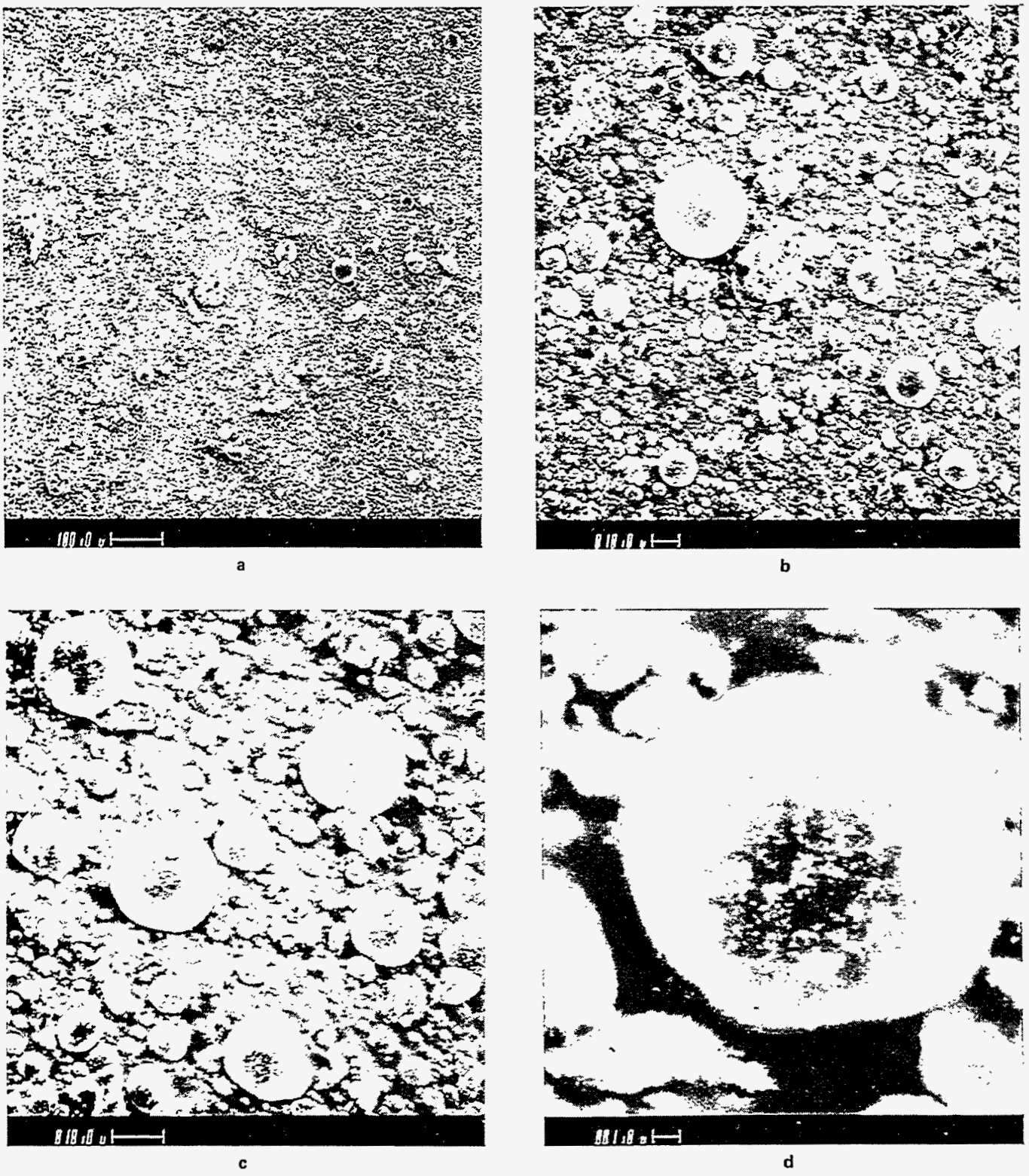

Figure 4-13. SEM photographs of leached Scholz dust cake ash (ID # 2101-W) taken at magnifications of a) 100X, b) 500X, c) 1000X, and d) 5000X.

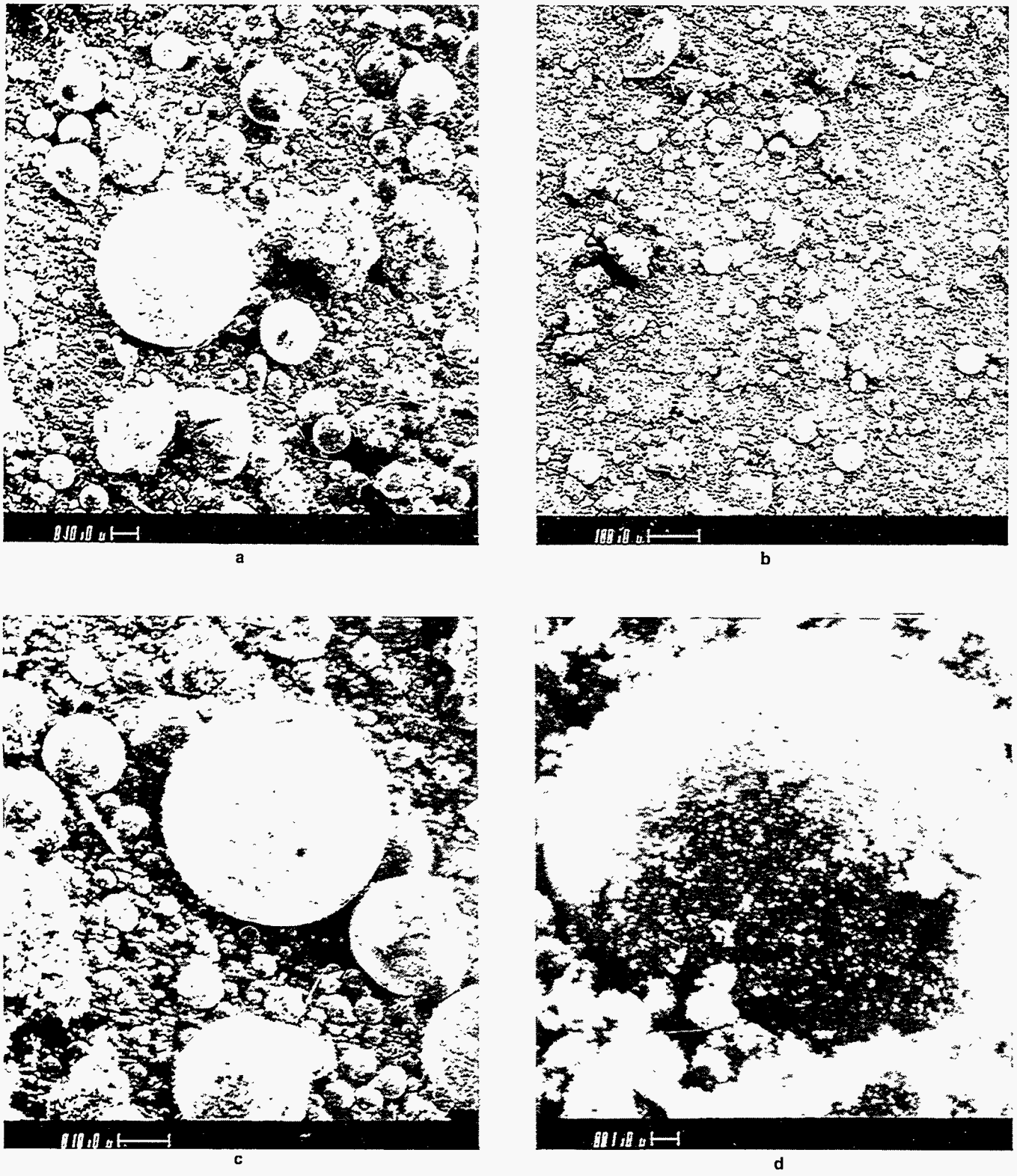

Figure 4-14. SEM photographs of leached Harrington dust cake ash (ID # 2514-W) taken at magnifications of a) 100X, b) 500X, c) 1000X, and d) 5000X.

are rougher than those of the Harrington ash particles. The AFBC ash (ID # 1994) has the finest size distribution and the highest specific surface area of the four unmodified dust cake ashes in our data base. The fineness is due to the recycle cyclone used in the process stream at the AFBC facility, as well as the influence of the sorbent added to the fluidized-bed combustor. The presence of the sorbent and the relatively low combustion temperatures of the AFBC account for the irregular shapes and the high surface area of the AFBC ash particles. These irregular particle shapes lead to the relatively low drag-equivalent diameter of this ash, and consequently to its relatively high specific gas flow resistance.

Because of their small particle size, no size distribution measurements were attempted on the three ultrafine silicon dioxide powders (ID #'s 3063, 3064, and 3065). However, the extremely high surface areas of these powders reflect their very small particle sizes, which are also evident in the SEM photographs of these powders (Figure 4-8). The relatively large size and smooth spherical particle shapes of the glass beads (ID # 1856), seen in Figure 4-9, account for the extremely low specific surface area of this sample. Although the MMD and specific surface area of the diatomaceous earth (ID # 2769) are the same as the values measured for the aluminosilicate powder (ID # 3238), the appearances of these two powders are quite different, as shown in Figure 4-10 and Figure 4-12. The chemical makeup (discussed in Section 4.3.2) of the diatomaceous earth and the aluminosilicate powder also differ. Permeability measurements of these two powders yielded similar results. Both powders, which can be used to precoat filtering fabrics, form filter cakes that have inherently low resistance to filtering flow.

Discussions of the physical characteristics of the ashes and powders conditioned with organosiloxane or SO_3 are discussed under Section 4.3.6. The chemical and physical characteristics of the leached dust cake ashes are discussed in Section 4.3.2.2.

4.3.2 Chemistry

The chemical composition of ash and powder particles often controls their interactions and their susceptibility to various conditioning mechanisms. Because of the pervasive influence of particle chemistry on ash and powder conditioning, we performed a variety of chemical analyses of the ashes and powders in our data base. These analyses included mineral analyses of unconditioned samples and leaching of dust cake ashes with water to determine their soluble components and the effects of removing these soluble compounds from the surfaces of the ash particles. (Other experiments designed to alter the chemical compounds on the surfaces of the particles included conditioning various ash and powder particles with organosiloxane and SO_3. These experiments are discussed in Section 4.3.6.)

4.3.2.1 Mineral Analyses

Tables 4-5, 4-6, and 4-7 present mineral analyses of most of the primary samples in our data base. (Table 4-7 also includes mineral analyses of the leached dust cake ashes. These data are discussed in Section 4.3.6.) In Table 4-5, the effect of the added sorbent on the overall chemical composition of the mixtures is especially evident in their relatively high concentrations of calcium and diminished concentrations (due to the large proportions of added sorbents) of Al_2O_3 and SiO_2. The mixtures of sorbents and ashes also contain large amounts of sulfur, expressed in the proportions of SO_3 and soluble sulfate identified in these samples, due to the capture of SO_2 in the particular desulfurization process used.

Our measurements of LOI, soluble sulfate ($SO_4^=$), and equilibrium pH were performed on as-received samples. Determinations of the various mineral constituents of the samples (Li_2O, Na_2O, K_2O, MgO, CaO, Fe_2O_3, Al_2O_3, SiO_2, TiO_2, P_2O_5, and SO_3) were performed on residues of the samples that remained after being baked overnight at 750 °C. In each of the tables presenting mineral analysis data, we have indicated the total % of the mass of the baked residue that is accounted for by these eleven oxides. Most of our chemical analyses included determinations of sulfur both as soluble sulfate ($SO_4^=$) and as sulfur oxide (SO_3). The soluble sulfate determination quantifies sulfur that is present as alkaline-sulfate salts or free sulfuric acid. These compounds are predominantly found on the surfaces of the particles. Baking the samples at 750 °C prior to the determination of sulfur oxide can cause some of the sulfur in the samples to volatilize. The determination of sulfur oxide, performed by controlled condensation, quantifies all of the sulfur remaining in the sample.

$CaCO_3$ present in some of these samples may calcine to form CaO due to the high temperature (750 °C) the samples are exposed to during determination of LOI. The evolution of CO_2 from $CaCO_3$ may account for a portion of the mass lost by the mixtures of sorbent and ash during the LOI measurement.

Table 4-5
Chemical Characteristics of Ashes and Sorbent and Ash Mixtures, % wt.*

ID #	2870	2871	2872	2873	2884	2885	2883	2890	2907
Li_2O	0.05	0.02	0.02	0.03	0.03	0.01	0.01	0.02	0.02
Na_2O	0.57	0.27	0.46	0.59	0.62	0.67	0.17	0.62	0.57
K_2O	1.9	0.83	0.87	0.97	1.6	0.48	0.63	1.6	0.85
MgO	1.3	0.9	1.1	1.0	0.8	0.6	1.0	0.88	1.4
CaO	2.1	48.6	38.5	31.5	3.0	36.5	46.9	17.3	36.0
Fe_2O_3	20.7	8.2	8.0	9.1	20.9	4.1	10.5	12.1	9.1
Al_2O_3	22.9	9.9	9.7	11.1	24.1	7.0	7.9	17.8	11.8
SiO_2	48.7	20.9	20.0	23.1	46.9	12.4	16.2	37.4	23.9
TiO_2	1.0	0.6	0.5	0.5	0.9	0.3	0.40	0.67	0.59
P_2O_5	0.20	0.09	0.11	0.10	0.46	0.19	0.08	0.12	0.19
SO_3	0.33	9.1	20.3	21.1	0.23	36.0	13.9	12.1	12.8
TOTAL	99.75	102.81	99.56	99.09	99.54	98.25	97.69	100.61	97.22
LOI	1.1	12.5	12.3	6.1	4.9	6.2	13.6	15.2	11.9
soluble $SO_4^=$	0.78	10.4	24.2	25.3	0.76	43.8	17.4	14.2	--
equilibrium pH	5.8	11.3	11.7	11.0	9.1	10.5	11.3	9.5	--

* equilibrium pH is a dimensionless quantity

Table 4-6
Chemical Characteristics of Diatomaceous Earth and Aluminosilicate Powder, % wt.

ID #	2769	3238
Li_2O	0.01	0.01
Na_2O	2.6	3.5
K_2O	0.07	4.6
MgO	0.60	0.27
CaO	0.77	0.63
Fe_2O_3	2.5	0.7
Al_2O_3	1.4	13.1
SiO_2	91.1	75.6
TiO_2	0.1	0.1
P_2O_5	0.05	0.05
SO_3	<0.01	<0.01
TOTAL	99.2	98.56
LOI	0.18	1.4

Diatomaceous earth (ID # 2769) is over 90 % SiO_2, while the aluminosilicate powder (ID # 3238) is over 75 % SiO_2 with a significant amount of Al_2O_3. The alumina powder (ID # 2874) is 99.9 % Al_2O_3.

Table 4-7
Chemical Characteristics of Dust Cake Ashes, % wt.*

Source	Scholz		Monticello		Harrington		AFBC	
ID #	2029	2029-W	2101	2101-W	2515	2515-W	1994	1994-W
Li_2O	0.02	0.02	0.02	0.02	0.02	0.02	0.02	0.02
Na_2O	0.45	0.52	0.82	0.62	1.3	1.2	0.35	0.39
K_2O	0.98	0.96	3.3	2.7	0.34	0.31	1.4	1.5
MgO	2.3	2.4	0.99	0.97	6.2	6.2	0.81	0.93
CaO	10.2	9.6	3.4	1.7	29.3	27.9	29.7	26.2
Fe_2O_3	3.5	3.2	19.9	19.9	5.5	5.3	14.4	13.9
Al_2O_3	20.3	20.3	19.2	19.7	18.8	18.7	11.0	12.6
SiO_2	60.4	60.4	50.1	49.9	31.7	33.7	23.6	26.5
TiO_2	1.6	1.3	1.0	1.1	1.3	1.2	0.54	0.58
P_2O_5	0.08	0.16	0.21	0.24	1.4	1.5	0.14	0.19
SO_3	0.53	0.08	1.00	0.13	2.5	1.5	17.4	15.4
TOTAL	100.36	98.94	99.94	96.98	98.36	97.53	99.36	98.21
LOI	0.37	0.65	11.8	8.0	0.24	6.1	12.7	18.6
soluble $SO_4^=$	0.52	0.13	3.8	0.32	3.0	2.5	18.4	15.1
equilibrium pH	9.9	8.7	4.8	5.7	11.2	10.7	11.5	10.2

* equilibrium pH is a dimensionless quantity

As discussed in Section 4.1, the chemical compositions of the four unmodified dust cake ashes vary widely. The alkaline Monticello ash is high in calcium, magnesium, and silica, all of which affect the adsorption and absorption of water by the ash particles. (Calcium and magnesium react with water in similar ways.) Because the lignite burned at Monticello is a low-sulfur fuel, the ash contains very little SO_3 or soluble $SO_4^=$, despite its relatively high calcium content. The Scholz ash contains somewhat less silica, and significantly less calcium and magnesium than the Monticello ash. The lesser amounts of these elements is predominately made up in the Scholz ash by a larger proportion of iron and also a higher LOI content. The high LOI of the Scholz ash is due to unburned carbon. This ash is acidic due to the high sulfur content of the coal. The unique chemical composition of Powder River Basin coal (very high calcium and magnesium, and low sulfur) accounts for the high alkalinity of the Harrington ash. This ash has much more calcium than is needed to trap the sulfur released during combustion. This ash is low in silica and iron. The low silica content and the high calcium and magnesium levels in this ash cause it to readily adsorb and bond with water vapor in the flue gas. In many ways, the chemical composition of the AFBC ash is like that of the Harrington ash. The AFBC ash has a high calcium content (due to the calcium-based sorbent added in the AFBC process), low silica content, and high overall alkalinity. However, the AFBC ash does not contain as much magnesium as the Harrington ash, because neither the high-sulfur fuel nor the sorbent contain much magnesium. The effectiveness of the AFBC

process in trapping SO_2 is reflected in the high SO_3, soluble $SO_4^=$, and LOI values measured for this ash. The high alkalinity of the AFBC ash indicates that this ash has excess capacity to react with SO_2 or other acidic compounds.

4.3.2.2 Solvent Leaching Studies

Analyses of unmodified and leached dust cake ashes provided some interesting insights into effects that compounds adsorbed on surfaces of ash particles can have on bulk ash behavior. Two sets of leaching tests were performed on the four unmodified dust cake ashes. We performed our first set of leaching tests to determine if we could remove significant amounts of soluble compounds from the surfaces of dust cake ash particles by exposing the ash particles to an excess of water. Leachate samples were produced by sequentially passing 10 ml samples of distilled, deionized water through a 5 gram sample bed of dust cake ash. A slight vacuum was used to pull the water and dissolved solids through a fritted glass filter (4-8 μm pore size) for collection. Additional distilled, deionized water was used to wash the walls of the collection vessel. Total collected leachate and wall washings were then diluted up to 25 ml total volume. This process was repeated ten times for each dust cake ash. The leachate samples were then submitted for chemical analyses. The resultant leached ashes from this first set of tests were assigned ID #'s 2029-W, 2101-W, 2515-W, and 1994-W. Results of these analyses demonstrated that significant quantities of several soluble compounds were removed from particle surfaces during leaching. To determine the effects of removal of soluble compounds on ash behavior, we performed a second set of leaching tests. In this set, 50 g samples of each of the dust cake ashes were leached using the same procedure and the same ratio of ash to distilled, deionized water as in our first set. We generated leached dust cake ashes identified as 2101-L, 2029-L, 2515-L and 1994-L and used them in a variety of subsequent analyses. (In our analyses of the key characteristics of these leached dust cake ashes, we often use the results obtained for these two sets of leached ashes interchangeably.)

The results of the chemical analyses of the leachate samples are presented in Tables 4-8 through 4-11. These results indicate that relatively large amounts of soluble compounds are present on the dust cake ashes. All four ashes lost some calcium, SO_3 (see Table 4-7), sodium, and soluble sulfate (see Tables 4-7 through 4-11) when leached.

Table 4-8
Chemical Constituents of Leachates from Solvent Leaching Test of Monticello Ash

	ppm in wash*							μeq/ml		
wash #	Na^+	Mg^{++}	K^+	Fe^{+++}	Ca^{++}	H^+	$SO_4^=$	Σ(cations)	$SO_4^=$	eq. pH
1	9.3	0.37	2.1	< 0.1	114	--	269.6	6.2	5.6	7.7
3	2.4	0.12	0.6	< 0.1	72	--	102.0	3.7	2.1	10.3
5	1.4	0.14	0.3	< 0.1	52	--	49.0	2.7	1.0	10.1
7	0.8	0.16	0.1	< 0.1	30	--	22.9	1.5	0.48	9.3
9	1.0	0.08	0.2	< 0.1	37	--	24.6	1.9	0.51	9.9

* 10 ml of leachate diluted with 15 ml of distilled, deionized water

Table 4-9
Chemical Constituents of Leachates from Solvent Leaching Test of Scholz Ash

	ppm in wash							μeq/ml		
wash #	Na^+	Mg^{++}	K^+	Fe^{+++}	Ca^{++}	H^+	$SO_4^=$	Σ(cations)	$SO_4^=$	eq. pH
1	250	**	128	5.2	460	0.63	4289	37.4	89.4	3.2
3	18	**	9	0.1	344	0.04	900	18.2	18.8	4.4
5	1.8	**	1.7	< 0.1	126	--	302	6.4	6.3	7.0
7	1.4	**	1.4	< 0.1	69	--	158	3.5	3.3	7.5
9	1.5	**	0.9	< 0.1	43	--	98.3	2.2	2.0	7.1

** analysis not run

Table 4-10
Chemical Constituents of Leachates from Solvent Leaching Test of Harrington Ash

	ppm in wash							μeq/ml		
wash #	Na^+	Mg^{++}	K^+	Fe^{+++}	Ca^{++}	H^+	$SO_4^=$	Σ(cations)	$SO_4^=$	eq. pH
1	55	< 0.03	5.7	< 0.1	126	--	253.6	6.3	5.3	10.7
3	14	< 0.03	2.4	< 0.1	134	--	16.4	7.4	0.34	11.4
5	3.7	< 0.03	0.6	< 0.1	82	--	15.9	4.3	0.33	11.0
7	1.9	< 0.03	0.3	< 0.1	72	--	14.7	3.7	0.31	11.0
9	1.5	< 0.03	0.2	< 0.1	60	--	14.1	3.1	0.29	10.9

Table 4-11
Chemical Constituents of Leachates from Solvent Leaching Test of AFBC Ash

	ppm in wash							μeq/ml		
wash #	Na^+	Mg^{++}	K^+	Fe^{+++}	Ca^{++}	H^+	$SO_4^=$	Σ(cations)	$SO_4^=$	eq. pH
1	9.2	< 0.03	10.5	< 0.1	870	--	1000.0	44.1	20.8	11.6
3	3.6	< 0.03	3.2	< 0.1	700	--	871.7	35.2	18.1	11.7
5	3.2	< 0.03	3.8	< 0.1	560	--	783.7	28.2	16.3	11.6
7	2.4	< 0.03	2.6	< 0.1	475	--	805.0	23.9	16.8	11.4
9	2.0	0.04	2.1	< 0.1	395	--	746.3	19.9	15.5	11.1

The analyses of the Monticello leachates described in Table 4-8 indicate that $CaSO_4$ is initially leached from the particles, followed by an excess of calcium, resulting in alkaline leachates. The concentrations of the sulfate ions and the cations both decrease gradually with repeated leachings.

There is good numerical agreement in Table 4-9 between the measured concentration of soluble $SO_4^=$ and the total soluble cations present in leachate samples #3, #5, #7 and #9 for the Scholz ash. The excess of $SO_4^=$ in leachate sample #1 indicates that this leachate was highly acidic. (Although the acidic nature of this leachate should be evident in the concentration of

H^+ ions, the equilibrium pH measurement is not a reliable indicator of H^+ concentration.) These results demonstrate that the relatively large amount of soluble $SO_4^=$ leached from the surfaces of the Scholz ash probably existed on the particles as salts of Ca, Na, K, and Fe, and as free sulfuric acid dissolved in the water on the surfaces of the ash particles.

The data in Table 4-10 demonstrate that leaching the Harrington ash rapidly removed the $SO_4^=$, leaving highly alkaline leachates as early as the third leaching. The soluble cations in the Harrington ash (primarily calcium) leached out more slowly, causing the leachates to become gradually less alkaline.

In contrast to the concentrations of soluble $SO_4^=$ measured for the pulverized coal ashes, the concentrations of $SO_4^=$ presented in Table 4-11 for the AFBC leachates dropped initially and then leveled off at a relatively high value (about 780 ppm). The total concentration of cations (dominated by calcium) continued to drop gradually with repeated leachings. We believe this behavior is indicative of two trends. During combustion, the calcium and sulfur have reacted to form calcium sulfite and calcium sulfate throughout the ash particles. Therefore the leaching process can affect the entire ash particle, not just its surface. In addition, there seems to be an excess of unreacted calcium in the AFBC ash.

Chemical analyses of the leached dust cake ashes (see Table 4-7) supplemented our analyses of the leachates, and also helped interpret the behavior and physical characteristics of these leached ashes. Monticello ash had the least reduction in alkali of the four ashes leached. Calcium content of leached ash was 6 % less by weight than unleached ash (9.6 vs. 10.2 %) and the potassium was 2 % less, but sodium was 16 % more (from 0.45 to 0.52 % wt) and magnesium was 4 % more. Overall, the content of these four alkali metals was reduced a little more than 3% by leaching the ash. Fe content was reduced from 3.5 to 3.2 % of the weight. The sulfur content of Monticello ash was reduced by about 80 % by leaching. Sulfur we measured as SO_3 went from 0.53 to 0.08 % of the weight of the ash. The content of soluble sulfate was reduced from 0.50 to 0.13 % of the weight. The net effect of leaching on pH was a decrease from 9.9 to 8.7.

Specific surface area of the Monticello ash (Table 4-3) increased from 0.98 to 1.6 m^2/g as a result of the leaching. The percent of weight the ash lost on ignition at 750 °C increased from 0.37 to 0.65 after leaching, suggesting more water was contained in the ash after it had been leached. We believe this water became hydrated to various calcium compounds during the leaching process. The inconsistency in water content prevents us from simply interpreting the relative roles of morphology and surface chemistry in adsorption of water by Monticello ash.

Scholz ash lost 50 % of its calcium when leached. This loss was especially significant since unleached Scholz ash has the lowest concentration of calcium among the ashes we tested. Furthermore, the concentration of alkali metals was lower in leached Scholz ash; sodium dropped 24 %, potassium 18 %, and magnesium 2 %. Scholz ash has a high concentration of

iron, some of which was evidently easily removed by leaching (5 ppm iron was found in the first leachate of the series of 10 leachates and none detected in subsequent leachates). However, there was no difference in iron contents of leached and unleached ashes.

For the Scholz ash, sulfur content that we determined as SO_3 was reduced by leaching from 1 % to 0.13 % of the mass of the ash. Sulfur that we determined as soluble sulfate was reduced from 3.8 to 0.32 % by weight. (There is some uncertainty about the soluble sulfate levels, since the leachate of Scholz ash suggested soluble sulfate amounts equivalent to 4.5 % of the weight of the ash, more than what was measured in the ash.) Reduction in sulfur was about three times more on a weight basis than the reduction in alkali. This result suggests that free sulfuric acid and sulfate salts were removed by leaching. Predictably, the effect of the leaching was a decrease in acidity (pH increased from 4.8 to 5.7).

Leaching Harrington ash removed only slightly more alkali metals than leaching Monticello ash. Small decreases in sodium and potassium content were probably within the margin of error of the measurements, and magnesium content was unchanged. Calcium content changed on a percentage basis less than any of the ashes, dropping from 29.3 to 27.9 % of the weight of the ash. Sulfur content of the Harrington ash was reduced by about 27 % by leaching. Sulfur measured as SO_3 went from 2.5 to 1.5 % of the weight of the ash. Soluble sulfate dropped from 3.3 to 2.5 % of the weight of the ash. The pH of the Harrington ash decreased from 11.2 to 10.7 as a result of leaching. The percentage of weight evolved on ignition at 750 °C increased from 0.24 for unleached ash to 6.1 for leached ash. Evidently, water used to leach Harrington ash reacted with calcium in the ash to form hydrates, hemihydrates, or other compounds, binding the water so that only part of it was removed by baking at 150 °C. The high weight loss on ignition of leached Harrington ash and potential chemical affinity of water and high-calcium ash suggest chemistry is equally, if not more, important in determining adsorption of water. These results indicate that surfaces of Harrington ash particles contain chemicals that are not only hydrophilic, but may chemically react with adsorbed water or sequester the water so that it is precluded from forming liquid bridges.

AFBC particulate matter is a combination of fly ash and particles of $CaCO_3$, $CaSO_4$, or $CaSO_3$ from the fluidized bed. The calcium content of unleached material is 29.7 %, which is almost exactly the same amount as is found in Harrington ash. Since calcium in AFBC particulate matter is in a different form than Harrington ash it is not surprising that results of leaching the two powders differed. AFBC particulate matter lost almost 12 % of calcium content when leached. There was a commensurate increase in percent of weight of Si and Al for leached ash, indicating that the source of reduction in calcium was the limestone added to the boiler. Total alkali content of AFBC particulate matter decreased by only 10%: the sodium, potassium, and magnesium fractions of the weight of leached ash increased slightly. AFBC ash has a relatively high concentration of sulfur because of the reaction between the limestone and sulfur oxides in the combustor. Sulfur content was reduced by about 15 % by leaching. Sulfur measured as SO_3 went from 17.4 to 15.4 % of the weight of the samples, and soluble

sulfate went from 18.4 to 15.1 %. The pH of the material became more neutral, decreasing from 11.5 to 10.2. Further analyses of the leached dust cake ashes were also performed, and are discussed in the remainder of Section 4.

4.3.3 Water Adsorption

We conditioned weighed samples in sealed environments having controlled levels of relative humidity. We then performed measurements of water content on these conditioned powders and dust cake ashes using Karl Fischer titration. This conditioning method does not necessarily imitate the exposure the ash would have in a flue gas stream; however, the intent of the experiment was to quantify differences in adsorption of water among the ashes so that we could learn what properties of ashes govern adsorption mechanisms. We heated each sample to 180 °C in an oven which served as the extraction chamber for the Karl Fischer device in order to extract the water from the ash or powder particles. Table 4-12 presents the results of our Karl Fischer determinations of water content.

Table 4-12
Water Contents of Ash and Powder Samples Titrated in the Karl Fischer Device, % wt.

	Relative Humidity used to Condition Samples, %						
ID #	1	11	33	50	75	82	93
2870	0.42	0.36	--	0.59	0.33	--	--
2871	1.3	1.6	--	2.2	2.0	--	--
2872	1.4	1.2	--	3.2	>2.9	--	5.5
2873	1.6	2.3	--	3.3	>3.6	--	8.8
2884	0.33	0.33	--	0.42	0.61	--	1.1
2885	2.1	2.5	--	>3.5	>4.5	--	--
2883	0.53	0.42	--	1.9	2.9	3.5	--
2890	4.3	6.9	--	9.9	12	--	8.8
2907	0.35	0.50	--	1.9	3.1	--	4.8
2029	0.15	0.16	--	0.18	0.25	--	0.36
2101	1.9	2.3	--	2.0	3.1	--	--
2515	0.25	0.18	--	0.22	0.27	--	--
1994	1.5	1.9	--	2.6	2.7	--	--
3063	0.20	0.27	0.35	0.63	1.4	--	--
3064	0.28	0.36	0.54	2.2	1.7	--	--
3065	0.60	1.4	1.9	5.0	2.6	--	--
1856	0.064	0.15	--	0.20	0.22	0.51	0.58
2769	0.040	0.16	--	0.20	0.41	--	--
2874	0.048	0.051	--	0.10	0.16	--	--
3238	2.2	2.0	--	2.7	2.0	--	2.2

Table 4-12 (continued)

ID #	Relative Humidity used to Condition Samples, %						
	1	11	33	50	75	82	93
2029-W	0.12	0.17	--	0.26	0.33	--	1.2
2101-W	0.62	0.79	--	1.1	1.3	--	1.7
2515-W	2.9	3.3	--	3.6	3.9	--	7.0
1994-W	1.3	2.8	--	3.5	4.2	--	--
2029-L-S	0.17	0.17	--	--	0.35	--	0.64
2101-L-S	0.66	--	0.88	--	0.99	--	--
2515-L-S	3.9	--	--	--	6.3	--	8.1
1994-L-S	4.1	4.5	--	--	6.5	--	8.4
1856-S	0.052	0.14	0.11	--	0.35	--	0.41
2769-S	0.063	--	--	--	0.54	--	--
2874-S	0.11	0.15	--	--	0.29	--	0.29
3238-S	1.0	--	--	--	2.3	--	2.2
2029-A	0.12	--	--	--	0.26	--	--
2101-A	1.0	--	--	--	1.6	--	1.7
2515-A	1.7	--	--	--	2.4	--	--
1994-A	1.0	--	--	--	2.8	--	--
1856-A	0.093	--	--	--	0.26	--	--
2769-A	0.075	--	--	--	0.20	--	--
2874-A	0.031	--	--	--	0.12	--	0.17
3238-A	0.89	--	0.44	--	2.3	--	--
2029-L-A	0.13	--	0.27	--	0.33	--	0.63
2101-L-A	0.28	--	1.2	--	1.5	--	1.8
2515-L-A	2.6	--	--	--	6.4	--	--
1994-L-A	0.85	--	--	--	4.6	--	--

Because of the very strong affinity sulfuric acid has for water, when samples with significant amounts of soluble sulfate on their particle surfaces adsorb water, it is very difficult for the Karl Fischer technique to separate the adsorbed water from the sulfuric acid that is formed on the particles. In general, temperatures exceeding 330 °C are needed to dissociate this water. Since this temperature is beyond the limit of our Karl Fischer device, the water contents of samples with significant amounts of soluble sulfate on their particle surfaces, such as unleached Scholz dust cake ash (ID # 2101), may actually be significantly higher than can be measured with this device.

These data contain some anomalies. For each sample, we expected that total water removed would increase with higher levels of relative humidity used for conditioning. Deviations from this trend occurred for several of the samples in Table 4-12. When some of these anomalies were first observed, we began to record the cumulative amount of water measured in the Karl Fischer device as a function of time the sample was in the oven. Therefore, for some of these data, it may be that the 30-minute extraction time we used for these samples was not always sufficient to reach equilibrium. When time-resolved data showed that water was still being removed from the sample at the end of the 30 minute extraction time, we have placed a > sign in front of the value reported in the table.

We also determined water contents of selected ash and powder samples by measuring their weight gain after being exposed to environments with controlled levels of relative humidity. As with the Karl Fischer data, these data, summarized in Table 4-13, also contain some inconsistencies. When this gain-in-weight method was used to determine the water content of sample # 2870 (Muskingum base line ESP hopper ash), an extraordinarily high value was measured. Since this single value (5.47 % wt. H_2O) is so different from the four values we determined for this sample with the Karl Fischer device, we believe that this single high value determined for ID # 2870 with the gain-in-weight method is not a true indication of the water adsorbed by this ash and should be ignored. The other inconsistencies in the data from the gain-in-weight and Karl Fischer methods are relatively minor.

Table 4-13
Water Contents of Conditioned Ashes and Powders Determined by Increases in Sample Weights

ID #	Relative Humidity used to Condition Samples, %	H_2O content, % wt.
2870	75	5.47
2871	75	0.18
2872	75	0.29
2873	75	1.01
2884	83	0.65
2884	93	0.87
2029	75	0.18
2029	83	0.15
2029	93	0.15
2101	75	2.28
2515	75	0.19
1994	75	2.26
1856	83	0.12
1856	93	0.52
2029-W	75	0.32
2029-W	83	0.24
2029-W	93	0.28
2101-W	75	1.08
2101-W	83	0.99
2101-W	93	1.3
2515-W	75	4.15
1994-W	75	5.30

The predominant trend in the data reported in Tables 4-12 and 4-13, as would be expected, was for each sample to adsorb more water as the conditioning environment became more humid. An exception to this trend was noted for the aluminosilicate powder (ID # 3238). This sample consistently adsorbed many times as much water as the glass beads (ID # 1856), diatomaceous earth (ID # 2769), or the alumina powder (ID # 2874). These result are in accord with the hydrophobic character of silica, and are clear evidence of the importance of particulate chemistry in adsorption. The unresponsiveness of the aluminosilicate powder to higher levels of relative humidity may be due to its unusual morphology (see Figure 4-12), but we cannot be certain based on the data we measured.

The water adsorption data clearly demonstrate the tendency for mixtures of sorbents and ashes to take up significantly more water than base line (no added sorbent) fly ashes. We attribute

the increased adsorption by these mixtures to their morphology (increased surface area) and their chemistry (high calcium contents). The extensive surfaces of the sorbent particles provide many locations for physical adsorption of the water molecules. Once the water is adsorbed, it can be drawn into the interior regions of the sorbent particles and also become chemically bound as hydrates to the various calcium-based compounds in these particles. Of the three mixtures of sorbent and ash from the DITF, (samples # 2871, 2872, and 2873), the sample spiked with $CaCl_2$ adsorbed the most water. This result supports the contention that a deliquescent additive increases the relative humidity in its immediate vicinity, leading to increased water adsorption. The ADVACATE sample (ID # 2890) adsorbed significantly more water than any of the other six mixtures of sorbents and ashes that we tested.

The Scholz and AFBC ashes adsorbed much more water than either the Monticello or Harrington ashes. We believe the Scholz ash (ID # 2101) adsorbed water easily because of the sulfate salts on the surfaces of the ash particles. These sulfate salts can promote increased water adsorption in the same way as $CaCl_2$ did for the sorbent and ash mixture from the DITF. This conclusion is supported by the reduced (by about 50 %) water adsorption by leached Scholz ash (ID # 2101-W). The sulfate compounds have been removed from the surfaces of this leached ash. Surface chemistry governs adsorption and retention of water by the Scholz ash more than does surface morphology. The AFBC ash (ID # 1994) adsorbs water in much the same way as the mixtures of sorbent and ash because of the sorbent used in the AFBC process. Water is adsorbed on the extensive surfaces of the AFBC ash particles and subsequently binds chemically with the ash in the form of hydrates formed with calcium-based compounds. The Monticello and Harrington ashes have less specific surface area than the Scholz or AFBC ashes (Table 4-3), and they have significantly different chemical compositions. The high silica content of the Monticello ash (ID # 2029) makes its particle surfaces hydrophobic, and subsequently this ash adsorbs little water. The adsorption of water by the Harrington ash (ID # 2515) is also limited by the low specific surface area of this ash. However, once the ash particles come in contact with water, as in the leaching procedures used to generate samples 2515-W and 2515-L, the large amounts of calcium in the Harrington ash provide multiple opportunities for this water to become chemically bound to the ash particles as hydrates. This effect can be seen in the high water contents of the leached Harrington ash (ID # 2515-W) compared with the low water contents of the unmodified Harrington ash. Apparently the hydrophobic nature of the Monticello ash particles overcomes much of the tendency for the leached Monticello ash (ID # 2029-W) to bind water as hydrates with the significant proportion (about 10 % by wt.) of calcium in the ash particles.

Data measured for the ultrafine silicon dioxide powders (ID #'s 3063, 3064, 3065) clearly demonstrate the effect of particle morphology on water adsorption. The only differences between these three powders are their particle size and specific surface area (Table 4-3). Increased surface area promotes increased water adsorption. The glass beads (ID # 1856), diatomaceous earth (ID # 2769) and the alumina powder (ID # 2874) all have relatively low specific surface areas, and very few, if any, chemical compounds on their particle surfaces to

promote the chemical binding of water to the particles. The water adsorption data measured for the samples conditioned with SO_3 or organosiloxane will be discussed in Section 4.3.6.

4.3.4 Cohesivity

We used two types of measurements, uncompacted bulk porosity (Table 4-14) and tensile strength (Table 4-15), to assess the relative cohesivity of the ashes and powders in our data base. We performed these two measurements on samples that had been conditioned with water vapor over a wide range of relative humidities. The data we obtained in these measurements generally show the consequences that different amounts of adsorbed water have on the bulk physical characteristics of the ashes and powders in our data base. The data reflect the influences of particle morphology and chemistry on the cohesivity of these samples because the amount of water adsorbed is dependent on the physical and chemical characteristics of the particles (Tables 4-12 and 4-13). Besides water present on the particle surfaces, particle shape (as shown in Figures 4-1 through 4-14) is a primary determinant of ash cohesivity. Prior studies have noted a positive correlation between irregular particle shape and increasing ash cohesivity (Bush *et al*, 1989).

4.3.4.1 Uncompacted Bulk Porosity

Uncompacted bulk porosities of ashes and powders that were conditioned and tested at a variety of relative humidities are summarized in Table 4-14. With the exception of the ADVACATE ash (ID # 2890) and the mixture of ash combined in the furnace with lignosulfonate-modified lime (ID # 2907) at very high relative humidities, the mixtures of sorbents and ashes were unresponsive to water vapor conditioning. This flat response is further evidence that water adsorbed by these mixtures is readily sequestered too deep within the sorbent particles to affect the way these particles interact.

Table 4-14
Uncompacted Bulk Porosities of Conditioned Ashes and Powders

ID #	Relative Humidity used to Condition and Test Samples, %						
	7	13	27	53	75	83	93
2870	61	--	61	--	62	--	66
2871	87	--	87	--	86	--	87
2872	88	--	87	--	85	--	87
2873	87	--	87	--	87	--	89
2884	59	--	--	63	64	62	67
2885	83	--	--	--	84	--	85
2883	89	--	--	--	--	--	88
2890	77	--	78	85	85	--	89
2907	82	--	--	--	83	--	86
2029	64	--	67	68	69	70	80
2101	77	--	76	78	82	84	87
2515	74	--	76	75	76	--	78
1994	90	--	88	90	89	--	91
1856	44	--	45	57	70	73*	77*
2769	91	--	--	--	--	--	92
2874	77	--	--	--	79	--	81
3238	94	--	--	--	--	--	95

Table 4-14 (continued)
Uncompacted Bulk Porosities of Conditioned Ashes and Powders

ID #	Relative Humidity used to Condition and Test Samples, %						
	7	13	27	53	75	83	93
2029-W	65	--	63	64	64	--	80
2101-W	73	--	72	72	72	73	80
2515-W	77	--	74	76	76	--	80
1994-W	90	--	89	91	90	--	91
2029-L	--	--	64	--	--	--	73
2101-L	--	--	72	--	--	--	79
2515-L	--	--	79	--	--	--	80
2029-L-S	--	65	65	--	68	--	76
2101-L-S	--	70	68	--	72	--	76
2515-L-S	--	85	84	--	87	--	83
1994-L-S	--	87	86	--	88	--	--
1856-S	--	73	73	--	74	--	--
2769-S	--	90	90	--	91	--	91
2874-S	--	65	64	--	65	--	66
3238-S	--	94	95	--	95	--	96
2029-A	--	66	--	--	70	--	83*
2101-A	--	71	--	--	79	--	87
2515-A	--	75	--	--	70	--	77
2769-A	--	--	--	--	--	--	93
2874-A	--	65	--	--	68	--	72
3238-A	--	--	--	--	--	--	95
2029-L-A	--	62	--	--	65	--	75
2101-L-A	--	72	--	--	74	--	81
2515-L-A	--	79	--	--	81	--	82
4118	--	--	74	--	--	--	--

* the powder got quite moist, sifting it created "gummy spindles"

The correlation between particle shape and ash cohesivity can be seen for the four dust cake ashes by comparing the measured specific surface areas (Table 4-3) and appearances of the ash particles in Figures 4-4 through 4-7 with the uncompacted bulk porosity values presented in Table 4-14. The uncompacted bulk porosity values we measured for the four unleached dust cake ashes demonstrate the relative cohesivity of these ashes. The Monticello ash (ID # 2029) is the least cohesive of the dust cake ashes. The second least cohesive of the four dust cake ashes is the Harrington ash (ID # 2515). The Scholz dust cake ash particles (ID # 2101) have rougher surfaces, and consequently the ash has a higher cohesivity than the Harrington ash.

The most cohesive of the four dust cake ashes is the AFBC ash. The AFBC ash particles have very irregular particle shapes.

Figure 4-15 presents a graph of these data for the four unleached and the four leached dust cake ashes. For Scholz, Monticello, and Harrington dust cake ashes, water conditioning increased ash cohesivity as measured by bulk porosity, although, except for unleached Scholz ash, relatively high humidities were required to significantly increase cohesivity. Because of sulfate salts and free sulfuric acid on the surfaces of the particles, unleached Scholz ash readily adsorbed water. This water was then available to form liquid bridges between the ash particles. We believe that porosity of AFBC ash stayed relatively constant as a function of the relative humidity used to condition the ash because all water adsorbed onto the surfaces of the ash particles was subsequently absorbed into the interior of the particles.

The only powder we tested that was more than mildly responsive to water vapor conditioning was the glass beads (ID # 1856). The low surface area of the glass beads is probably responsible for limiting the response of the glass beads to relative humidities greater than 27 %. However, once enough water was adsorbed onto the surfaces of the glass beads, the hydrophobic surfaces of the glass caused the water to be highly mobile. In this respect, the adsorbed water on the surfaces of the glass beads behaved like water adsorbed on the hydrophobic surfaces of the Monticello ash particles. Because mobile water on hydrophobic particle surfaces has a greater tendency to bond with itself than with the particle surface, it readily forms the liquid bridges that in turn increase ash or powder cohesivity.

4.3.4.2 Tensile Strength

We measured the tensile strengths of most of the samples in our data base with an electrostatic tensiometer (Pontius and Snyder, 1991). These data are summarized in Table 4-15. Although the magnitude of the tensile strengths of the samples varied widely, almost all of the samples displayed a minimum in tensile strength for samples conditioned and tested at relative humidities between 34 and 50 %. The increases in tensile strength for samples conditioned at relative humidities above 50 % are generally explainable in terms of the formation of liquid bridges between adjacent particles. However, we are not certain what leads to the high tensile strengths we measured for samples conditioned and tested at low relative humidities. We suspect that changes in van der Waals forces caused by changes in materials at contact points or closeness of contact points are involved in these results, as may be the strengths of ionic bonds. We also cannot rule out electrostatic effects at very low humidities.

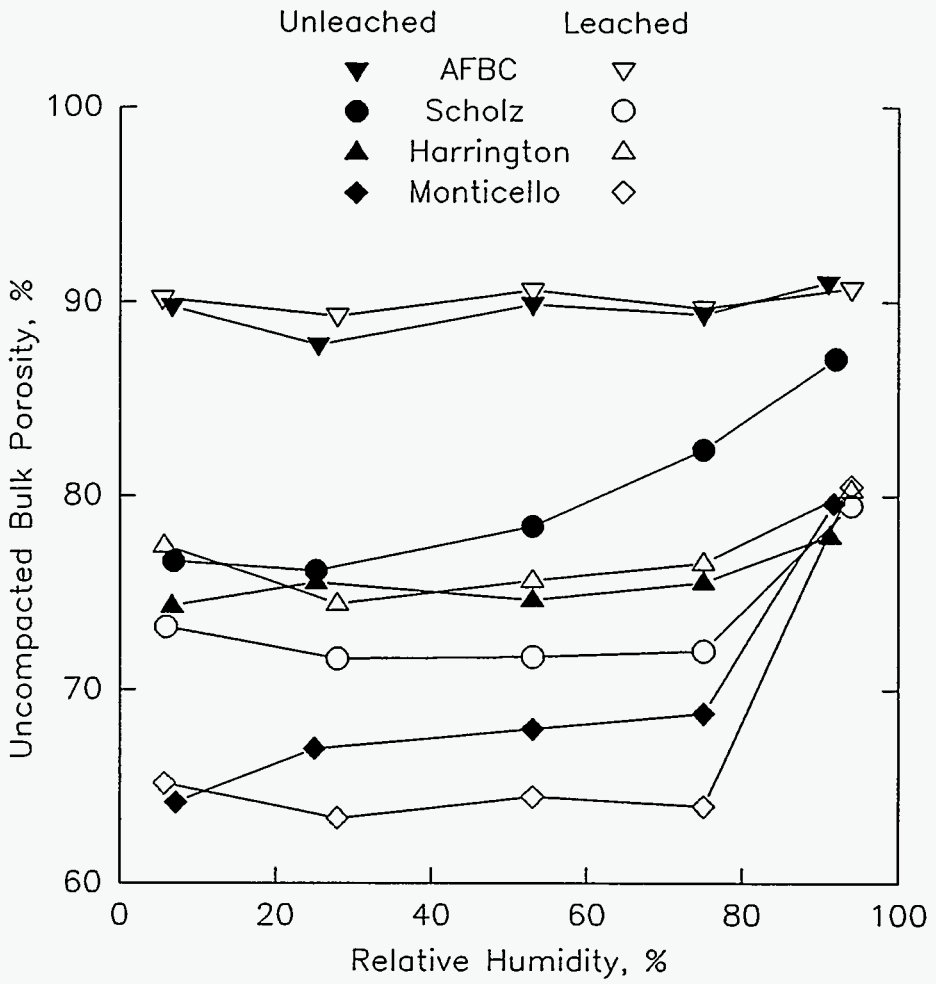

Figure 4-15. Uncompacted bulk porosity of leached and unleached dust cake ashes as a function of the relative humidity used to condition the ashes.

Table 4-15
Tensile Strengths of Conditioned Ashes and Powders, N/m^2

ID #	Relative Humidity used to Condition and Test Samples, %							
	1	11	22	34	50	75	83	93
2870	19	7.3	7.3	1.1	1.6	5.1	>30	--
2871	>32	>32	24	3.1	3.7	--	3.4	8.0
2872	--	--	--	>28	>9.5	--	15	>24
2873	--	--	--	>18	>6.8	--	>14	--
2884	1.9	--	--	0.6	0.6	--	0.5	--
2885	>30	18	11	2.8	4.2	--	6.8	12
2883	--	--	>32	31	7.5	12	>23	--
2890	>32	--	13	11	18	--	>32	>32
2907	--	--	--	>14	9.3	--	>21	--
2029	>32	19	--	4.1	8.2	8.5	8.5	12
2101	11	4.7	--	1.5	5.1	5.4	28	--
2515	--	>32	>32	19	15	>26	30	--
1994	--	--	--	>13	>7.7	--	--	--
1856	7.9	3.6	--	0.6	0.8	>27	32	--
2769	--	--	--	>6.6	>4.4	--	--	--
2874	3.3	1.5	--	0.8	0.8	--	1.2	2.1
3238	>30	4.9	--	2.0	1.4	--	1.9	3.4
2029-W	>30	15	--	3.1	3.2	3.6	3.8	6.1
2101-W	15	6.3	--	1.8	2.8	--	3.9	3.1
2515-W	>32	8.8	--	2.0	1.6	2.5	3.4	3.8
1994-W	--	--	--	>14	>9.5	--	--	--
2029-L-S	--	--	--	5.3	--	9.0	--	11
2101-L-S	--	--	--	6.1	--	3.8	--	--
2515-L-S	--	--	--	24	13	19	--	--
1856-S	--	--	--	>32	--	--	--	--
2874-S	--	--	--	1.3	--	--	--	1.8
2029-A	--	--	--	10	--	10	--	>32
2101-A	--	--	--	--	--	6.1	--	--
2515-A	--	--	--	--	--	>20	--	--
3238-A	--	--	--	2.5	--	--	--	--
2029-L-A	--	--	--	7.7	--	6.1	--	--
2101-L-A	--	--	--	6.3	--	6.3	--	--
2515-L-A	--	--	--	>23	--	18	--	--
4058	>21	13	8.5	4.7	8.5	--	--	--
4118	>21	11	11	6.1	6.8	12	--	--

Many of the higher tensile strengths were measured for various mixtures of sorbents and ashes. This trend agrees with the uncompacted bulk porosity data we measured, and demonstrates the influence of particle shape and size on cohesivity. The samples with the lowest minimum tensile strengths were also the samples for which we measured the largest MMD values (Table 4-3: ID #'s 2870, 2884, 1856, and 2874). This was expected because of the strong van der Waals forces between particles less than about 4 μm diameter. The samples with the lowest tensile strengths also have relatively low specific surface areas (Table 4-3). These same samples, with the exception of the alumina powder (ID # 2874), also displayed relatively low uncompacted bulk porosity values. The uncompacted bulk porosity of the alumina powder may be somewhat higher than these other coarse powders because of its internal porosity. The relatively coarse alumina particles (Figure 4-11) seem to be agglomerates of finer primary particles of about 1 μm diameter. The open volume between these fine, primary particles increases the overall uncompacted bulk porosity of the powder. Lower tensile strength and lower porosity are compatible results since it is presumably weaker cohesive forces between particles that allow the particles to pack in less open (less porous) arrangements.

The influence of particle size on tensile strength may be responsible for the fact that the minimum tensile strength of the unleached Scholz dust cake ash is less than the minimum values measured for either the unleached Monticello or Harrington ashes. If the morphology of the ash particles from these three plants were identical, their different surface chemistries (specifically the soluble $SO_4^=$ levels listed in Table 4-7) would probably cause the Scholz ash to adsorb more water and exhibit a higher tensile strength than the Monticello ash. The Scholz ash does adsorb more water than the Monticello or Harrington ashes. However, in this case the effect of the coarser size distribution of the Scholz ash apparently overrides the effect of surface chemistry on tensile strength.

The data in Table 4-15 show that the tensile strength of the unleached Harrington ash is significantly greater than the tensile strength of the Monticello ash over the range of humidities tested. This is true even though these two ashes have similar morphology (MMD's, specific surface areas, and particle shape as shown in SEM photographs) and adsorb similar amounts of water at comparable relative humidities (Table 4-12). The behaviors of these two ashes are apparently affected by differences in their chemical compositions. The high silica content, and the resultant hydrophobic behavior, of the Monticello ash apparently makes the bulk cohesivity of this ash more responsive to very high relative humidities than the Harrington ash (note the uncompacted bulk porosity values above 75 % RH for these ashes in Table 4-14). This difference in uncompacted bulk porosity values does not have a parallel in the tensile strength data. The tensile strengths of all three of the unleached pulverized-coal (PC) dust cake ashes increase with increasing humidities (above 50 % RH). A factor which may promote the higher tensile strengths of the Harrington ash is the soluble $SO_4^=$ content of the Harrington ash (Table 4-7), which is six times higher than that of the Monticello ash. This sulfate may combine with the adsorbed water to form an especially sticky glue between particles, although this mechanism is not verified.

Our tensile strength measurements of the leached dust cake ashes showed the effects of the removal of soluble $SO_4^=$ from the surfaces of the Scholz ash particles and also the apparent effect of the attachment of water of hydration to calcium in the Harrington, and possibly also the Monticello ashes. The reduced levels of adsorbed water on the leached Scholz ash (Table 4-12) are probably responsible for the lower tensile strengths measured for the leached Scholz ash (ID # 2101-W) at relative humidities above 50 %. The tensile strength of the leached and unleached Scholz ashes are similar at dryer conditions. The Harrington ash exhibited much lower tensile strengths after leaching. However, leaching removed a lesser proportion (about 17 %) of the soluble $SO_4^=$ from the Harrington ash than from the Scholz ash (about 92 %), although the soluble $SO_4^=$ contents of both ashes were about the same prior to leaching. Even though the effects of leaching on the surface chemistry of the Harrington ash may be minimal, the leaching process did apparently cause a significant amount of water to become attached as water of hydration to the calcium in the ash (see Table 4-12 and the LOI values in Table 4-7). We suspect, but are not certain, that this hydrated water reduced the tensile strength of the leached Harrington ash. Similar, but greatly diminished, hydration of water and reductions in tensile strength were obtained for the Monticello ash.

4.3.5 Resistivity

Because the resistivity of an ash is a primary characteristic governing its collection in an ESP, we performed laboratory determinations of resistivity for many of the samples in our data base. In each of these determinations resistivity was measured as a function of temperature. Most of these measurements were made in descending temperature mode, and a few were made when the temperature was increased between measurement points. We conditioned and tested many of the powder and ash samples in environments with different levels of water vapor.

In order to determine the resistivity effects of different types of sorbent addition on the characteristics of the base line ash, we measured the resistivity of the Muskingum base line ash (ID # 2870) and the three sorbent and ash mixtures from the DITF (ID #'s 2871, 2872, and 2873). These samples were conditioned and tested in an environment having 11.9 % H_2O by volume. The ascending temperature data we measured are presented in Figure 4-16, and the descending temperature determinations are plotted in Figure 4-17.

Comparisons of the resistivity data measured for the three sorbent and ash mixtures in ascending and descending temperature modes demonstrate that measured resistivity may vary because of the temperature history of the sample. Procedures have not been established to ensure that resistivity data measured for mixtures of sorbent and ash accurately reflect the resistivity of the mixture at the time of collection. Since the resistivity of these mixtures plays a crucial role in the effectiveness of ESP's used to collect them, we recommend research to

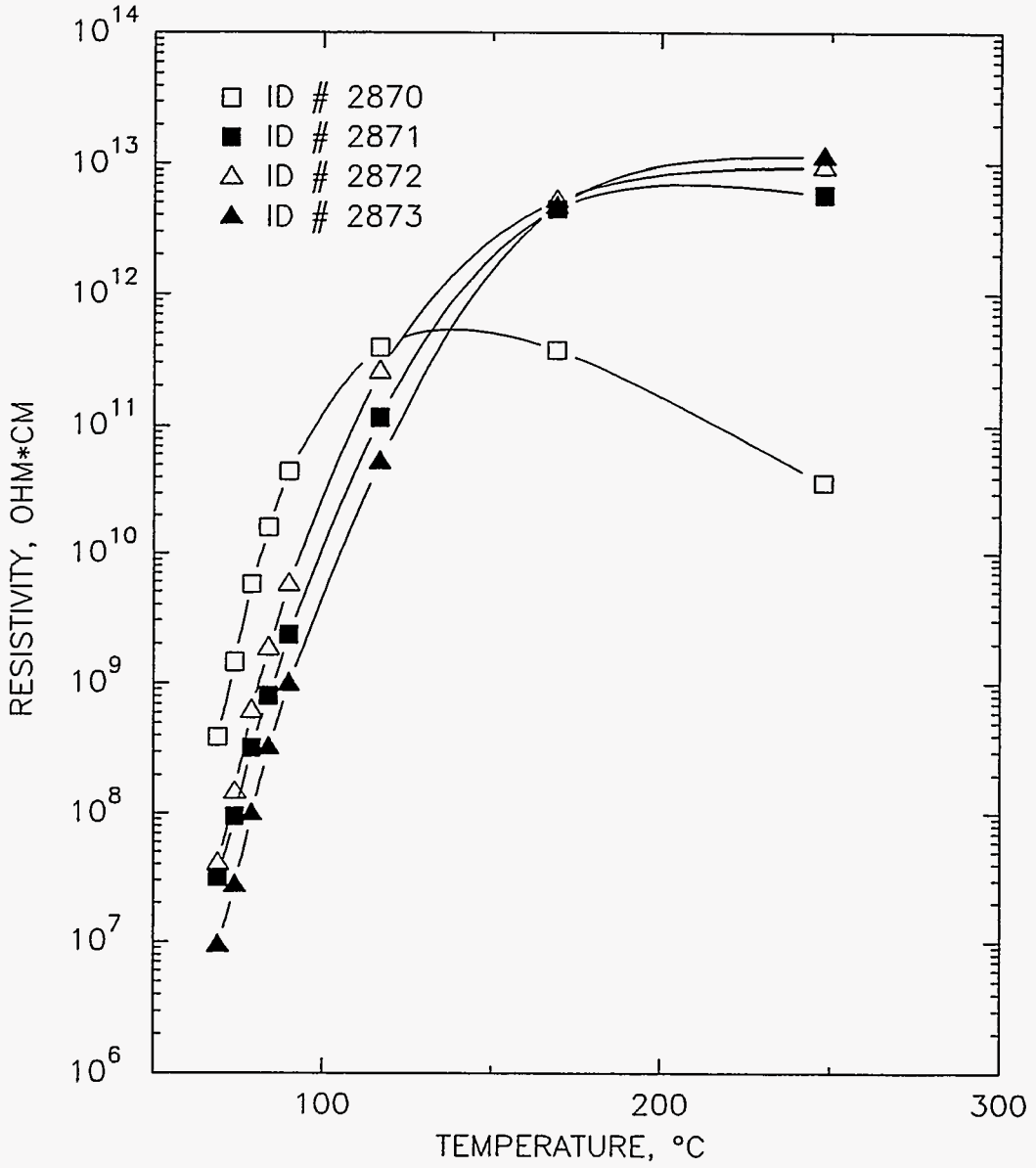

Figure 4-16. Data obtained from ascending temperature resistivity determinations of the Muskingum base line ESP hopper ash (ID # 2870), a mixture of sorbent and ash from tests of dry $Ca(OH)_2$ injection at the DITF (ID # 2871), a mixture of sorbent and ash from tests of $Ca(OH)_2$ slurry injection at the DITF (ID # 2872), and a mixture of sorbent and ash from tests of $Ca(OH)_2$ slurry injection with $CaCl_2$ addition at the DITF (ID # 2873).

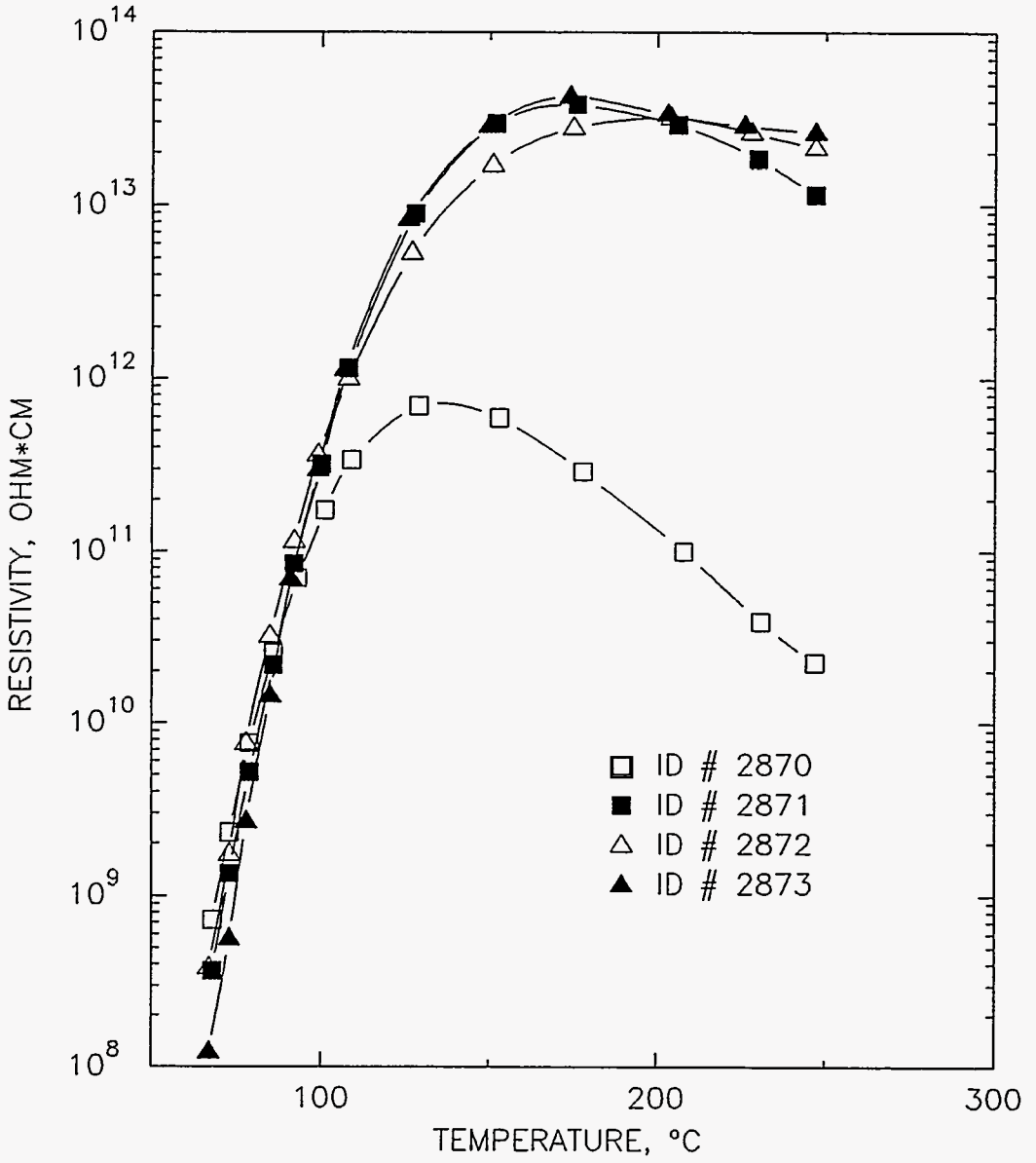

Figure 4-17. Data obtained from descending temperature resistivity determinations of the Muskingum base line ESP hopper ash (ID # 2870), a mixture of sorbent and ash from tests of dry $Ca(OH)_2$ injection at the DITF (ID # 2871), a mixture of sorbent and ash from tests of $Ca(OH)_2$ slurry injection at the DITF (ID # 2872), and a mixture of sorbent and ash from tests of $Ca(OH)_2$ slurry injection with $CaCl_2$ addition at the DITF (ID # 2873).

define the proper resistivity measurement procedures for the various types of sorbent and ash mixtures encountered at utility and industrial applications.

Despite the differences in ascending and descending temperature data for the three sorbent and ash mixtures from the DITF, it is apparent from the data presented in Figure 4-16 and 4-17 that the resistivities of these three mixtures are similar. These data also show that sorbent addition can modify the resistivity of the ash by at least one order of magnitude at a given temperature. Temperature reductions during sorbent injection processes can cause even greater changes in the resistivity of the material being collected. Sorbent injection processes performed at the DITF lowered the duct temperature to around 165° F from about 350° F for base line operation. Consequently, during collection in the ESP, the particulate matter from the sorbent injection processes had a significantly lower resistivity (approximately 4×10^7 $\Omega \cdot cm$) than the base line ash (approximately 3×10^{11} $\Omega \cdot cm$ at 350° F).

We measured resistivity as a function of ash temperature for the leached dust cake ashes in descending temperature mode. These data and corresponding data taken for unleached dust cake ashes are shown in Figures 4-18 through 4-29. Amounts of adsorbed water and soluble compounds on the surfaces of ash particles are prime determinants of the degree of surface conduction. (Overall conduction of current through an ash layer combines surface conduction and volume conduction.) For all eight ashes tested, conditioning samples with increased levels of water vapor decreased the ash resistivity for temperatures below 200 to 300 °C. At temperatures above 300 °C, the amount of water that could be adsorbed onto surfaces of ash particles was apparently too low to promote surface conduction.

We believe that the unleached Monticello ash has a higher resistivity than unleached Harrington ash because of a difference in surface conduction. In our analyses of leachate samples, a much larger amount of soluble Na^+ was removed from Harrington ash during the leaching cycles than from Monticello ash. Sodium present on the surface of ash particles serves as a very effective, mobile charge carrier. After each of these two ashes had most of the Na^+ (and SO_3 and $SO_4^=$) removed from their particle surfaces during leaching, their overall resistivities were increased, and became much more similar. Although sodium was effectively removed from the surfaces of the Harrington ash particles during leaching, the total amount of sodium present in the ash dropped only slightly. Therefore the sodium within particles was still available for promoting volume conduction at higher ash temperatures. A possible explanation of the apparent decrease in volume conduction of leached Harrington ash is given below.

One of the changes that occurred in Monticello and Harrington ashes during leaching was inclusion of significant quantities of water in the form of hydrates with alkaline metals (Na, K, Mg, and Ca). Presence of these metallic hydrates is evident in increased LOI values measured for these two leached ashes (Table 4-7). LOI nearly doubled for Monticello ash, and increased by a factor of twenty five for Harrington ash. Water contents of Harrington ashes measured

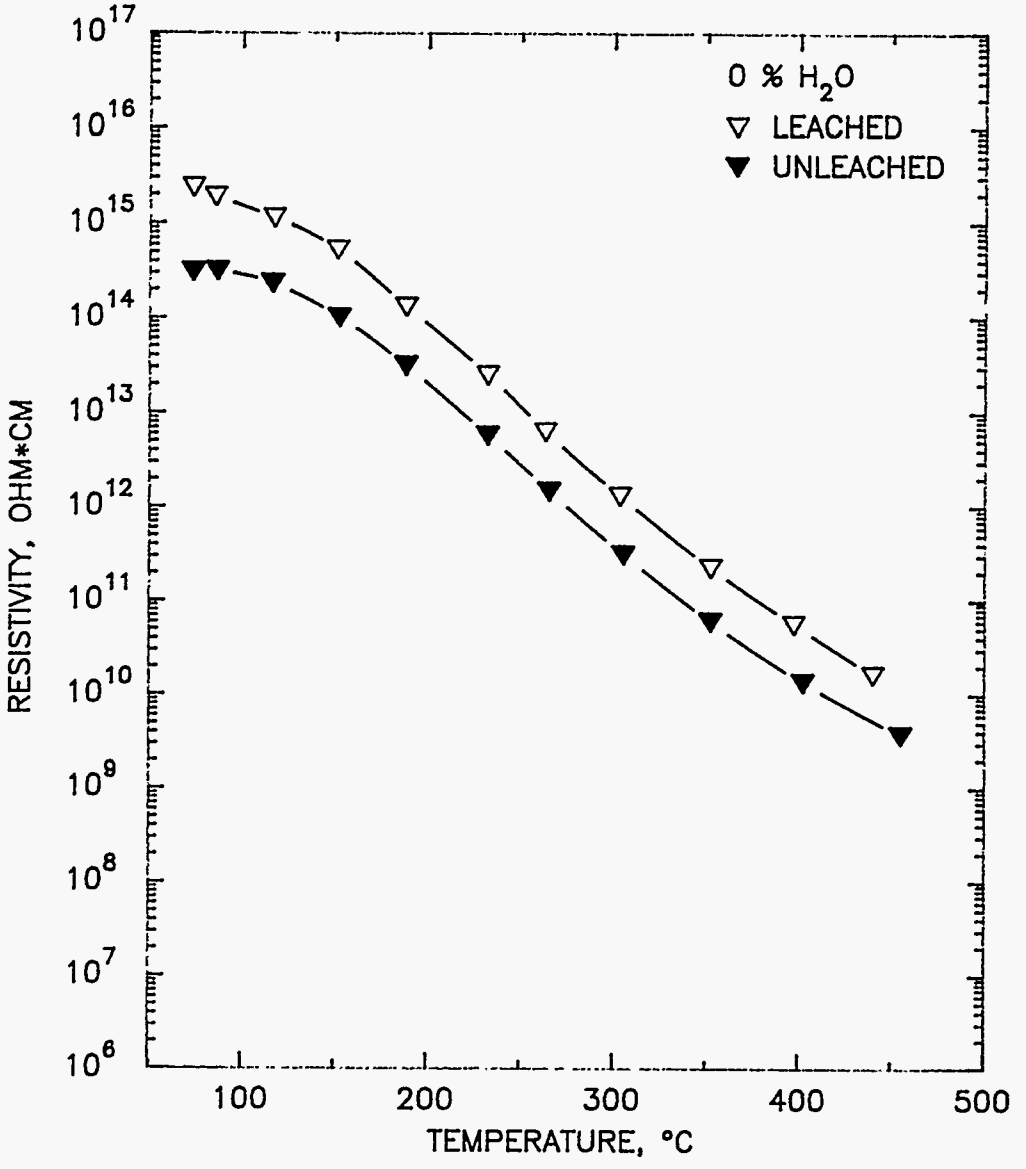

Figure 4-18. Leached (ID # 2029-W) and unleached (ID # 2029) Monticello dustcake ash resistivity as a function of temperature during descending-temperature resistivity determinations made in a dry (0 % water) environment.

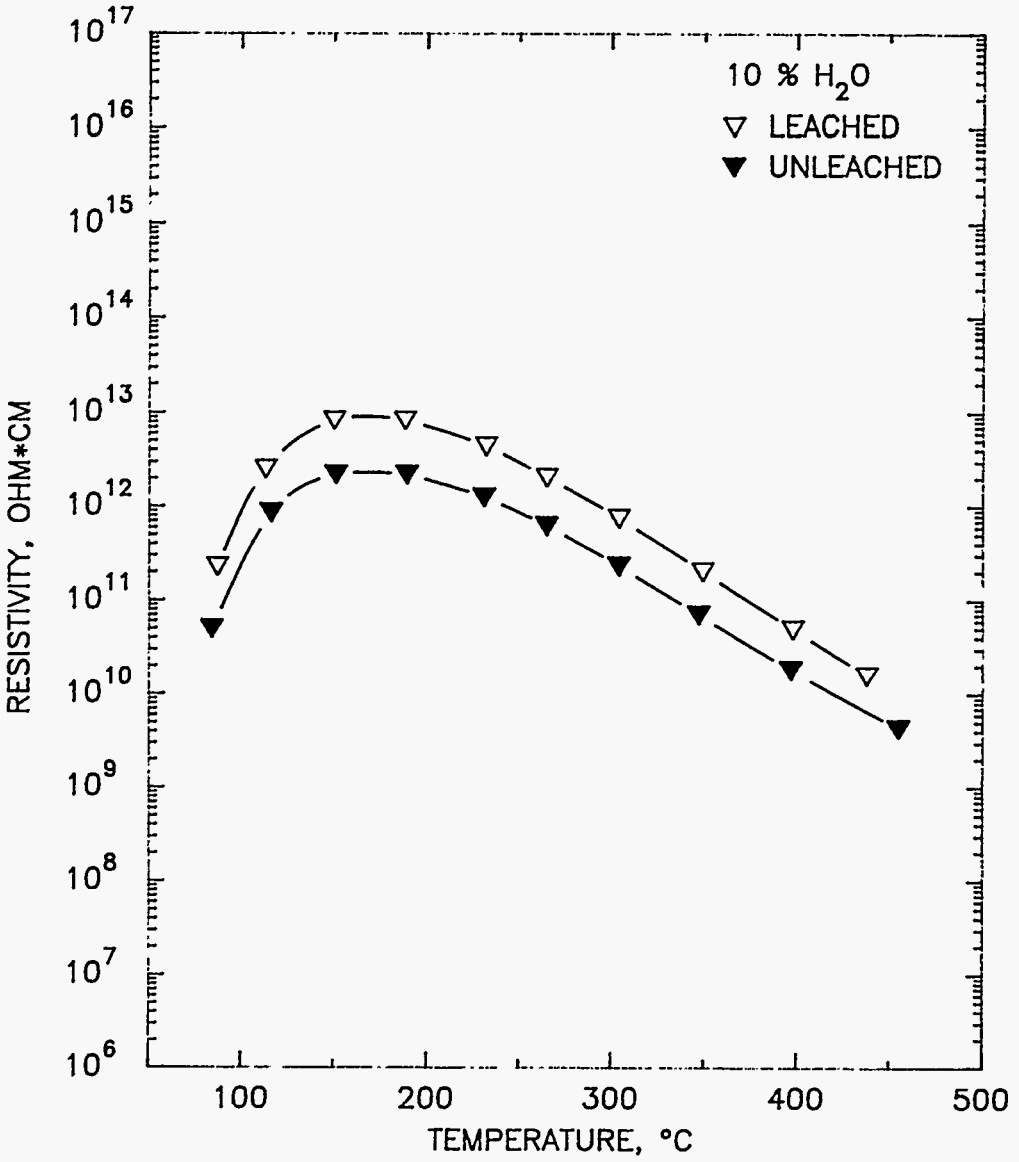

Figure 4-19. Leached (ID # 2029-W) and unleached (ID # 2029) Monticello dustcake ash resistivity as a function of temperature during descending-temperature resistivity determinations made in a moist (10 % water) environment.

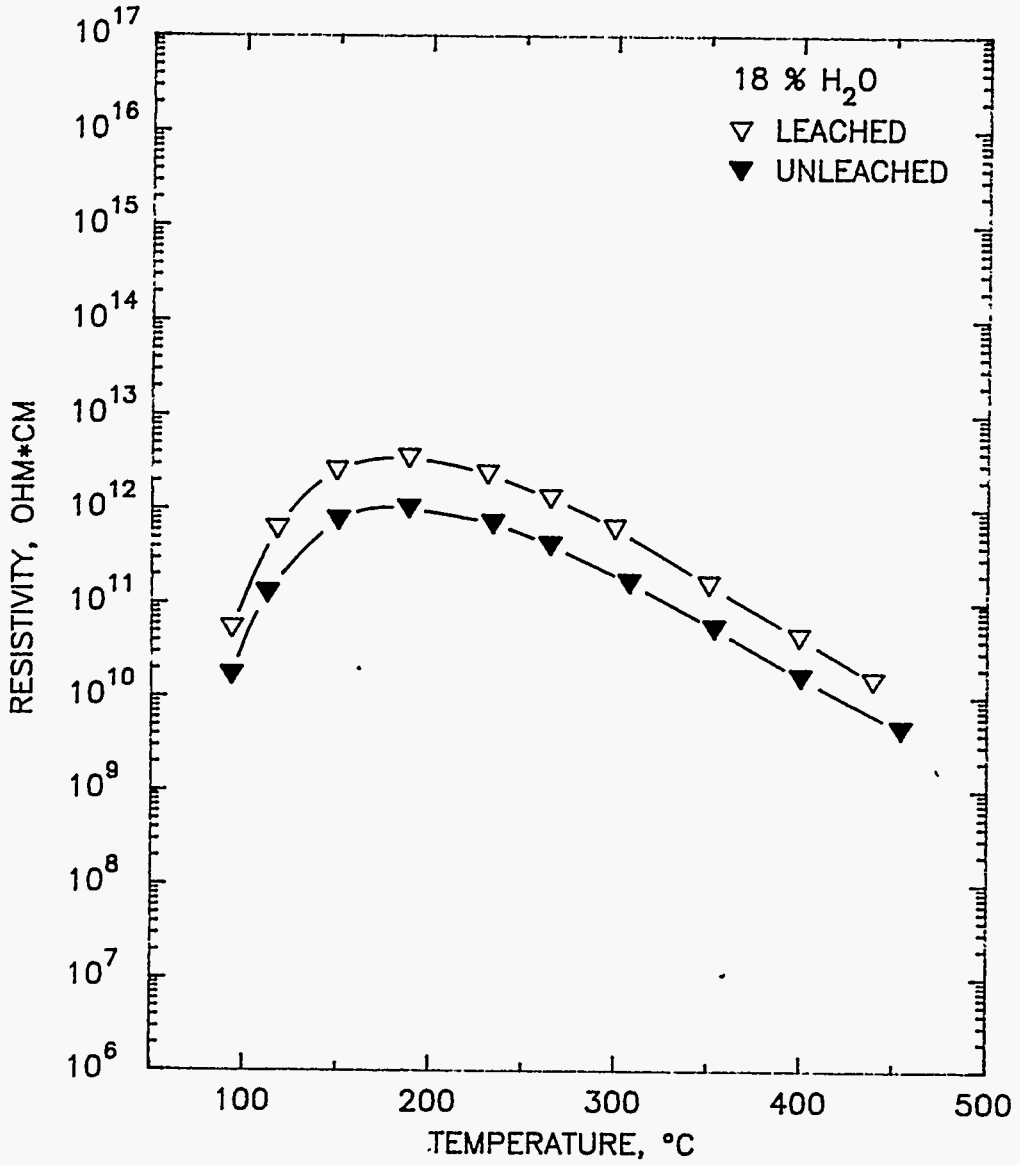

Figure 4-20. Leached (ID # 2029-W) and unleached (ID # 2029) Monticello dustcake ash resistivity as a function of temperature during descending-temperature resistivity determinations made in a moist (18 % water) environment.

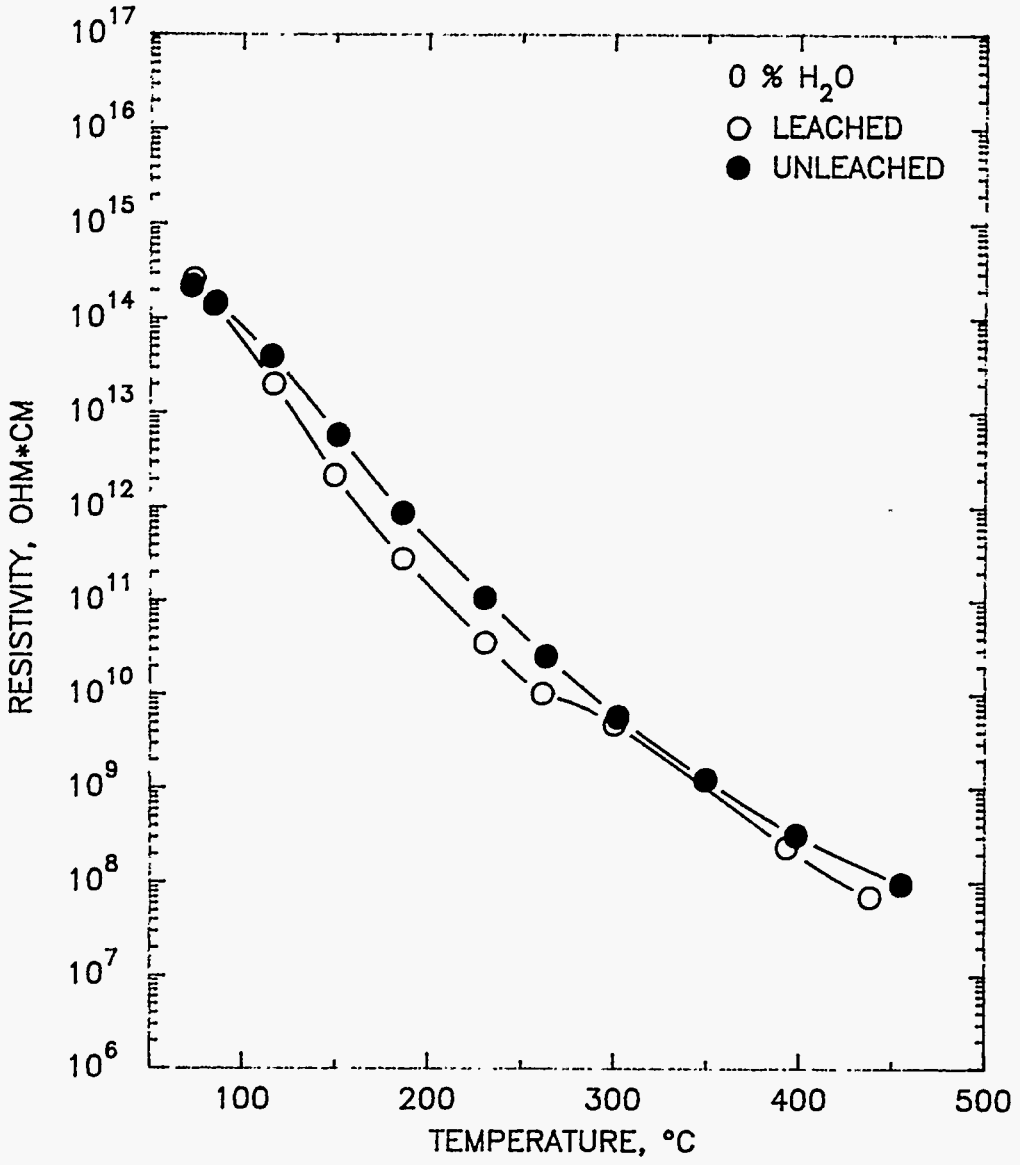

Figure 4-21. Leached (ID # 2101-W) and unleached (ID # 2101) Scholz dustcake ash resistivity as a function of temperature during descending-temperature resistivity determinations made in a dry (0 % water) environment.

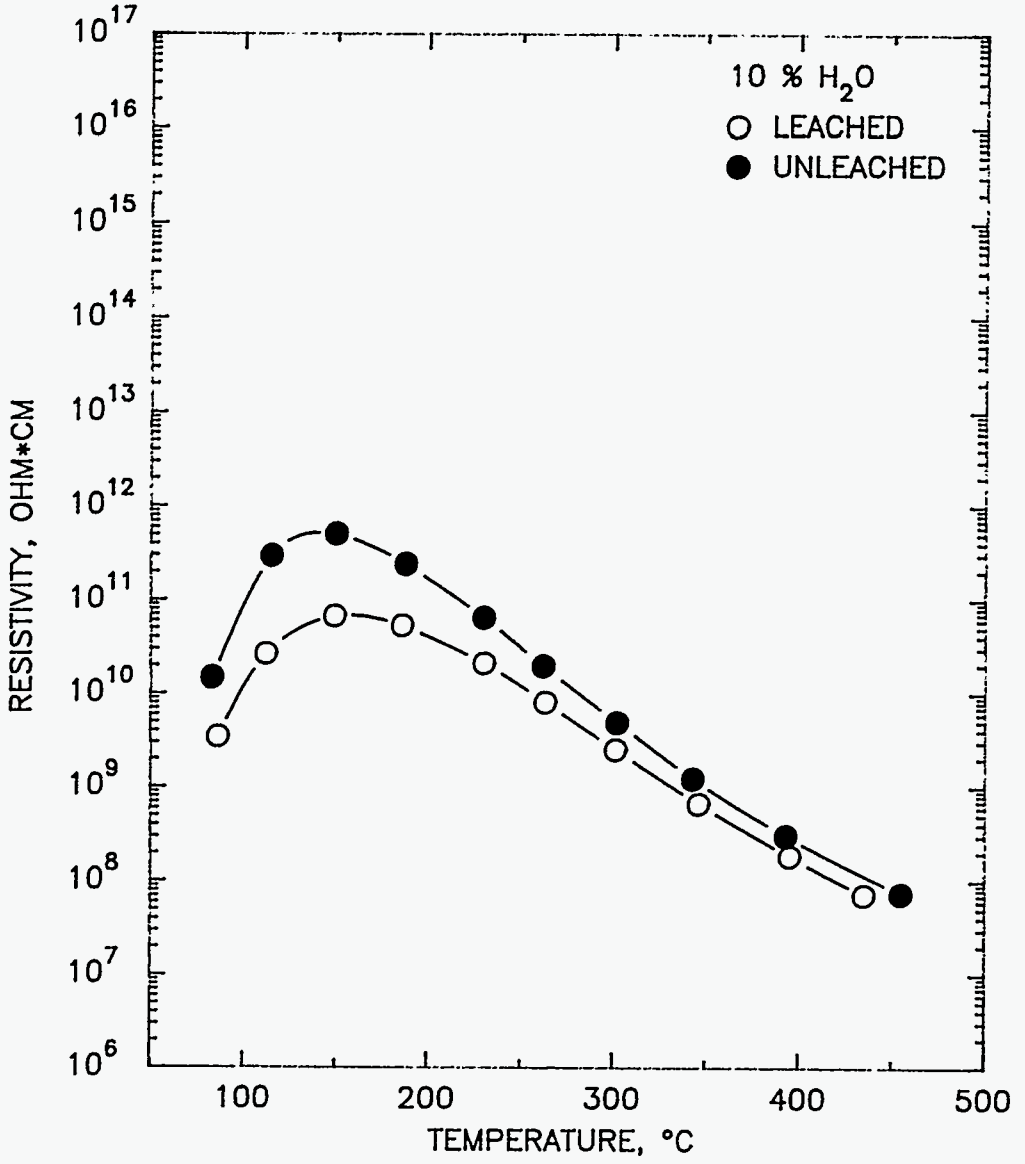

Figure 4-22. Leached (ID # 2101-W) and unleached (ID # 2101) Scholz dustcake ash resistivity as a function of temperature during descending-temperature resistivity determinations made in a moist (10 % water) environment.

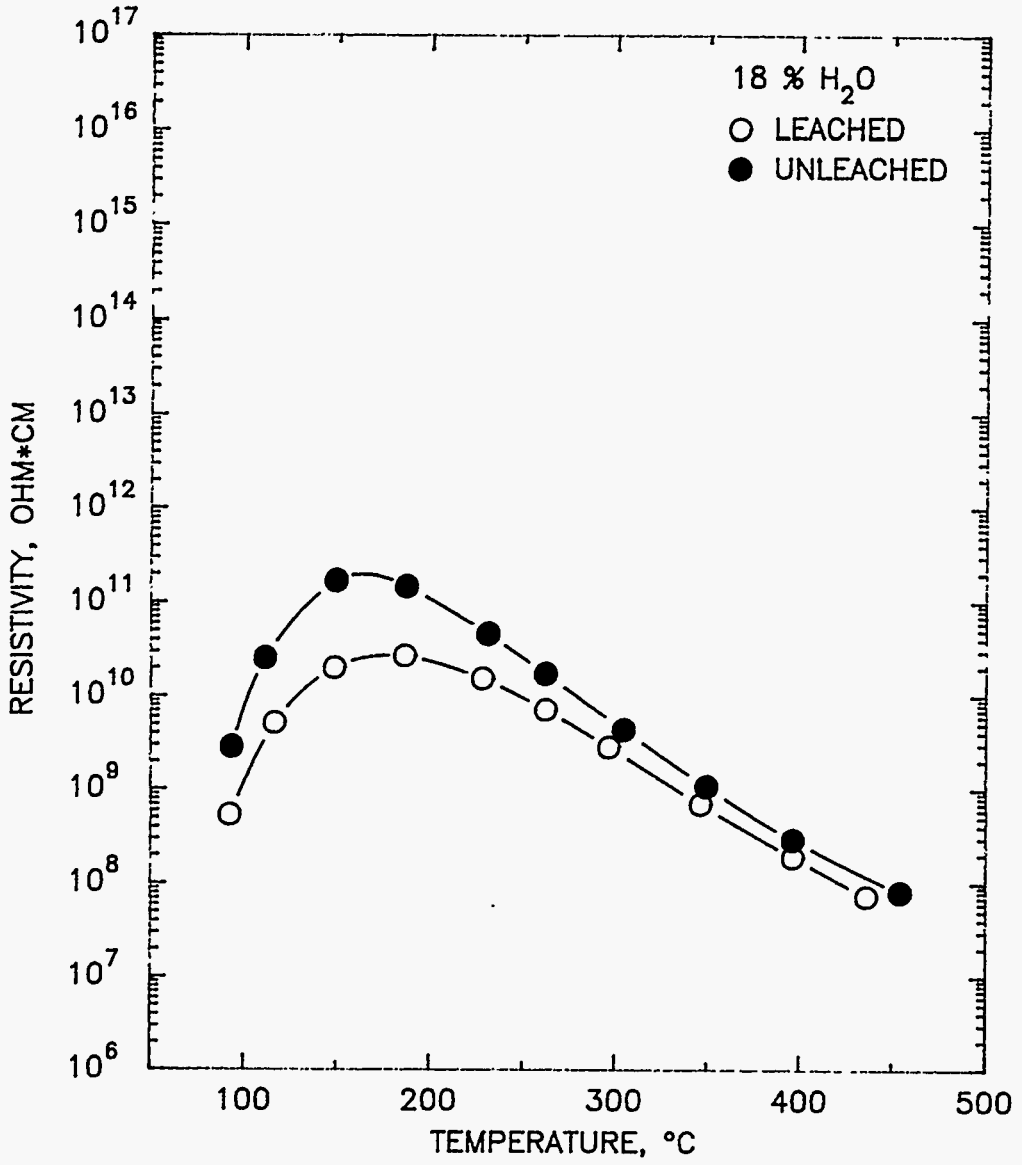

Figure 4-23. Leached (ID # 2101-W) and unleached (ID # 2101) Scholz dustcake ash resistivity as a function of temperature during descending-temperature resistivity determinations made in a moist (18 % water) environment.

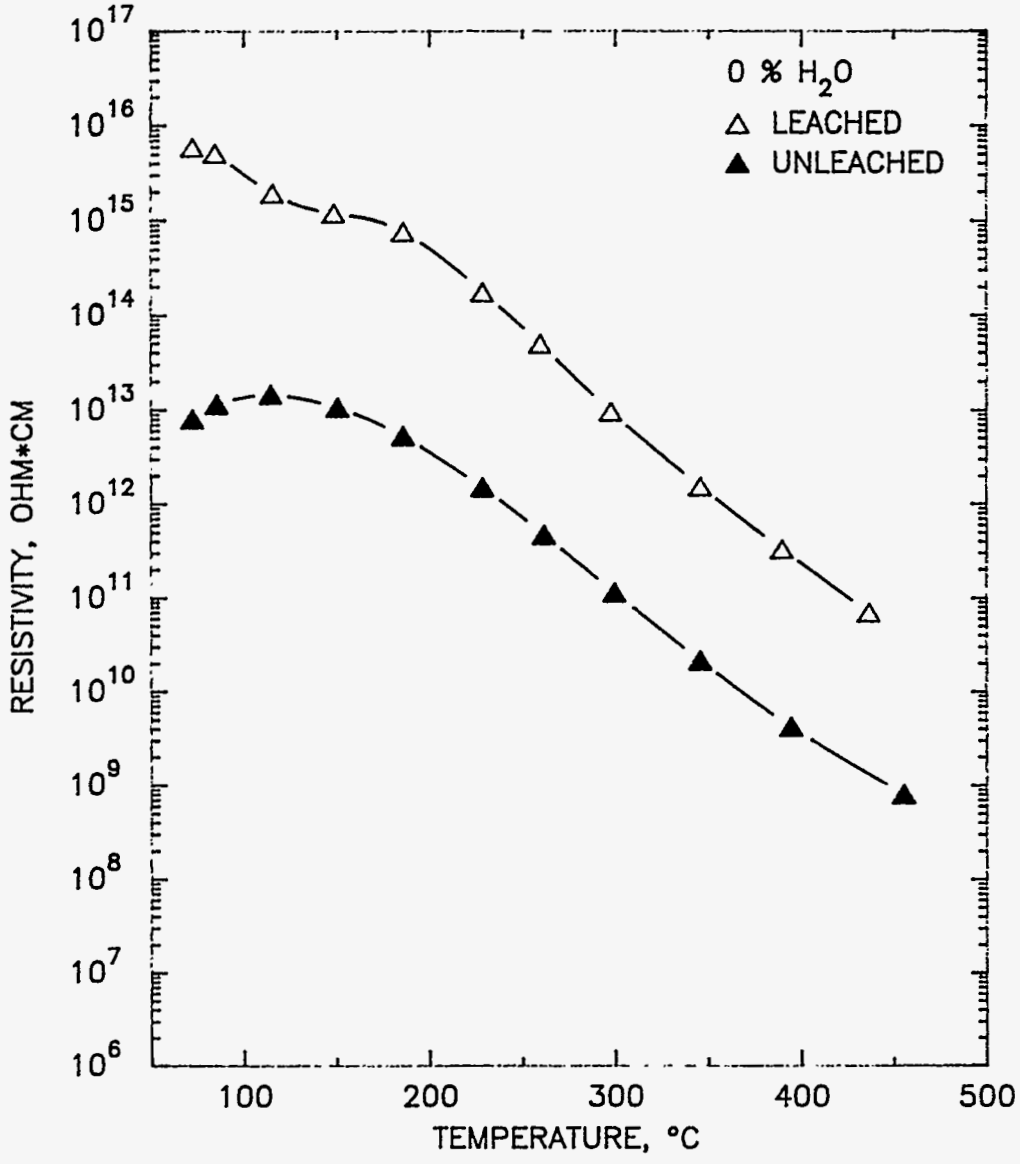

Figure 4-24. Leached (ID # 2515-W) and unleached (ID # 2515) Harrington dustcake ash resistivity as a function of temperature during descending-temperature resistivity determinations made in a dry (0 % water) environment.

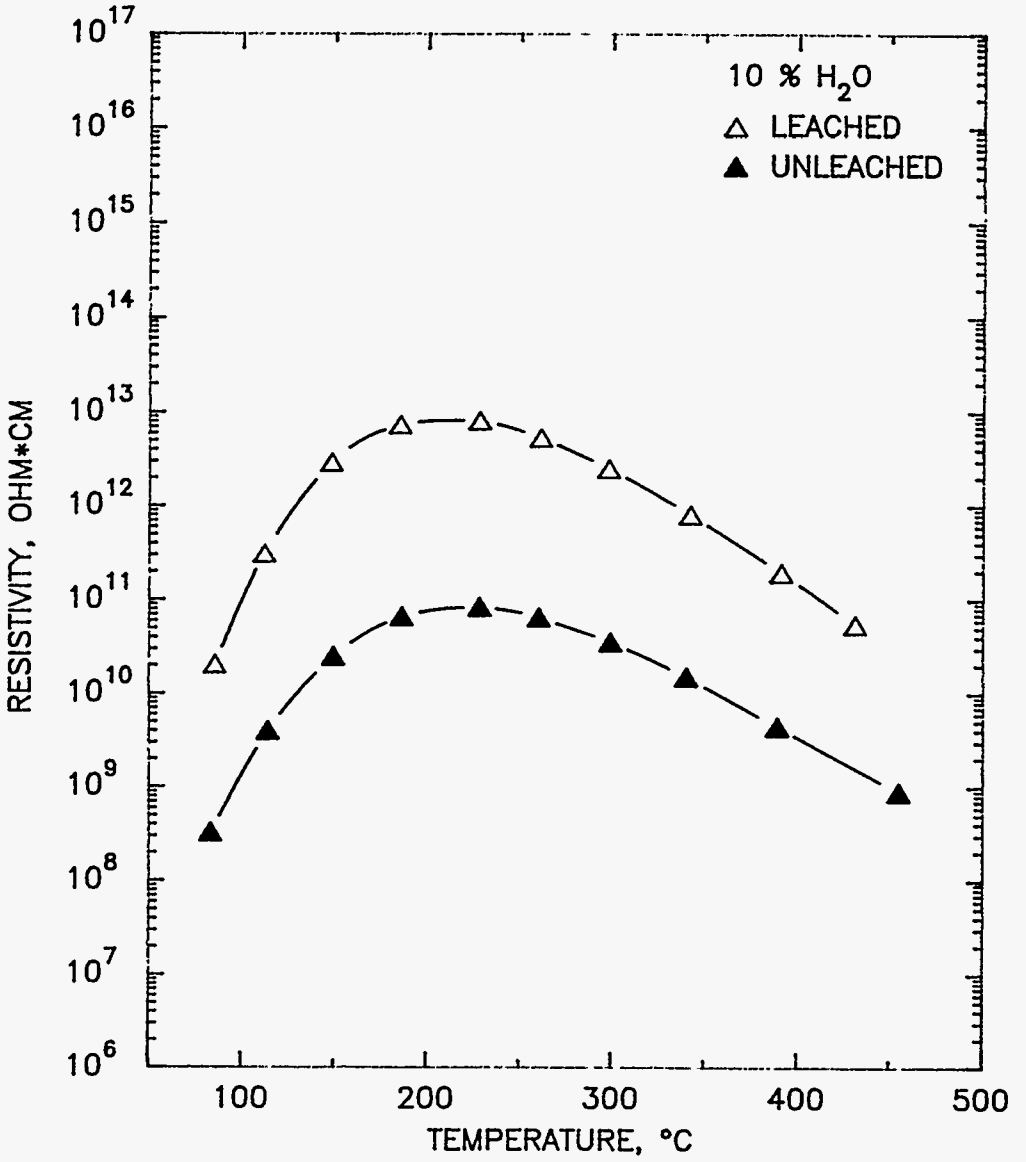

Figure 4-25. Leached (ID # 2515-W) and unleached (ID # 2515) Harrington dustcake ash resistivity as a function of temperature during descending-temperature resistivity determinations made in a moist (10 % water) environment.

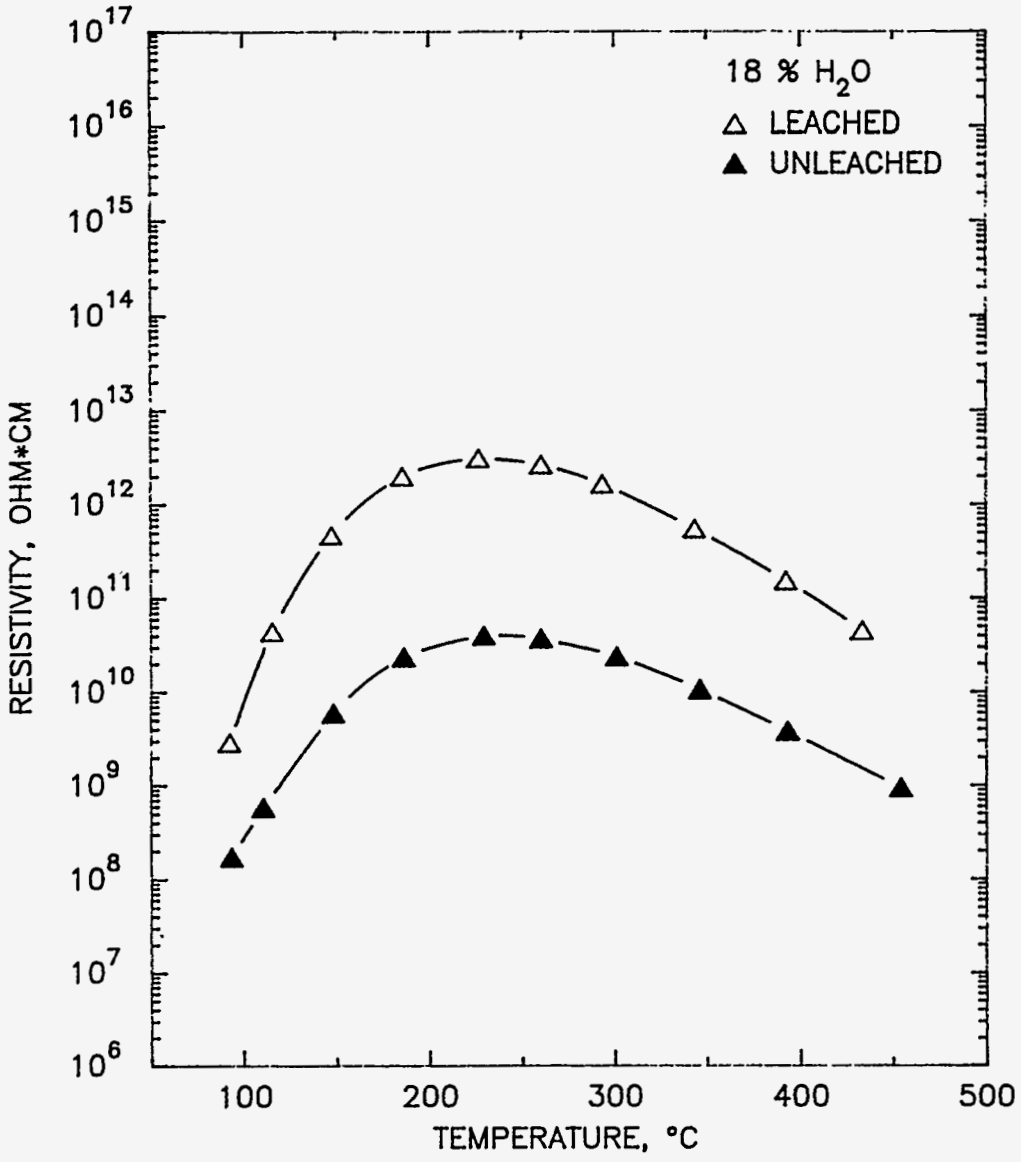

Figure 4-26. Leached (ID # 2515-W) and unleached (ID # 2515) Harrington dustcake ash resistivity as a function of temperature during descending-temperature resistivity determinations made in a moist (18 % water) environment.

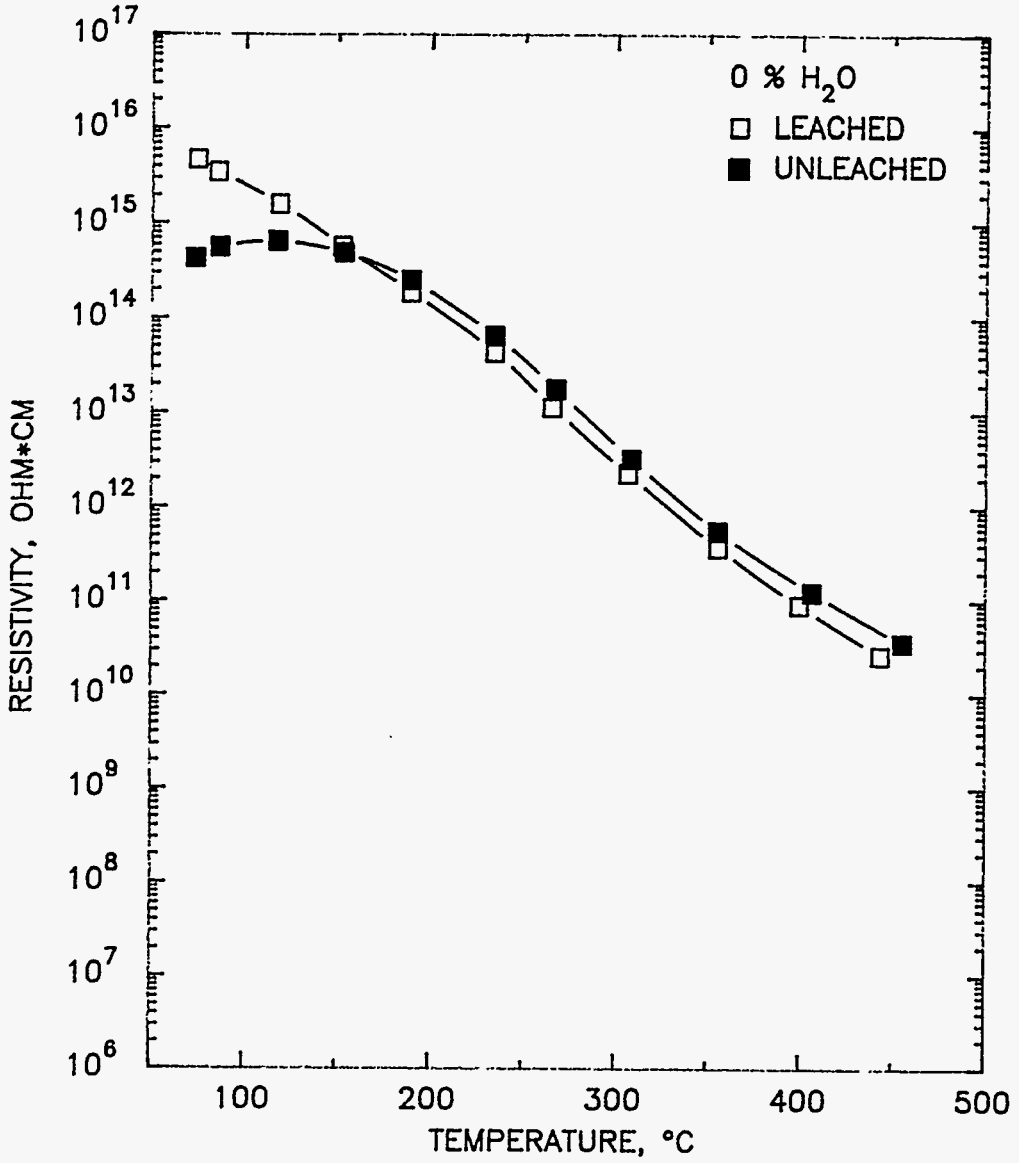

Figure 4-27. Leached (ID # 1994-W) and unleached (ID # 1994) AFBC dustcake ash resistivity as a function of temperature during descending-temperature resistivity determinations made in a dry (0 % water) environment.

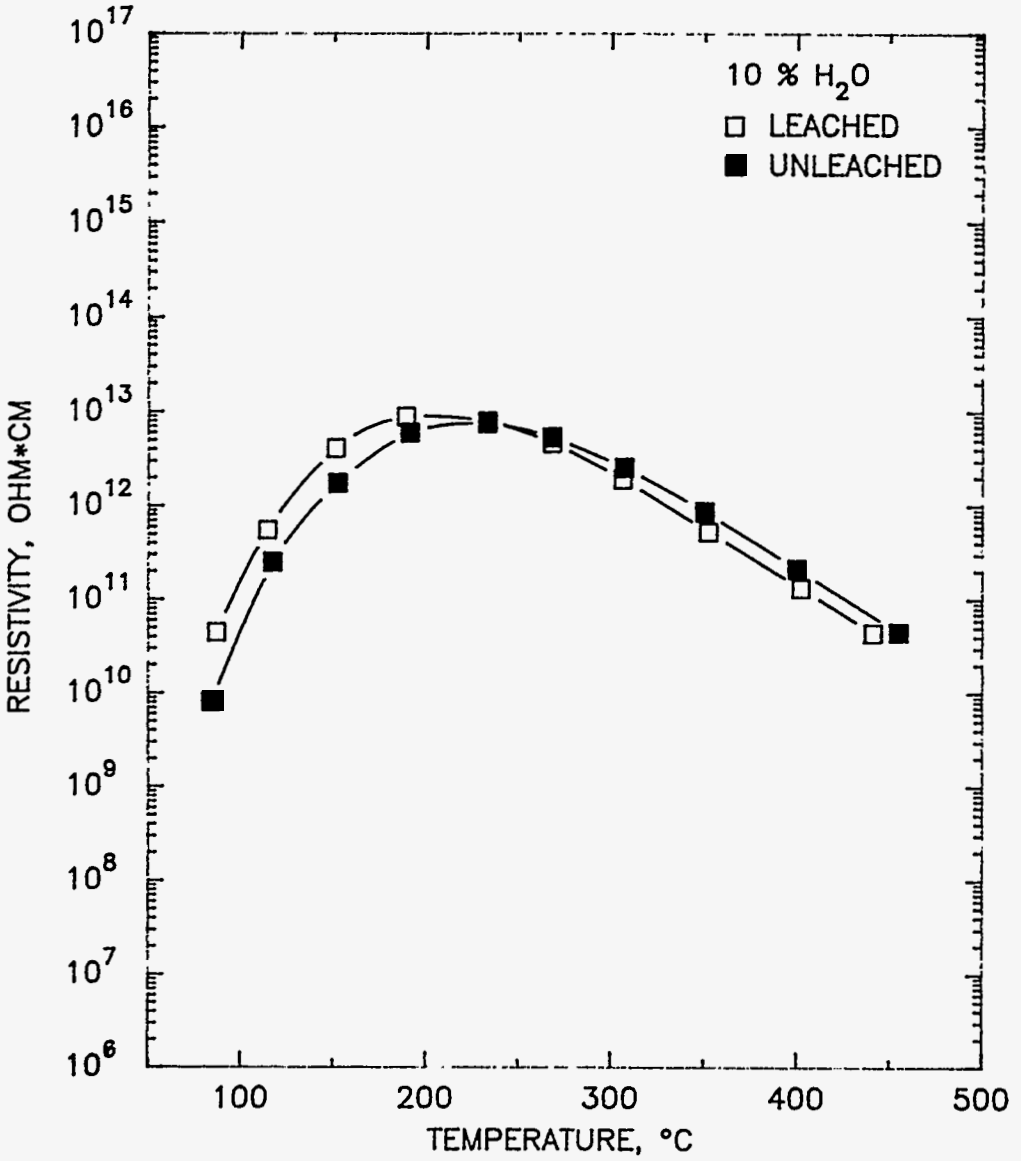

Figure 4-28. Leached (ID # 1994-W) and unleached (ID # 1994) AFBC dustcake ash resistivity as a function of temperature during descending-temperature resistivity determinations made in a moist (10 % water) environment.

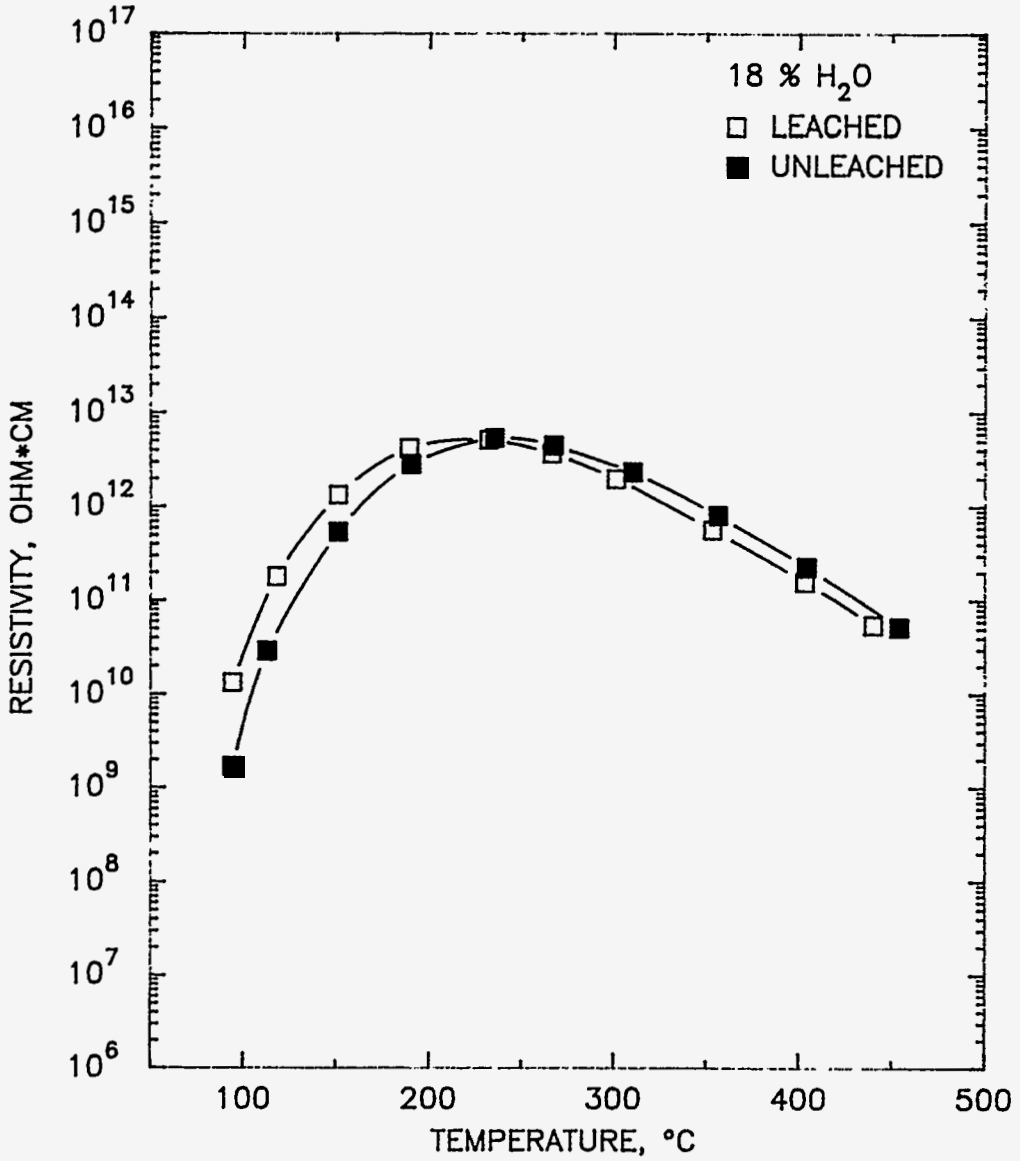

Figure 4-29. Leached (ID # 1994-W) and unleached (ID # 1994) AFBC dustcake ash resistivity as a function of temperature during descending-temperature resistivity determinations made in a moist (18 % water) environment.

with Karl Fischer titration also demonstrate about an order of magnitude increase in water content of leached ash in comparison with unleached ash. We postulate that pozzolanic reactions occur, binding water with ash to form hydrocalcium silicates. This cement-like material is very stable. The apparent reduction in volume conductivity of Harrington ash caused by leaching can be attributed to formation of these hydrocalcium silicates. Calcium ions which are available for charge transfer in unleached ash form hydrogen bonds with water during leaching. This bonding may inhibit charge transfer that the calcium would otherwise be available for, thereby significantly decreasing volume conduction. We believe that, on a reduced scale, a similar process occurs with Monticello ash.

Leaching produced quite unexpected results for measured resistivities of Scholz ash. Although leaching removed Na^+, SO_3 and $SO_4^=$ from particle surfaces, resistivity at the lower temperature range (where surface conduction is dominant) was *decreased* by about one order of magnitude. At higher temperatures reduction in resistivity was not as pronounced. Several factors may have influenced this behavior. Bickelhaupt (1975) has stated that resistivity can be expected to decrease when surface area increases because of increased water adsorption. Our data support this statement. Leaching increased the specific surface area of Scholz ash from 3.0 to 8.3 m^2/g. A decrease in the resistivity of leached Scholz ash was measured only when samples were conditioned and tested in moist environments, and the difference in the resistivities of leached and unleached Scholz ashes became less significant as ash temperature increased. (However, an even larger increase in surface area, from 1.5 to 7.1 m^2/g, for Harrington ash was accompanied by an *increase* in resistivity for moist and dry samples.) Another change in Scholz ash caused by leaching was the decrease in cohesivity of leached ash. A loosely packed bulk sample of leached Scholz ash would be less porous, and contain more contact points, than a similar sample of unleached Scholz ash. (Resistivity is measured for loosely packed samples of ash.) More contact points may promote better surface and volume conduction. A third possibility for increased surface conduction for leached Scholz ash is rearrangement and deposition of soluble salts on the particle surfaces and especially at contact points between particles. Although the leaching technique we used removed the vast majority of soluble compounds from the particle surfaces, enough salts may accumulate when the sample was being dried following the leaching procedure to build salt bridges between particles. If conductivity of this bridge was sufficiently high, electrical conduction between particles could be significantly enhanced. A crystalline salt was found in large quantities in the first few leachate samples from the leaching of Scholz ash. Because of its golden color and crystalline structure, we believe this salt to be $Fe_2(SO_4)_3$. If this compound were present in increased concentrations at contact points between particles in leached ash, or if some type of matrix of highly conductive salt were deposited in a film-like structure on the particles, surface conduction might improve. We are not able to say which, if any, of these mechanisms explain Scholz resistivity data.

The only increase in the resistivity of AFBC ash caused by leaching was for very dry ash at very low temperatures. AFBC resistivity data tend to support the argument relating reduced

volume conduction in leached Harrington ash to the presence of hydrocalcium silicates. Because of the high concentration of calcium in AFBC ash, similar pozzolanic reactions could occur with this ash. Resistivities of leached Harrington and leached AFBC ashes are very similar at all three moisture contents.

The resistivity prediction model that Southern Research Institute developed for the U. S. Environmental Protection Agency was run for leached and unleached dust cake ashes from Scholz, Monticello, and Harrington. Mineral analyses of the samples from Table 4-7 were used as the inputs to the model. Predicted relationships between temperature and resistivity in an environment containing 10 % water were compared with data measured for Scholz and Monticello ashes (Figures 4-30 and 4-31). These comparisons show that the model does not accurately predict resistivity for these ashes. Predicted resistivity data for Harrington also differed significantly from measured values.

We measured the resistivity of the Kintigh base line ash (ID # 2884), diatomaceous earth (ID # 2769), the alumina powder (ID # 2874), and the aluminosilicate powder (ID # 3238) at three different moisture levels. These data are presented in Figures 4-32 through 4-35. As with the resistivity measurements of the leached and unleached dust cake ashes, the effect of water adsorption can be clearly seen for each of these samples. The resistivity data measured for the Kintigh base line ash is typical for high-sulfur coal ashes. The diatomaceous earth and the aluminosilicate powder have relatively low resistivities. Because the alumina powder is 99.9 % pure Al_2O_3, there are essentially no charge carriers, such as sodium ions, on the dry alumina powder particles. This absence of charge carriers makes the resistivity of the dry alumina powder quite high. As with the other samples, adsorbed water significantly improves current conduction on the surfaces of the alumina particles.

As stated in the summary of the literature review, resistivity plays a crucial role in determining the conditions for electrostatic reentrainment. Part of our pilot-scale tests, which are discussed in Section 5, were directed towards a detailed examination of this phenomenon. As part of these analyses, we measured the resistivities of ashes collected during these pilot-scale tests. These resistivity data are presented and discussed in Section 5 along with the rest of the pilot-scale test data.

4.3.6 Laboratory Conditioning with Organosiloxane and SO_3

We designed a series of tests to determine if the characteristics of ashes or powders could be significantly altered by the surface deposition of silanes or SO_3. Our literature review indicated that deposition of silanes on particle surfaces should make these surfaces more hydrophobic. Our literature review and our laboratory examinations of the effects of soluble $SO_4^=$ indicated this compound promotes the adsorption of water onto particle surfaces. To verify these effects for the types of ashes and powders we had in our data base, we conditioned

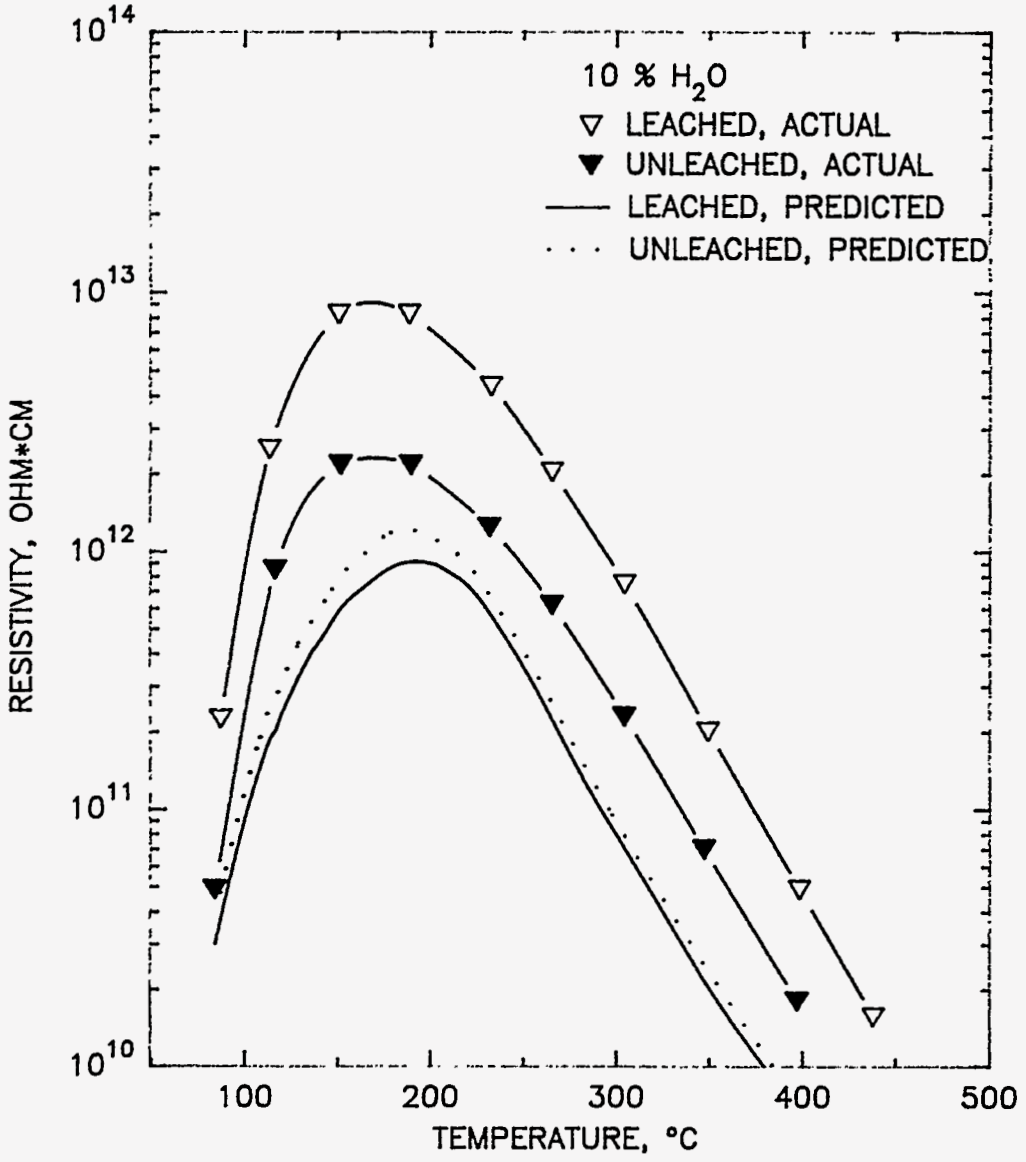

Figure 4-30. Measured and predicted values of ash resistivity of leached (ID # 2029-W) and unleached (ID # 2029) Monticello dustcake ashes in a moist (10 % water) environment.

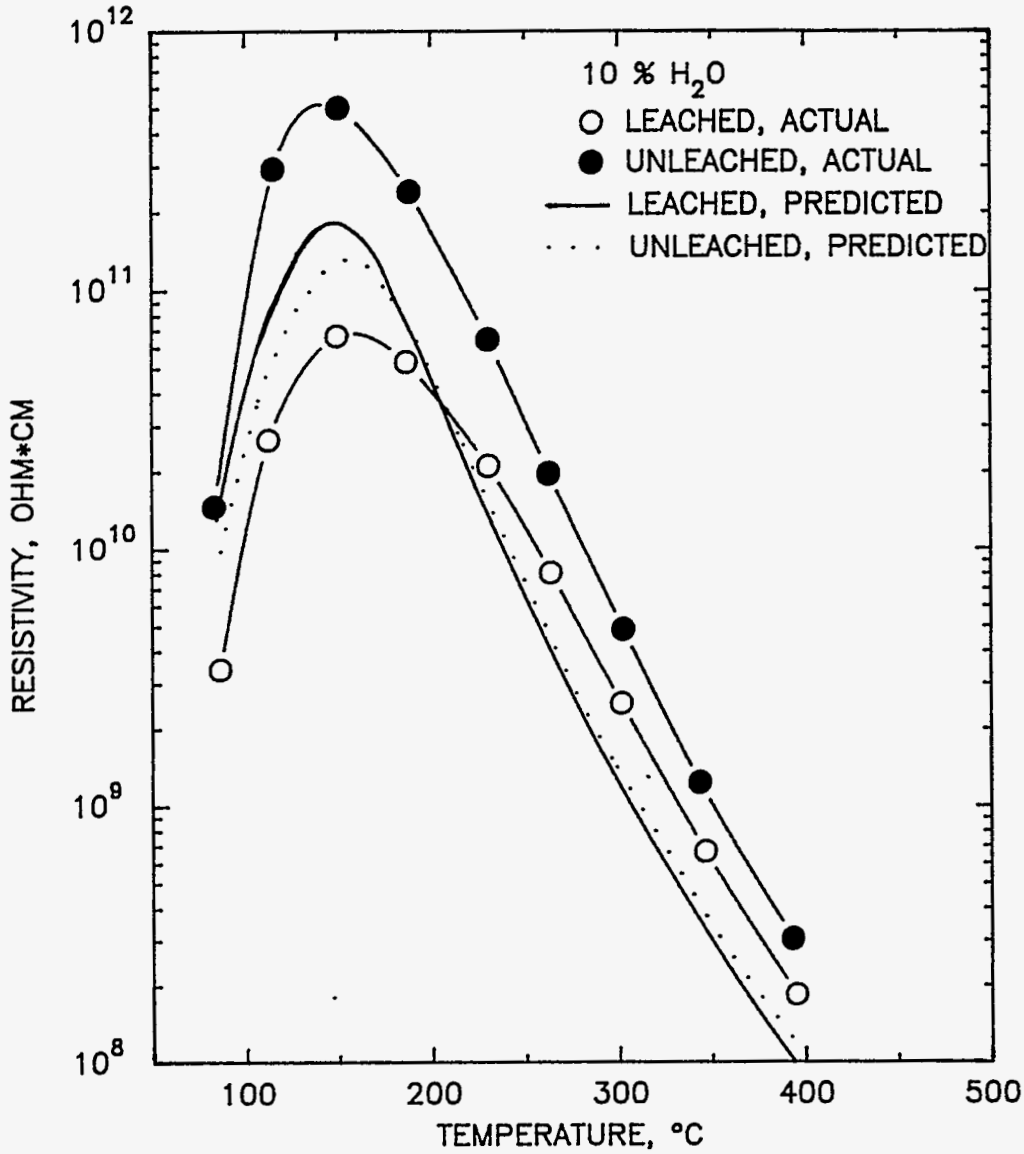

Figure 4-31. Measured and predicted values of ash resistivity of leached (ID # 2101-W) and unleached (ID # 2101) Scholz dustcake ashes in a moist (10 % water) environment.

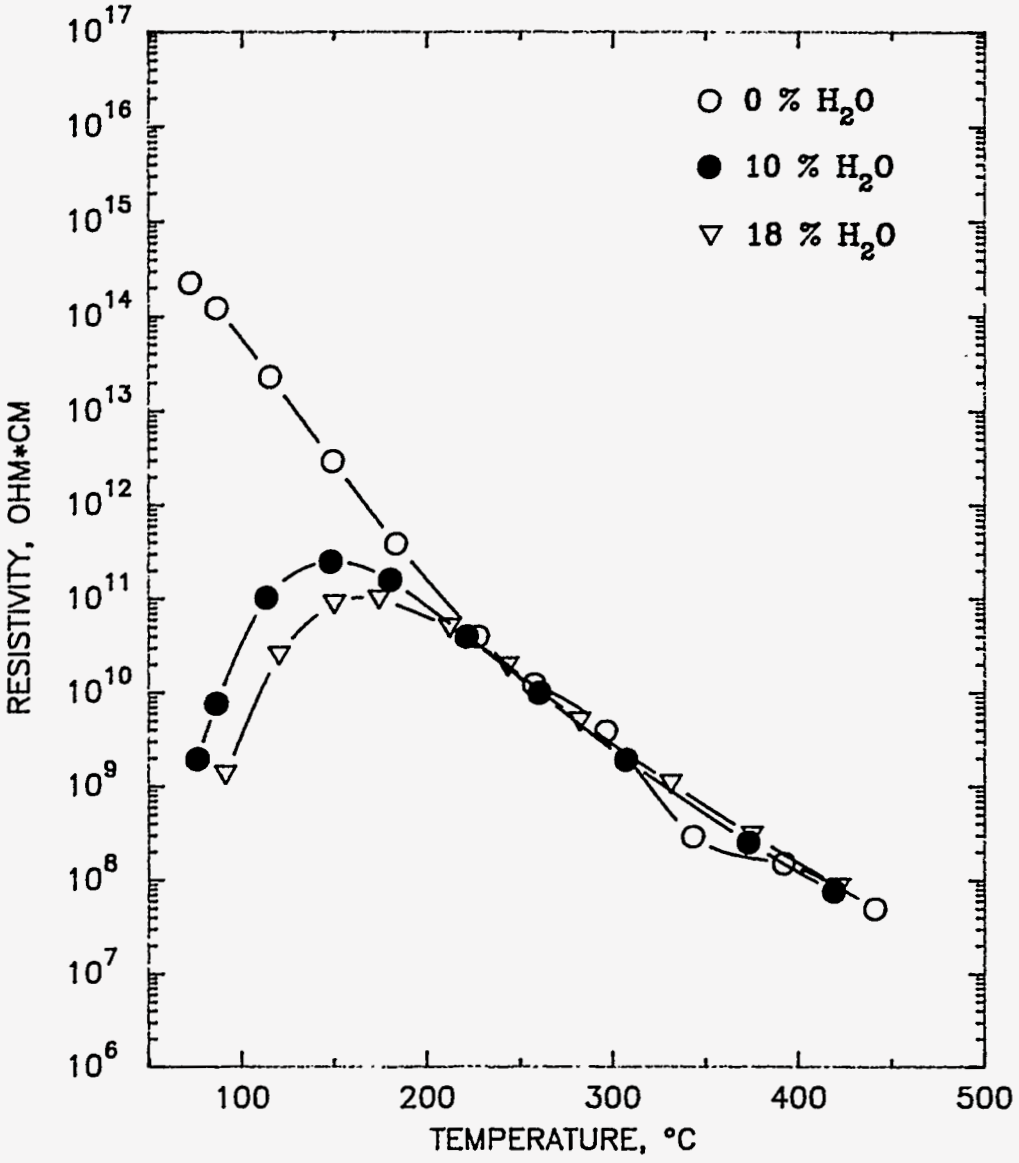

Figure 4-32. Resistivity of the Kintigh base line ESP hopper ash (ID # 2884) as a function of temperature during descending-temperature resistivity determinations made in environments with three different moisture levels.

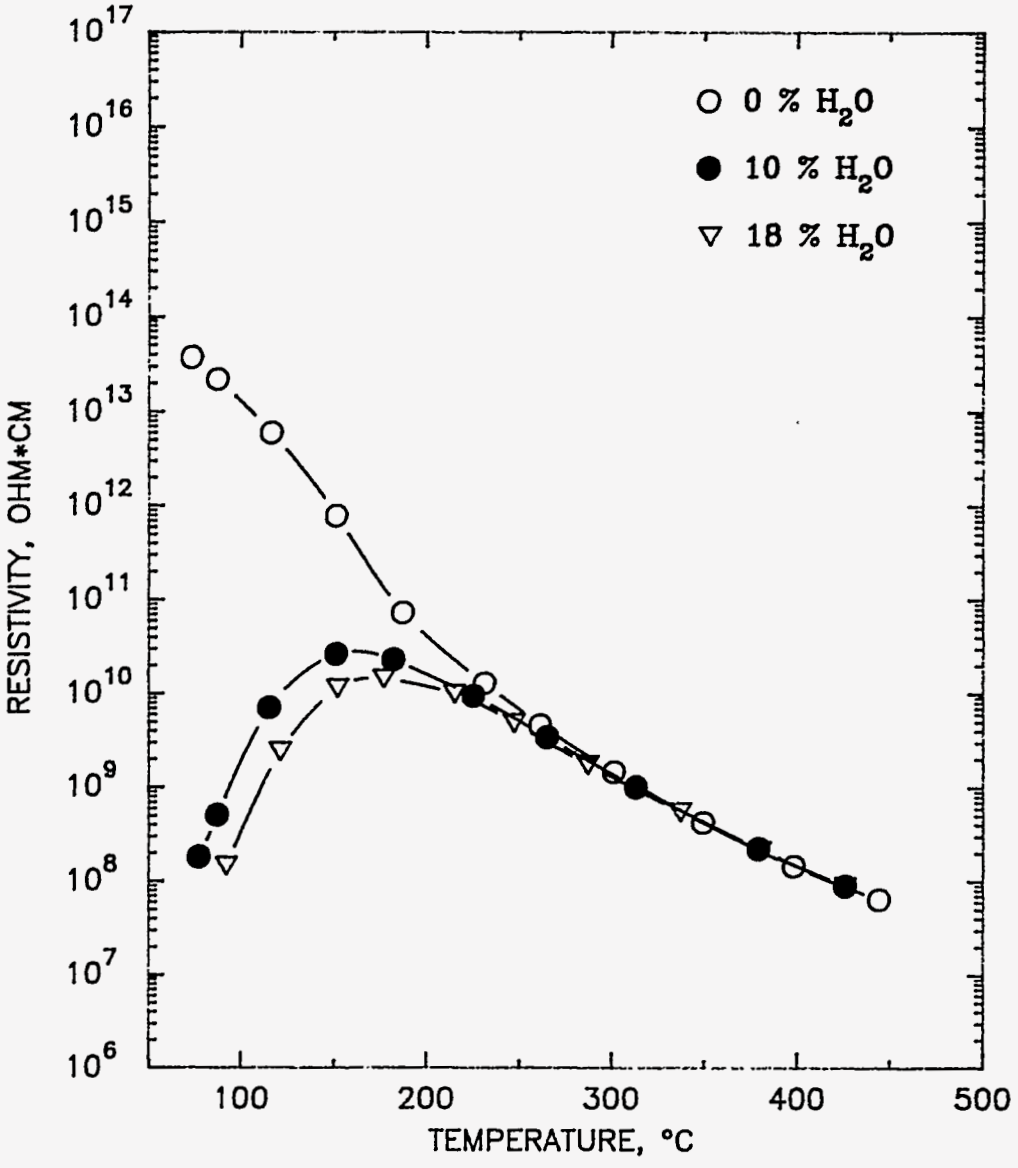

Figure 4-33. Resistivity of the diatomaceous earth (ID # 2769) as a function of temperature during descending-temperature resistivity determinations made in environments with three different moisture levels.

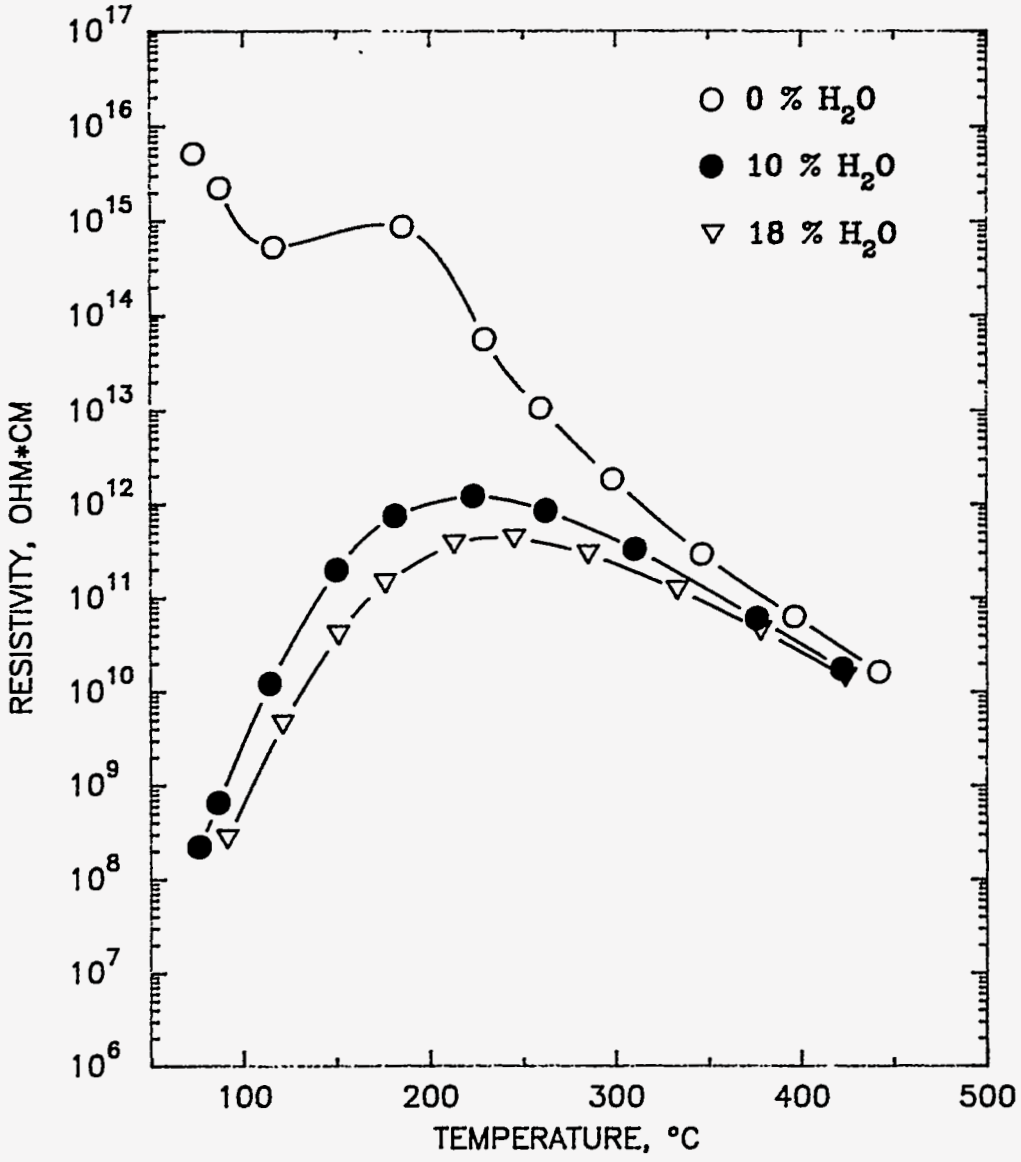

Figure 4-34. Resistivity of the alumina powder (ID # 2874) as a function of temperature during descending-temperature resistivity determinations made in environments with three different moisture levels.

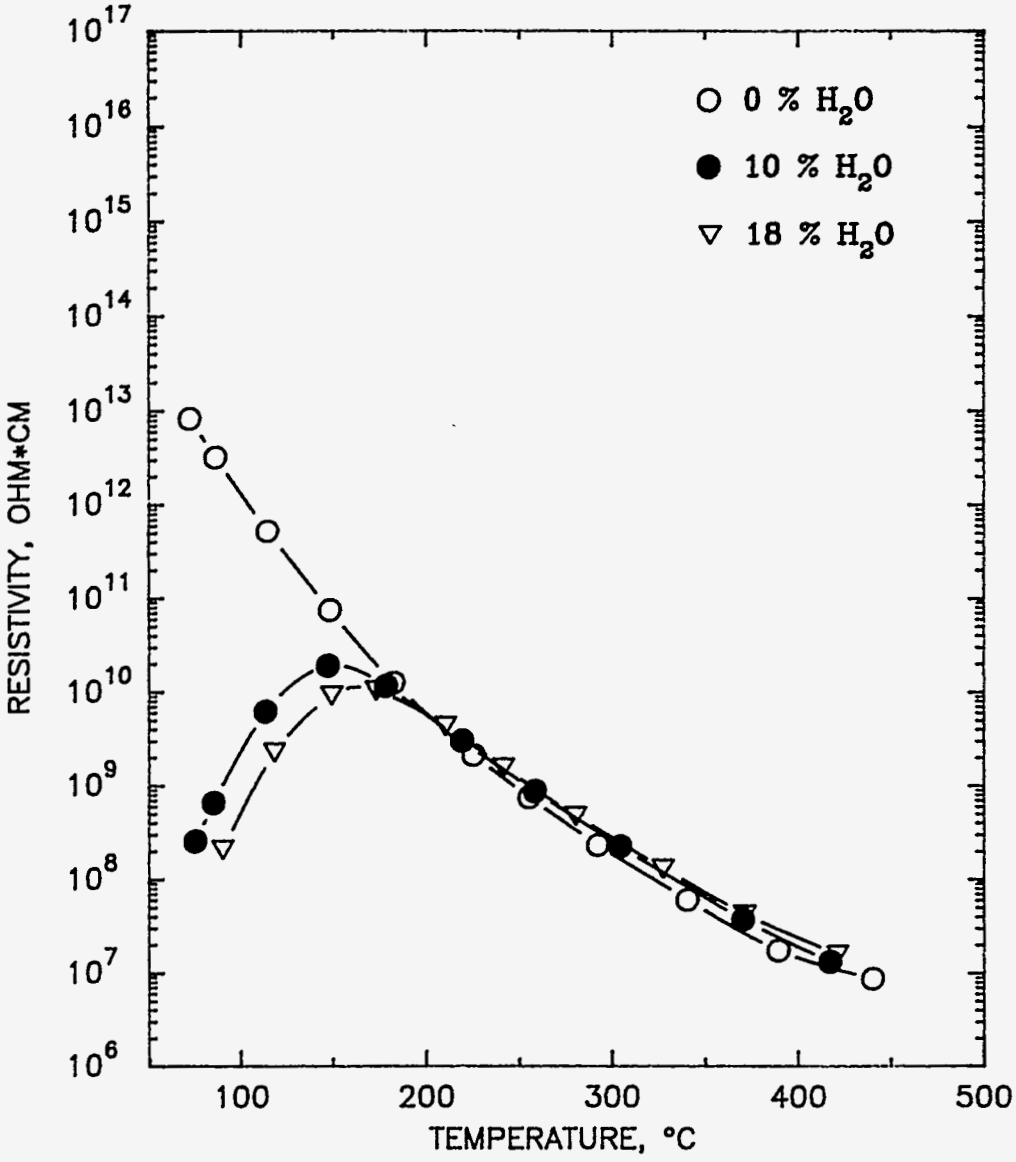

Figure 4-35. Resistivity of the aluminosilicate powder (ID # 3238) as a function of temperature during descending-temperature resistivity determinations made in environments with three different moisture levels.

selected ashes and powders with organosiloxane and SO_3. The organosiloxane we used was a type of silanizing agent marketed for the treatment of glassware.

We conditioned eight ashes and powders with organosiloxane. To condition these samples we mixed 1 part by weight of organosiloxane concentrate with 100 parts by weight of sample in a water slurry. The mixture was stirred for 15 minutes, filtered, and then oven baked to remove excess water. The samples we prepared in this manner are listed in Table 4-1 and are identified by the suffix *-S* at the end of the sample ID #. Because alumina tends to pick up relatively large amounts of water of hydration during exposure to excess water, suspending this powder in a water/organosiloxane slurry may have obscured data on water adsorption measured for this sample. Although Harrington and AFBC ashes also tend to pick up relatively large amounts of water by hydration during exposure to excess water, the samples of Harrington and AFBC ash (ID #'s 2515-L and 1994-L) that we conditioned with organosiloxane were already exposed to excess water during the leaching process.

We selected twelve samples for conditioning with SO_3. Our conditioning system generated SO_3 vapor by the passage of metered, dry N_2 over a container of heated, fuming sulfuric acid. Several trials were made to establish a concentration of SO_3 between 10 and 30 ppm. We settled on a final concentration of 24 ppm SO_3 in our conditioning gas stream. The conditioning process passed this SO_3-laden gas stream through a porous bed of the powder or ash to be conditioned and then on through a water bath to absorb any excess SO_3. The samples we prepared in this manner are listed in Table 4-1 and are identified by the suffix *-A* at the end of the sample ID #.

After conditioning the selected samples, we characterized the effect of relative humidity on their adsorption of water and relative cohesivities (assessed with uncompacted bulk porosity and tensile strength measurements). We also measured the specific surface areas of the samples conditioned with organosiloxane. We compared these data with data obtained for unconditioned samples. The reader is directed to reexamine Table 4-12 (water contents), Table 4-14 (uncompacted bulk porosities), and Table 4-15 (tensile strengths) as needed to supplement this discussion.

Conditioning with organosiloxane did not have much effect on the amounts of water adsorbed by the various samples tested (Table 4-12). The only sample we conditioned with organosiloxane that had consistently higher water contents after the conditioning process was the alumina powder (ID # 2874). However, because of the tendency for Al_2O_3 molecules to form hydrates with one, two, or three times as many molecules of water, we believe the elevated water contents of sample 2874-S are due to the exposure of the sample to the water used to dilute the organosiloxane and suspend the powder particles during conditioning.

The deposition of organosiloxane onto particle surfaces did affect the cohesivity of two of the samples (ID #'s 1856-S and 2515-L-S). Both of these samples exhibited higher values of

uncompacted bulk porosity (see Table 4-14) after being conditioned with organosiloxane. We attribute these changes to the increased hydrophobicity of the particle surfaces. As the surfaces became more hydrophobic, even small amounts of water were easily concentrated at particle-to-particle contact points, resulting in the formation of liquid bridges.

Conditioning with organosiloxane decreased the uncompacted bulk porosity of the alumina powder. Possibly the particle morphology of the alumina powder and the hydration of water account for this behavior. The alumina particles (mean size 45 μm) appear to be agglomerates of smaller (approximately 1 μm) particles. (See Figure 4-11 for SEM photographs of this sample.) If it is true that the conditioning process caused the Al_2O_3 molecules to bind with up to three molecules of water, this would increase the molecular weight of the resulting compound by over 50 %. The morphology of the alumina powder we used might allow this water to be located in the large pores within the coarser agglomerated alumina particles. Therefore the density of the alumina might have increased significantly without altering the external shape of the particle very much. This type of change would result in lower values of uncompacted bulk porosity, like those we measured for this sample. This explanation is supported by the tensile strength of the alumina powder conditioned with organosiloxane. This type of conditioning had little, if any, effect on the tensile strength of the alumina powder. (Tensile strength should not be affected by changes in particle density.)

Conditioning with SO_3 had the greatest effect on Harrington ash (ID # 2515-A), increasing water content by 7 to 8 times. Apparently the high calcium content of the Harrington ash does not alter the hydrophilic nature of the SO_3 adsorbed on the surfaces of the ash particles. Although the unconditioned Monticello ash (ID # 2029) might be expected to react to SO_3 conditioning in much the same way as the Harrington ash, no significant increase in water content was measured for this ash. Possibly high silica content, or the way the calcium is bound within the Monticello ash particles may explain this difference. Another distinct possibility is that the adsorbed SO_3 subsequently caused more water to be adsorbed, but that this water has combined with the adsorbed SO_3 to form sulfuric acid, from which the water is extremely difficult to remove. For the AFBC ash (ID # 1994-A), either its high calcium content, and/or its particle morphology prevented adsorbed SO_3 from increasing overall water content significantly. The formation of sulfuric acid on the surfaces of the AFBC ash particles is less likely because of the high calcium content of this ash. We measured less adsorbed water for the Scholz ash conditioned with SO_3 (ID # 2101-A) than for its unconditioned counterpart. This is probably due to the formation of sulfuric acid on the particle surfaces as described above.

The only significant change we measured in the amount of water adsorbed by powders conditioned with SO_3 was for the aluminosilicate powder (ID # 3238-A) at low relative humidities. We believe the SO_3 deposited on the surfaces of the particles may combine with adsorbed water to form sulfuric acid. As discussed above, this formation may limit the

amount of water detected by the Karl Fischer device. We cannot be certain if this type of effect is masking enhanced water adsorption by the other powders we conditioned with SO_3.

Conditioning with SO_3 apparently caused some changes in the cohesivity of several of the samples. One unexpected result was obtained with the alumina powder (ID # 2874). Conditioning with SO_3 lowered the uncompacted bulk porosity of this powder across the range of relative humidities tested. We are not certain what mechanism is responsible for this apparent drop in the cohesivity of this powder. The cohesivity of unleached Monticello dust cake ash (ID # 2029) increased somewhat after being conditioned with SO_3. We attribute the small increase in the uncompacted bulk porosity at 93 % RH and large increases in the tensile strength at 34 and 75 % RH to increased adsorbed water. We believe that the SO_3 promoted the adsorption of additional water, even though the Karl Fischer determinations were not able to detect it. Our tensile strength measurements were also able to detect increases in the cohesivities of the Monticello, Scholz, and Harrington leached dust cake ashes (ID #'s 2029-L, 2101-L, and 2515-L). SO_3 conditioning resulted in moderate increases in the tensile strengths of the Monticello and Scholz ashes at 34 and 75 % RH. Much larger increases in tensile strength were measured for the Harrington ash. SO_3 conditioning apparently restored the cohesivity of the leached Harrington ash to the high values it exhibited prior to being leached. This may be due to the SO_3 taking the water away from the hydrates formed with the calcium in the ash during the leaching process. It is also possible that the SO_3 caused additional water to be adsorbed, increasing the strength of the bonds between the ash particles. For all of these dust cake ashes, we believe the strong bonds between adsorbed water and the adsorbed SO_3 prevented the Karl Fischer device from detecting all of the adsorbed water.

We have not been able to correlate any of the changes in the cohesivity or water adsorption data to the measured specific surface areas (Table 4-3) of the samples conditioned with organosiloxane or SO_3. If the specific surface area data truly represent changes in the morphology of the ash and powder particles, then the chemical nature of the surfaces of these conditioned particles seems to be the predominant factor controlling the behavior of these conditioned ashes and powders.

5 PILOT-SCALE TESTS TO VERIFY THE ROLES OF ADSORBED LIQUID

We performed three pilot-scale tests designed to determine and verify the effects that adsorbed water has on fabric filtration and electrostatic precipitation of entrained fly ash particles in actual flue gas environments. Southern Research Institute's 6 million Btu/hr Coal Combustion Facility provided a valuable test location for our studies. We investigated two specific phenomena in these pilot-scale tests. The first was the ability of flue gas humidification to increase ash cohesivity through the creation of liquid bridges between particles collected in a fabric filter. Increasing cohesivity through the development of liquid bridges was demonstrated in our laboratory measurements of tensile strength and uncompacted bulk porosity, and in filtration studies performed for DOE/PETC under an earlier contract (Contract No. DE-AC22-88PC88868).

The second phenomenon we studied was the electrostatic reentrainment of previously collected ash particles in an ESP. We prepared a small ESP for use in our pilot-scale tests. Our laboratory studies showed the effects that relative humidity can have on the forces (resistivity, cohesivity, and tensile strength) that hold the collected ash on the grounded ESP plate. These laboratory studies, our literature review, and our review of field experiences indicated that severe reentrainment can occur when these three forces have been modified by changes in flue gas temperature and/or water content. Therefore we intentionally modified these factors in attempts to induce this type of electrostatic reentrainment.

5.1 DESCRIPTION OF TEST FACILITIES

5.1.1 Coal Combustion Facility

The designed firing rate of Southern Research Institute's CCF is six million Btu per hour (1.75 megawatts thermal or 0.6 megawatts electric). The design of the facility provides a close simulation of the physical processes in a full-scale utility boiler. The facility consists of a coal preparation area, a coal feeding system, a vertical refractory-lined furnace, a single up-fired burner, a horizontal convective section pass with air-cooled tube banks, a series of heat exchangers, an electrostatic precipitator, a pulse jet baghouse, and a caustic scrubber. The basic components of the CCF are shown in Figure 5-1. The furnace is a vertical, up-fired 30-foot cylinder with a 42-inch inner diameter. The vertical furnace is assembled from seven 4-foot sections, which are water-cooled shells with 6 inches of cast refractory on the inside. This refractory lining serves to ensure the proper simulation of the radiation environment found in full-scale boilers. The furnace height and diameter were chosen as a compromise to best match utility boiler residence times and gas velocities, with the pilot furnace having a gas velocity of 20 ft/s and a 1.2-s residence time through the radiant section.

The burner is designed for up-firing on coal or natural gas. A closed-circuit television camera with a control room monitor displays the view from the top of the furnace through the flame

PILOT SCALE PULVERIZED COAL COMBUSTOR

Southern Research Institute
and
Southern Company Services, Inc.

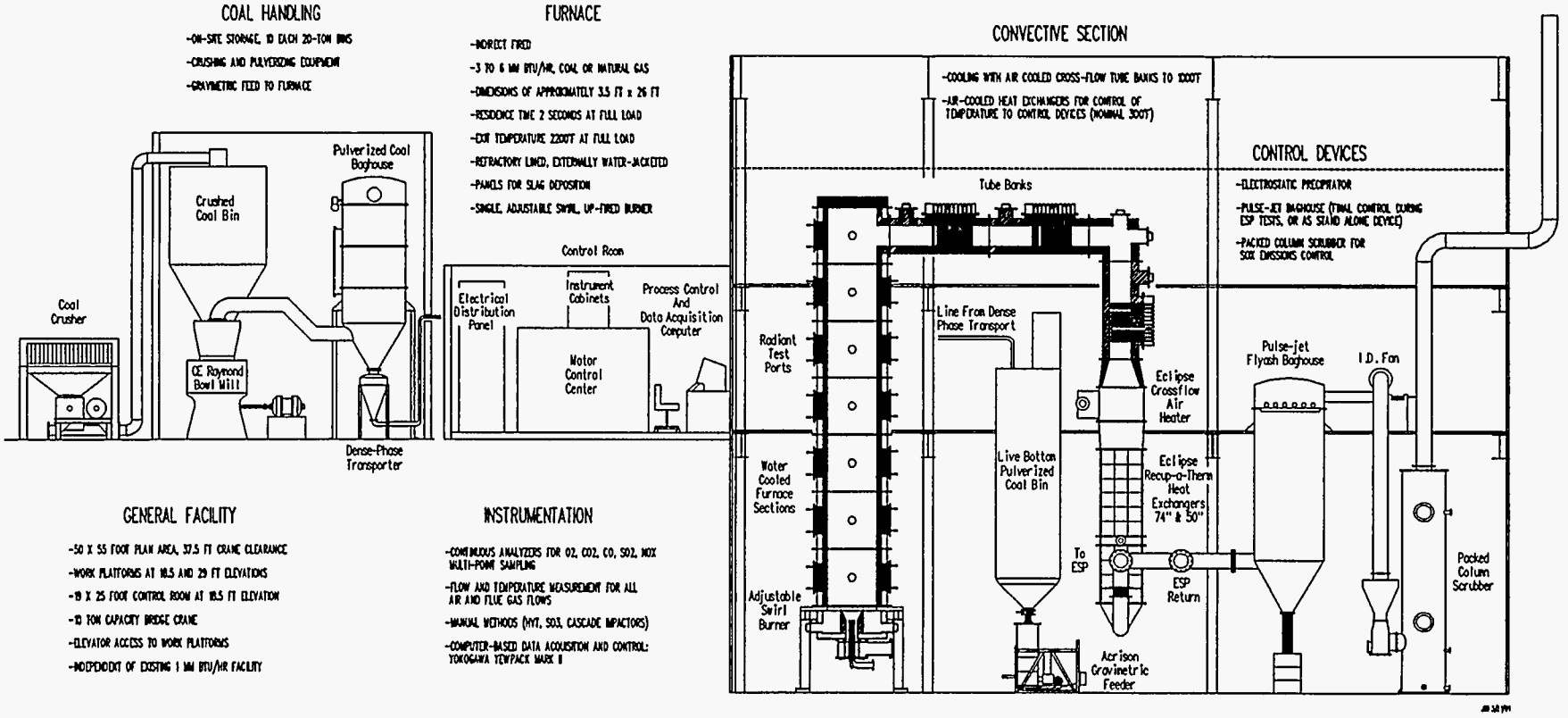

Figure 5-1. Basic components of the Coal Combustion Facility.

into the burner. This system allows continuous monitoring of the flame for stable operation. The convective section of the pilot furnace is designed to remove a substantial part of the heat from the flue gases to maintain the time-temperature profile needed to simulate that found in a utility boiler. A series of three air-cooled tube banks are installed in the upper section of the facility. Two air-to-flue-gas recuperators are used to cool the flue gas down before the gas enters the particulate control devices. The facility is controlled by a combined process control-data acquisition computer. Flue gas composition is continuously monitored by a set of gas analyzers which measure O_2, NO_X, CO, CO_2, and SO_2 levels.

5.1.2 Pilot-Scale Slipstream System

The arrangement of the major components of our pilot-scale slipstream system are shown in Figure 5-2. Flue gas extracted from the main duct of the CCF passes through a heat exchanger and a spray/steam tower to establish the desired temperature and relative humidity conditions. The flow passed through the ESP and a venturi, and into the main pulse-jet baghouse used to provide particle collection for the CCF. The venturi was being used to monitor actual flow rate through the ESP. The operation of the CCF facility was maintained such that the pressure drop between the points where we accessed the CCF process stream was sufficient to induce the desired flow of 280 acfm through the ESP. The Fabric Filter Sampling System (FFSS) that we built for DOE/PETC used its own regulated pump to withdraw about 2.5 acfm of flue gas from the conditioned stream upstream of the pilot-scale ESP.

The cylindrical spray tower we used to condition the flue gas stream was 10-ft tall and had a diameter of 36 inches. Flue gas entered at the top of the chamber. Residence time in the chamber was around 18 seconds. We were able to inject a fine spray of water droplets with a wide-angle spray, air-atomizing nozzle or wet, high-pressure steam into the chamber to add moisture to the flue gas. After leaving the lower end of the chamber the flue gas entered a transform to the ESP.

The ESP we used was a small, single field, single flow passage unit, and was only about 88 % efficient at removing the fly ash from the slipstream of flue gas. These factors aided in our characterizations of reentrainment. The ESP had six 1/8-inch diameter wires in series. Plate-to-plate spacing was nine inches in the single field of this ESP. Each plate could be rapped with up to 100 g force. The ESP was equipped with windows on the inlet and outlet transforms. At a flow of 280 acfm the ESP had a SCA of about 31 ft^2/kacfm.

The FFSS was used to simulate the operation of a fabric filter with reverse-gas cleaning. The FFSS drew flue gas isokinetically from the transform immediately upstream of the ESP. The system consists of modules for holding the filter medium, for controlling and monitoring flow and temperature in the system, for cooling and drying the flue gas after it has been filtered, and for data acquisition and analysis. We placed an absolute filter in parallel with the FFSS filtration cabinet so that we could periodically measure the total mass loading entering the

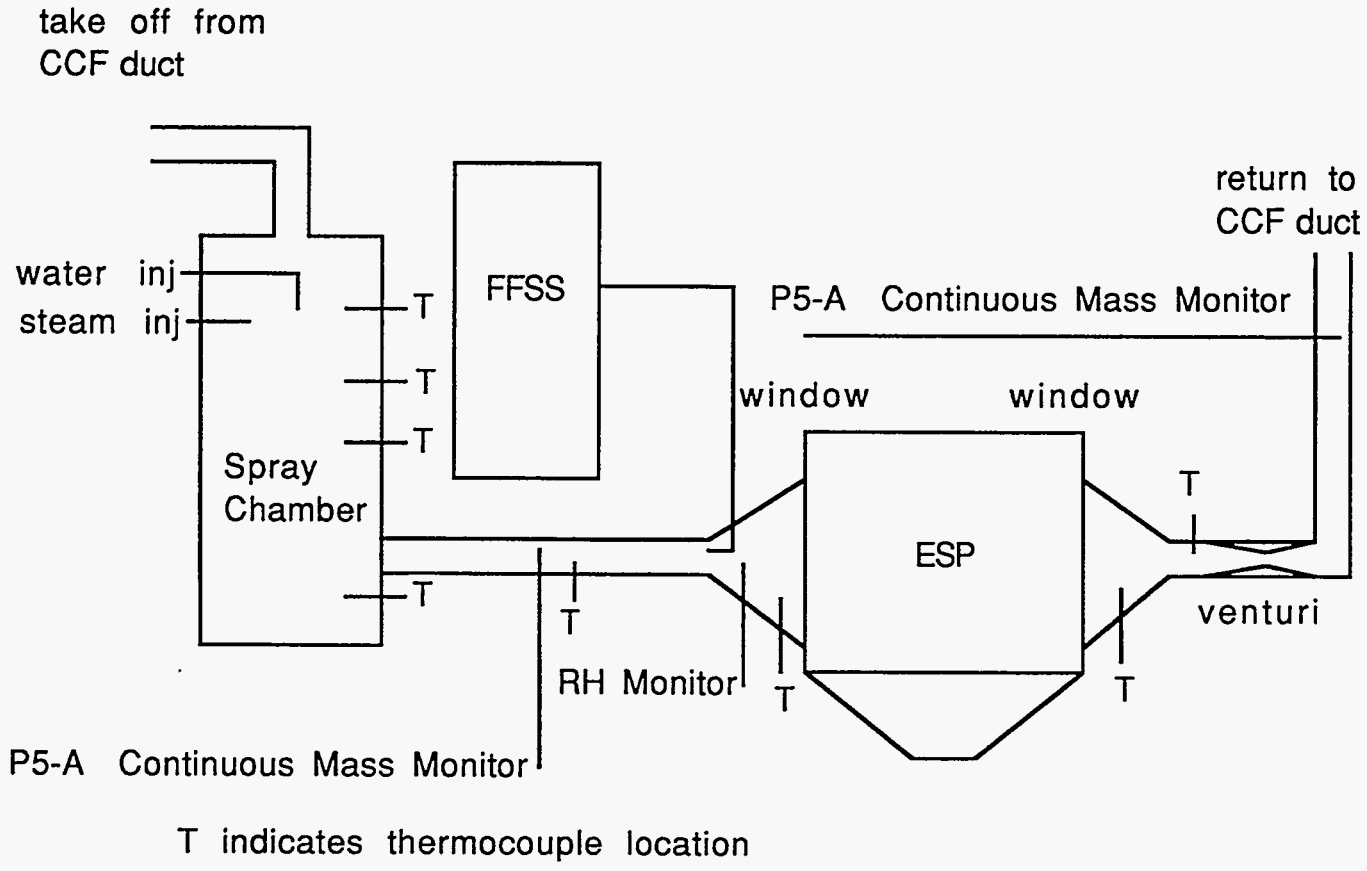

Figure 5-2. Schematic diagram showing the major components of our pilot-scale test setup.

device during the CCF tests. The temperature of the FFSS filtration cabinet was controlled independently of the rest of the system and maintained at the target temperature for the test condition. The gas was passed through a circular swatch of fabric, 11 inches in diameter, mounted opposite the inlet port. A viewport in the FFSS exists for visual observation of the dust cake and fabric during operation. Fittings located on each side of the fabric allowed monitoring of the filtering pressure drop. The flue gas passed through the test fabric and entered a highly-efficient inertial cyclone which collected any ash penetrating the fabric. The cyclone could be isolated while the FFSS continued to sample normally to allow retrieval of the collected ash. The flow rate through the fabric was measured by a metering orifice located downstream of the cyclone. After passing through the orifice, the flue gas passed out of the heated sampling cabinet. After the flue gas exited the filtration cabinet it was dried and filtered before it entered the control cabinet. The control cabinet was used to control and monitor temperature, flow rate, pressures, and operating mode of the system. When reverse-gas cleaning was initiated, the cleaning air flow was preheated by passing through a coil of copper tubing mounted inside the cabinet. This periodic reverse-gas cleaning simulated full-scale baghouse operation. Operating temperatures, flows and filtering pressure drop were output to the data acquisition system.

We installed a continuous monitor (Environmental Systems Corporation model P-5A) downstream of the ESP to measure total mass emissions through the ESP. This instrument collected and measured back-scattered light from fly ash particles entrained in the flue gas. Because accurate assessments of temperature and relative humidity were critical to the interpretation of the FFSS and ESP data, we monitored these parameters very closely. Thermocouples were located at critical points throughout the system, and relative humidity was assessed by direct measurement of the water content of the flue gas, and with a continuous monitor located just upstream of the ESP.

A computer utilizing Labtech Notebook® software acquired and stored data for our system. This data acquisition system displayed and recorded temperatures, flowrates, FFSS pressure drops, and ESP outlet mass concentration. Values from all monitors connected to the data acquisition system were read every 2 seconds and recorded to a data file every 30 seconds. During the third pilot-scale test, data acquisition for the FFSS was performed by an independent computer dedicated entirely to that system.

We used two different means for identifying the onset of electrostatic reentrainment from the ESP collection plates. Because the ESP we used had windows at both ends that allowed illumination and viewing of the wires and plates, visual inspection of the plates was a very valuable observation tool. We also observed the output of our continuous mass monitor located in the outlet duct as we attempted to induce reentrainment.

5.2 TEST ACTIVITIES

Our laboratory studies indicated that the response of different types of fly ashes to water vapor conditioning varied greatly. In our pilot-scale tests, the effects of actual flue gas, a variety of coal types, and true size distributions of entrained fly ash particles allowed us to verify the effects of flue gas humidification for two distinctly different fly ashes. Our laboratory data indicated that the most likely conditions for electrostatic reentrainment would be high relative humidity and relatively cool flue gas. We also expected that the strongest liquid bridges that we could form in the dust cake in the FFSS would result from very moist conditions. Therefore we planned to create these conditions in the ESP and FFSS. Unconditioned CCF flue gas normally contained about 8 % water by volume. Therefore the base line relative humidity in the 300 °F flue gas extracted from the CCF duct was around 1.7 %.

The first of our pilot-scale tests was conducted during December 1993 and lasted approximately 240 hours. During this test our primary objectives were to exercise the system, and determine factors such as temperature loss, inleakage of ambient air, and stability of flow rates and mass loadings. Two different Illinois No. 6 coals were burned in series during this test. The first coal was from the Galatia mine. Midway through the test the CCF changed to another bituminous Illinois No. 6 coal from the Jader mine. During this first test the flue gas conditions we examined were limited to the base line conditions of the flue gas extracted from the CCF duct.

Our second pilot-scale test occurred during January 1994. During this test the CCF burned a mixture of two medium-sulfur Alabama coals from the Cedrum and Shoal Creek mines. We were able to condition the flue gas and fly ash particles during this second test by the injection of a fine water spray into the large conditioning chamber in our slipstream system. This conditioning method increased flue gas water content and decreased flue gas temperature concurrently. Using this method for conditioning the flue gas we were able to reproducibly induce electrostatic reentrainment in the pilot-scale ESP and reduce the specific flow resistance of the filter cake formed in the FFSS. In order to assess the roles that ash properties had in these two phenomena, we collected and analyzed ash collected on the plates of the pilot-scale ESP during this test.

After completion of our second pilot-scale test we added a new, more sensitive optical mass monitor at the outlet location. The less sensitive optical mass monitor we used previously at the outlet was moved to the duct upstream of the ESP inlet. We also modified a high-voltage power supply and our data acquisition system so that current and voltage applied to the ESP could be recorded automatically. We shortened and simplified the sample line leading to the FFSS to minimize probe losses.

The CCF was fired with Powder River Basin Coal from the Bell Ayr mine for the duration of our third pilot-scale test, which occurred in November, 1994. Since we evaluated ash from

Powder River Basin coal fly ash in our laboratory studies, CCF tests of this coal provided an excellent opportunity for the comparison of the results of our pilot-scale tests to our laboratory results.

Because we funded several days of CCF operation during this test, we were able to use several conditioning and control options in the CCF process stream that were not available to us during the first two tests. The design of the CCF allowed us to control duct moisture and temperature independently. We used in-line heat exchangers to cool the flue gas without increasing its moisture content. By injecting water just downstream of the combustion zone, we were also able to moisten the flue gas without lowering its temperature. As in the second test, we were able to lower the specific flow resistance of the filter cake formed in the FFSS. However, none of the range of flue gas conditions we created in the ESP were able to induce electrostatic reentrainment from the ESP collection plates. We attribute this to the characteristics of the Powder River Basin coal ash. Following this test we collected some of this ash for laboratory analysis.

The laboratory tests we performed on the ash samples we collected during these tests included tensile strength, uncompacted bulk porosity, size distribution, true particle density, resistivity, and chemical analysis. Detailed discussions of our activities during each of the three pilot-scale tests and the analyses we performed on the ash samples we collected are presented in the following sections.

5.2.1 Test 1

The first pilot-scale test we participated in was a CCF test of two Illinois No. 6 coals (Galatia and Jader) in December, 1993. During this test, we exercised the system (except for the conditioning chamber, which was not ready for operation at that time) and evaluated the baseline operation of the ESP and FFSS. Operation of the CCF commenced on December 6 and continued through December 16. The CCF was initially fired with natural gas (used to preheat the combustor). During the first day of operation, the fuel was gradually changed over from natural gas to a high-chlorine bituminous Illinois No. 6 coal from the Galatia mine. Midway through the test period (on December 13), the CCF changed to another bituminous Illinois No. 6 coal from the Jader mine. Selected analyses of these two coals are presented in Table 5-1. The ESP was brought on line to heat up on December 6, and was fully operational by December 7. The FFSS was brought on line late on December 8. Except for brief interruptions in the smooth, continuous operation of the CCF (primarily for maintenance), the ESP and FFSS operated successfully until the end of the CCF test period.

Table 5-1
Proximate Analyses and Chlorine Contents of Coals Burned in the CCF (Test 1)

Source	Galatia		Jader	
	As received	Dry basis	As received	Dry basis
% Moisture	10.25	--	5.23	--
% Ash	6.09	6.78	8.83	9.32
% Volatile	33.27	37.07	34.27	36.16
% Fixed carbon	50.39	56.15	51.67	54.52
Btu/lb	12297	13701	13005	13723
% Sulfur	1.21	1.35	2.76	2.91
% Chlorine	0.4	--	0.1	--

The key operating parameters we were examining in this test included temperature loss through the ESP and associated ductwork, V-I characteristics of the ESP, rapping procedures for the ESP, rate of ash accumulation in the ESP and FFSS hoppers, length of FFSS cleaning cycles, degree of air in-leakage, maintenance and stability of flue gas flowrates, mass loadings in the flue gas, flue gas moisture content, operation and sensitivity of the continuous mass monitor, sample collection, and collection of data with our automated data acquisition system.

We closely examined our data analysis and operating procedures to provide rapid evaluations of ESP and FFSS performance. Key parameters include the buildup of properly conditioned ash layers on the ESP collection plates and the FFSS fabric, and analysis of the sensitivity of the P-5A mass monitor to entrained particulate levels at the outlet of the ESP. Operation of our pilot-scale system was also affected by the maintenance procedures performed on the CCF during the test period. Daily soot blows rendered 1 to 2 hours of each day unavailable for meaningful ESP or FFSS operation. In our second and third tests we attempted to coordinate our daily schedule with CCF maintenance in order to optimize periods available for testing.

During this first test, current and voltage levels for the ESP power supply were recorded manually. Glass windows located at the inlet and outlet of the ESP were used to observe ash levels in the hopper and the effects of rapping on the ash layers accumulated on the ESPs grounded collection plates. Method 17 mass trains were performed downstream of the ESP with the voltage on and off. The total flowrate through the ESP was maintained at about 280 acfm. During normal operation, the temperature at the inlet of the ESP was about 292 °F. Flue gas temperature dropped by about 8 to 10 °F through the length of the ESP. Normal operating voltage of the ESP power supply was set at 36 kV and its total current output normally ranged between 0.5 and 0.6 mA. These current levels correspond to a current density between 30 and 40 nA/cm^2. V-I data measured for the ESP during operation with the Galatia and Jader coals are given in Figure 5-3.

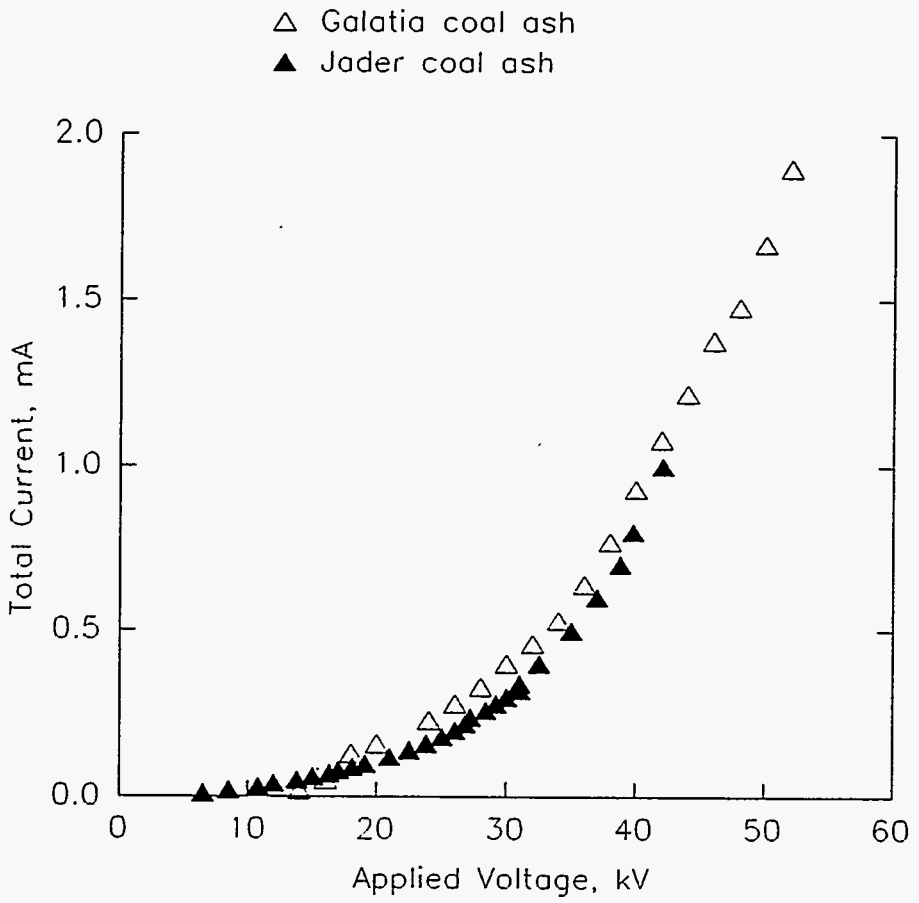

Figure 5-3. Voltage-current characteristics of the pilot-scale ESP measured while operating at about 275 °F and collecting fly ashes generated by the Coal Combustion Facility during test 1.

For the Galatia coal, we measured mass loadings of 0.69 gr/acf at the outlet of the ESP with ESP power off and 0.08 gr/acf with the power on. For the Jader coal, the corresponding values were 1.02 gr/acf and 0.11 gr/acf. Although time limitations precluded direct measurements of mass loadings at the inlet to the ESP, the efficiency of the ESP operating at a current density of about 40 nA/cm^2 can be estimated to be about 88 %. (This value assumes the mass loadings at the ESP inlet are the same as the loadings measured at the ESP outlet with the power off.) Our continuous mass monitor served as a reliable indicator of relative changes in mass concentrations in the outlet duct. Our evaluations of the effectiveness of rapping the ESP collection plates during this first test indicated that subsequently we should only rap the plates after evaluating a particular combination of flue gas temperature and moisture. More frequent rapping would cause the buildup of ash on the plates to be too slow.

We operated the FFSS with a fabric temperature of 285 °F for the duration of our first test. We used woven fiberglass fabric with a 25 % exposed surface texturization as our filtration substrate. This is fabric commonly used at utility reverse-gas baghouses. Since one of our primary objectives for this test was to establish the cleaning schedule that would provide the fastest, most accurate assessment of the pressure drop characteristics of the ash, we operated the FFSS with 1- and 2-hour filtering cycles.

We use K_2, the specific drag coefficient of the ash, as the comparative parameter of filtration performance. Because the calculation of K_2 requires knowledge of the rate of accumulation of ash on the fabric, we used the rate of pressure drop accumulation at a constant flowrate as our parameter for evaluation of ash filtration characteristics during this first test. (The mass of ash reaching the filter cake could not be directly measured because of the near-continuous operation of the FFSS, and effects that the geometry of the FFSS transform had on selective particle settling.) Our data indicated that a filtering period of two hours should be sufficient to establish a measurable, constant rate of increase in pressure drop across the fabric. We measured differences in the rate of pressure drop increase for the Galatia and Jader coal ashes. The steady-state rate of pressure drop increase in the FFSS (at a face velocity of 2 ft/min) for the Galatia coal ash was 0.169 ± 0.037 in. H_2O/min compared with 0.261 ± 0.031 in. H_2O/min for the Jader coal. Essentially all of this difference can be attributed to the higher concentration of ash in the flue gas with the Jader coal. Our mass train measurements made at the outlet of the ESP (with power off) and the proximate analyses of the Jader coal indicate that this coal should generate 45 to 48 % more ash than the Galatia coal. Therefore the 54 % increase in the rate of pressure drop accumulation we observed with the Jader coal was quite reasonable.

5.2.2 Test 2

Our second pilot-scale test was performed during scheduled operation of the CCF that was funded by another research project. Therefore the temperature and moisture content of the flue gas we extracted from the CCF duct remained constant throughout the test. We used a

fine spray of water droplets to moisten and cool the flue gas and condition the fly ash particles in our large conditioning chamber. Without the cooling induced by the water spray, the temperature at the inlet of the ESP was about 292 °F. Flue gas temperature dropped by about 8 to 10 °F through the length of the ESP.

For our second test, we measured the mass loading entering the FFSS by placing a thimble filter in parallel with the FFSS. (Time limitations precluded the performance of Method 17 mass measurements during this test.) This allowed us to normalize the rate of pressure drop increase by the mass concentration entering the FFSS. (The mass of ash actually reaching the filter cake could not be directly measured because of the near-continuous operation of the FFSS, and effects that the geometry of the FFSS transform had on selective particle settling.)

The ESP was operated around 40 kV and 0.48 mA total current. This setting resulted in a current density of 30 nA/cm^2. (Periodically during our tests we measured V-I curves for the ESP. We maintained the applied voltage between 38 and 43 kV to build ash layers on the grounded plates. At these voltages, the current density ranged from 2.5 to 33 nA/cm^2.) Relatively stable operation was maintained for the FFSS and ESP at about 290 °F for about 6 hours. We collected a relatively thick ash layer on the ESP plates and then began injection of a water spray into our conditioning chamber to cool the ESP inlet to around 168 °F. While the flue gas and slipstream ducting were cooling, we also lowered the set points on the FFSS ovens and probe heaters to around 165 °F. After temperatures stabilized at these lower values we operated the ESP and the FFSS for several hours. We then began to increase the temperature in the ESP by reducing the volume of water spray. (We discontinued FFSS operation during the period of transition in flue gas temperature.) Severe reentrainment from the ESP plates was observed at an ESP inlet temperature of about 193 °F. We reestablished stable ESP and FFSS operation at about 220 °F. Figure 5-4 presents a record of this and subsequent reentrainment events as observed by our P5-A optical monitor.

From an ESP operating temperature of around 220 °F, we gradually lowered the flue gas and ESP temperature to around 165 °F by increasing the water spray. However, during this drop in temperature, we were not able to reproduce the reentrainment phenomenon we observed during the temperature rise through 193 °F. We then cleaned the ESP plates and re-deposited an ash layer at an operating temperature of about 165 °F. The FFSS was also brought back on line at this temperature and allowed to operate for four hours. During this period, the filtering pressure drop across the fabric in the FFSS did not increase. Our experiences at other operating temperatures would tend to attribute much of this inability to build pressure drop to a decrease in the fundamental gas flow resistance (K_2) of the filter cake. However, even a much lower K_2 should still result in a gradual increase in filtering pressure drop. We also measured lower mass loadings at the inlet to the FFSS at this temperature, but we would still predict some increase in pressure loss through the fabric. Our analyses of the FFSS sampling line following this test indicated that severe probe losses occurred in this sampling line when the flue gas was extremely moist.

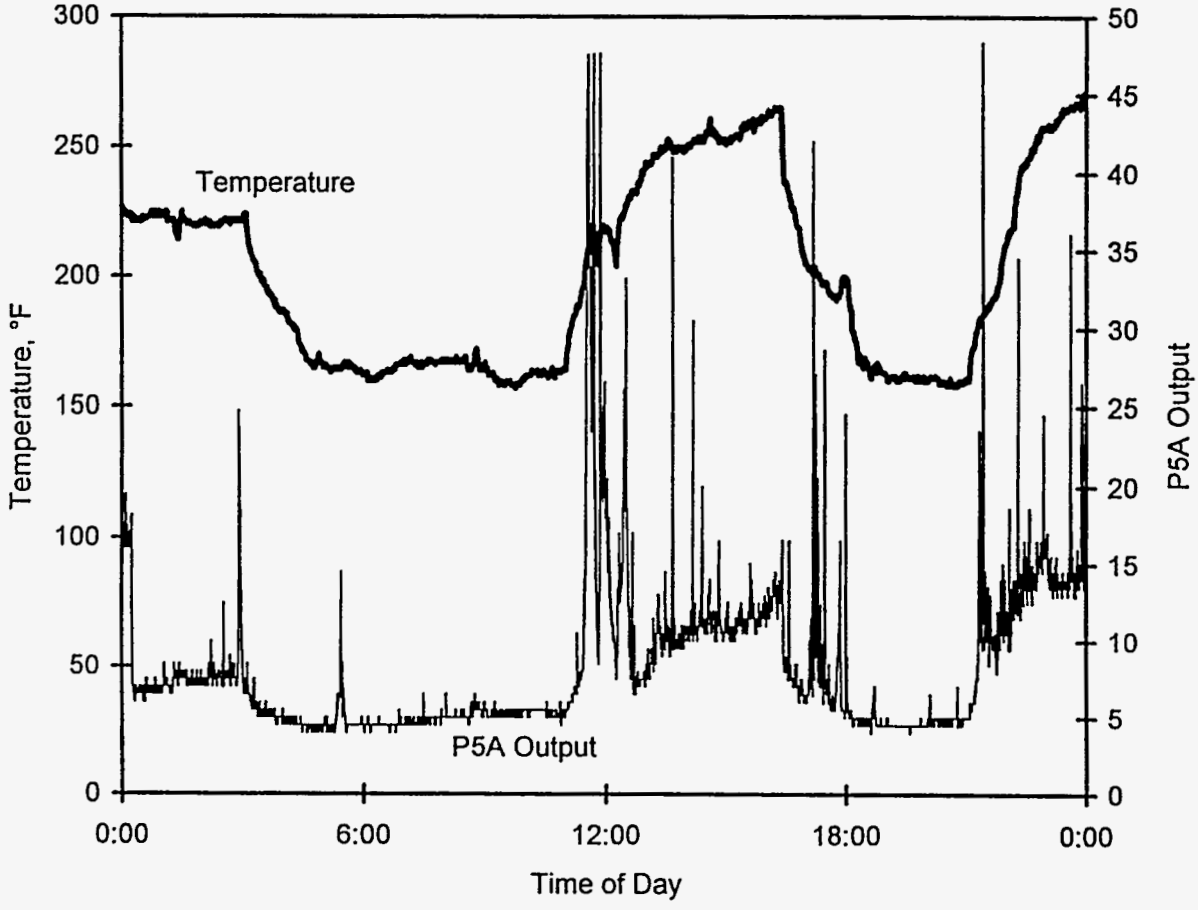

Figure 5-4. Comparisons of ESP inlet temperature and P5-A outlet monitor output. Distinct reentrainment events correspond to periods when the ESP temperature was being increased.

After an ash layer had been formed in the ESP at 165 °F, we isolated the FFSS and began slowly increasing the temperature by decreasing the water spray. Once again, we observed severe reentrainment at ESP inlet temperatures between 198 and 218 °F. After cleaning the ESP plates and reheating the system to around 260 °F, we maintained stable operation of the FFSS at this temperature. After operation at 260 °F, we once again attempted to induce reentrainment by gradually decreasing operating temperatures. We did observe an increase in emissions from the ESP at about 203 °F. Unfortunately, this event coincided with a soot blow in the CCF, and we cannot be certain the emissions we saw were due to reentrainment from the ESP. Visual observations through the ESP window did show significant amounts of ash falling off the plate during this period; however, similar reentrainment was often viewed through the window when no significant increases in outlet emissions were being measured by the P5-A.

We once again dropped the system temperature to about 165 °F and built a new ash layer on the ESP plates. After building the layer, we gradually increased the system temperature and once again observed highly active reentrainment of the collected ash. This time the reentrainment occurred at an ESP inlet temperature of about 182 to 187 °F. During this episode of reentrainment (shown in Figure 5-5) the relative humidity in the ESP was about 16 %. (This value of relative humidity has been adjusted to account for the difference in the temperatures of the ESP and the relative humidity monitor.) We continued to increase system temperature all the way up to about 220 °F, but we did not observe additional significant reentrainment. We then reheated the system to about 272 °F to obtain more FFSS operating data. We also rebuilt ash layers on the ESP plates at this temperature. As we had done before, we attempted to induce reentrainment of these ash layers by gradually dropping system temperature with water spray injection. No significant reentrainment was observed as we slowly lowered the system temperature to 150 °F. However, when we raised the temperature of the inlet to the ESP back up to around 203 °F, we again observed the reentrainment phenomenon.

5.2.3 Test 3

The third pilot-scale test was conducted in three parts during November, 1994. The CCF fired Powder River Basin Coal throughout the entire test. For the first three days, the CCF evaluated various combustion parameters of this coal for Southern Company Services, Inc. Mass loadings of about 0.64 gr/acf were measured during this initial three day-period in the CCF duct from which our slipstream was taken. Representative data obtained with a cascade impactor are presented in Figure 5-6. These data show a relatively coarse mass median diameter of 22 μm. In-situ resistivity data taken at the same location during this period gave values around 2.8×10^{11} ohm-cm at temperatures around 270 °F. A proximate analysis performed on a sample of the pulverized coal burned during the test is presented in Table 5-2.

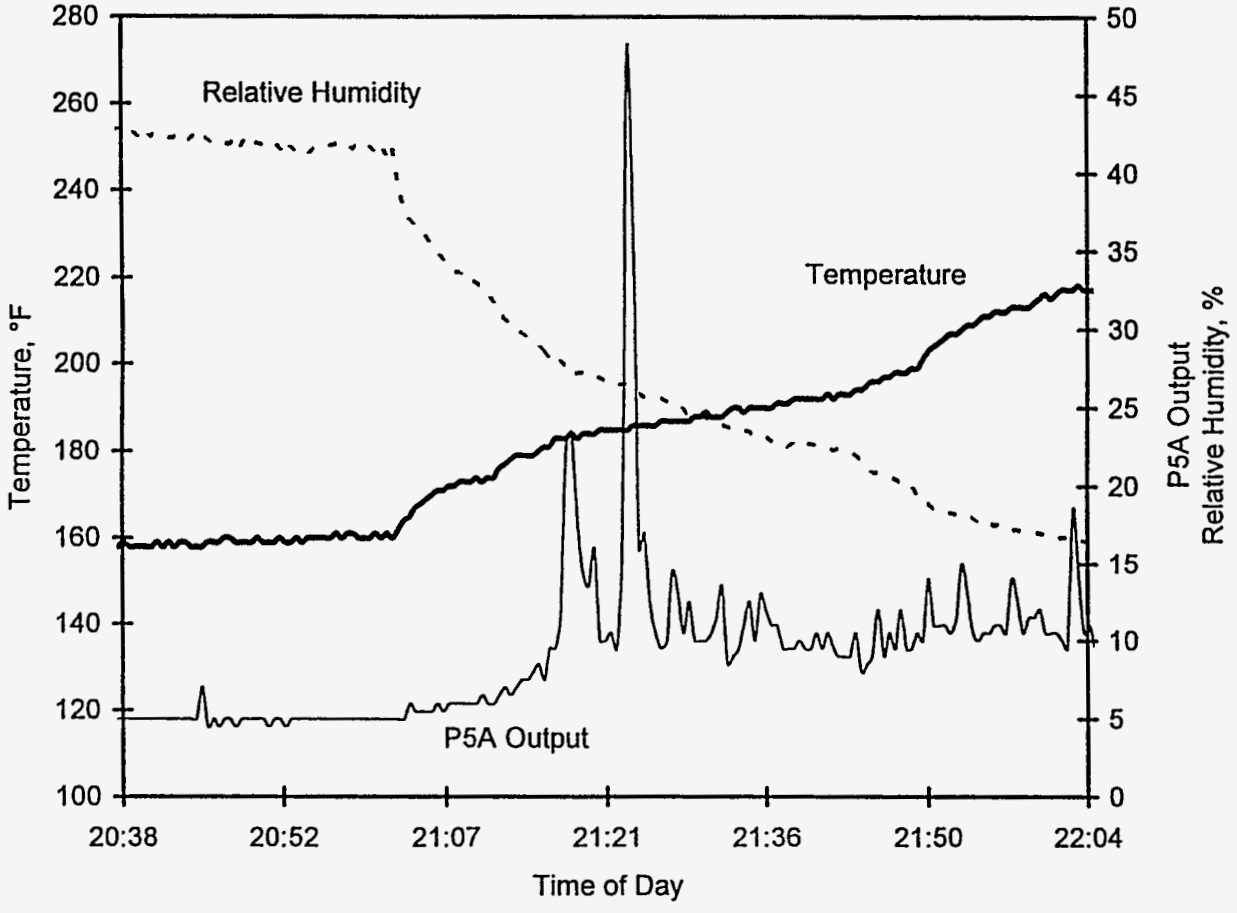

Figure 5-5. Comparisons of ESP inlet temperature and P5-A outlet monitor output. Distinct reentrainment events correspond to periods when the ESP temperature was being increased. Actual values of relative humidity in the ESP were somewhat lower than the values presented on this graph due to differences in temperature.

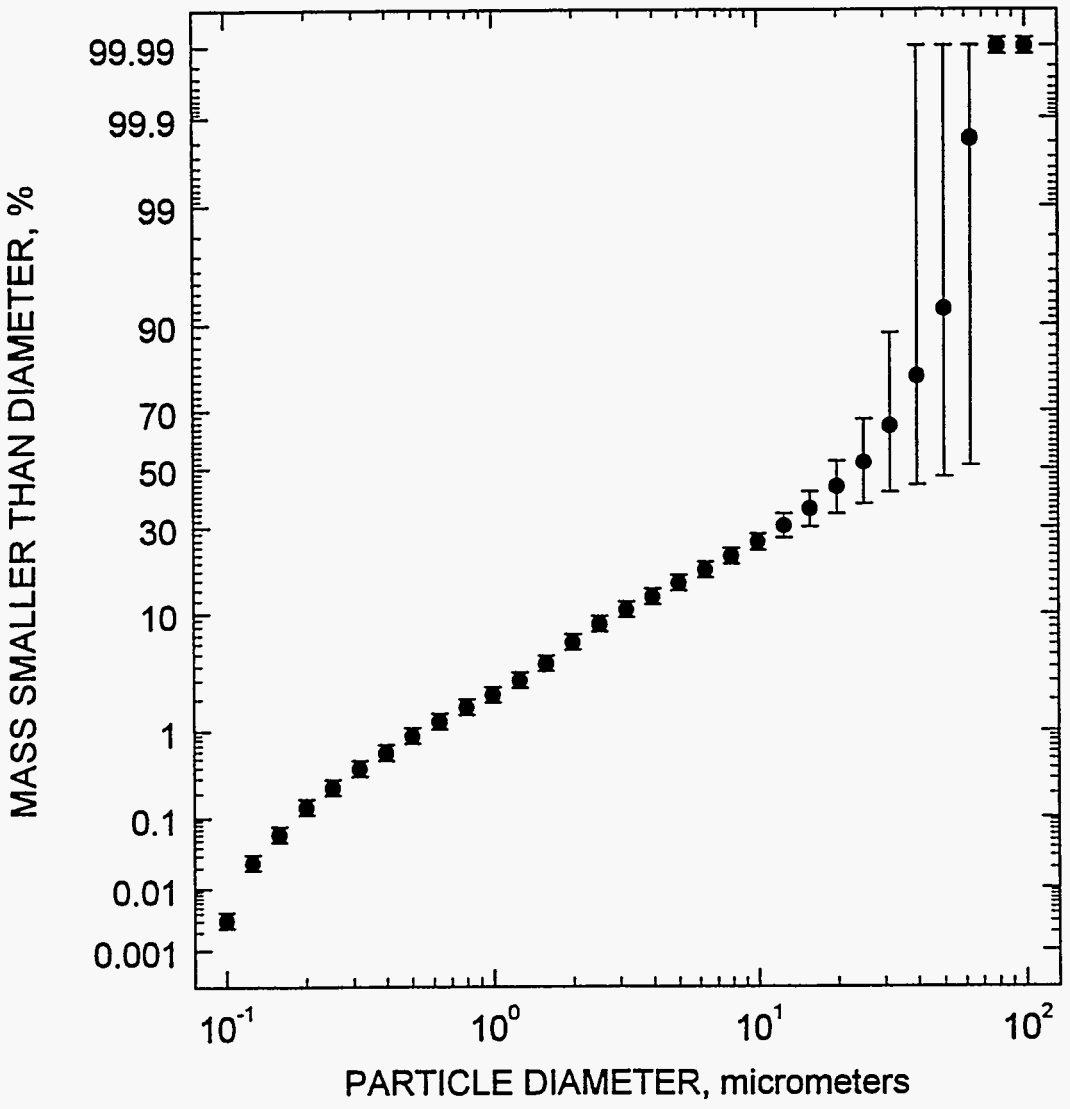

Figure 5-6. Representative cumulative size distribution data obtained during test 3 with a cascade impactor at the CCF duct location where the flue gas slipstream was extracted. The D_{50} of this size distribution is 22 μm.

Table 5-2
Analyses (As Received Basis) of Pulverized Powder River Basin Coal - Bell Ayr Mine

Quantity	Value
Total moisture	26.28 % by wt.
Ash content	5.80 % by wt.
Heat of combustion	8695 BTU/lb
Fixed carbon	36.40 % by wt.
Total chlorine	214 mg/kg
Volatiles	31.52 % by wt.
Sulfur	0.38 % by wt.

Toward the end of this first period of operation, we began on November 14 to preheat our slipstream system by pulling flue gas through the system and warming up heaters placed at various points throughout our system. In the afternoon of November 14 we began to collect data. Unfortunately, a spark from our ESP high-voltage power supply during a clean-plate V-I measurement found its way into our data acquisition system, our two optical mass monitors, and our continuous relative humidity monitor. Consequently, the two mass monitors had to be removed and taken to Environmental Systems Corporation for immediate repair. The data acquisition system was repaired early on November 15. The mass monitors were repaired and reinstalled in the system on the afternoon of November 15. Our slipstream system then resumed operation.

The failure of the relative humidity monitor was not immediately apparent. Once it was discovered (late on November 15), we attempted to identify and repair it, but were not successful. We then investigated several other means for quickly determining the water content of the flue gas. One of the options we investigated involved passing a known volume of extracted flue gas through a preweighed drying column. We had used this technique successfully in past tests; however, the length of time (about 40 minutes) required to obtain a final value with this method limited our ability to accurately determine the flue gas moisture when conditions in the slipstream system were rapidly changing. Therefore, we also investigated using an alternative continuous relative humidity monitor. However, this second monitor was not designed to withstand temperatures exceeding 176 °F. We constructed a heated extractive probe to gradually decrease the temperature of the extracted gas down to about 170 °F. The monitor was installed in the probe where it would be constantly exposed to newly extracted flue gas. Although the probe provided the flue gas to the monitor's sensor at the proper temperature, the values we were able to measure with this monitor were much lower than values we measured with the drying column technique mentioned above. We also installed a wet-bulb thermocouple at the outlet of the ESP to compare with dry thermocouple readings from the same location. The readings we obtained from these two thermocouples were used to derive moisture contents of the flue gas from a standard psychrometric chart. Data obtained with this system generally agreed with the extractive/drying column technique.

This wet-bulb/dry-bulb thermocouple system worked well throughout most of the rest of the test.

Throughout the second period of the test (which extended until 0700 on November 18) we created a range of moisture and temperature conditions in the slipstream ESP and the FFSS. We injected water directly into the CCF process stream at several points downstream of the combustion chamber to increase the water content of the flue gas. We also injected steam into the CCF duct downstream of the combustion chamber to increase the water content of the flue gas when we wanted the flue gas entering our slipstream system to be moist and also as hot as possible. The heat exchangers in the CCF ductwork were used to vary the temperature of the flue gas without modifying its water content. Because of its configuration in the slipstream system, the temperature of the FFSS was controlled independently of the rest of the system.

As in our previous tests, the total flow rate through the ESP was maintained at about 280 acfm. Because the inlet and outlet optical mass monitors required significant amounts of ambient purge air to cool the optics and keep the lenses clean, the level of moisture in our system was somewhat less than the moisture level in the CCF duct from which we withdrew our gas stream. Another factor that placed a limit on the levels of moisture that we were able to create in our system was the requirements of the CCF pulse-jet baghouse. If moisture levels were allowed to get too high in the baghouse, the ash could not be cleaned effectively from the bags. The CCF control system also placed limits on the upper temperature of the duct from which we obtained our flue gas. Despite these limits, we were able to explore a range of temperature and moisture conditions in the ESP.

Several attempts were made to induce electrostatic reentrainment in the ESP. Our general approach was to establish a stable condition (moisture and temperature) in the ESP and then to build an ash layer (without rapping the plates) at these conditions. The ESP was typically operated at an applied voltage of 38 - 41 kV and current densities ranging between 0.8 and 3 nA/cm^2. (Higher voltage and current settings were avoided due to the possibility of high-voltage sparks and corresponding damage to the data acquisition system and/or optical mass monitors.) Once the layer was formed, we would alter the flue gas moisture and/or temperature while we observed the ash layer. In our second test this approach allowed us to reproducibly generate electrostatic reentrainment. In our third test, our initial attempt at inducing reentrainment in the ESP was with an ash layer we formed at around 200 °F and with flue gas having about 22 % H_2O by volume (27 % RH). We used water and steam injection into the CCF duct to create and hold these conditions. The ash layer on the ESP plates was formed into plateaus up to 0.25 in. thick. We began a gradual increase in ESP temperature by adjusting the CCF's heat exchangers while attempting to hold the water content constant at about 22 % by volume. During this increase in temperature, the steam generator malfunctioned and over the two hours we increased the ESP temperature up to about 220 °F, the water content of the flue gas dropped to about 15 % H_2O by volume. During this period we did not observe any significant non-rapping reentrainment.

For our next attempt at inducing electrostatic reentrainment, we built an ash layer at about 200 °F and about 30 % H_2O by volume (37 % RH). We then observed it as we decreased the water content of the flue gas while holding gas temperature constant. We continued this trial until the water content had been reduced to 15 % H_2O by volume (18 % RH). As before, we observed no electrostatic reentrainment of the ash layer. We continued to observe the layer as we increased the flue gas temperature in the ESP up to about 265 °F and gradually decreased the water content to about 8 % by volume (3 % RH). This trial also failed to induce reentrainment. We then rapped the plates and built a new ash layer at 210 °F and 24.5 % H_2O by volume (24 % RH). Once the ash layer had matured, we discontinued all water and steam injection and observed the ash layer as it dried out gradually while the CCF used its heat exchangers to hold the temperature constant. As before, no electrostatic reentrainment was observed during this transition period. Our final attempt to induce reentrainment began with the formation of a new ash layer at about 200 °F and 10.5 % H_2O by volume (13 % RH). No water or steam were injected into the CCF duct during this period. After the ash layer had been collected at these conditions, we increased the ESP temperature up to 270 °F. By the end of this period of rising temperatures, the relative humidity in the flue gas was 3.5 %. No reentrainment was generated during this procedure. Following this trial, the slipstream system was prepared for the testing conducted by ADA Technologies, Inc. under DOE Contract No. DE-AC22-91PC90364.

The third period of operation commenced at 0700 on November 18 and continued for 16 hours. During this time ADA Technologies, Inc. evaluated some of their additives for reducing resistivity using our slipstream ESP. Full discussions of their results are contained in technical reports issued to DOE\PETC by ADA Technologies, Inc. under Contract No. DE-AC22-91PC90364.

5.3 RESULTS AND OBSERVATIONS - FABRIC FILTRATION

In order to analyze the effects that duct humidification had on the filtration characteristics of the ash collected in the FFSS, we observed two main parameters: the rate of pressure drop increase across the filtering fabric, and the amount of ash entering the FFSS filtration cabinet. These data, which were collected during tests 2 and 3, are summarized in Tables 5-3 and 5-4. The final columns in these tables normalize the rate of pressure drop increase by the mass loading we measured with the thimble filter we placed upstream of the FFSS. These normalized values provide a fair indication of relative changes in K_2 at different flue gas conditions. The relative humidity values presented in Table 5-3 were calculated from moisture determinations performed on samples taken from the ESP outlet duct during the corresponding FFSS test periods. The RH values presented in Table 5-4 were calculated from moisture determinations performed on samples taken from the ESP inlet duct and on wet-bulb/dry-bulb thermocouple readings made during the corresponding FFSS test periods.

Table 5-3
Summary of FFSS Operation (Test 2)

FFSS fabric temperature, °F	δΔP/δt, in. H_2O/ hr (a)	Inlet mass load rate, g/hr	Approximate RH in FFSS, %	δΔP/(δ+δM), in. H_2O/g (b)
300	0.23	7.6	1.3	0.030
300	0.22	7.6	1.3	0.029
300	0.40	11	1.2	0.037
260	0.30	6.8	2.5	0.044
220	0.11	4.9	6.1	0.022
190	0.00	--	--	--
165	0.01	2.5	22	0.0040
165	0.01	3.0	23	0.0034

(a) ΔP is the pressure drop across dustcake and fabric, δt is the time interval.
(b) δM is the inlet mass loading increment over the time increment δt.

Table 5-4
Summary of FFSS Operation (Test 3)

FFSS fabric temperature, °F	δΔP/δt, in. H_2O/ hr	Inlet mass load rate, g/hr	Approximate RH in FFSS, %	δΔP/(δ+δM), in. H_2O/g
225	0.375	1.720	5.2	0.218
220	0.394	--	9.1	--
217	0.449	*	15.1	--
231	0.325	--	16.3	--
231	0.259	0.834	7.7	0.310
229	0.293	1.501	7.3	0.195
281	0.218	0.672	3.0	0.324
343	0.442	1.180	1.2	0.375

* Although this measurement was made, the sample contained large agglomerates of ash that appeared to have broken loose from the sample line upstream of the thimble filter. Pluggage and/or condensation in the sample line leading to the mass train thimble may be ultimately responsible for the problem with this inlet mass measurement.

Except for the data obtained at 2.5 % RH during test 2 and the data obtained at 7.7 % RH during test 3, the data show that increasing the relative humidity decreases the characteristic pressure drop associated with the dust cake. The last two columns in these tables are plotted in Figure 5-7 and Figure 5-8. As discussed above, we attribute this reduction in the

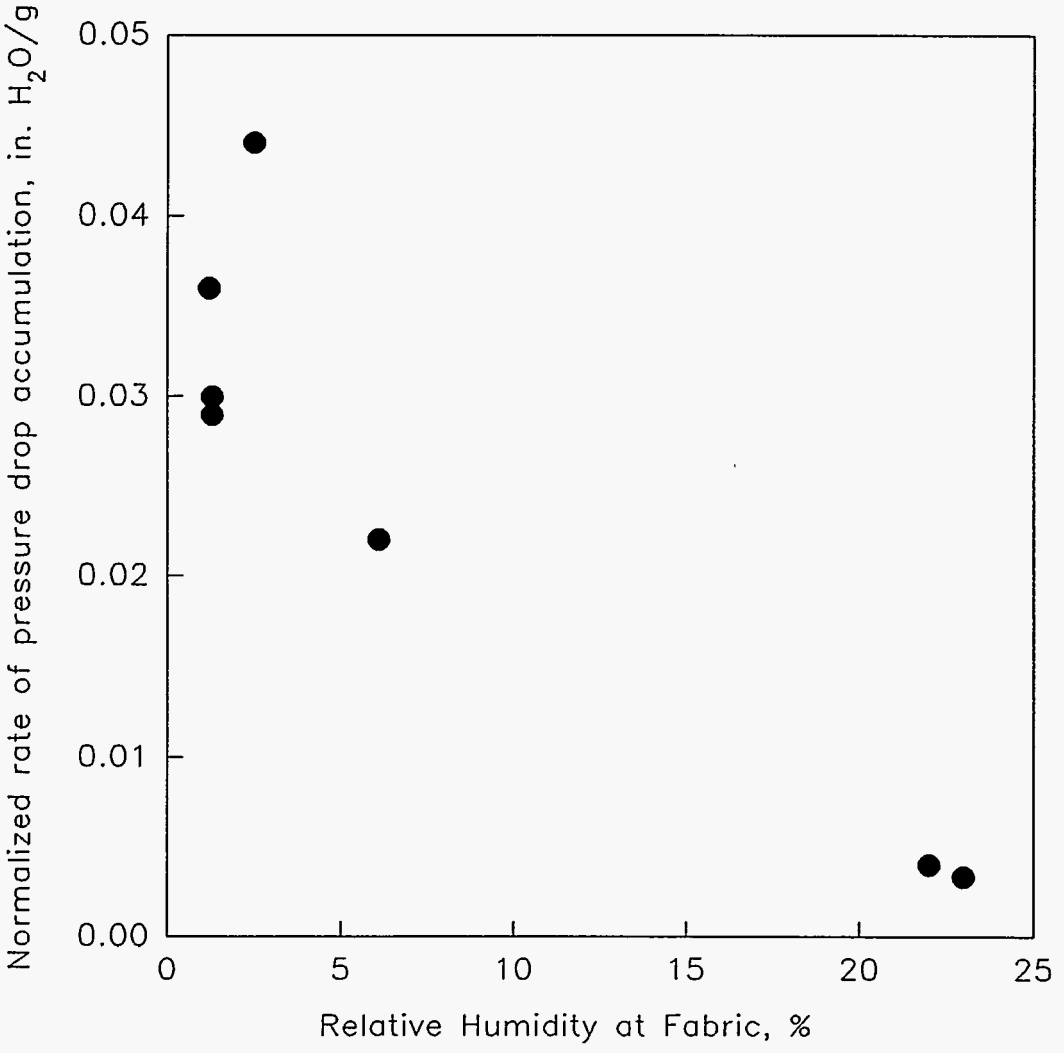

Figure 5-7. Relationship showing the dependence of the accumulation of filtering pressure drop on the relative humidity of the flue gas during our second pilot-scale test.

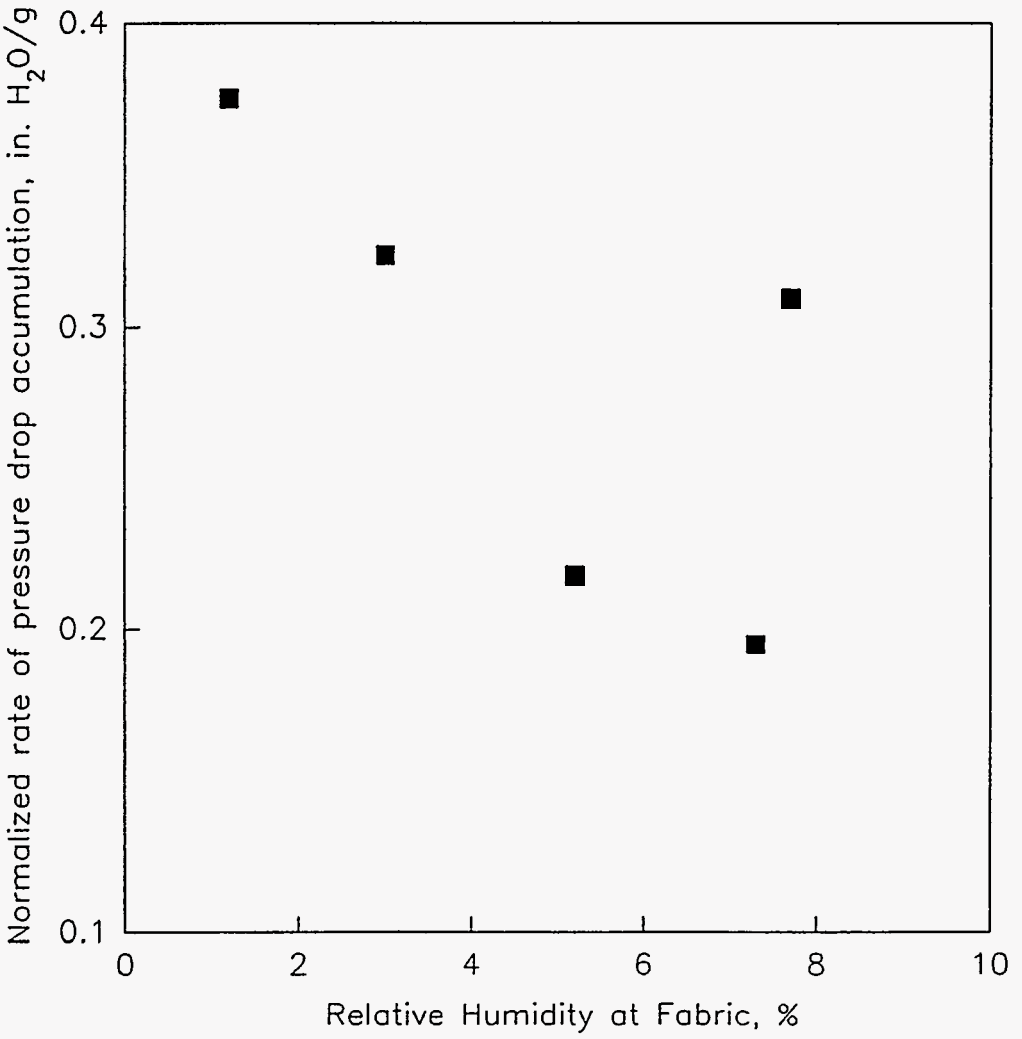

Figure 5-8. Relationship showing the dependence of the accumulation of filtering pressure drop on the relative humidity of the flue gas during our third pilot-scale test.

accumulation of pressure drop at higher relative humidities to increased porosity induced by liquid bridging between particles.

The results of our tests indicate that the Cedrum/Shoal Creek and Powder River Basin ashes can be conditioned with water to improve filtration characteristics by increasing dust cake porosity. For liquid bridges to be able to increase dust cake porosity above the characteristic value associated with an ash, free, mobile water must exist on the surfaces of the particles. Once the cake is formed at an elevated porosity, that porosity should remain intact even if the adsorbed surface water is subsequently immobilized. In our laboratory studies, we related the high calcium content of Powder River Basin ash to the immobilization of adsorbed water. We believe that the calcium and the silica present in the ash undergo a pozzalonic reaction with water that adsorbs on the surface of the ash particles to form hydrocalcium silicates. In the dust cake, additional water is continuously adsorbed on the particle surfaces in the dust cake because fresh flue gas is continuously passing through the cake and over the surfaces of the collected particles. Therefore, we postulate that free water is always available for the formation of liquid bridges between the particles on the surface of the dust cake and the newly arriving particles as they are captured by the cake. Eastern, bituminous coals like the mixture of Cedrum and Shoal Creek coals burned in the second test generally have low calcium content. Because water adsorbed on the surfaces of low-calcium ashes remains mobile and can easily form liquid bridges, the ash we collected in our second test was a good candidate for humidification to lower specific filtering flow resistance.

5.4 RESULTS AND OBSERVATIONS - ELECTROSTATIC PRECIPITATION

Several factors combined to yield the phenomenon of electrostatic reentrainment from the ESP plates that we observed during our second pilot-scale test. Our visual observations of the ash layers deposited on the ESP plates indicated that the appearance of the layer depended on the relative humidity in the ESP during deposition. When ash layers were deposited at around 275 °F (1.2 % RH), the ash layer looked smooth, with many large craters in its surface. In contrast, the ash layers deposited under high humidity conditions (22 % RH at about 165 °F) appeared fluffy, and the surface of the layer seemed to be composed of small (1/32 inch diameter) agglomerates of ash particles. This appearance agrees with the kind of fluffy structures we observed in laboratory measurements of uncompacted bulk porosity at relatively high humidities. We would expect that these fluffy ash layers have a higher porosity and probably a different inherent tensile strength associated with the physical configuration of particles than the smooth layers formed at lower relative humidities. Since the major reentrainment phenomena we observed were from these fluffy ash layers, the characteristics (porosity and tensile strength) of the layer may have been key factors in inducing reentrainment during the second test.

Because the temperature and humidity of the flue gas were changing as we approached conditions where reentrainment was likely (around 190 °F and 18 % RH), the ash layers on

the ESP plates were either drying out or adsorbing additional moisture as the ESP passed through the conditions most conducive to reentrainment. The actual water content of the ash layer may not have been the same during ascending and descending temperature conditions.

Ash resistivity is a key factor in the reentrainment phenomenon. Resistivity is strongly influenced by adsorbed water on the ash, as well as by ash temperature. Therefore the same factors mentioned above that may have affected the porosity and tensile strength of the ash layer, may also have significantly influenced ash resistivity. We measured the resistivity of ash we obtained from the ESP plates after the conclusion of the second test. These data are presented in Figure 5-9.

The ash we saw being ejected from the ash layers on the plates usually came off as small (~1/8 inch) chunks. It was not possible to tell from visual observation what became of the chunks after they fell into the gas stream. Since the bulk cohesivities of the ash layers formed at high and low relative humidities are probably quite different, the chunks of ash that we observed reentering the flue gas stream from the ash layers may have behaved differently in the inter-electrode region. In the laboratory, we observed the decrepitation, or breaking up, of agglomerates of ash lofted into the inter-electrode space in the electrostatic tensiometer we used to measure tensile strength. If the degree of difference in cohesivity was sufficient to induce or prevent significant decrepitation of the chunks of ash entrained from the ash layer, then we may actually have been inducing reentrainment during our descending-temperature transitions. The reentrained chunks of ash may have been too cohesive to decrepitate, and therefore may have fallen rather quickly and directly into the ESP hopper. This type of reentrainment would have been visible through the ESP window, but would not have been detected by our continuous mass monitor. On the other hand, the fluffier chunks of ash formed at high humidities may have decrepitated more fully, and led to the large increases in outlet emissions sensed by our P5-A monitor.

Rather large deposits built up on the discharge electrodes during test 2 operation at low temperatures and high humidities. The deposits were about 1 inch wide transverse to flow and up to 4 1/2 inches long in the direction of gas flow. Deposits formed on the wires at higher temperatures and lower humidities were only about 1/8-inch thick and seemed to be more radially symmetrical. We are not sure what effects these buildups might have had on reentrainment (other than an alteration of the field strength required to obtain a given total current).

As stated in our summaries of test activities, we were able to reproducibly cause the eastern, bituminous coal ash we collected to reentrain from the ESP collection plates during the second test. However, despite being better able to control the flue gas temperature and moisture content during the third test, we were not able to generate conditions that induced reentrainment of the Bell Ayr Powder River Basin coal ash. In order to identify and understand the differences in ash characteristics that contributed to these different behaviors,

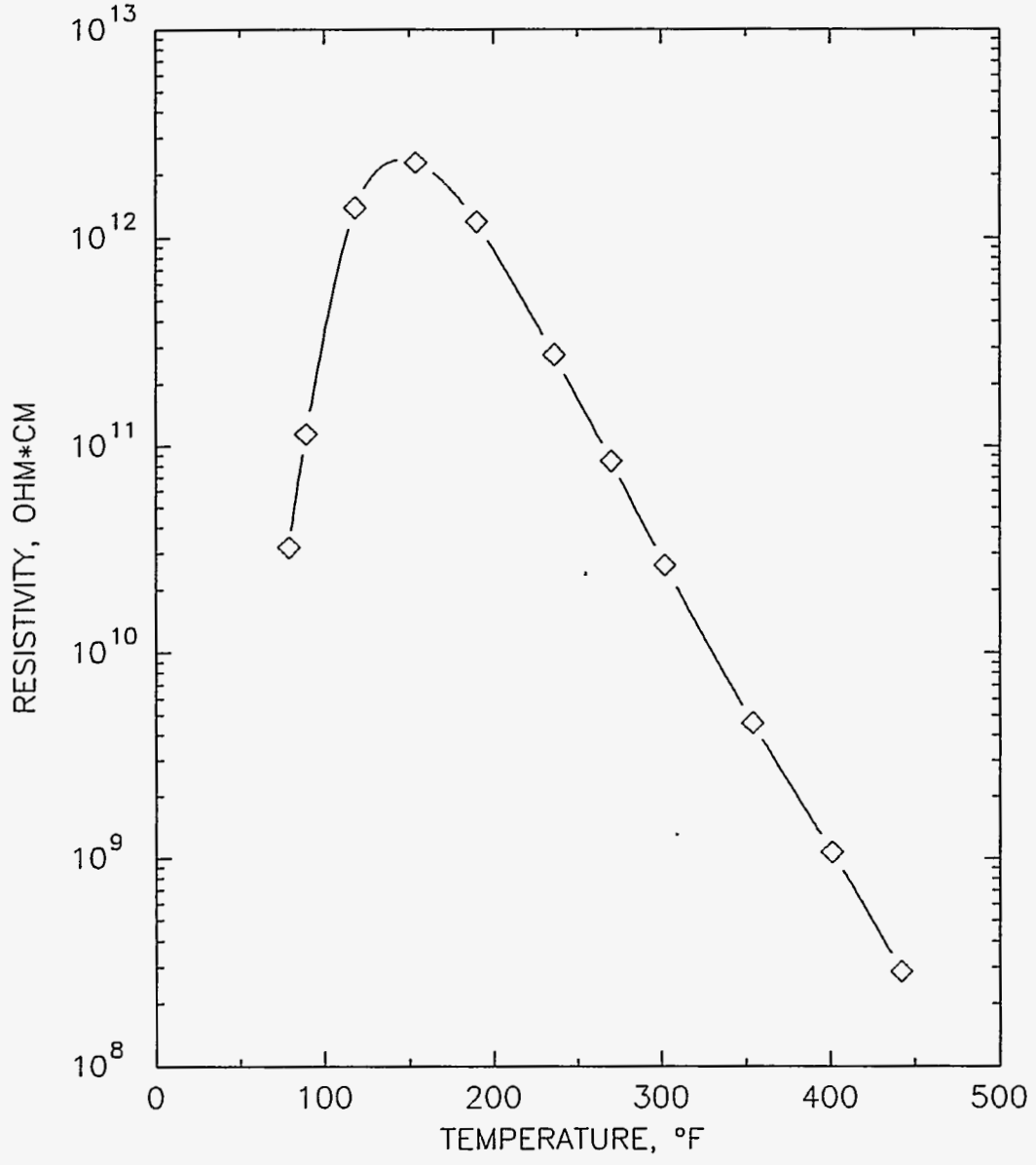

Figure 5-9. Resistivity of the Cedrum/Shoal Creek coal ash collected from the ESP plates following our second CCF test. Resistivity was measured with 9.5 % H_2O by volume.

we performed several analyses of the ashes collected during these tests. Analyses of these two ashes included size distribution, particle density, tensile strength and resistivity. Further analyses performed on the Bell Ayr Powder River Basin coal ash included chemical composition, specific gas flow resistance, and uncompacted bulk porosity. (The results of all of these analyses, except the chemical composition and the resistivity measurements, have been presented in Section 4.) Table 5-5 contains the results of chemical analysis of the Bell Ayr Powder River Basin coal ash (ID # 4118).

The ashes collected in the second and third pilot-scale tests each exhibited a relative minimum in tensile strength at around 34 % RH. The tensile strength data measured as a function of relative humidity for these two ashes are presented in Figure 5-10.

Table 5-5
Chemical Analysis of Bell Ayr Powder River Basin Coal Ash (ID # 4118)

Constituent	Value, % wt.
Na_2O	1.87
K_2O	0.71
MgO	4.53
CaO	23.92
Fe_2O_3	5.78
Al_2O_3	19.96
SiO_2	33.42
TiO_2	1.48
P_2O_5	1.08
SO_3	6.15
SrO	0.39
BaO	0.60
MnO_2	0.11
TOTAL	100.00

For adsorbed water to affect tensile strength and cohesivity, it must exist and remain as free water on the surfaces of the ash particles. If the water originally adsorbed on the particle surfaces becomes strongly bound up as hydrocalcium silicates (or possibly other compounds), it is no longer available to form or maintain liquid bridges. With respect to ash resistivity, the inclusion of hydrated water in the chemical matrix of the ash particles does affect volume conduction through the ash layer collected in an ESP; however, continuously present free surface water is needed for improved surface conduction. Because of the high calcium content of the Bell Ayr Powder River Basin coal ash, hydration of water through mechanisms like the one described here may have significantly affected the cohesivity, tensile strength, and resistivity of this ash.

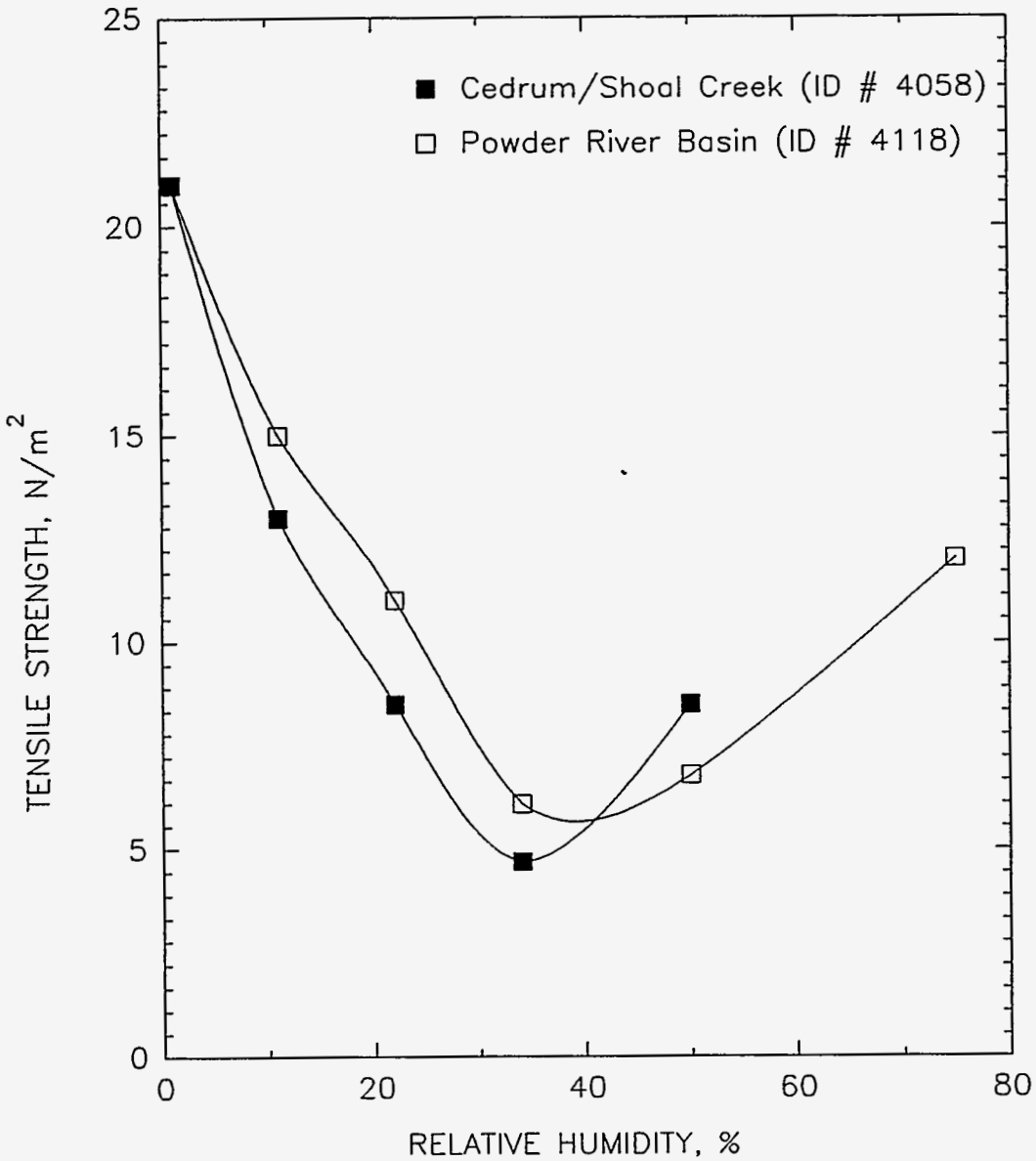

Figure 5-10. Tensile strength as a function of relative humidity for Bell Ayr Powder River Basin coal ash (ID # 4118) and Cedrum/Shoal Creek coal ash (ID # 4058).

Two factors tend to hold previously precipitated ash on an ESP plate. In most cases, the electrical clamping force derived from the particle charge, the applied electric field across the ash layer, and the resistance to current flow through the layer is sufficient to hold the collected ash on the plate. However, this clamping force will diminish and possibly even become a repelling force as the resistivity of the ash drops due to a drop in ash temperature and/or the adsorption of water or other conditioning agent onto the surfaces of the particles. The magnitude of the effects of temperature changes and adsorbed water on ash resistivity and clamping force depend on the particular characteristics of the ash and the structure of the ash layer. Figure 5-11 shows the dependence of resistivity on temperature for the ashes collected in our second and third pilot-scale tests. Figure 5-12 shows the effects that water vapor conditioning has on the laboratory-measured resistivity of the Bell Ayr Powder River Basin coal ash. (Similar behavior has been noted for the other ashes we have characterized.) Because in many of our pilot-scale trials we increased the relative humidity and lowered the ash temperature concurrently (as would occur with simple water injection), the reduction in clamping force can be linked to an increase in relative humidity.

The overall tensile strength of the ash layer provides the second factor that helps to hold the collected ash layer on the ESP plate. Although we have observed that the magnitude of this tensile strength varies as a function of the amount of water adsorbed on the surfaces of the ash particles (Figure 5-10), its overall contribution to holding the ash on the plate is always positive.

Because of the dependence of the electrical clamping force and the tensile strength on ash temperature and adsorbed water, the overall force adhering the ash to the plate can change significantly as temperature and humidity change. Figure 5-13 demonstrates how relative humidity affects the way these two factors combine with the characteristics of the collected ash to either hold the ash on the plate or cause electrostatic reentrainment. Figure 5-13(a) shows for two ashes how the electrical clamping force becomes negative after enough water is adsorbed on the surfaces of the ash particles. (As mentioned above, this increase in adsorbed water is usually accompanied by decreases in ash temperature and subsequent reductions in the resistivity of dry ash.) Figure 5-13(b) presents a generalized relationship between tensile strength and relative humidity for these same two hypothetical ashes. In Figure 5-13(c), the electrical clamping force has been added to the adhering force due to the tensile strengths of the ashes to demonstrate that for an ash with the proper characteristics, electrostatic reentrainment can occur over a finite range of conditions.

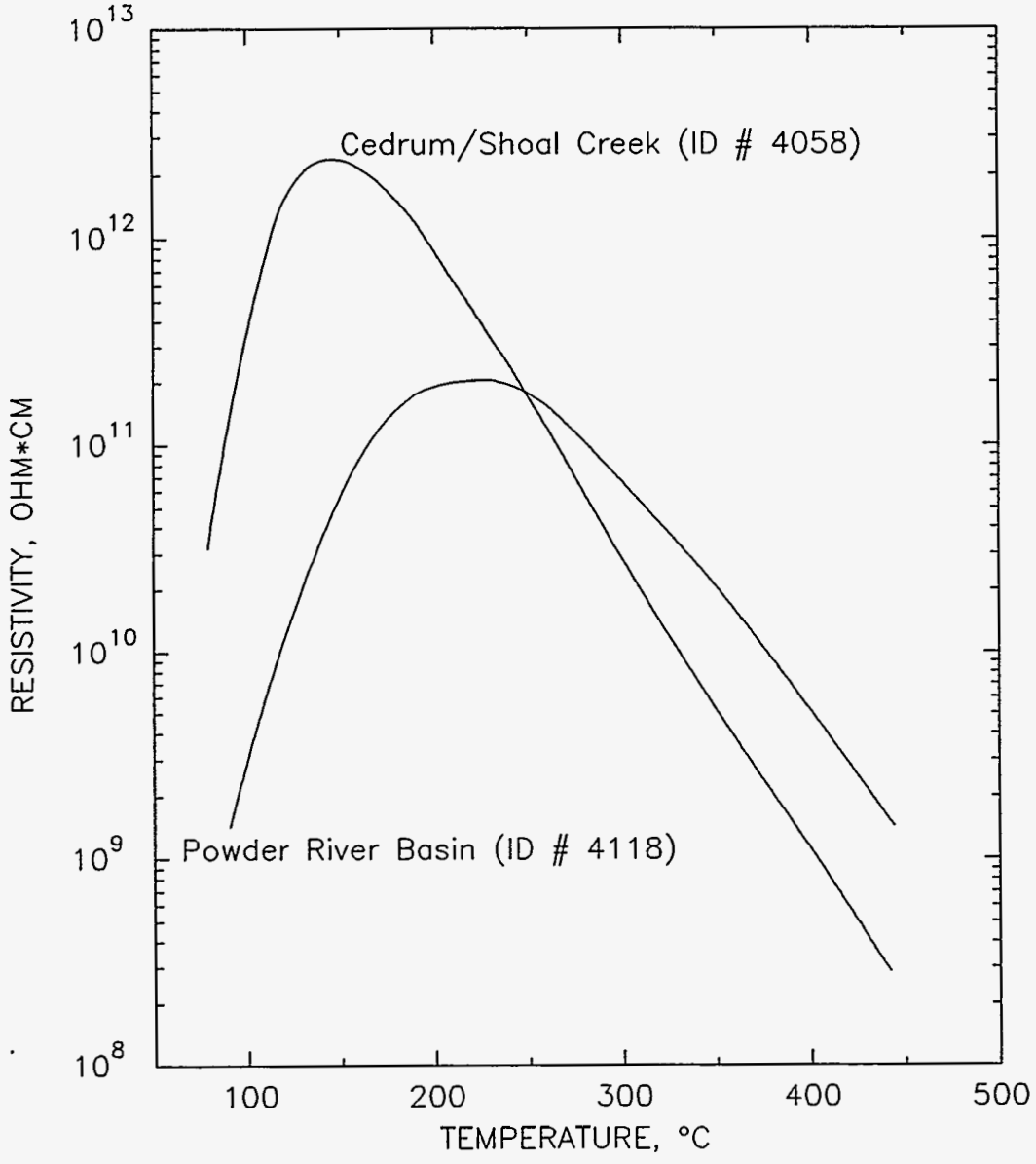

Figure 5-11. Resistivity as a function of temperature for Bell Ayr Powder River Basin coal ash (ID # 4118) and Cedrum/Shoal Creek coal ash (ID # 4058). These data were measured for ash samples conditioned at about 9 % water by volume.

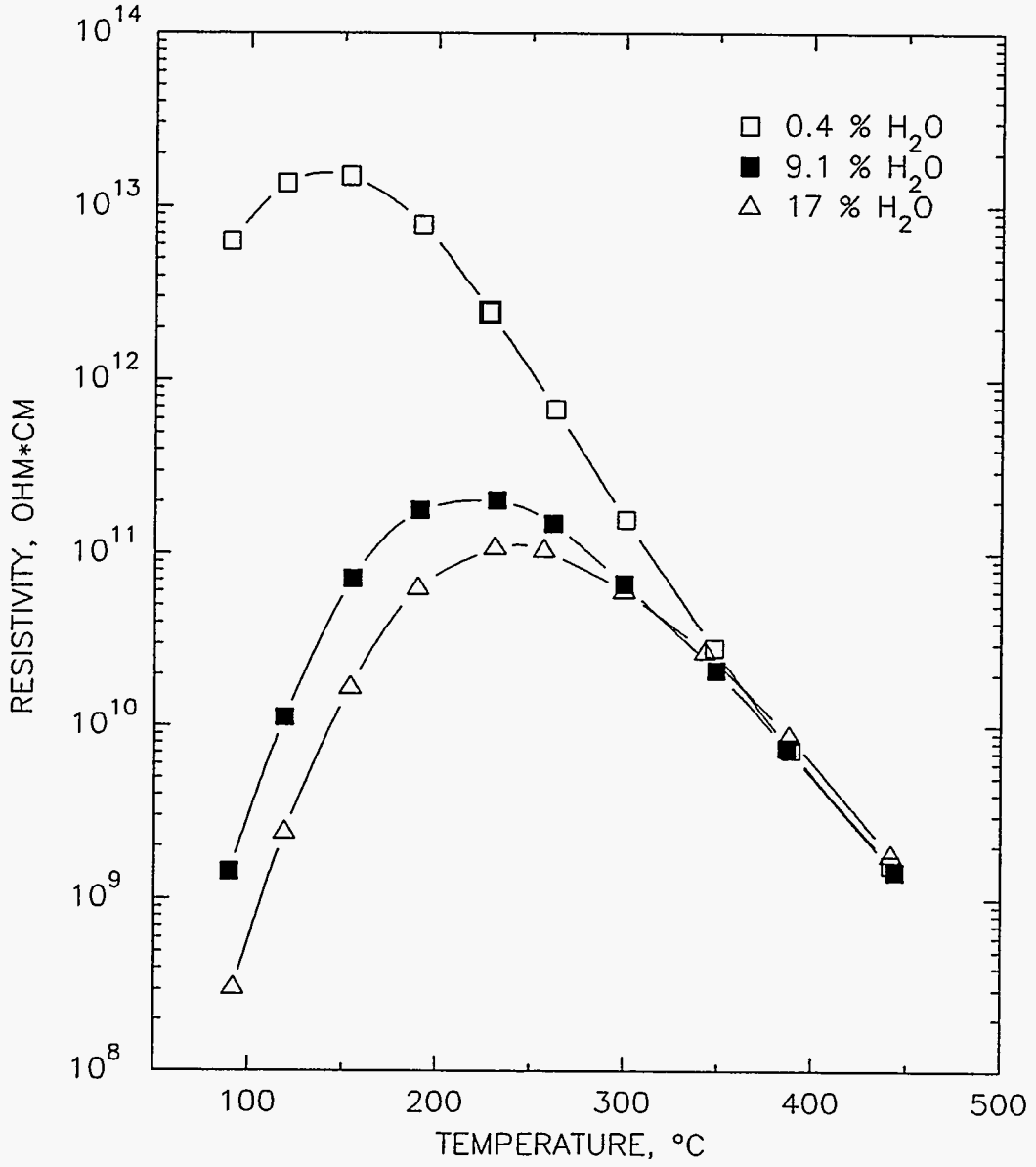

Figure 5-12. Resistivity as a function of temperature for Bell Ayr Powder River Basin coal ash (ID # 4118). These data were measured during descending temperature resistivity determinations in environments with 0.4, 9.1, and 17 % water by volume.

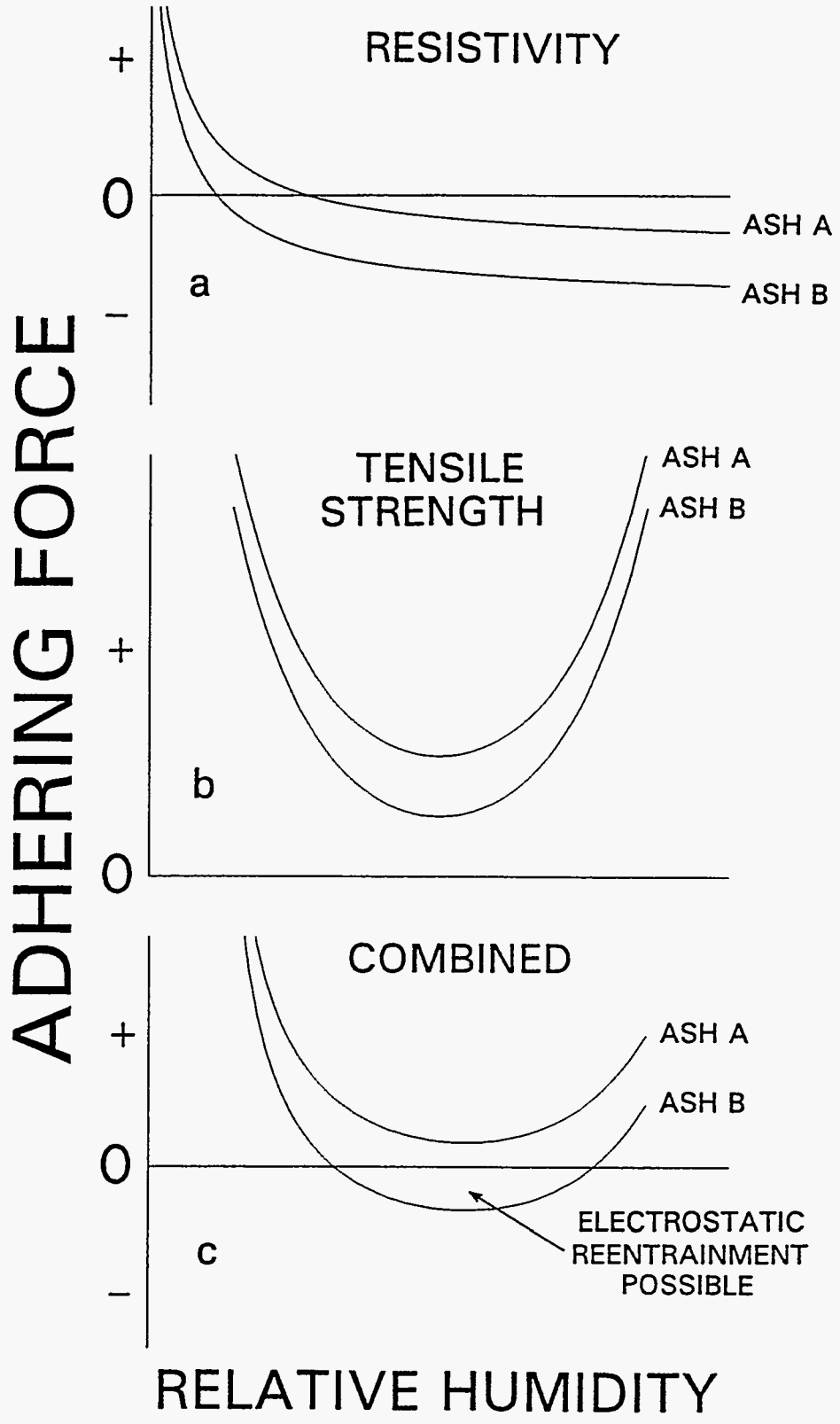

Figure 5-13. This figure demonstrates how relative humidity affects the way the electrical clamping force and tensile strength combine to yield conditions that can be conducive to electrostatic reentrainment.

6 MODELING THE EFFECTS OF FLUE GAS CONDITIONING

We took a pragmatic and phenomenological approach to the development of a model of flue gas conditioning that could be used in conjunction with existing models of particulate control devices. The nature and scope of this project precluded the derivation of anything but a generalized, empirical model. We, nevertheless, studied the fundamental interactions between particles and their environment in order to make sure that our empirical findings were consistent with the basic mechanisms that govern interparticle interactions. Our study entailed the literature survey described in Section 3, and the laboratory analyses reported in Section 4.

We found in our study that conditioning agents affect fine particle collection in control devices by one of two mechanisms that alter particulate properties: adsorption of the agent onto particle surfaces, or addition of sufficient numbers of particles of different surface chemistry and morphology to change the bulk properties. The latter mechanism applies largely to processes whereby solid sorbents are added to a gas stream to capture vapors (e.g., lime for SO_2 capture, or carbon for Hg capture), although the use of additives to improve filtration performance is another application of this mechanism. In general, this mechanism by which bulk properties are changed does not require a distinct model; rather, existing models of particulate control processes apply when the new bulk chemistry of the particulate matter is used as input to the models.

The mechanism of adsorption of conditioning agents onto particle surfaces does entail more subtle effects on particulate control systems. There are, in fact, distinct effects on electrostatic precipitation and fabric filtration that can be predicted. Therefore, these effects can be incorporated into the models of these particulate control processes. The following discussion describes separately the enhancements to the models of fabric filtration and electrostatic precipitation.

6.1 FABRIC FILTRATION

The existing model of fabric filter performance was developed at Southern Research Institute for the Electric Power Research Institute (Pontius and Marchant, 1991). The model describes the pressure drop across a fabric filter as sum of resistances to flow, some of which are in series and some are in parallel. The relationships of the parameters included in the model are shown in Figure 6-1.

Flue gas conditioning affects, primarily, the filtering resistance of the dust cake. This is affected by altering ash properties in some way. Our research in this project has demonstrated that the adsorption of agent onto the surface of particles tends to increase the cohesivity of the bulk powder. This is evident in Table 4-14 which shows the effect of adsorbed water on the uncompacted bulk porosity of powders. As discussed earlier in this report, the formation of liquid bridges between particles increases the interparticle bonds. Since the particles adhere to

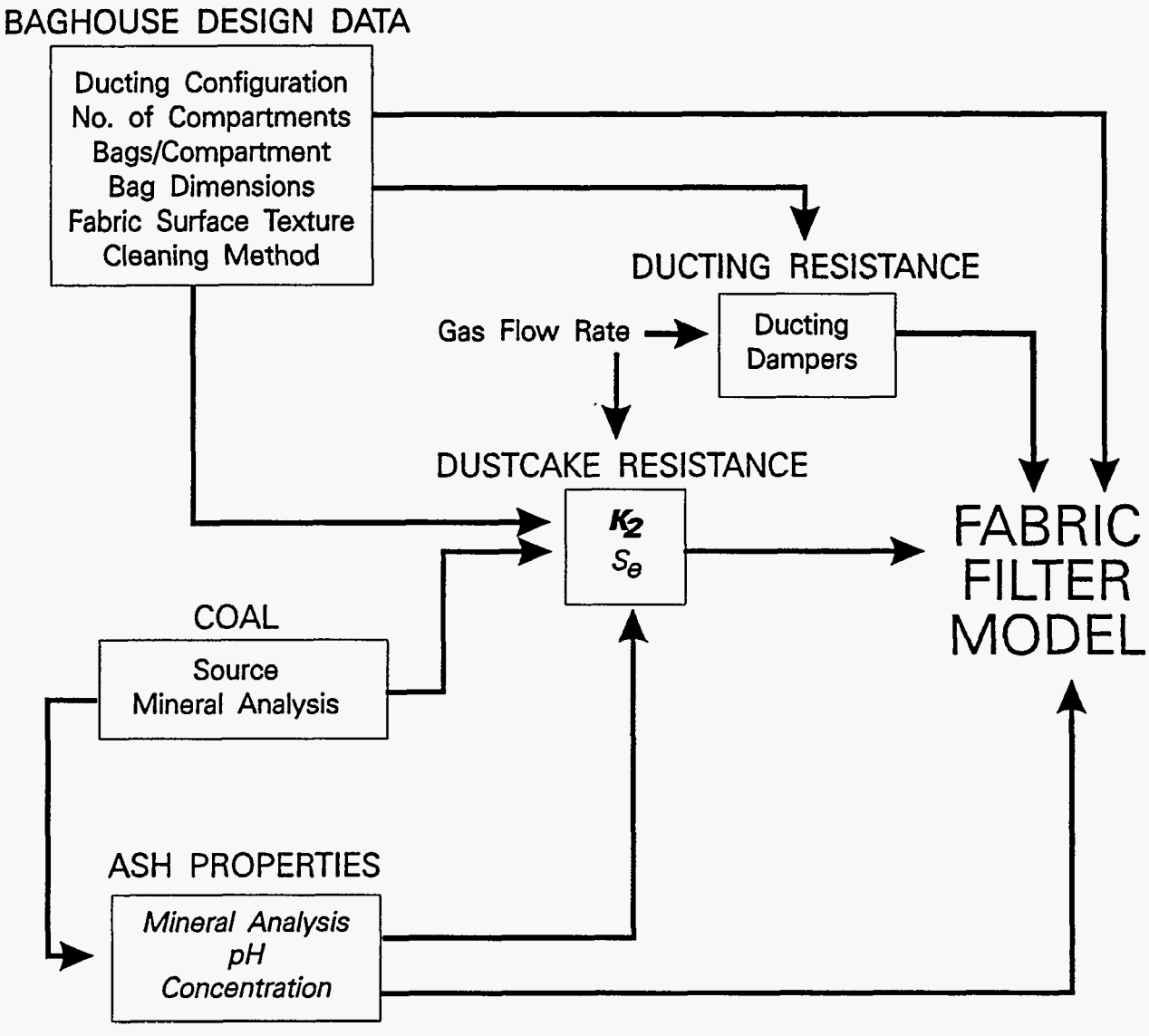

Figure 6-1. Fabric Filter Model Components.

one another more firmly, they build a more porous agglomerate. Porosity is a major variable in determining the resistance to flow through an agglomerate. The following equation expressed the dependence of flow resistance on porosity:

$$R = \Delta p/(WU) = (\mu/D^2)\cdot[1/(\rho(1-\varepsilon))]\cdot[(1-\varepsilon)^2/\varepsilon]\cdot[30+36.2(1-\varepsilon)-143(1-\varepsilon)^2+2240(1-\varepsilon)^3]$$

in which:

R = specific gas flow resistance of the porous bed, μbar/[(g/cm^2)·(cm/s)]
Δp = pressure drop across the porous bed, μbar
W = areal mass loading of the porous bed, g/cm^2
U = face velocity of the gas, cm/s
μ = gas viscosity, poise
D = drag-equivalent diameter of the ash, cm
ρ = average true density of the ash particles, g/cm^3
ε = porosity of the porous bed, dimensionless ($0 < \varepsilon < 1$).

Anything that increases porosity without altering other ash properties (in particular, particle morphology) will decrease the flow resistance. We have shown in this project that flue gas conditioning, in the form of elevated water vapor content, decreases the flow resistance through filter cakes. The data are discussed in Section 5. Our conclusion is that increasing relative humidity forms liquid bridges among the particles so that the filter cake that is built up as the ash is deposited has an increased porosity.

Increased porosity, or decreased flow resistance, is expressed as a component of fabric filter models in the parameter known as K_2, the specific drag coefficient of the filtered material. K_2 is equivalent to the relative gas flow resistance, R. The definition of K_2 is as follows.

$$K_2 \propto (\Delta Pt-\Delta P_e)/tV^2c$$

in which:

ΔP = pressure drop
t = filtration time
ΔP_e = effective pressure drop after cleaning
V = air-to-cloth ratio
c = mass loading.

K_2 is implemented in the fabric filter model, as shown in Figure 6-1, through empirical relationships that we developed between filtering drag and ash properties. Our approach for including the effects of conditioning agents on fabric filter performance is to add an adjustment to K_2 as a module on the existing fabric filter model. With the empirical results given in

Section 5, and previous data, we can estimate the nature and scale of the adjustment factor required to predict the effects of a conditioning agent on K_2.

Data that we have collected suggest that the degree to which a conditioning agent alters K_2 is mainly dependent on the concentration of the additive. In our study, we evaluated water vapor as the additive, and there were noticeable effects of particle surface chemistry and morphology on the relationship between K_2 and water vapor concentration. In the case of a generic additive, added as a liquid or vapor to the particle-laden flue gas, we can not assume exactly the same moderating effects of surface chemistry or morphology (though morphology is likely to have similar effects). So, we propose a model of flue gas conditioning that expresses a simple relationship between K_2 and the concentration of the additive.

We have taken the data from laboratory and pilot-scale filtration tests to determine the empirical dependence of K_2 on the concentration of conditioning agent (in this case, water vapor). Relative humidity is the expression of water vapor concentration that normalizes all of our data; this choice is necessary because of the usually non-isothermal effect of the addition of water vapor, or the purposeful variation of temperature to change the relative partial pressure of water in the flue gases. The values of K_2 assigned to the data were derived from the rates of change of pressure drop, normalized by the filtering face velocities and the particulate loadings of the filtered gases. Filtration data plotted in Figure 6-2 show a consistent, monotonic relationship between K_2 and water vapor concentration.

A logarithmic relationship, also shown in Figure 6-2, provides an acceptable model with which to predict K_2 as additive concentration changes. We can use this relationship as the basis of a model for the effects of conditioning agents on filtration properties. A primary justification for this approach is the finding from this project that the mechanism by which any agent alters particulate properties is at least analogous to, if not equivalent to, the adsorption of water vapor onto the particle surfaces. Furthermore, we have shown that the effects of coal and ash properties on filtration performance also follows a logarithmic relationship (Bush *et al*, 1989). This is additional support for our interpretation of the mechanism involved in conditioning particles.

Therefore, we propose that the following adjustment be incorporated into filtration models whenever flue gas conditioning is used for the purpose of altering ash cohesivity:

$$K'_2 = K_2 \cdot (-\alpha \cdot \mathrm{LOG}(\eta) - 1)$$

in which α is the scale factor defined for each additive, and η is the concentration of additive in the flue gas. In the case of water vapor, as shown in Figure 6-2, the value of α is approximately 0.25, with the concentration, η, expressed in terms of relative humidity.

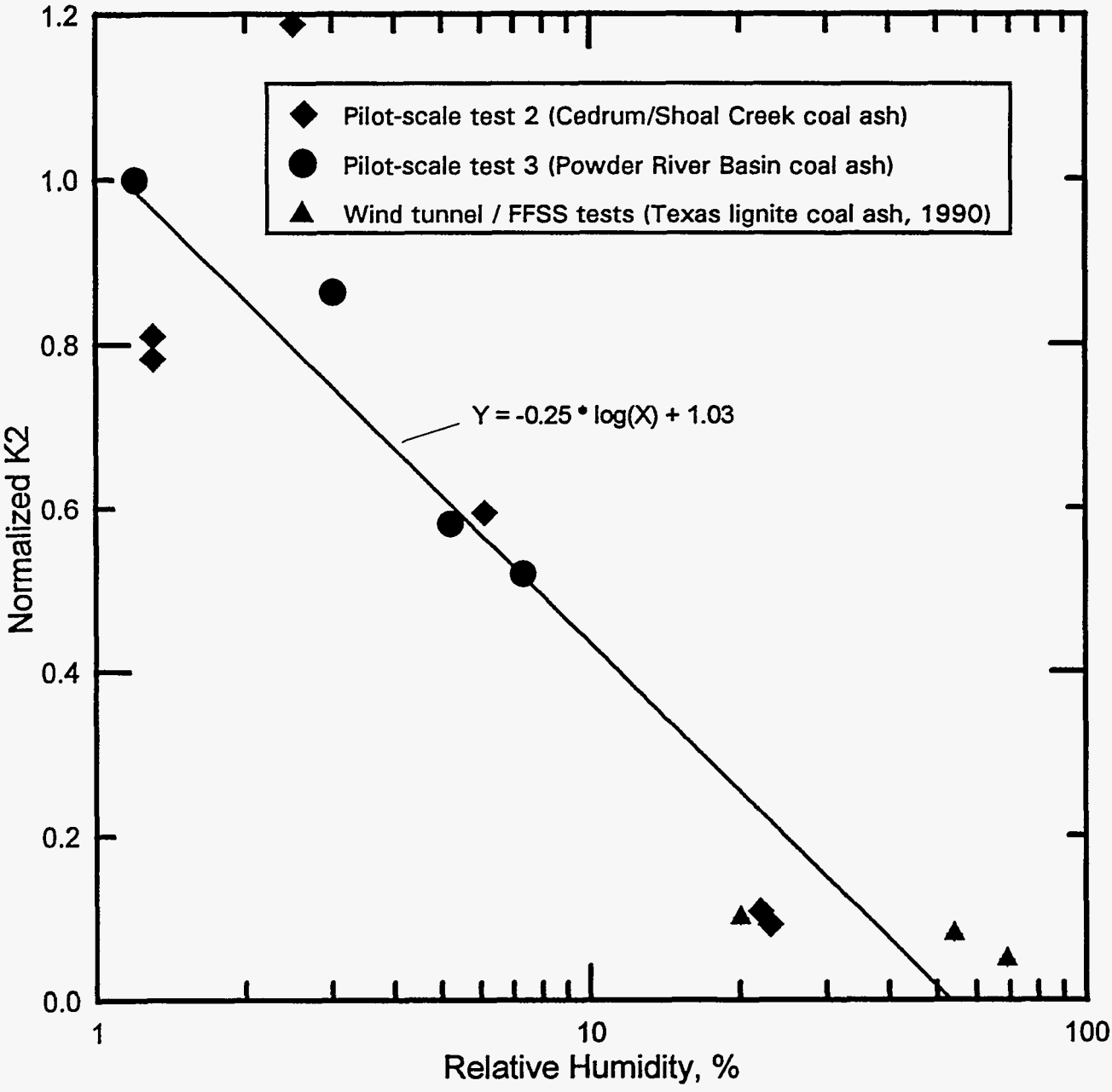

Figure 6-2. Relationship showing the dependence of normalized K_2 on the relative humidity of the gas being filtered. The logarithmic relationship shown provides an acceptable model with which to predict K_2 as additive concentration changes.

This expression for modifying K_2 is the only modeling extension that we feel is reasonable to formulate based on our data. The mechanism by which conditioning agents alter dust cake porosity is also the mechanism governing the tendency of particles to penetrate through the dust cake. Certainly it is true that increasing ash cohesivity through the use of additives affects emissions (Felix *et al*, 1986, Miller and Laudal, 1987). In the exceptional cases where ashes are very non-cohesive, the use of additives can have dramatic effects on emissions. Nevertheless, we have not addressed any effects of additives on fine particle collection efficiency in the context of predictive modeling. There are no existing models of industrial filtration processes that can predict emissions. Generally, emissions in industrial filters are dominated by leaks not directly associated with dust cake properties. (This is the main reason fabric filters tend to have constant efficiency performance for all particle sizes.)

6.2 ELECTROSTATIC PRECIPITATION

Parameters that are involved in the modeling of electrostatic precipitation are shown in Figure 6-3. The two inputs that are modified by conditioning agents are electrical resistivity and emissions from so-called 'non-ideal effects', such as rapping. Electrical resistivity modifications are extremely important to the performance of ESPs, evidenced by the fact that almost all flue gas conditioning for ESPs has focused on this parameter. And flue gas conditioning for resistivity modification is a mature technology, with roots as far back as 1912 (White, 1963). Because of its importance and the wealth of experience in practice, the effects of flue gas conditioning on electrical resistivity are well known. Predictive models of the electrical resistivity of fly ash were developed in the 1970s at Southern Research Institute (Bickelhaupt, 1975, Bickelhaupt, 1979). These resistivity predictions have become accepted components of ESP models, and the work described in this report does not add to these capabilities.

We can bring some new understanding of the effects of flue gas conditioning on emissions associated with reentrainment. Reentrainment in an ESP is the process by which a fraction of emissions are attributable to particles that have been, at one or more times in their passage through the ESP, precipitated onto the collection plates. These particles are either scoured off of the collecting surfaces, are electrostatically repelled from the collecting surfaces, or reenter the gas stream when the electrodes are rapped because they do not form agglomerates of sufficient size to settle into the ESP hoppers. In any case, reentrainment can be considered a phenomenon dependent on the combined effects of electrical and cohesive forces.

By decreasing electrical resistivity of ash, the electrical force that holds ash to the collecting plate (called the electrical clamping force) is reduced. For ashes with very high resistivity, conditioning and the resulting lower resistivity would lessen the clamping force enough to improve rapping efficiency and reduce the dust layer thickness on collecting electrodes. The resistivity of ash would have to be below 5×10^8 ohm-cm before any appreciable non-rapping reentrainment would be expected. The amount of conditioning agent injected to accrue the

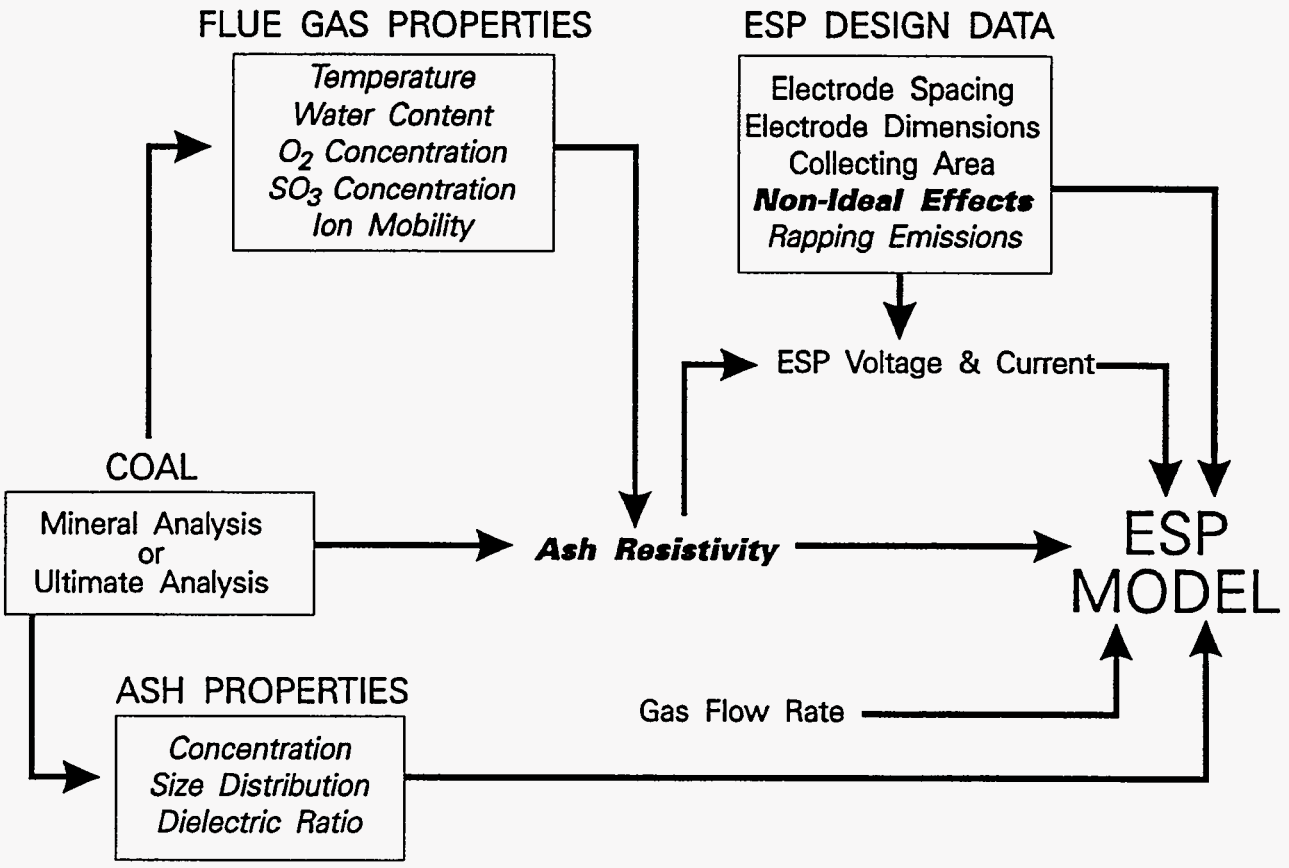

Figure 6-3. ESP Model Components.

benefits of lower resistivity should be limited to the amount that results in ash resistivity in the range of 5×10^8 to 2×10^{10} ohm-cm.

Flue gas conditioning, while reducing the electrical clamping force, can alter the tensile forces holding the collected particles together. Depending on the conditioning agent and the ash, it is possible to increase the tensile strength enough to suppress reentrainment. There is a body of empirical data that shows that water and calcium chloride have both acted in this manner (Brindle *et al*, 1995, Durham, Holstein *et al*, 1991).

Reentrainment is incorporated into existing ESP models through the selection of the non-ideal parameters s, representing sneakage and reentrainment, and σ_g, representing the non-uniformity of gas flow. In the absence of mechanical problems, the performance of ESPs collecting fly ash is typically bracketed by values for (s, σ_g) of 0.05, 0.15 and 0.10, 0.25 (Dubard and Dahlin, 1987).

Data on ESP performance for cases in which particulate properties were altered by processes for flue gas desulfurization show that the existing models of ESP performance provide acceptable predictions if appropriate values of the non-ideal parameters, (s, σ_g), are used (Landham and Cushing, 1994). Based on field tests for a variety of FGD processes, the conclusion was made that there was the potential for increased reentrainment from those processes in which water spray is used to enhance the reaction between a sorbent and SO_2. The explanation for these observed increases in emissions was the combination of a reduction in electrical resistivity of the particulate matter (caused by low temperature and high water vapor content) and an inherently low tensile strength of the mixture of sorbent and ash (Landham and Cushing, 1994). These findings are consistent with the information presented in Section 3.1 and Section 5 of this report.

We propose adopting the following modeling approach for ESPs with flue gas conditioning:

1. Use the existing model to predict electrical resistivity of the particulate matter in the presence of the flue gas conditioning agent, incorporating the chemistry and temperature effects of the conditioning process.
2. If the resultant electrical resistivity of the particulate matter is greater than 10^9 ohm-cm with the flue gas conditioning process, use the standard range of ESP model non-ideal parameters (for s a range of 0.05 to 0.10, and for σ_g a range of 0.15 to 0.25) to model the ESP performance.
3. If the resultant electrical resistivity of the particulate matter is less than 10^9 ohm-cm with the flue gas conditioning process, use for s a range of 0.25 to 0.40, and for σ_g a value of 0.25.

7 CONCLUSIONS

Flue gas conditioning, which involves the modification of one or more of the parameters which determine the magnitude of the forces acting on the fly ash particles, can take place through many different methods. Resistivity, chemistry, cohesivity, size distribution, and particle morphology are among the basic properties of fly ash that significantly influence fine particle collection. Modifications of these particulate properties can result in improved or degraded control device performance. These modifications can be caused by changes to the flue gas, addition of particulate matter such as FGD sorbents, or the addition of reactive gases or liquids.

In high-temperature sorbent injection applications, the resistivity of the mixtures of sorbent and ash particles have significantly higher resistivities than the base line fly ashes. Precipitators collecting these mixtures often have problems with back corona. Although SO_3 conditioning is generally not effective for reducing the resistivities of these types of mixtures because of the presence of unreacted sorbent material, water vapor conditioning has been used successfully to accomplish this goal (Gooch *et al*, 1987; Nolan *et al*, 1990). However, the computer model produced by DuBard *et al* (1986) simulating humidification of mixtures of sorbent and ash suggests that humidification may not be able to overcome the detrimental effects of sorbent addition on resistivity. The model produced by Helfritch *et al* (1986) is more optimistic about the ability of humidification to lower the resistivity of these mixtures. The key to the effectiveness of humidification may lie in the specific chemical and morphological properties of the sorbent and ash particles in the mixture.

At furnace temperatures, the limestone or hydrated lime added to the furnace is rapidly calcined, and the resulting lime undergoes a pozzolanic reaction with the aluminosilicates in the fly ash, forming a modified ash with cementitious qualities. In addition to these changes, furnace sorbent injection produces a shift in the particle size distribution toward smaller sizes. Ashes produced from high-temperature have irregular particle shapes and relatively high specific surface areas.

For low-temperature sorbent injection applications, a primary concern is that the electrical resistivity of the ash/sorbent mixture may become too low. As the resistivity of the mixture drops much below 1×10^8 ohm-cm, the electrical force holding the particles on the ESP plates vanishes and then reverses direction to become a repulsive force. If this repulsive force becomes large enough, it can overcome the tensile strength of the particulate layer, resulting in reentrainment of the particles into the flue gas. Problems with electrostatic reentrainment have been addressed by the addition of a deliquescent additive, $CaCl_2$, to increase the relative humidity in the immediate vicinity of the ash and sorbent particles. This increase in relative humidity promoted increased cohesive strength in the collected ash layer, diminishing the reentrainment.

Both low- and high-temperature sorbent injection processes significantly increase the mass loading entering the particulate control device. Sorbent particles are often quite porous, and they are largely composed of calcium compounds that readily form hydrates. Once these hydrates form, it is very difficult to detach the water molecules. Highly porous, calcium-based sorbents adsorb relatively large amounts of water from the surrounding flue gas. However, sorbent particles can sequester the adsorbed water into the interior of the particles, where it is unavailable for modifying the surface characteristics of the ash and sorbent mixture.

The primary forces or physical changes that affect the interaction of particles, and subsequently the performance of particulate control devices are van der Waals forces, electrostatic forces, ionic forces, adsorbed liquid layers, capillary forces (liquid bridges), and solid bridges. van der Waals forces, adsorption, and liquid and crystalline bridges all intimately depend upon the nature of the particle surface. The morphology of particles, their surface chemistry, and the adsorption of vapors (in particular, water vapor) determine the forces of interaction among particles.

In the particle size regime of coal fly ash, van der Waals forces are generally considered the most fundamental of the interparticle forces. Other forces become important after the van der Waals forces have attracted particles close enough together for the shorter-range forces to participate in the adhesion. At this point, forces other than van der Waals forces may become dominant, as in the case of capillary forces.

Particle morphology governs van der Waals forces. Particle morphology combined with external forces applied to the particles (electrical or fluid dynamic forces) determine the number of contacts, or points of close proximity, each particle has with neighboring particles or surfaces. Adhesive forces increase with increasing proximate or contact area. Thus, decreasing particle size, particle sphericity, or particle surface smoothness will generally increase the strength of adhesive forces between particles.

Physical adsorption of gases is attributed to van der Waals forces and depends largely on particle morphology. Geometry of the particles near the contact point will promote adsorption and condensation of molecules from the gas phase. Adsorption will occur even when the concentration of gas molecules is far below the level for condensation. Physical adsorption can result in multiple layers of adsorbed molecules on the surface of particles. The adsorbed layers increase the area over which the interparticle forces are acting, effectively decrease the separation distance between particles, and, if extensive enough, can lead to the formation of liquid bridges between particles. Adsorbed layers may increase adhesion due to van der Waals forces by as much as a factor of five. Only the first atomic layers on the surface of particles interact in van der Waals forces, so surface chemistry is important in determining adhesion. However, compared to the morphology the chemical nature of the particle surface is of secondary importance for these forces.

Chemical properties of particle surfaces affect the adsorption of gases, as in the use of sorbents to collect gaseous pollutants such as SO_2 and NO_X. Chemical adsorption is usually limited to a monolayer, and creates stronger bonds than do physically adsorbed gases. These strong chemical bonds normally involve ionic-covalent interactions, as is often the case with adsorbed water. The hydrogen-bonding component of interactions with adsorbed water generally makes a far greater contribution to adhesion than the change in van der Waals forces.

The deposition of layers of liquid on the surfaces of fly ash particles is the most common mechanism for altering the behavior of these particles during filtration or precipitation. Ammonium bisulfate, generated on fly ash particle surfaces during conditioning with ammonia in the presence of SO_3, has been shown to be effective in field applications for reducing resistivity and for increasing cohesivity. The effectiveness of this compound for increasing cohesivity is linked to the fact that it melts at 296 °F. Because it may exist as a liquid at the flue gas temperatures encountered in many particle control devices, it can collect at the contact points between particles through capillary action. When this occurs, liquid bridges are formed between adjacent particles. Liquid bridges are the most common mechanism for increasing ash cohesivity. Water adsorbed from the flue gas can also form these liquid bridges.

Adsorbed water is almost a universal factor in the interaction of particles, even in cases of very low relative humidities. Water can be present in different forms: adsorbed monolayers or multilayers on particle surfaces, 'free' mobile water on the surface, physically adsorbed within pores in the particles, or strongly bound by chemisorption. The form of the water depends on the relative humidity of the gas, the morphology of the particles, the geometry of the contact points, and the surface chemistry of the particles. Hydrophilic particles provide binding sites all over the particle surface allowing the formation of a monolayer and then subsequent multilayers of water. For a hydrophobic particle surface there may be only a few sites suitable for water binding, which when saturated act as anchor points for adsorbed droplets. Agents can be applied to particles to alter the affinity of their surfaces to water, and thereby affect adhesion of water. Adsorbed water will form liquid bridges between particles when the relative humidity exceeds some critical level for condensation to occur at contact points. A meniscus forms around the point of contact between particles, and surface tension of the liquid exerts a capillary force between the particles. Drying surfaces after liquid bridges have been formed can leave residual solid bridges between particles. Solid bridges are the strongest of interparticle bonds.

The primary variable determining the degree to which water adsorbs on suspended fly ash and sorbent particles is the relative humidity of the flue gas. As the relative humidity of the flue gas is increased, additional water is deposited on the surfaces of these particles. Even at the temperatures commonly encountered in fabric filters and electrostatic precipitators (~300 °F), layers of water are present on the surfaces of the entrained fly ash particles. Depending on the physical and chemical characteristics of the particles, enough water may become available to affect the strength of the bonds between particles through liquid bridge formation, or to reduce

resistivity by providing conductive paths along the surfaces of the particles. The first layer of water initially deposited on fly ash particles usually forms strong chemical bonds with the compounds on the surfaces of the ash particles. Subsequent layers of water that are adsorbed as relative humidity increases become physically bonded to the particles. This physically bonded water is more mobile than the chemically bonded water, and can form liquid bridges and/or dissolve soluble salts on the particle surfaces.

In our laboratory studies we found that the amount of water adsorbed on the ashes and powders we tested was a function of the relative humidity used to condition them, and also strongly affected by the surface chemistry and morphology of the particles. Water adsorption was promoted by the presence of soluble salts and acids on the surfaces of fly ash particles. Water adsorbed on hydrophobic surfaces (often high in silica), was more likely to migrate to interparticle contact points than similar amounts of water adsorbed onto hydrophilic particle surfaces. The fate of adsorbed water was also strongly affected by the structure of the particles. Porous sorbent particles sequestered water in the interior of the particles, rendering it unavailable for building liquid bridges. We also verified that calcium present in coal fly ash particles often forms hydrates with adsorbed water, limiting the ability of the water to form liquid bridges.

The tensile strength of ashes and fine powders is often predominantly controlled by their size distribution. Ashes and powders with coarse size distributions usually have relatively low tensile strengths. For ashes and powders with similar size distributions, surface chemistry and adsorbed liquid layers can also greatly affect tensile strength.

Existing fabric filtration and electrostatic precipitation models do not adequately account for the various effects flue gas conditioning can have on particle collection. Our data indicate that water vapor conditioning holds promise as a fabric filter conditioning agent. We verified the ability of adsorbed water to lower the specific flow resistance of filter cakes in the laboratory and in our pilot-scale tests. The modifications we suggest for the existing Electric Power Research Institute filtration model account for reductions in the specific resistance of the filter cake due to adsorbed water on the fly ash particles resulting from flue gas humidification.

Our pilot-scale studies also demonstrated that electrostatic reentrainment can occur when the electrical clamping force becomes negative for an ash with inherently low tensile strength. Specific conditions of resistivity and tensile strength must be met to induce this type of reentrainment. Our results also suggest that the overall tensile strength of the ash layer is dependent on the porosity of the layer. Based on our pilot-scale studies, we recommended adjustments to the precipitation model developed for the EPA. These adjustments account for electrostatic reentrainment by modifying the parameters that calculate the effects of non-ideal conditions.

8 RECOMMENDATIONS

Humidification is a flue gas conditioning technique applicable to both electrostatic precipitators and fabric filters to produce improved particulate control. Our studies have shown that water adsorbed on ash particles during humidification of flue gas increases bulk ash cohesivity and decreases bulk ash resistivity. An additional benefit of humidification is a reduction in gas volume due to evaporative cooling. Reductions in gas volume lead directly to increased specific collection area in ESPs and reduced pressure drop in fabric filters.

We recommend that humidification should be seriously considered as a flue gas conditioning option. Unlike many flue gas conditioning systems, humidification does not add any toxic or hazardous compound to the plant site, flue gas, or collected ash. The reductions in resistivity and gas volume that result from flue gas humidification have the potential to significantly enhance ESP performance. These benefits are additive, so that the net effect can be very substantially reduced emissions. Since emissions are exponentially related to SCA, the gas volume reductions that come from evaporative cooling may favor humidification over other flue gas conditioning options. However, our studies have shown that care must be taken to prevent resistivity levels from becoming too low, in order to reduce the likelihood of electrostatic reentrainment of previously collected ash layers. Other potential benefits of increasing the cohesivity of the ash layer that builds on the ESP plates are reduction of rapping emissions and emissions from hopper boil up when ash dislodged from the plates during rapping falls into the collection hopper.

In order to realize the maximum benefit from flue gas humidification upstream of an ESP, it is necessary to closely monitor flue gas temperature and humidity in the ESP and associated ductwork. These data should be combined with continuous outlet mass measurements in order to optimize the degree of humidification used.

In instances where electrostatic reentrainment is suspected, we recommend that efforts be made to characterize the temperature and relative humidity of the flue gas, as well as in situ measurements of ash resistivity. These measurements, as well as ESP voltage and current levels, and inlet and outlet mass concentration data should help to further characterize electrostatic reentrainment, and possibly to establish operating parameters that minimize its harmful effects.

Reductions in flue gas volume and increases in dust cake porosity that result from flue gas humidification upstream of fabric filters directly benefit filter performance. Although the degree to which filtering pressure drop will be reduced will vary at different installations, the mechanisms for these performance improvements are well understood. Furthermore, proper operation and monitoring of the flue gas humidification process should prevent any detrimental occurrences such as dew point excursions. In a few cases where extremely low ash cohesivity

is causing ash particles to gradually bleed through the filtering fabric, water adsorbed onto the ash particles during humidification can also improve overall particle collection efficiency.

In order to optimize flue gas humidification for fabric filter operation, an array of data must be closely monitored. These data include on-line measurements of water consumption, and flue gas temperature, relative humidity, and flow rate. Important parameters describing the condition of the filter bags and cakes must also be closely watched. Key measurements include real time assessments of filtering pressure drop and representative bag weights.

Humidification offers a potentially unique advantage for enhanced control of air toxic emissions. Reducing total particulate emissions is the most direct way to reduce emissions of most of the trace elements that are classified as hazardous air pollutants, or air toxics. Humidification can lower particulate emissions, and thus air toxic emissions, for both ESPs and fabric filters. The unique opportunity humidification may offer is the prospect of condensing vaporous elements. Elements such as selenium and arsenic may be near their dew point temperature at typical flue gas temperatures. Because of the cooling that is achieved with humidification, these elements that would otherwise be emitted as vapors may be collected as solids in the particulate control device. Humidification is a candidate for enhancing control of air toxics.

The positive effects of humidification on particulate control justify serious consideration for this flue gas conditioning technique. Developments in reliable and energy-efficient systems for flue gas humidification need to be evaluated so that this promising technology can mature as an option for improving particulate control.

We also recommend that work investigating novel conditioning agents be continued. Research into the effectiveness of various conditioning agents should include a full array of measurements designed to identify and elucidate the mechanisms active in novel conditioning processes.

9 BIBLIOGRAPHY

Ariman, T. and D. J. Helfritch. How Relative Humidity Cuts Pressure Drop in Fabric Filters, *Filtration and Separation* **14** (1977).

Bickelhaupt, R.E. Effect of Chemical Composition on Surface Resistivity of Fly Ash, EPA-600/2-75-017 (1975).

Bickelhaupt, R.E. A Technique for Predicting Fly Ash Resistivity, EPA-600/7-79-204, US EPA NTIS PB80-102379 (1979).

Bickelhaupt, R.E., R.S. Dahlin, J.P. Gooch, E.C. Landham, Jr., and G.H. Marchant, Jr. Sodium Conditioning for Improved Hot-Side Precipitator Performance, Volume 1: Field and Laboratory Studies, EPRI CS-3711, vol. 1 (1984).

Blythe, G., R. Smith, M. McElroy, R. Rhudy, V. Bland, and C. Martin. EPRI Pilot Testing of SO_2 Removal by Calcium Injection Upstream of a Particulate Control Device. In: Proceedings: 1986 Joint Symposium on Dry SO_2 and Simultaneous SO_2/NO_X Control Technologies, Volume 2. EPA-600/9-86-029b (NTIS PB87-120457). October 1986.

Borgwardt, R. H. and K. R. Bruce. EPA Study of Hydroxide Reactivity in a Differential Reactor. In: Proceedings: 1986 Joint Symposium on Dry SO_2 and Simultaneous SO_2/NO_X Control Technologies, Volume 1. EPA-600/9-86-029a (NTIS PB87-120465). October 1986.

Boynton, R. S. Chemistry and Technology of Lime and Limestone. John Wiley & Sons, Inc. New York, NY. 1966.

Brindle, D. E., T. L. File, and S. L. Thomas. Reducing Flue Gas Temperature by Moisture Conditioning, Presented at the 57th Annual American Power Conference, Chcago, IL (1995).

Brown, C. A., G. M. Blythe, L. R. Humphries, R. F. Robards, R. A. Runyan, and R. G. Rhudy. Results from the TVA 10-MW Spray Dryer/ESP Evaluation, Presented at the First Combined FGD and Dry SO_2 Control Symposium, St. Louis, MO (1988).

Buckton, G. Contact Angle, Adsorption and Wettability - A Review with Respect to Powders, *Powder Technology* **61** (1990).

Bush, P. V., T. R. Snyder, and W. B. Smith. Filtration Properties of Fly Ash from Fluidized Bed Combustion. *J. Air Pollut. Control Assoc.* 37, 1292 (1987).

Bush, P. V., T.R. Snyder, and R.L. Chang. Determination of Baghouse Performance from Coal and Ash Properties: Part I, *JAPCA* **39** (1989).

Bush, P. V., T.R. Snyder, and R.L. Chang. Determination of Baghouse Performance from Coal and Ash Properties: Part II, *JAPCA* **39** (1989).

Bush, P. V. and T. R. Snyder. Literature Review and Assembly of Theories on the Interactions of Ash and Conditioning Agents. Topical Report No. 2; Contract No. DE-AC22-91PC90365. U. S. Department of Energy, Pittsburgh Energy Technology Center. January 1992.

Carr, R. C., A.V. Conti, R.L.Merritt, D.J. Mormille, and J. Pirkey. Pilot Demonstration of a Pulse-Jet Fabric Filter for Particulate Matter Control at an Oil-Fired Utility Boiler, Proceedings of the Ninth Symposium on the Transfer and Utilization of Particulate Control Technology, Williamsburg, VA (1991).

Coelho, M. C. and N. Harnby. The Effect of Humidity on the Form of Water Retention in a Powder, *Powder Technology* **20** (1978).

Coelho, M.C. and N. Harnby. Moisture Bonding in Powders, *Powder Technology* **20** (1978).

Cushing, K. M., V. H. Belba, R. L. Chang, and T. J. Boyd. Fabric Filtration Experience Downstream from Atmospheric Fluidized Bed Combustion Boilers. Presented at the Ninth Particulate Control Symposium. Williamsburg, VA. October 15-18, 1991.

Dahlin, R. S. and R. F. Altman. Prediction of Mass Loading and Particle Size Distribution for Use in a Precipitator Sizing Procedure. In: Proceedings: Conference on Electrostatic Precipitator Technology for Coal-Fired Power Plants. EPRI CS-2908. Electric Power Research Institute. Palo Alto, CA. April 1983.

Dahlin, R. S., R. Beittel, and J. P. Gooch. Pilot-Scale Evaluation of LIMB Technology. EPA Final Report No. EPA/600-87-019 (NTIS PB 87-224630). Environmental Protection Agency. Research Triangle Park, NC. September 1987.

Dahlin, R. S. and T. D. Brown. Control of Acid Mist Emissions from FGD Systems. Presented at the 1991 SO_2 Control Symposium. Washington, DC. December 3-6, 1991.

Dahlin, R. S., C. L. Lishawa, and N. Kaplan. Analysis of LIMB Waste Management Options. In: Proceedings: 1986 Joint Symposium on Dry SO_2 and Simultaneous SO_2/NO_X Control Technologies, Volume 2. EPA-600/9-86-029b (NTIS PB87-120457). October 1986.

Dahlin, R. S., P. V. Bush, and T. R. Snyder. Literature Review and Assembly of Theories on the Interactions of Ash and FGD Sorbents. Topical Report No. 1; Contract No. DE-AC22-91PC90365. U. S. Department of Energy, Pittsburgh Energy Technology Center. January 1992.

Dalmon, J. and D. Tidy. The Cohesive Properties of Fly Ash in Electrostatic Precipitation, *Atmospheric Environment* **6** (1972).

Davison, R. L., D.F.S. Natusch and J.R. Wallace. Trace Elements in Fly Ash Dependence of Concentration on Particle Size, *Environmental Science and Technology* **8** (1974).

Dismukes, E. B. Conditioning of Fly Ash with Sulfur Trioxide and Ammonia, EPA-600/2-75-015 (1975).

Donsi, G. and L. Massimilla. Particle to Particle Forces in Fluidization of Fine Powders, Fluid Ses Appl. Conference (1974).

Doyle, J. B., B. J. Jankura, and R. C. Vetterick. Comparison of Dry Scrubbing Operation of Laramie River and Craig Stations. Presented at the Tenth Symposium on Flue Gas Desulfurization. Atlanta, GA. November 16-21, 1986.

DuBard, J. L., J. P. Gooch, R. Beittel, S. L. Rakes, and G. R. Offen. Particle Properties Related to ESP Performance with Sorbent Injection and Gas Conditioning, In: Proceedings: 1986 Joint Symposium on Dry SO_2 and Simultaneous SO_2/NO_X Control Technologies, Volume 2. EPA-600/9-86-029b (NTIS PB87-120467). October 1986.

DuBard, J. L. and R. S. Dahlin. Precipitation Performance Estimation Procedure, EPRI CS-5040. Electric Power Research Institute. Palo Alto, CA. April 1987.

Durham, M. D., T. G. Ebner, D. B. Holstein, C. A. Brown, and L. G. McGuire. Pilot Plant Investigation of ESP Performance and Upgrade Strategies for In-Duct Sorbent Injection, Presented at the Ninth Particulate Control Symposium, Williamsburg, VA (1991).

Durham, M. D., D. B. Holstein, G. Blythe, K. A. Hieneken, R. G. Rhudy, R. F. Altman, T. A. Burnett, R.A. Barton, and C. W. Dawson. High Efficiency Electrostatic Precipitator Operation at Spray Dryer Conditions, Presented at the Ninth Particulate Control Symposium, Williamsburg, VA (1991).

Emmel, T. E. and N. Kaplan. Lime/Limestone FGD and Sorbent Injection Technology Retrofit Difficulty at 60 Coal-Fired Utility Power Plants, Presented at the First Combined FGD and Dry SO_2 Control Symposium, St. Louis, MO (1988).

Felix, L.G., R.L.Merritt, and K. Duncan. Improving Baghouse Performance, *JAPCA* **36** (1986).

Fuller, E.L., Jr. and K.A. Thompson. Chemical and Geometric Factors in Physical Adsorption/Desorption of Gases and Solids, *Langmuir* **3** (1987).

Gillespie, T. The Contribution of Electrostatic Induction to the Long Range Forces between Solid Particles. Particulate and Multiphase Processes: Vol. 3 Colloidal and Interfacial Phenomena (1987).

Gooch, J. P., J. L. DuBard, and R. Beittel. The Influence of Furnace Sorbent Injection on Precipitator Performance and Methods of Improving Performance. In: Proceedings of the Third International Conference on Electrostatic Precipitation. University of Padua. Abano-Padova, Italy. 1987.

Gullett, B. K. and K. R. Bruce. Pore Distribution Changes of Calcium-Based Sorbents Reacting with Sulfur Dioxide. *AIChE J.* 33 (10), 1719 (1987).

Harker, J.H. and P.M. Pimparker. The Effect of Additives on the Electrostatic Precipitation of Fly Ash, *Journal of the Institute of Energy* **61** (1988).

Helfritch, D. J., P. L. Feldman, B. Weinstein, and M. W. McElroy. Electrostatic Precipitator Upgrades for Furnace Sorbent Injection, In: Proceedings: 1986 Joint Symposium on Dry SO_2 and Simultaneous SO_2/NO_X Control Technologies, Volume 2. EPA-600/9-86-029b (NTIS PB87-120467). October 1986.

Hench, L. L. Characterization of Powder Surfaces - Chapter 16 of Ceramics published by Marcel Dekker. (1971).

Henzel, D. S. and W. Ellison. Commercial Utilization of SO_2 Removal Wastes in the Application of New Advanced Control Technology. Presented at the 1990 SO_2 Control Symposium. New Orleans, LA. May 8-11, 1990.

Hobbel, E.F. Cohesion and Interparticle Forces. Dissertation (1988).

Jayasinghe, S.S. The Cohesion and Flow of Particulate Solids, *Process Technology International* **17** (1972).

Jøns, E., K. Felsvang, and R. Madhok. Limestone Spray Drying Absorption for SO_2 Control. Presented at the Tenth Symposium on Flue Gas Desulfurization. Atlanta, GA. November 17-21, 1986.

Jozewicz, W., J. C. S. Chang, C. B. Sedman, and T. G. Brna. Characterization of Advanced Sorbents for Dry SO_2 Control. *Reactivity of Solids.* 6, 243 (1988).

Karra, V.K. and D.W. Fuerstenau. The Effect of Humidity on the Trace Mixing Kinetics in Fine Powders, *Powder Technology* **16** (1977).

Kaufherr, N., M. Shenasa, and D. Lichtman. X-ray Photoelectron Spectroscopy Studies of Coal Fly Ashes with Emphasis on Depth Profiling of Submicrometer Particle Size Fractions, *Environmental Science and Technology* **19** (1985).

Keller, D.V., Jr. et al. Investigation of Physics of Adhesion of Coal Aerosols, Bureau of Mines Report 16-75 (1973).

Khan, F. and N. Pilpel. The Effect of Particle Size and Moisture on the Tensile Strength of Microcrystalline Cellulose Powder, *Powder Technology* **48** (1986).

Kirchgessner, D. A. and J. M. Lorrain. Lignosulfonate-Modified Calcium Hydroxide for Sulfur Dioxide Control. *Ind. Eng. Chem. Res.* 26, 2397 (1987).

Klingspor, J. Kinetic and Engineering Aspects of the Wet-Dry FGD Process. Licenciate Thesis. Lund Institute of Technology. Lund, Sweden. 1983.

Klein, D.H. et al. Pathways of Thirty-seven Trace Elements Through Coal-Fired Power Plant, *Environmental Science and Technology* **9** (1975).

Landham, E. C., Jr., K. M. Cushing. Guidelines for Particulate Control for Advanced SO_2 Control Processes, EPRI TR104594. Electric Power Research Institute. Palo Alto, CA. December 1994.

Landham, E. C., Jr., K. M. Cushing, R. F. Altman, B. D. Larson, and J. B. Doyle. Effects of Spray Dryer Effluent on the Performance of the Laramie River Unit 3 ESP, Presented at the Ninth Particulate Control Symposium, Williamsburg, VA (1991).

Lauga, C., J. Chaouki, D. Klvana and C. Chavarie. Improvement of the Fluidisability of Ni/SiO_2 Aerogels by Reducing Interparticle Forces, *Powder Technology* **65** (1991).

Leong, K.H., J.J. Stukel, and P.K. Hopke. Effects of Surface Properties of Collectors on the Removal of Charged and Uncharged Particles from Aerosol Suspensions, EPA Report EPA-600/7-82-006 (1981).

Livengood, C. D., H. S. Huang, J. W. Allen, and P. S. Farber. Combined SO_X/NO_X Removal in a High-Sulfur Spray Dryer/Fabric Filter System. Presented at the First Combined FGD and Dry SO_2 Control Symposium. St. Louis, MO. October 25-28, 1988.

Luckham, P.F. The Measurement of Interparticle Forces. (An Invited Review), *Powder Technology* **58** (1989).

Mamane, Y., J.L. Miller and T.G. Dzubay. Characterization of Individual Fly Ash Particles Emitted from Coal- and Oil-Fired Power Plants, *Atmospheric Environment* **20** (1986).

Merritt, R.L. P.V. Bush, N.H. Wagner, P.J. Knapp, and R.L. Chang. Demonstration of Strategies for Improved Baghouse Performance, Proceedings of the Ninth Symposium on the Transfer and Utilization of Particulate Control Technology, Williamsburg, VA (1991).

Miller, S.J. and D.L. Laudal. Flue Gas Conditioning for Improved Fine Particle Capture in Fabric Filters: Comparative Technical and Economic Assessment, DOE/MC/10637-2414, vol. 2 (1987).

Miller, S. J., D. L. Laudal, and R. Chang. Flue Gas Conditioning for Improved Pulse-Jet Baghouse Performance. Presented at the Ninth Particulate Control Symposium. Williamsburg, VA. October 15-18, 1991.

Milne, C. R., G. D. Silcox, D. W. Pershing, and D. A. Kirchgessner. High-Temperature, Short-Time Sulfation of Calcium-Based Sorbents. 1. Theoretical Sulfation Model, *Ind. Eng. Chem. Res.* **29** (1990).

Natusch, D.F.S. Characterization of Fly Ash from Coal Combustion, NTIS # COO-4347-4 Workshop on measurement technology and characterization of primary sulfur oxides emission from combustion sources, Southern Pines, NC, USA (1978).

Natusch, D.F.S., E.R. Denoyer, T.R. Keyser, S.E. Kirton, D.R. Taylor, and M.V. Zeller. Surface Analysis of Particles Emitted to the Atmosphere, *AIChE Symposium* **201** (1980).

Pontius, D. H. and G. H. Marchant, Jr. Laboratory and Field Studies of Electrical Reentrainment Associated with Calcium-Based Sorbents, Presented at the Ninth Particulate Control Symposium, Williamsburg, VA (1991).

Pontius, D. H. and T. R. Snyder. Measurement of the Tensile Strength of Uncompacted Dust Aggregates, *Powder Technology* **68** (1991).

Rietma, K. Powders, What Are They?, *Powder Technology* **37** (1984).

Rothenberg, S.J. Coal Combustion Fly Ash Characterization: Adsorption of Nitrogen and Water, *Atmospheric Environment* **14** (1980).

Sedman, C. B., R. E. Valentine, and N. Plaks. Evaluation of Pilot ESP Performance with Elevated Loadings from Sorbent Injection Processes. Presented at the Ninth Particulate Control Symposium. Williamsburg, VA. October 15-18, 1991.

Slaughter, D. M., S. L. Chen, W. R. Seeker, D. W. Pershing, and D. A. Kirchgessner. Increased SO_2 Removal with the Addition of Alkali Metals and Chromium to Calcium-Based Sorbents. In: Proceedings of the 22nd Symposium (International) on Combustion. Combustion Institute. 1988.

Snyder, T.R., P.V. Bush, and M.S. Robinson. Characterization and Modification of Particulate Properties to Enhance Filtration Performance, DOE/PC/88868-T5 (1990).

Tidy, D. A Leaching Technique for Determining the Surface Composition of Pulverized Fuel Ash (PFA), *Journal of the Institute of Energy* **59** (1986).

van Oss, C. J. and R. J. Good. On the Mechanism of "Hydrophobic" Interactions, *J. Dispersion Science and Technology* **9** (1988).

Visser, J. Adhesion of Colliodal Particles, Manuscript for Surface and Colloid Science.

White, H.J. Industrial Electrostatic Precipitation, (1963).

Williams, R. and R.W. Nosker. Adherent Dust Particles, *RCA Engineer* **28** (1983).

Yoon, H., J. A. Withum, W. A. Rosenhoover, and F. P. Burke. Sorbent Improvement and Computer Modeling Studies for Coolside Desulfurization. In: Proceedings: 1986 Joint Symposium on Dry SO_2 and Simultaneous SO_2/NO_x Control Technologies, Volume 2. EPA-600/9-86-029b (NTIS PB87-120457). October 1986.

Zimon, A. D. Adhesion of Dust and Powder. 2nd Edition. Consultants Bureau/Plenum Publishing Corporation. New York, NY. 1982.

APPENDIX A
LITERATURE SEARCH PROCEDURES

An abstract search was performed through the DIALOG Information Services. This computer-based service was used to access the National Technical Information Service (NTIS), COMPENDEX PLUS, and Chemical Abstracts data bases. The NTIS data base consists of unclassified government-sponsored research, development and engineering reports, and other analyses prepared by government agencies. The COMPENDEX PLUS data base provides coverage of the worlds significant engineering and technical literature. This data base corresponds to the printed publication "Engineering Index", plus additional conference records from the Engineering Meetings file. The Chemical Abstracts data base provides the most current indexing and abstracting of the major chemical literature. The search terms used are presented in Table A-1. This search was performed on July 29, 1991.

Table A-1
Terms Used in Abstract Search

Set	Items	Description
1	127886	powder? or particle? or particulat? or sorbent? or ash?
2	127886	S1/ENG,NPT
3	120912	S2 not (Chromatog? or extract? or soil? or virus?? ? or viral? or pollen? or pharmaceut? or drug?)
4	6789	S3 and (inject? or spray( )(dry? or drie?) or hydroxide? or reentrai? or cohesi? or adhesi? or adsor?)
5	16328	S3 and (propert? or interpartic?)
6	21722	S4-S5
7	7195	S3 and (propert? or interpartic?)
8	13463	S4 or S7

Over 35,000 abstracts were returned from this search and examined. 136 articles and reports that appeared to contain information describing the factors involved in either the interactions of ashes and sorbents or in the general conditioning of ash or other fine particles were selected. Many of these articles and reports were obtained from the holdings of Southern Research Institute's Library. The other articles and reports selected were ordered through various NTIS and interlibrary loan services.

APPENDIX B
ANALYTICAL METHODS USED TO CHARACTERIZE SAMPLES

SIZE DISTRIBUTION - This technique provides a measurement of the size distribution and Stokes' mean diameter of the fly ash or powder size distribution based on aerodynamic classification of the individual ash particles. The results of this test indicate whether an ash is typically sized in comparison to other ashes tested, or abnormally fine or coarse. An abnormal size distribution can have significant effects on filtration behavior. In general, filter cakes composed of extremely fine ash particles exhibit abnormally high filtering drags.

SPECIFIC SURFACE AREA - This measurement utilizes the Brunaeur-Emmett-Teller (BET) technique for determining the total surface area of a known mass of ash or powder. Ashes with high specific surface areas are usually highly cohesive, and form filter cakes with relatively high porosities.

UNCOMPACTED BULK POROSITY - This value expresses the porosity of a container of sifted ash or powder . Ashes and powders exhibiting relatively high uncompacted bulk porosity values are generally highly cohesive. The uncompacted bulk porosity of an ash sample can be used as an estimate of the porosity of the filter cake that would be formed in a conventional fabric filter.

PARTICLE DENSITY - This standard measurement is obtained with a helium pycnometer. This measurement determines the true density, or specific gravity of the ash or powder particles in the sample tested. Particle density is a factor in calculating porosity, and Stokes' diameter.

TENSILE STRENGTH - This test measures the magnitude of the attractive forces between ash or powder particles. An electrostatic tensiometer is used to apply a mechanical stress on a layer of particles as an effect of an imposed electrostatic field. This electrostatic technique allows the measurement to be performed on uncompacted powder or ash samples.

GAS FLOW RESISTANCE - This value is obtained by filtering air at a known flow rate through a simulated dust cake of known porosity in a laboratory test device while measuring the resistance to the air flow. When this measurement is made with the porosity of the simulated dust cake equal to the estimated characteristic dust cake porosity of the ash, the resultant gas flow resistance is defined as the specific gas flow resistance. This value is the resistance that this simulated dust cake (with an areal loading of 1.0 lb/ft^2) exhibits for an air flow of 1.0 $acfm/ft^2$.

DRAG-EQUIVALENT DIAMETER - This quantity is not a measurement of physical size, but rather a fitted parameter ranking the characteristic gas flow resistances of ashes at equal porosities. Increasing values of drag-equivalent diameter indicate a lower resistance to gas flow at a given porosity. Measurements of physical size generally correlate with this expression; however, the drag-equivalent diameter best expresses the fineness of an ash or powder as it relates to its effect on gas flow resistance. Ashes and powders with smaller values of drag-equivalent diameter are generally more cohesive.

SCANNING ELECTRON MICROSCOPE PHOTOGRAPHS - Representative photographs of the ash and powder samples were taken at a range of magnifications. The appearance of the ash and powder particles often provided valuable insight into bulk sample characteristics and behavior. These photographs also allowed quick comparison of different samples and qualitative verification of particle sizing data.

CHEMICAL ANALYSES - Standard techniques are used to determine the mineral constituents of ash and powder samples that are ignited overnight at 750 °C. Loss on ignition (LOI) is determined gravimetrically. Soluble $SO_4^{=}$ and equilibrium pH values are measured for as-received samples.

Table B-1
Primary Methods and Equipment Used in Laboratory Analyses

Test	Equipment	Data obtained	Limitations
sedigraphic analysis	Shimadzu SA-CP4	aerodynamic size distribution	agglomeration of particles, measurement performed in liquid environment
uncompacted bulk porosity	uncompacted bulk porosity tester	porosity of sample	testing at high temperature not possible
surface area analysis	Monosorb Surface Area Analyzer	specific surface area	removes adsorbed materials from sample prior to measurement
tensile strength	electrostatic tensiometer	tensile strength	tensile strength of some samples may exceed the upper limit of device
SEM photo micrographs	scanning electron microscope	visual record of particle appearance	adsorbed compounds may be lost during preparation
drag-equivalent diameter	permeability tester	calculated diameter based on bulk permeability	algorithm used in calculation tends to fail for highly irregular particles
specific gas flow resistance	permeability tester	flow resistance of bulk ash sample	value is strongly dependent on measurements of bulk porosity
water content	Karl Fischer titrator	water content of powder sample	measurement cannot be done in situ
solvent leaching	solvent leaching apparatus	amounts, types of soluble compounds on particle surfaces	technique does not reveal distribution of compounds on particle surfaces
chemical analysis	various standard techniques	chemical constituents	
particle density	helium pycnometer	particle density	method cannot distinguish internal pore structure
resistivity	IEEE Standard Method 548-1984	resistivity at various temperatures and gas conditions	

APPENDIX C
MEASURED SIZE DISTRIBUTIONS OF POWDERS AND ASHES

The following pages contain the size distributions of the various samples in the data base of ashes, powders, and mixtures of sorbents and ashes.

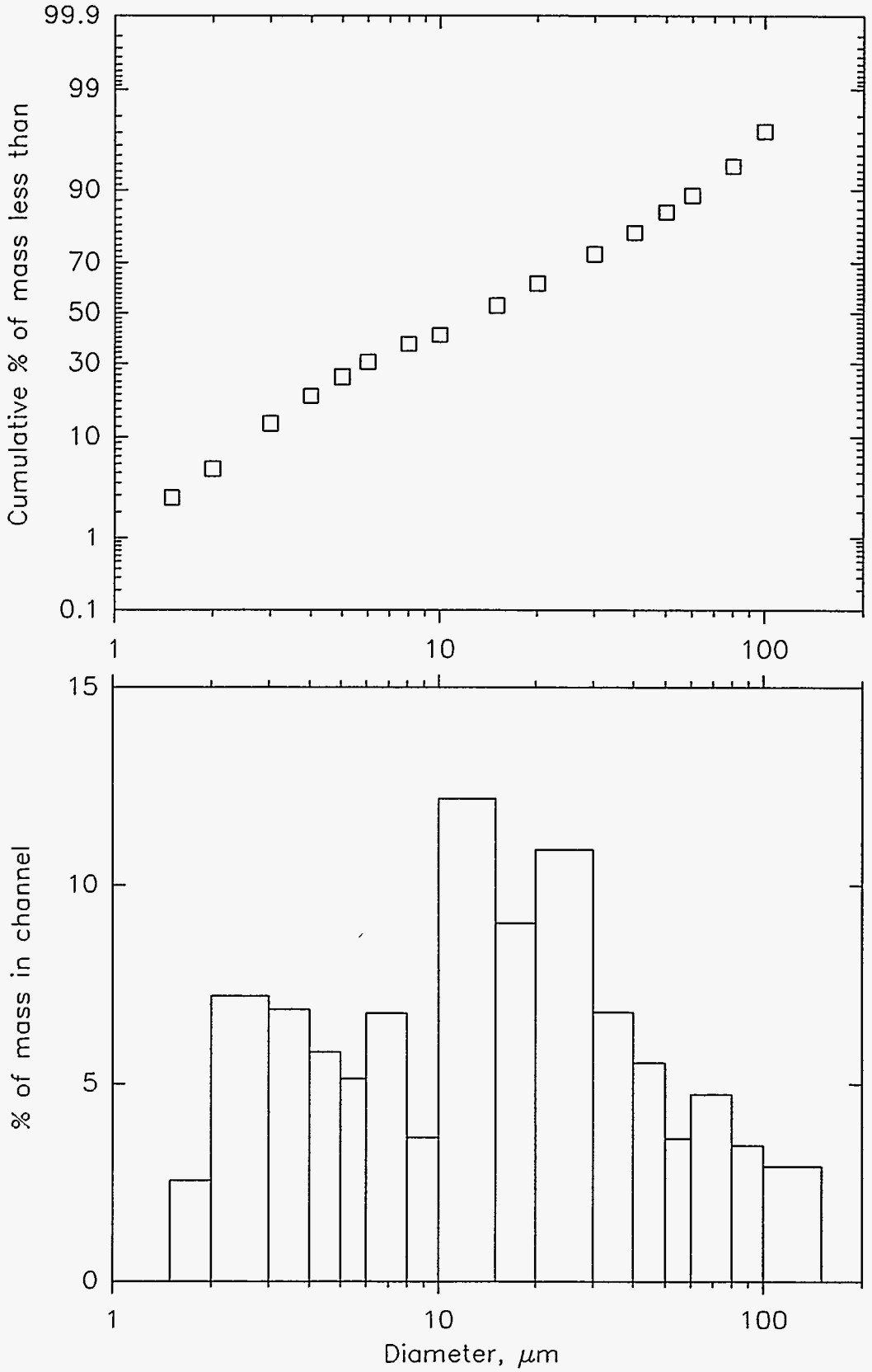

Figure C-1. Cumulative and differential size distribution data measured with a sedigraph for the Muskingum base line ESP hopper ash (ID # 2870).

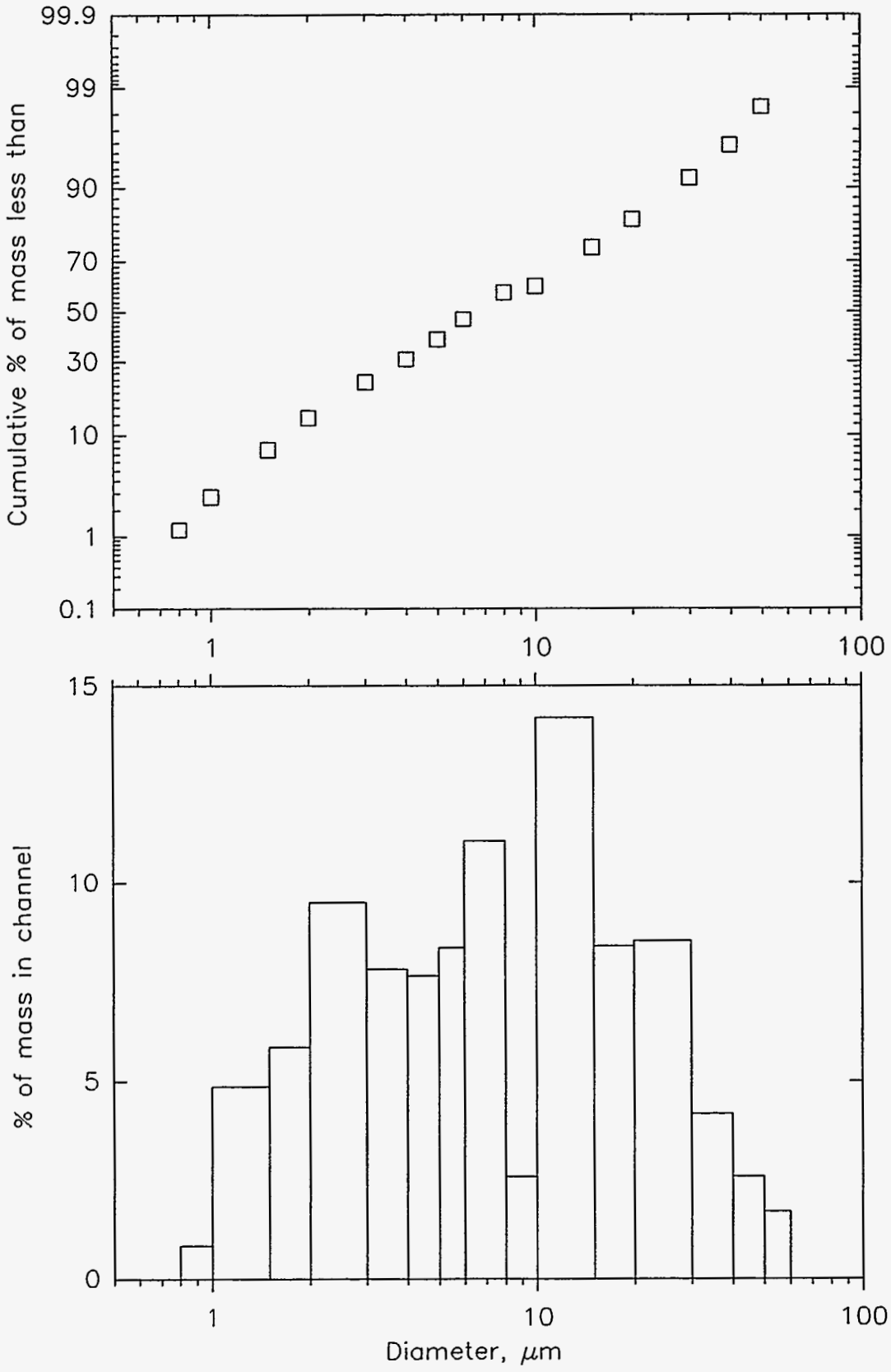

Figure C-2. Cumulative and differential size distribution data measured with a sedigraph for the sorbent and ash mixture from tests of dry $Ca(OH)_2$ injection at the DITF (ID # 2871).

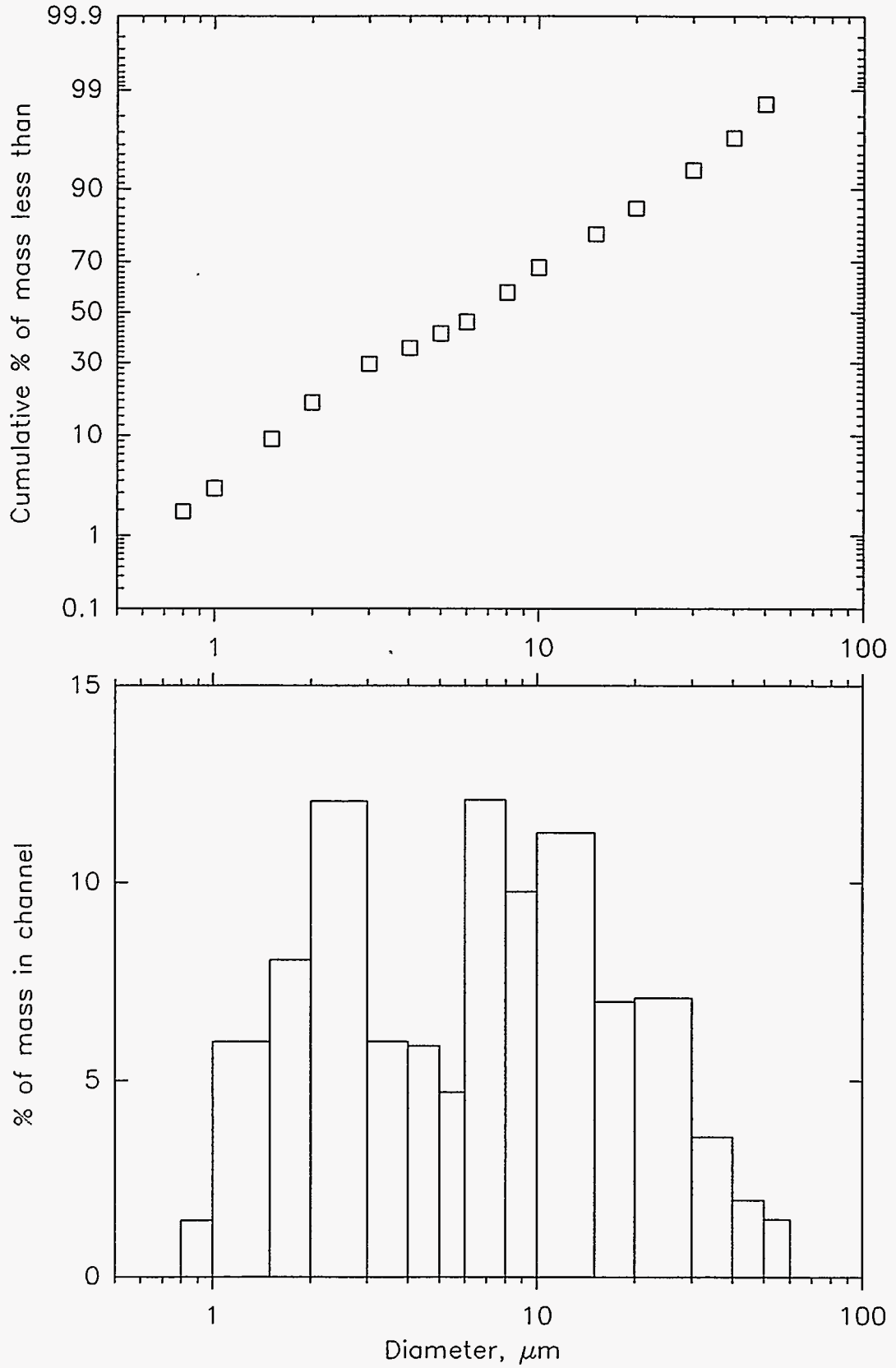

Figure C-3. Cumulative and differential size distribution data measured with a sedigraph for the sorbent and ash mixture from tests of $Ca(OH)_2$ slurry injection at the DITF (ID # 2872).

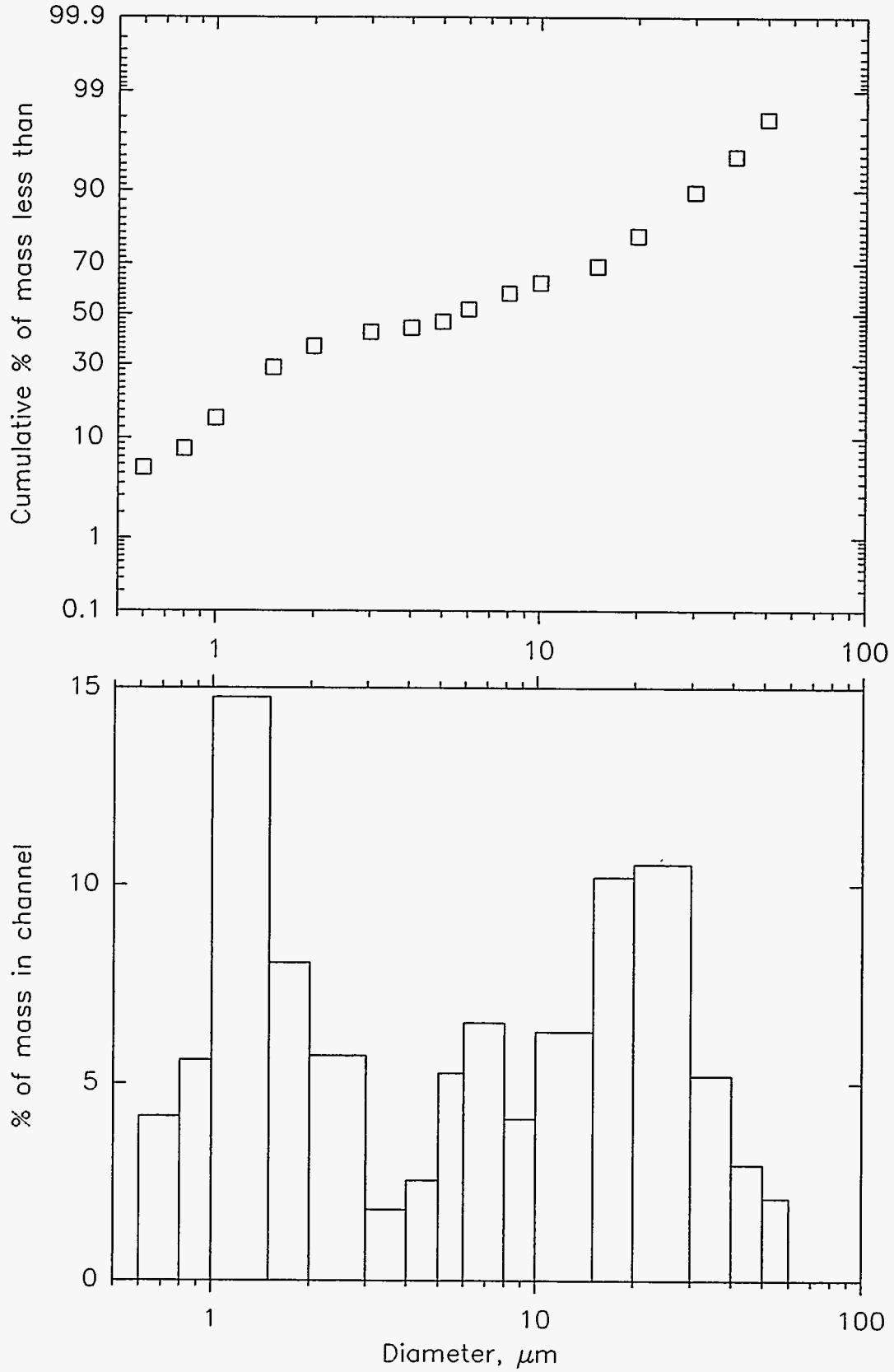

Figure C-4. Cumulative and differential size distribution data measured with a sedigraph for the sorbent and ash mixture from tests of $Ca(OH)_2$ slurry injection with $CaCl_2$ addition at the DITF (ID # 2873).

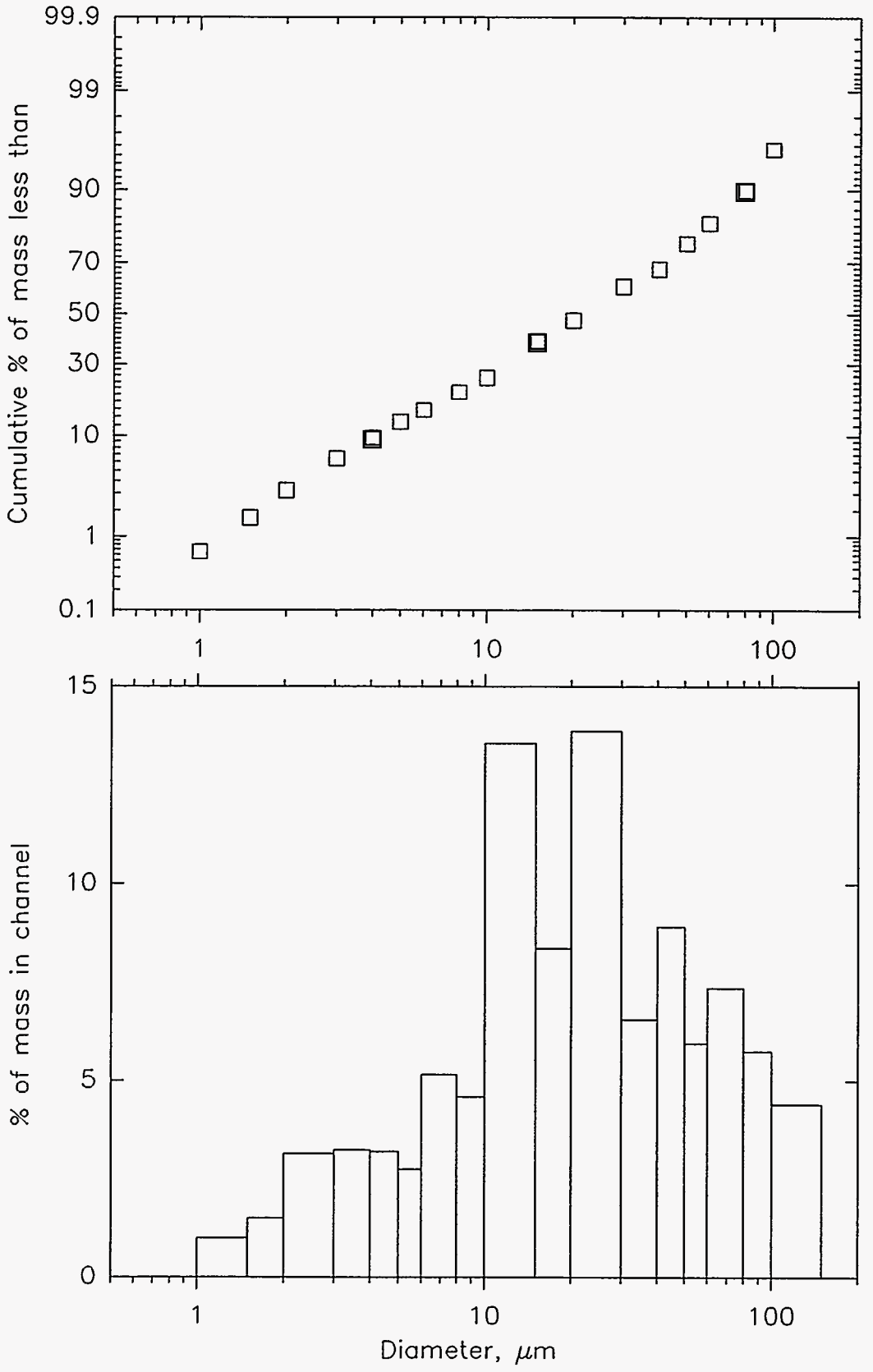

Figure C-5. Cumulative and differential size distribution data measured with a sedigraph for the Plant Kintigh base line ESP hopper ash (ID # 2884).

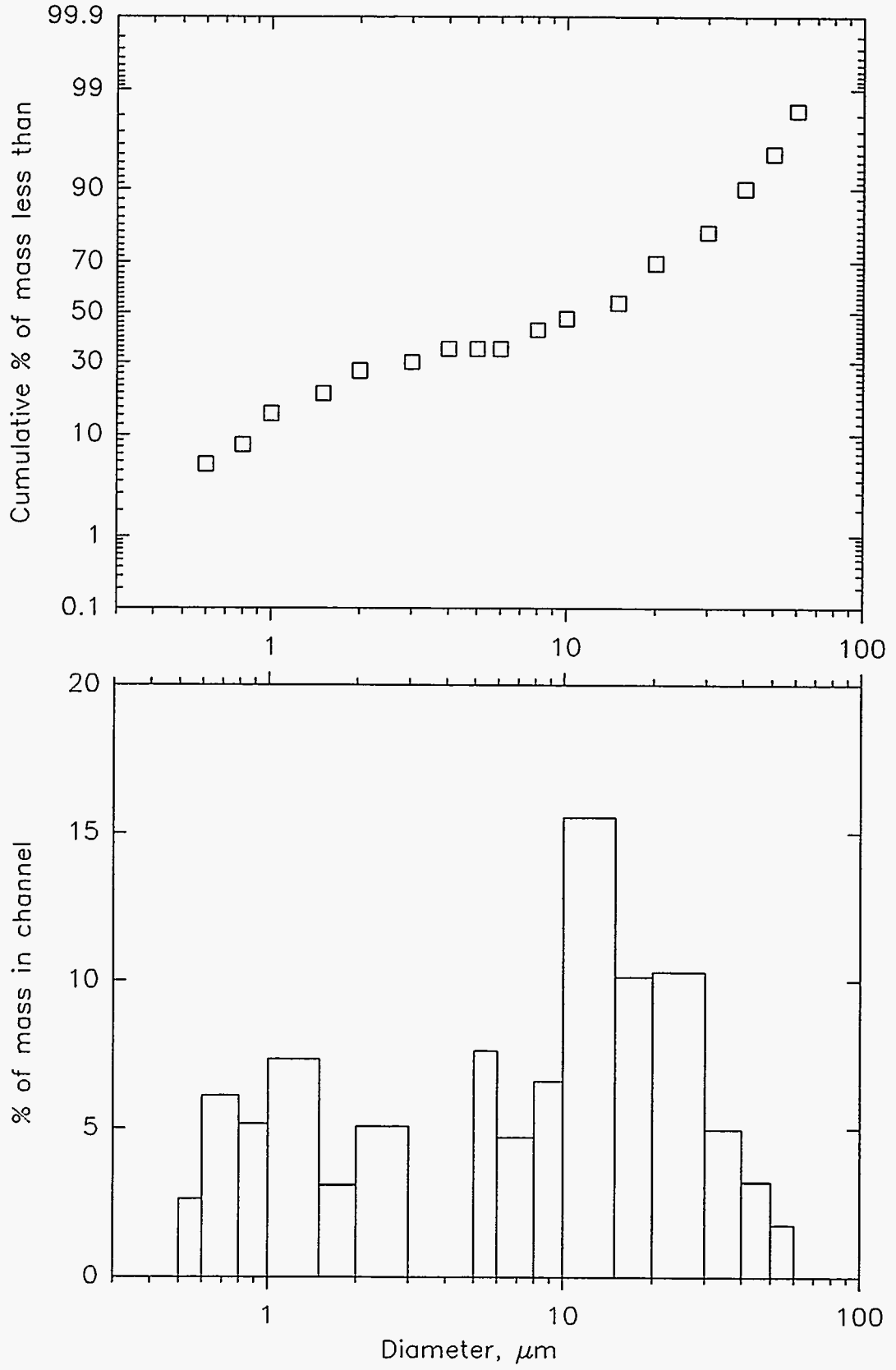

Figure C-6. Cumulative and differential size distribution data measured with a sedigraph for the sorbent and ash mixture produced in the conventional spray dryer located at the High Sulfur Test Center (ID # 2885).

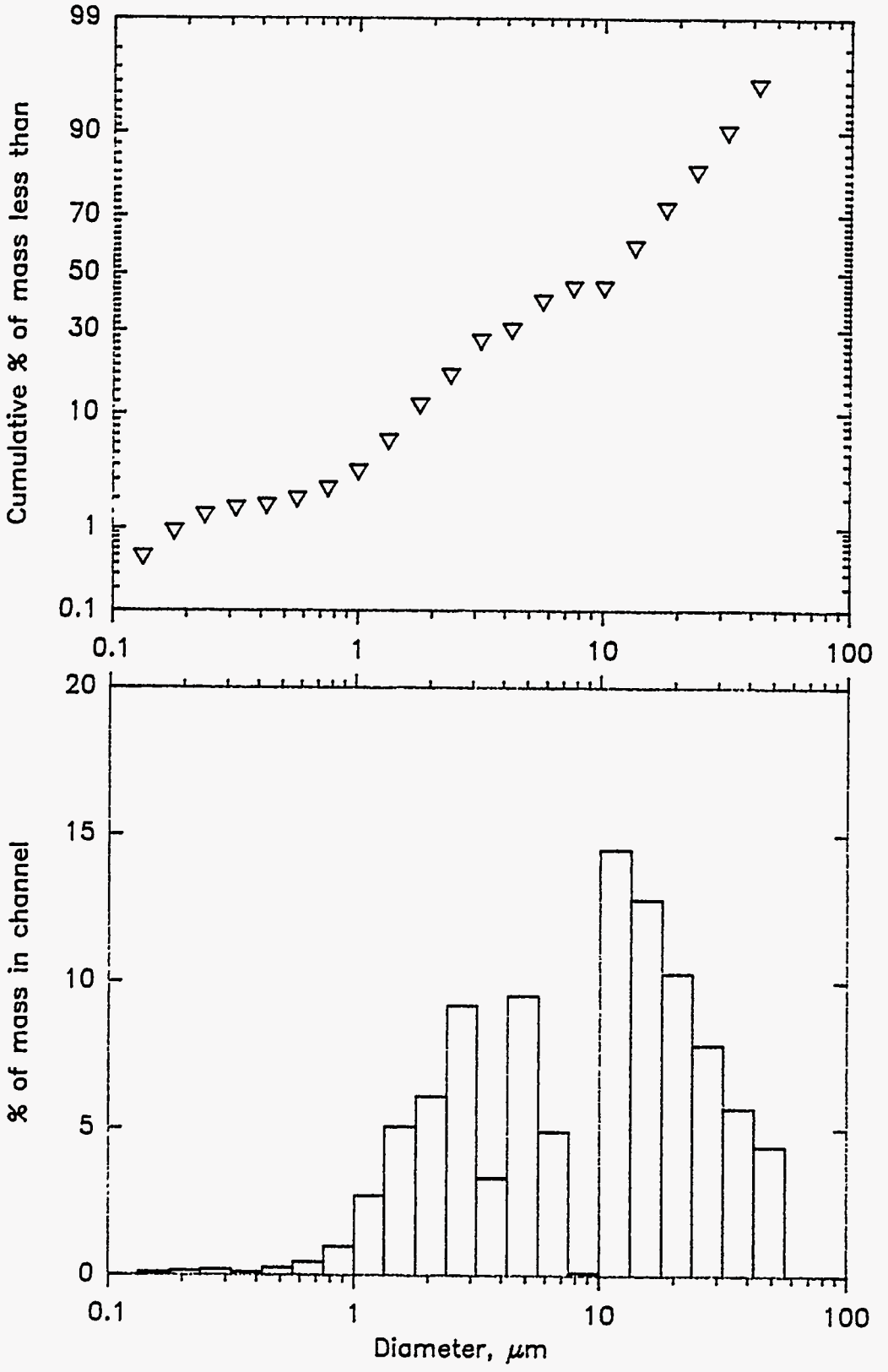

Figure C-7. Cumulative and differential size distribution data measured with a sedigraph for the sorbent and ash mixture from furnace injection of $Ca(OH)_2$ at Edgewater (ID # 2883).

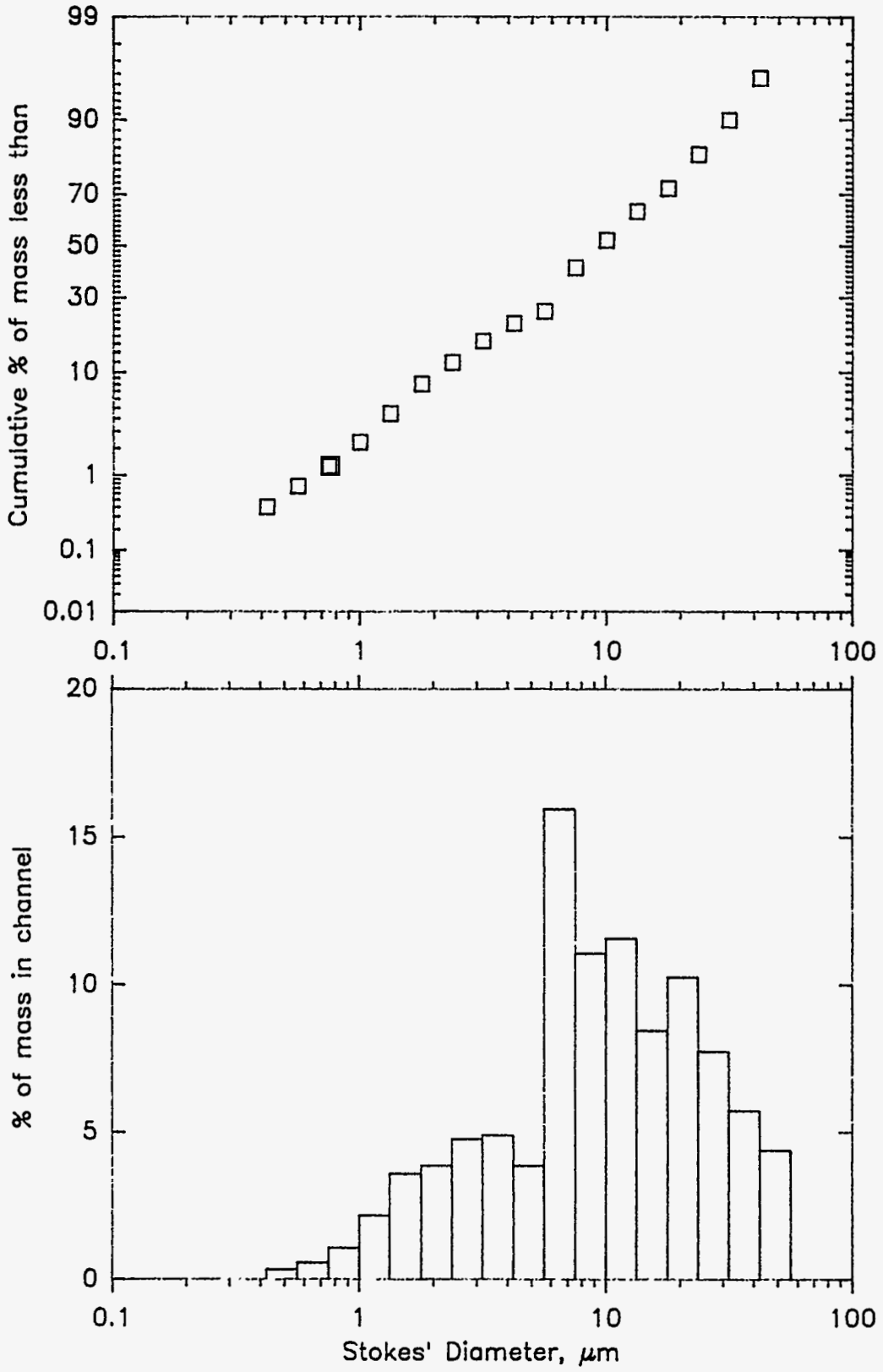

Figure C-8. Cumulative and differential size distribution data measured with a sedigraph for the sorbent and ash mixture produced from ADVACATE injection (ID # 2890).

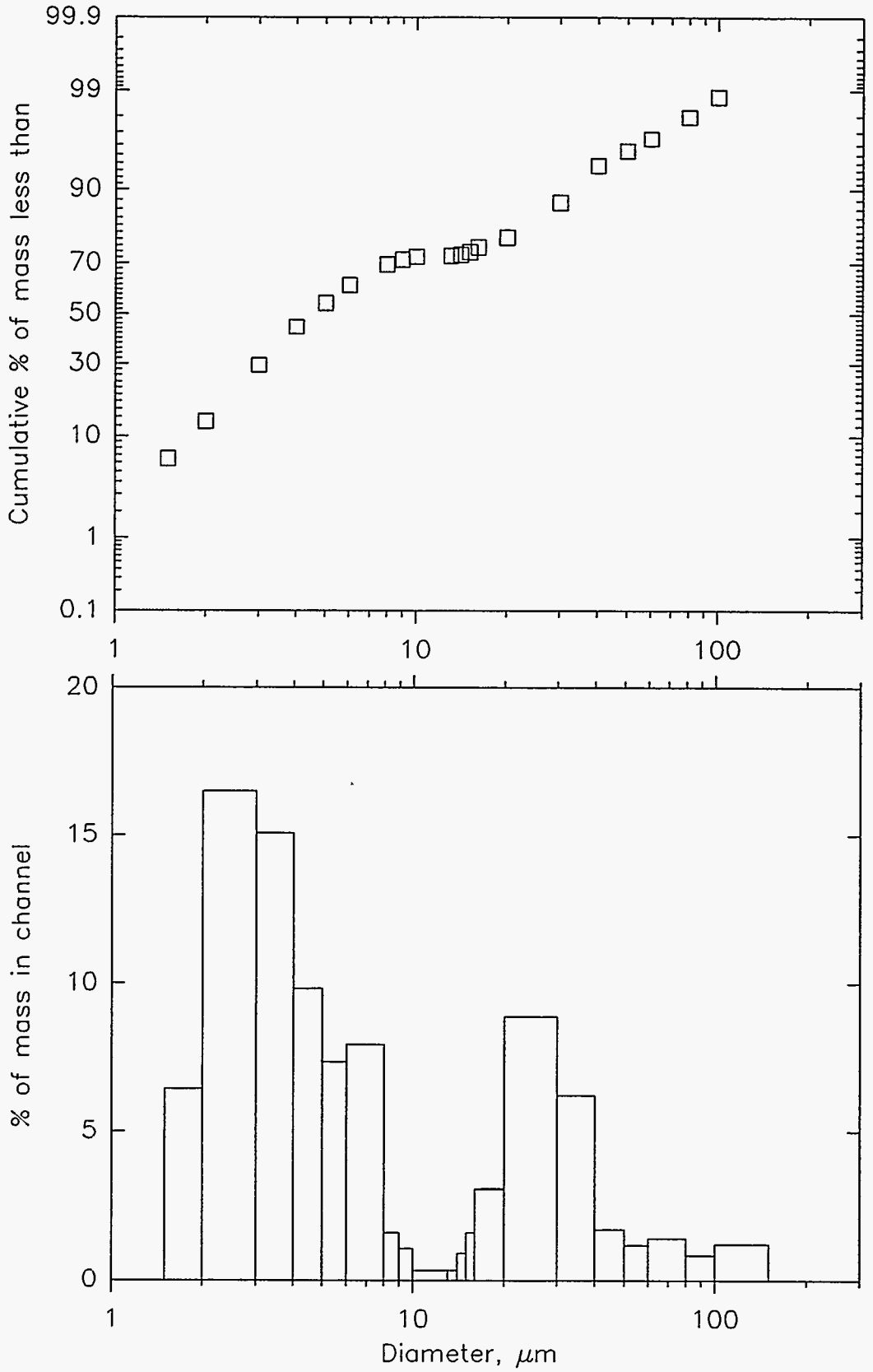

Figure C-9. Cumulative and differential size distribution data measured with a sedigraph for the Monticello dust cake ash (ID # 2029).

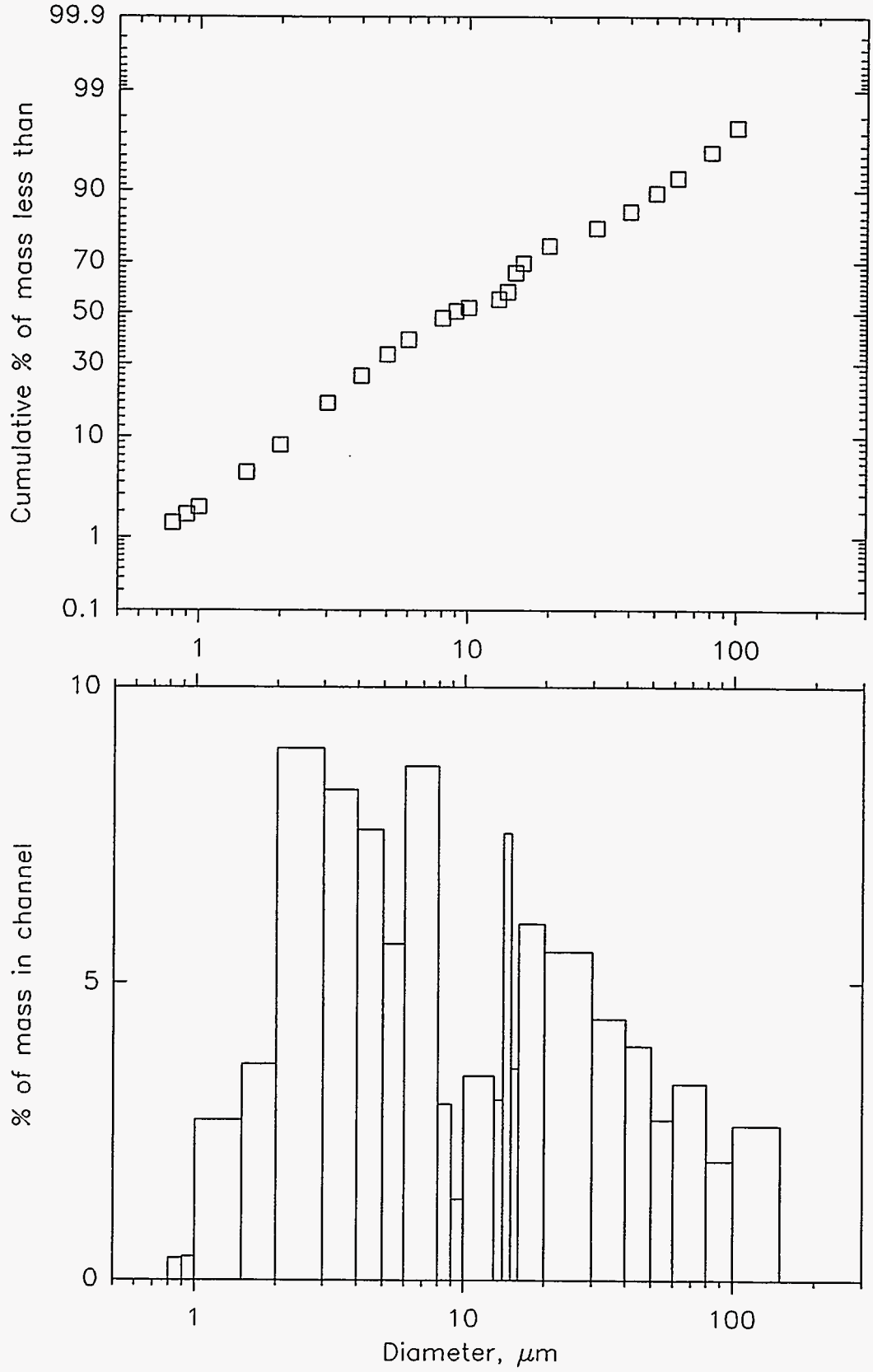

Figure C-10. Cumulative and differential size distribution data measured with a sedigraph for the Scholz dust cake ash (ID # 2101).

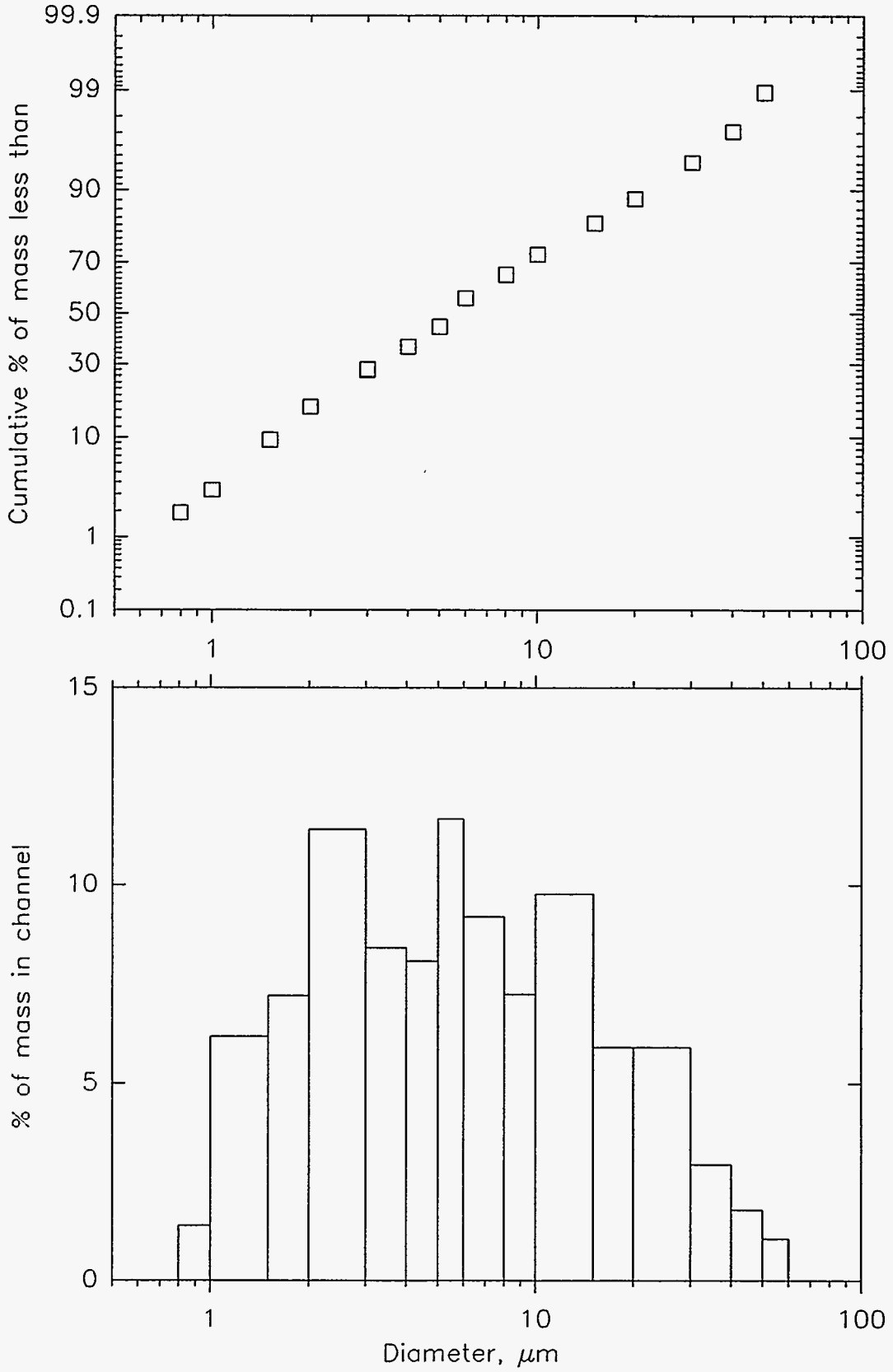

Figure C-11. Cumulative and differential size distribution data measured with a sedigraph for the Harrington dust cake ash (ID # 2515).

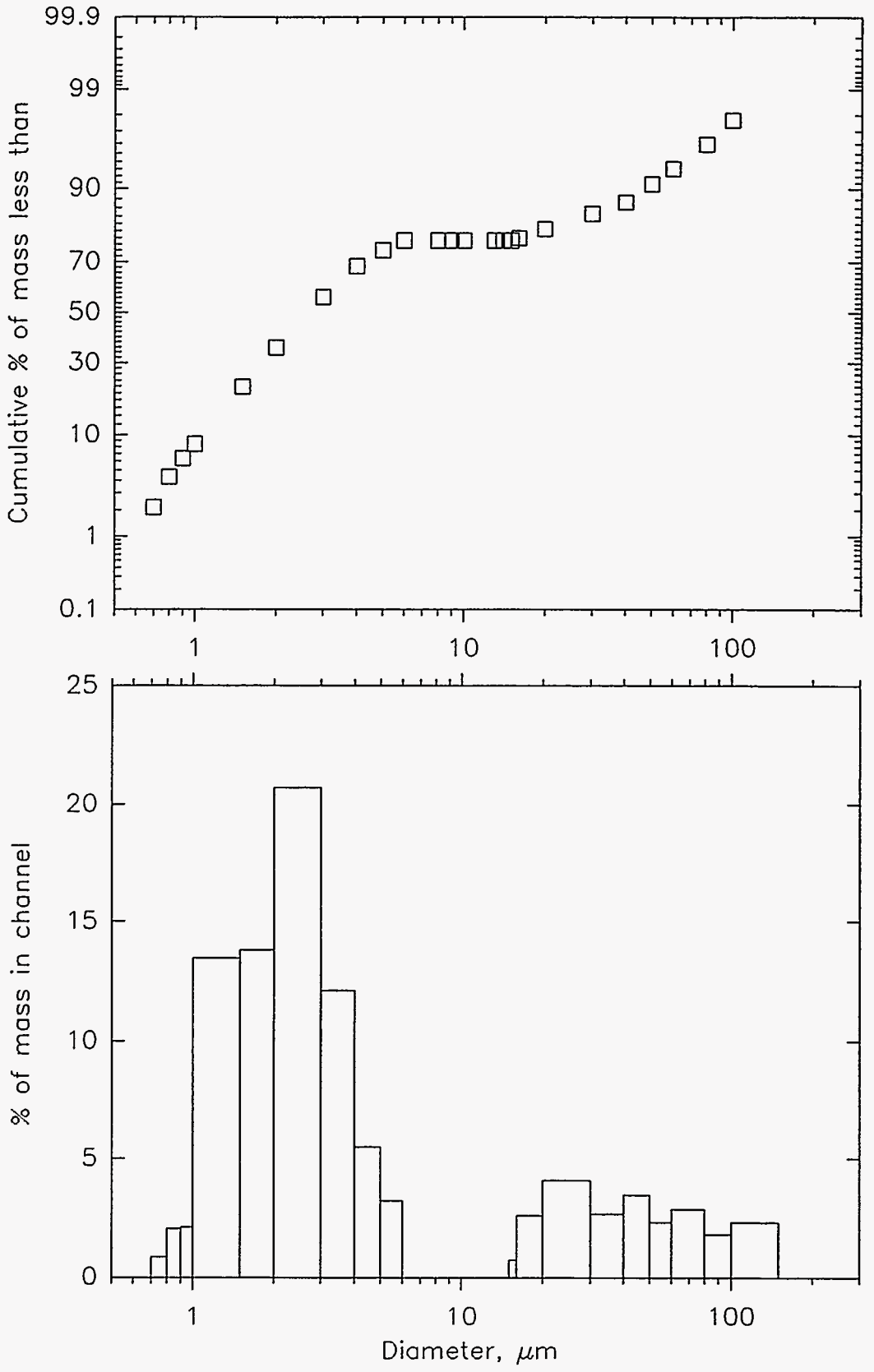

Figure C-12. Cumulative and differential size distribution data measured with a sedigraph for the AFBC dust cake ash (ID # 1994).

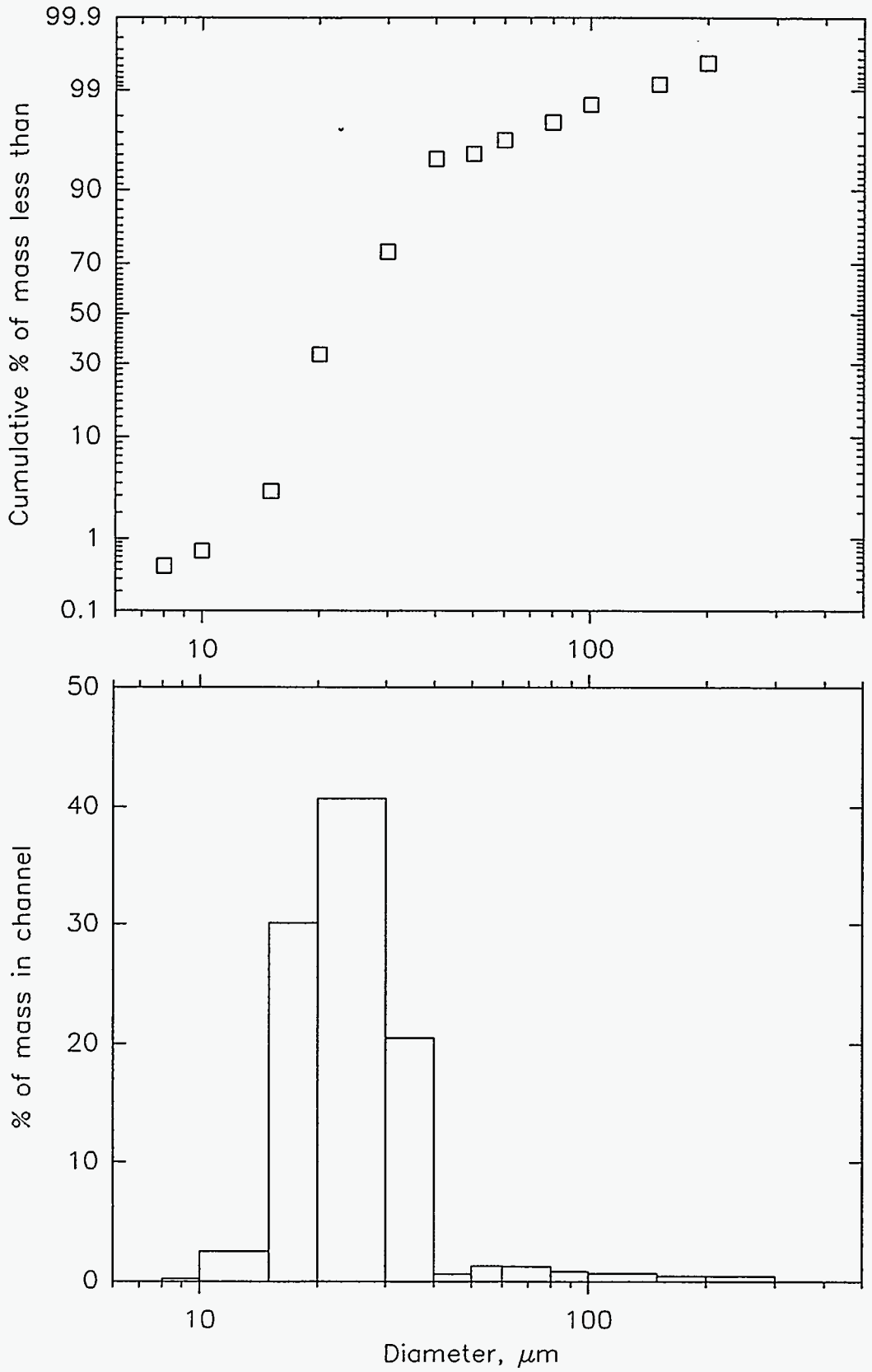

Figure C-13. Cumulative and differential size distribution data measured with a sedigraph for the glass beads (ID # 1856).

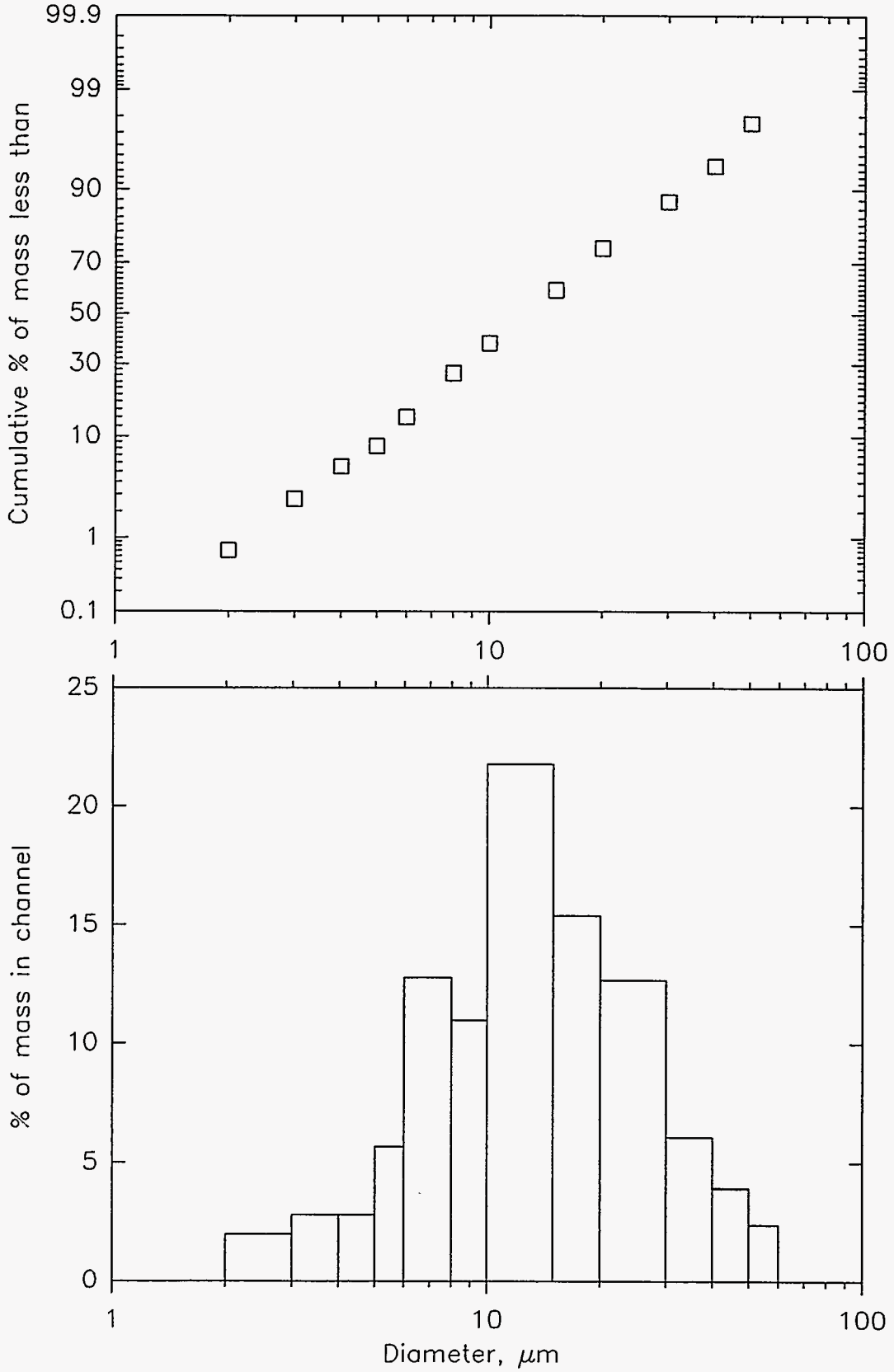

Figure C-14. Cumulative and differential size distribution data measured with a sedigraph for the diatomaceous earth (ID # 2769).

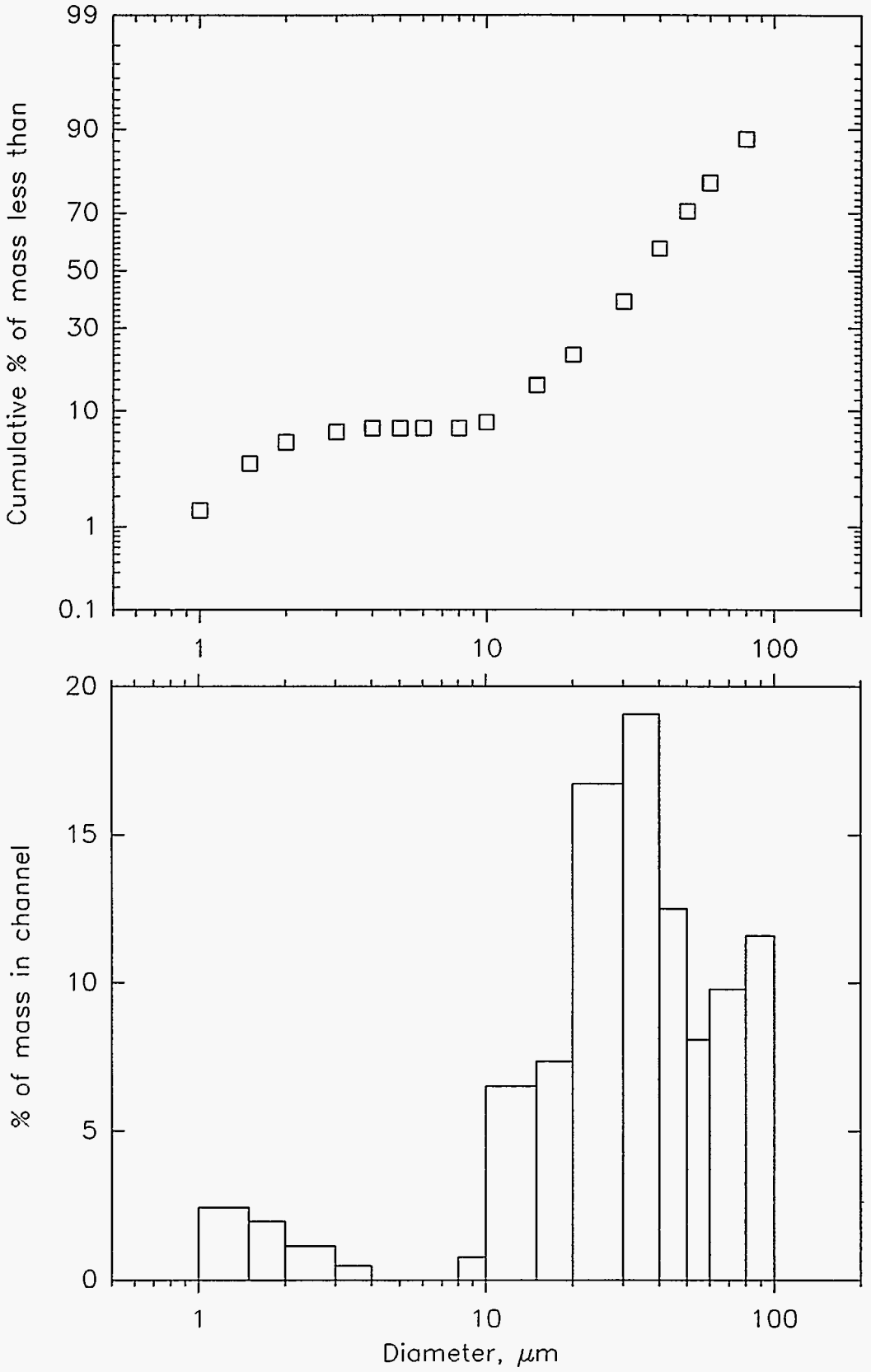

Figure C-15. Cumulative and differential size distribution data measured with a sedigraph for the alumina powder (ID # 2874).

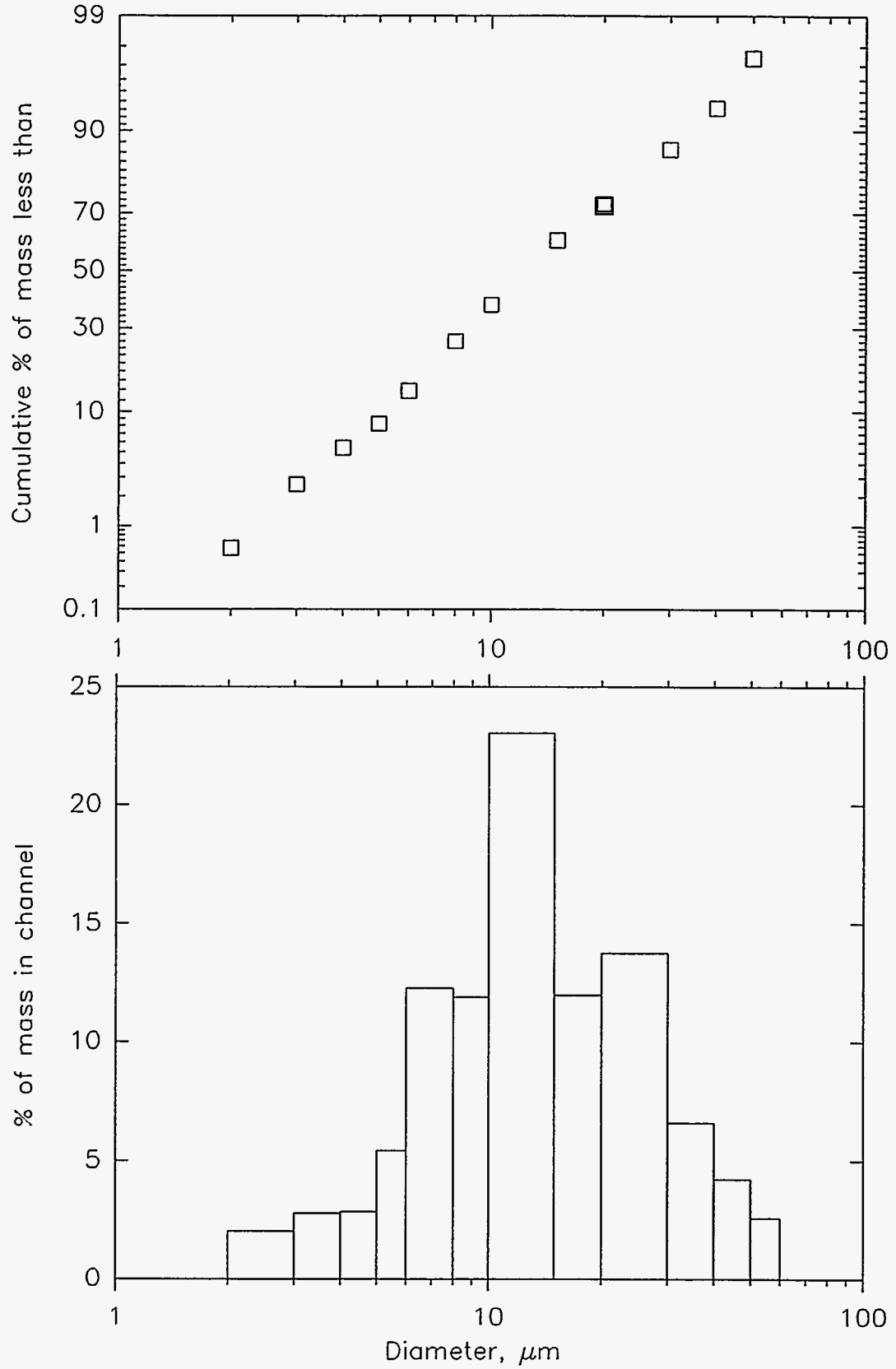

Figure C-16. Cumulative and differential size distribution data measured with a sedigraph for the aluminosilicate powder (ID # 3238).

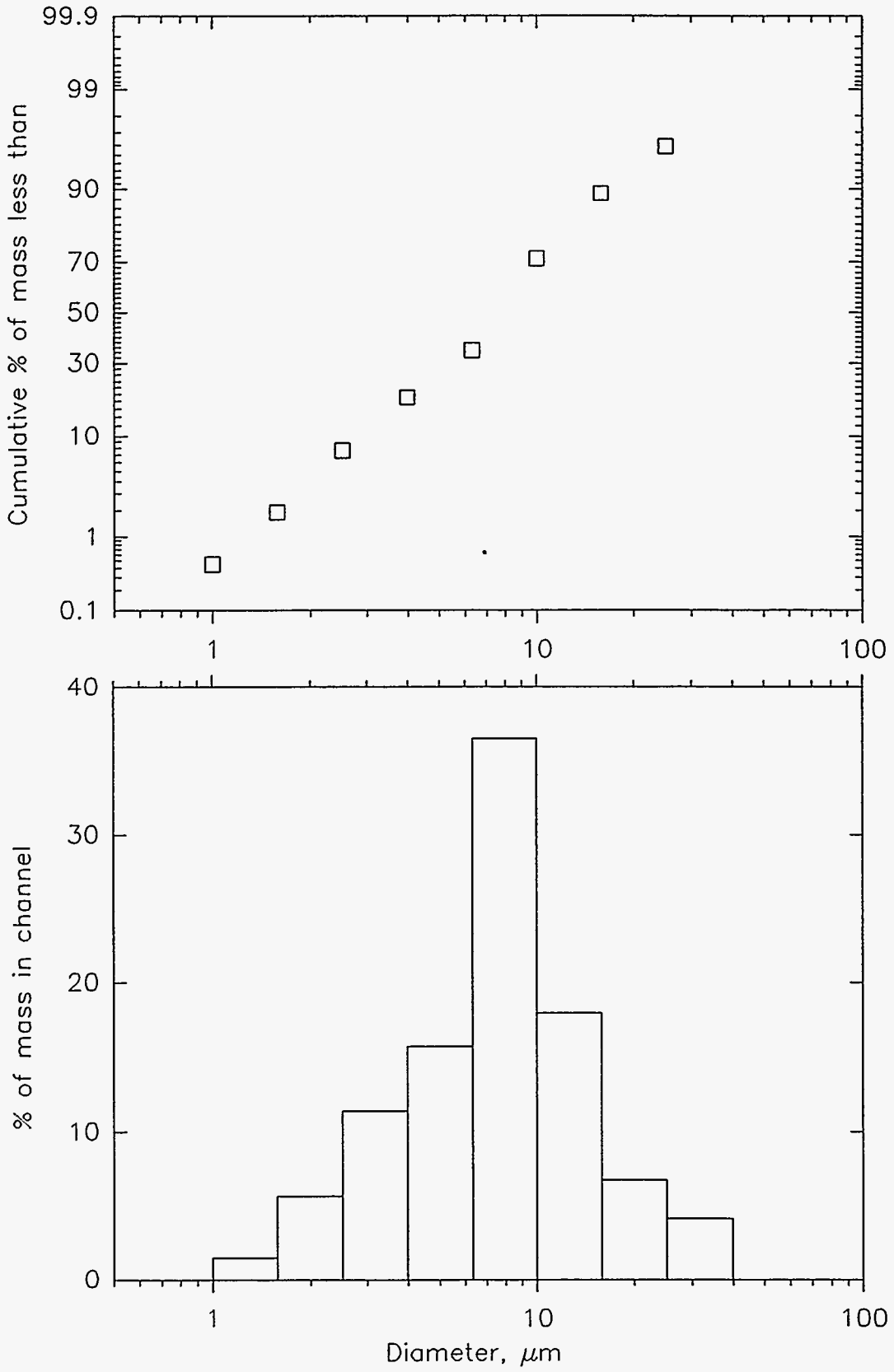

Figure C-17. Cumulative and differential size distribution data measured with a sedigraph for the Cedrum/Shoal Creek coal fly ash (ID # 4058) collected during our second pilot-scale test. The MMD of this ash is 7.7 μm, the D_{16} of this mass distribution = 3.5 μm, and the D_{84} of this mass distribution = 14 μm.

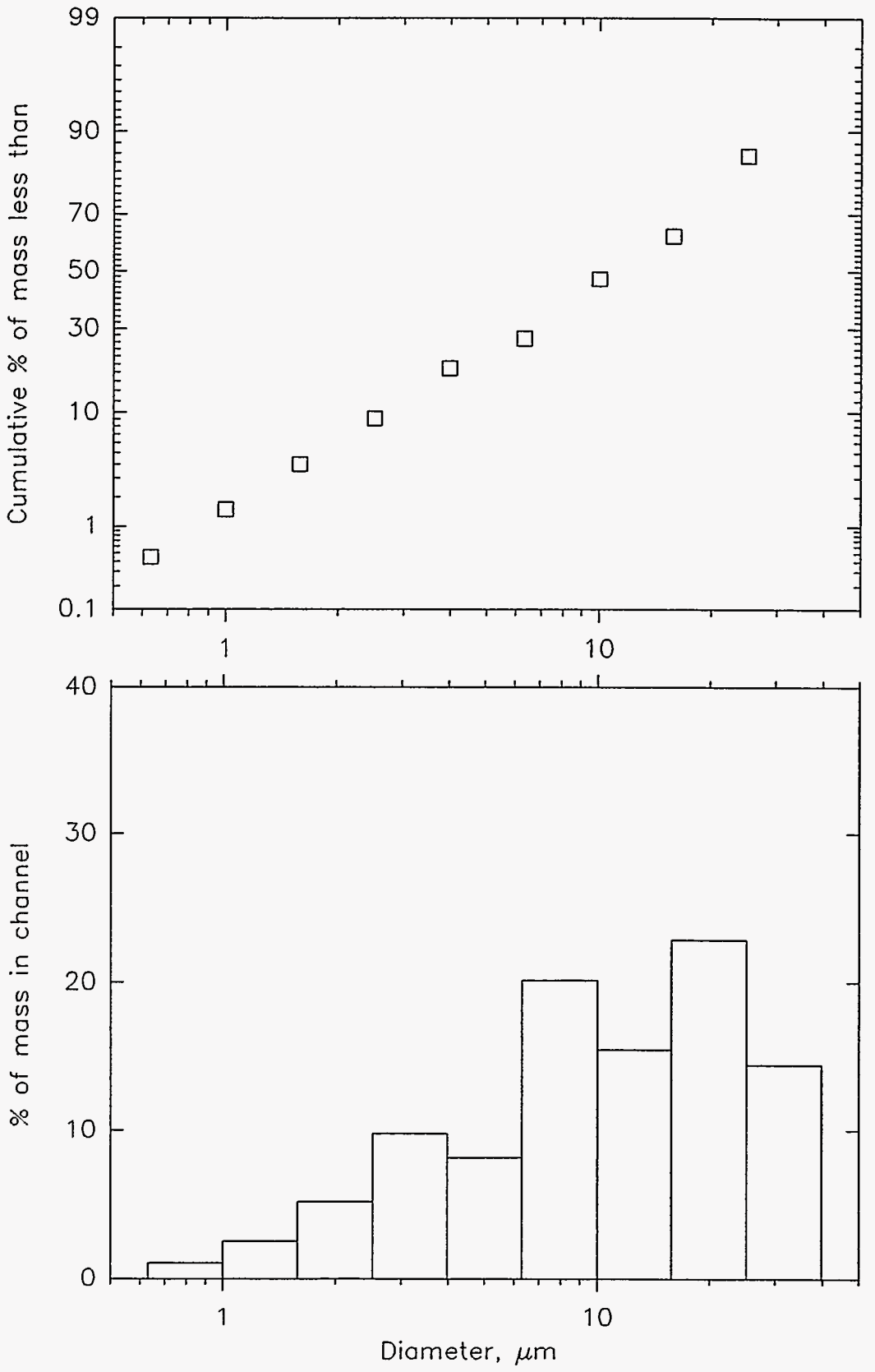

Figure C-18. Cumulative and differential size distribution data measured with a sedigraph for the Powder River Basin Bell Ayr coal fly ash (ID # 4118) collected during our third pilot-scale test. The MMD of this ash is 7.7 μm, the D_{16} of this mass distribution = 2.5 μm, and the D_{84} of this mass distribution = 18 μm.